Experimental, Computational and Sustainability Study of Energy-Efficient Technologies for Residential Buildings in Hot Countries

A thesis submitted for the degree of Doctor of Philosophy (PhD)

by

Emmanuel Shittu

Department of Mechanical and Aerospace Engineering
College of Engineering, Design and Physical Science
Brunel University London

June 2021

Abstract

Residential buildings account for the highest share of the global final energy use and related carbon dioxide emissions; 22 % and 17 %, respectively while energy for cooling is the fastest growing demand worldwide. Demand for cooling is higher in countries with high ambient temperatures and solar radiation leading to the installation of air-conditioning systems to improve internal thermal comfort. In addition, residential building retrofit has shown high energy savings potential due to the high percentage of existing stock in comparison to new built. This study investigates both the energy and environmental impacts associated with energy use in existing residential buildings in hot countries using two selected case studies.

The research involved experimental, computational and sustainability studies of building energy-efficient technologies focussing on external building envelope retrofit and reduction of internal heat gains, and renewable energy production focussing on solar energy systems. Three suitable envelope retrofit strategies were identified through literature review; (a) cool roof paint, (b) roof thermal insulation, and (c) window shading. For the reduction of internal heat gains, household A-rated appliances and energy-efficient lighting were identified as suitable technologies. Literature review also revealed that solar systems are very efficient in locations with high solar radiation, especially if thermal energy is also produced. The study considered Photovoltaic (PV) systems and Photovoltaic Thermal (PVT) systems focussing on the novel High Concentrator Photovoltaic Thermal (HCPV/T) 2000x system which is capable of providing electricity and thermal power with high efficiency. The identified technologies were applied to two case study existing low-rise single-family houses in Portmore, Jamaica and Palermo, Sicily. The experimental study involved monitoring the two case study houses and the HCPV/T system. These were used to calibrate the developed thermal EnergyPlus model used to investigate the houses' energy consumption and indoor thermal performance. There were also used to develop an analytical model for the HCPVT/T system. The environmental impact analysis was based on Life Cycle Assessment (LCA) methods using SimaPro and the ReCiPe method.

The thermal modelling study indicated that the cool roof paint is an attractive low-cost house retrofit solution for energy savings and indoor thermal comfort compared to roof thermal insulation. The cool roof paint and roof thermal insulation show similar energy savings in

Jamaica (-189 $kWh/m^2/year$ with the cool roof paint and -194 $kWh/m^2/year$ with the roof thermal insulation) while a heating penalty was experienced in Sicily. The heating penalty in Sicily results in higher energy savings with roof thermal insulation (influenced by the low U-value of roof thermal insulation); -22 $kWh/m^2/year$ for cool roof paint and -30 $kWh/m^2/year$ for roof thermal insulation.

Results indicate that the studied HCPV/T 2000x system has a high operational efficiency of ~80 % (30 % for electrical efficiency and 50 % for thermal efficiency) compared to PVT (11 % for electrical efficiency and 48 % for thermal) and PV (10 % for electrical efficiency). Therefore, it is the most attractive solar energy system because of its high energy production capability. The annual produced energy by the HCPV/T 2000x system in Sicily (1738 $kWh/year$ and 4125 $kWh/year$ electrical and thermal energy) is higher than the PV (1144 $kWh/year$ electrical energy) and PVT systems (1463 $kWh/year$ and 2695 $kWh/year$). In Jamaica, the annual produced energy by the HCPV/T 2000x system (1111 $kWh/year$ and 2662 $kWh/year$ electrical and thermal energy) is higher than PV (1100 $kWh/year$ electrical energy) and PVT (814 $kWh/year$ and 1980 $kWh/year$).

The sustainability study critically assessed the environmental impacts of the cool paint and the HCPV/T 2000x system in both case-study locations. It was found that the environmental impacts of cool roof paint are lower than thermal insulation; for example, the Global Warming Potential (GWP) of cool roof paint were 4 – 7-fold lower than thermal insulation materials. The environmental impact (which includes GWP) of the HCPV/T 2000x are lower than fuel-based Combined Heat and Power and non-RES systems; for example, the GWP of the HCPV/T 2000x system was up to 4-fold lower than coal and natural gas systems.

Based on these findings it is concluded that the potential of operational energy use reduction and the whole life environmental impact of renovation components should both be considered to ensure the least impacting solution for building renovation.

Contents

List of Figures

List of Tables

Nomenclature

Nomenclature	*Description*	*Unit*
A_c	InGaP/InGaAs/Ge solar cell area	m^2
C_p	Pressure coefficients	-
$E_{el,p,HCPVT}$	Analytical HCPV/T 2000x produced electrical energy	kWh
$E_{th,p,HCPVT}$	Analytical HCPV/T 2000x produced thermal energy	kWh
$G_{i,met}$	Meteonorm DNI	$\mathrm{W/m}^2$
G_i	Onsite measured DNI	$\mathrm{W/m}^2$
P_d	Dynamic pressure	$\mathrm{N/m}^2$
$P_{el,p,HCPVT,exp}$	Experimental HCPV/T 2000x produced electrical power	W
$P_{el,p,HCPVT}$	Analytical HCPV/T 2000x produced electrical power	W
P_{mp}	Power at maximum power point	W
P_x and P_o	Static pressure	$\mathrm{N/m}^2$
$Q_{th,p,HCPVT,exp}$	Experimental HCPV/T 2000x produced thermal power	W
$Q_{th,p,HCPVT}$	Analytical HCPV/T 2000x produced thermal power	W
$Q_{th,p,PVT}$	Analytical PVT 2000x produced thermal power	W
T_{in}	Inlet water temperature	°C
T_{out}	Outlet water temperature	°C
$\dot{V}$	Volumetric flowrate	m^3/s
$\eta_{c,HCPVT,exp}$	Experimental InGaP/InGaAs/Ge solar cell efficiency	-
$\eta_{c,HCPVT}$	Analytical InGaP/InGaAs/Ge solar cell efficiency	-
$\eta_{c,PV}$	PV cell efficiency	-
$\eta_{c,PVT}$	PVT cell efficiency	-
$\eta_{el,HCPVT,exp}$	Experimental HCPV/T 2000x electrical efficiency	-
$\eta_{el,HCPVT}$	Analytical HCPV/T 2000x electrical efficiency	-
$\eta_{th,HCPVT,exp}$	Experimental HCPV/T 2000x system thermal efficiency	-
$\eta_{th,HCPVT}$	Analytical HCPV/T 2000x thermal efficiency	-
ρ_w	Water density	$\mathrm{kg/m}^3$
I	Current	A
Q	Heat/Cooling energy	kWh

U	Upstream wind speed	$\mathrm{m/s}$
V	Voltage	V
ρ	Air density	$\mathrm{kg/m^3}$
ϕ	Heat transmission rate	W

Abbreviations

Abbreviations	*Definition*
BEM	Building Energy Modelling
BIM	Building Information Modelling
CAD	Computer Aided Design
CEPMD	Council for European Producers of Materials for Construction
CFD	Computational Fluid Dynamics
CR	Concentration Ratio
CSP	Concentrator Solar Power
CTGA	Cradle to Gate
CTGR	Cradle to Grave
CTSI	Cradle to Site
CVRMSE	Coefficient of Variance of the Root Mean Square Error
DHI	Diffuse Horizontal Irradiance
DNI	Direct Normal Irradiance
DTM	Dynamic Thermal Model
EC	European Commission
EEIA	Electrical Energy Impact Allocation
EJ	Exa-Joules
EMS	Energy Management System
EP	EnergyPlus
EPBD	Energy Performance of Buildings Directive
EPS	Expanded Polystyrene
EU	European Union
FDM	Finite Difference Method
GHG	GreenHouse Gases
GHI	Global Horizontal Irradiance
HCPV/T	High Concentrator Photovoltaic Thermal
HVAC	Heating, Ventilation, and Air Conditioning
InGaP/InGaAs/Ge	Indium-Gallium-Phosphide/Indium-Gallium-Arsenide/Germanium
IoT	Internet of Things
LC	Life Cycle

LCA	Life Cycle Assessment
LCI	Life Cycle Inventory
LCIA	Life Cycle Impact Assessment
LED	Light-Emitting Diode
MBE	Mean Bias Error
MPPT	Maximum Power Point Tracking
NREL	National Renewable Energy Laboratory
NZEB	Nearly Zero Energy Buildings
OS	OpenStudio
PV	Photovoltaic
PVT	Photovoltaic Thermal
RES	Renewable Energy Source
SDG	Sustainable Development Goal
SES	Solar Energy System
TEIA	Thermal Energy Impact Allocation
TMY	Typical Meteornorm Year
UN	United Nation
ZEB	Zero Energy Building

To the memory of my grandmother, Florence Folorunso Shittu

"The greatest threat to freedom is the absence of criticism."

Wole Soyinka

Acknowledgements

The completion of this PhD programme which was full of challenges and adventures was made possible due to the endless support and advice of many people.

First and foremost, I would like to express my deepest gratitude to my principal supervisor, Professor Maria Kolokotroni for the advice and guidance that steered me through the 4 years of my research project. Also, I would like to thank my second supervisor, Dr Valentina Stojceska for supporting the completion of my research project.

I would like to thank Marie Curie SMART GEMS partners (IDEA SRL in Sicily, Loccioni in Marche and Elgama – Elektronika in Lithuania) for the opportunities to acquire international industrial experience. Also, I would like to acknowledge my colleagues from IDEA SRL, in particular Benedetto Schiavo, Luca Venezia, Sergio Milone, Filippo Paredes and Fabio Montagnino from IDEA SRL for providing access to the HCPV/T 2000x system and data. To seconded staffs, Nikos Kampelis, Martina Senzacqua, Laura Standardi and Lukas Samulevičius for the great secondment experiences.

To colleagues from CSEF Brunel University London. Zoi Mylona and Thiago Santos for provided the buddy system needed at the start of my research project for smooth integration into the world of academia. Matteo Marchionni and Ioannis Katsaros for providing a friendly working environment.

To my parents, Bamidele and Patricia Shittu, and my brother Anthony Shittu for their words of encouragement, great and never-ending support. Finally, to my beautiful partner Sima Banelyte for the endless encouragement and emotional support during frustrations and challenging times.

Chapter 1: Introduction

1.1 Research Context

The global share of the building sector final energy use (125 EJ) and related carbon dioxide (CO_2) emissions (9.7 $GtCO_2$) as of 2018 is 36 % and 39 % respectively; the residential building sector accounted for the highest share (22 %) and CO_2 emissions (17 %) as shown in Figure 1-1. This share has continuously increased yearly due to the increase in floor area and population. Final energy use increased by 7 % from 2010 to 2018 (1 % increase from 2017) and a 2 % related increase in CO_2 emissions from 2017 to 2018 (IEA, 2019). The long lifecycle of buildings means that a large percentage of the present total building stock in developed countries will exist in 2050 (IPCC, 2014); globally, this is expected to double by 2050 (IEA, 2019). High energy performance retrofits are key mitigation strategies to reduce building energy consumption which includes heating and cooling energy which accounts for 77 % of global final energy demand in buildings in 2017 (REN21, 2020). In particular, residential building energy-efficient retrofit presents good opportunities to reduce final energy use because residential building accounts for nearly three-quarters of the global final energy use (REN21, 2020), hence large external envelope area which offers high energy saving potential. Countries with high ambient temperature and solar radiation, cooling energy demand is a significant part of the energy demand because of the weather conditions (Kwame et al., 2020). There is evidence that demand for air conditioning is increasing in the residential sector to provide improved internal comfort conditions (IEA, 2019, 2018a). In addition, there is increasing effort to reduce the environmental impact of buildings throughout their life cycle from production to demolition. The reduction of environmental impacts in buildings is achieved by increasing building energy efficiency and integration of Renewable Energy Source (RES) systems in buildings (Desideri and Asdrubali, 2018).

The renovation rates of existing building stock in industrialised countries should increase by an average of 2 % per year by 2025, and to 3 % by 2040. While renovation rates in developing countries should reach 1.5 % by 2025 and 2 % by 2040 (IEA, 2019). Some key challenges of building renovation are costly, further research needed to understand the effect of building fabric insulation, and the reduction of internal space (Khairi et al., 2017).

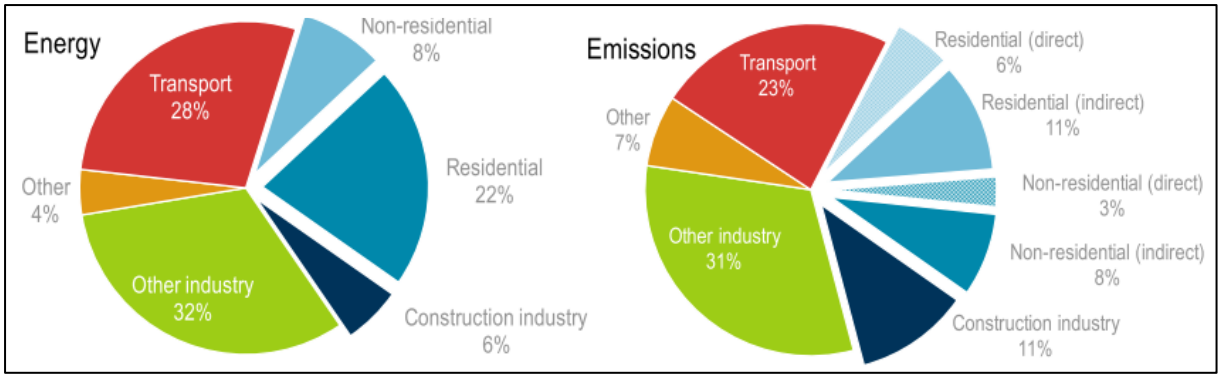

Figure 1-1: "Global share of buildings and construction final energy and emissions, 2018 Energy" (IEA, 2019).

The effort to reduce existing residential buildings' final energy use and related environmental impacts can be achieved in several ways. For example, by reducing direct energy consumption by adopting energy-efficient appliances and lighting (European Commission, 2019a; Serrano et al., 2017) and retrofitting existing building envelope (walls, roof, windows, etc.) to reduce heating and cooling energy demand. Also, building integration of RES systems will help displace some percentage of the non-RES systems such as high level of coal which is still used for electricity generation (European Commission, 2019a; IEA, 2019). The global increase in the share of RES systems is key to achieving net zero GreenHouse Gases (GHG) by 2050; a global share of 90 % for total electricity generation is expected to achieve this goal according to the roadmap for the energy sector (IEA, 2021). The increase in RES systems also addresses Sustainable Development Goal (SDG) 7 of the United Nation (UN), which is to "ensure access to affordable, reliable, sustainable and modern energy for all" (United Nations, 2018). The SDG 7 is one of the 17 UN SDGs (see Figure 1-2) with 169 targets (detailed list of challenges through which the SDGs can come alive) that the UN endorsed in September 2015 as a universal agenda; "Transforming our World: the 2030 Agenda for Sustainable Development". The Agenda aims "to take the bold and transformative steps which are urgently needed to shift the world onto a sustainable and resilient path" (IPCC, 2018). The 17 UN SDGs build on decades of work of the Agenda 21 adopted in June 1992 which aimed to improve human lives, protect and the environment; and the eight Millennium Development Goals adopted in September 2000 which aimed to reduce extreme poverty by 2015.

Figure 1-2: The UN 17 SDGs (United Nations Department of Global Communications, 2020).

The research project was developed under the Marie Curie Research and Innovation Staff Exchange (RISE) Smart Grids Energy Management Staff (SMART GEMS) project, which aimed to investigate smart buildings, systems and grid infrastructural technologies as the common bias for collaboration among all stakeholders from academia and industry partners (European Commission, 2014). The collaborative approach contributed to the advancement of knowledge in architecture, smart buildings, smart communities, and urban engineering.

Part of the work presented in this thesis contributed to work package 4 (Smart Communities and Smart Grids) and work package 5 (Integration, Innovation) of the Marie Curie SMART GEMS project which is made of six work packages. The presented thesis focuses on energy and environmental performance by using RES systems and energy-efficient solutions for residential buildings. The building energy-efficient solutions studied are at the building envelope level, and reduction of internal heat gains. The RES systems studied under the Marie Curie Research and Innovation Staff Exchange (RISE) Smart Grids Energy Management Staff (SMART GEMS) project was based on operational state-of-the-art solar energy systems installed on the site of the Marie Curie SMART GEMS industry partners; these include High Concentrator Photovoltaic Thermal (HCPV/T) 2000x, Photovoltaic (PV) and Concentrator Solar Power (CSP) systems (European Commission, 2014). The performance of these systems was compared in terms of efficiency, energy production potential and environmental impacts.

The following sections present the research aim and objectives, methods adopted to meet the aim and objectives, the research novelty and significance, thesis structure and published research outcome.

1.2 Research Aim and Objectives

The research study contributes to the international effort to increase the energy efficiency of buildings by the renovation of their envelopes and the use of RES systems to provide the required energy need (European Commission, 2019a). In addition, it focuses on the environmental impacts of the selected systems to provide information on life-cycle impacts. Low-rise buildings are characterised with larger envelope areas than high-rise buildings for heat gains and losses (Du et al., 2015), therefore, their retrofit offers high energy savings potential. The study focuses on low-rise single family residential buildings because energy-efficient retrofit is decided by the occupants/owners and therefore can be implemented once information on possible improvements is available to them. Therefore, this research project aims to critically assess the energy efficiency and environmental impact performance of selected building energy-efficient technologies and solar energy systems suitable for low-rise residential buildings in regions with high ambient air temperature and solar radiation where cooling is the predominant energy demand.

To achieve this, the following specific objectives were set:

Objective 1: Through literature review, identify the building energy-efficient technologies and solar energy systems applicable for improving the energy and environmental performance of existing residential buildings in hot countries.

Objective 2: Define case study locations and existing residential building types to demonstrate the energy and environmental performance of the building energy-efficient technologies and solar energy systems identified in objective 1. The study of the building energy-efficient technologies and solar energy systems at the different locations helps to understand their effectiveness in varying climatic conditions.

Objective 3: Investigate experimentally and computationally, the energy reduction and thermal comfort improvement potential by the building energy-efficient technologies, and the electrical and/or thermal energy production potential of the solar energy systems. A validated computational model can be used to accurately predict energy demand, energy savings, and

thermal comfort improvement by the different building energy-efficient technologies. Also, via experimental monitoring data and/or analytical study of energy production, the most energy-efficient solar energy system can be identified.

Objective 4: Develop cradle to grave Life Cycle Assessment (LCA) system boundary for the most energy-efficient building solution and solar energy system.

Objective 5: Critically evaluate the magnitude and significance of the lifecycle environmental impacts of the most energy-efficient building solution and solar energy system, using the developed LCA system boundaries developed in objective 4. The energy savings and energy production findings from the study to achieve objective 3 are used as an input (functional unit) to conduct the lifecycle environmental impact study.

1.3 Research Methods

The work presented in this thesis is a combination of experimental and computational study to meet the set objectives. Table 1-1 summarises the research methods, techniques, and studies undertaken to meet these objectives. Experimental monitoring and computational studies were carried out for two case-study houses in the high solar radiation regions of Sicily (with some heating demand) and Jamaica (with no heating demand), to study the implementation of the most efficient building energy solution and solar energy system. The purpose of the experimental monitoring of the two case-study houses was to collect data required to accurately model and validate the computational model. Finally, the environmental impacts of the most efficient building energy solution and solar energy system were assessed using the LCA method and compared with literature studies of the environmental impact of other energy systems (which includes RES and non-RES) and building energy-efficient solutions (including indoor thermal comfort) respectively, which provide the same functions.

Table 1-1: Research objectives and methods.

Objective	Method	Technique	Study/Research
1, 2	Literature Review	Journal Papers and Books	Residential Building Energy and Environmental Performance
3	Experimental, Analytical and Numerical	Dynamic Thermal Modelling and Data Monitoring	Residential Building Energy and Thermal Performance, and Energy Production
4	Literature Review and Data Collection	Journal Papers, Books, and Data Collection	LCA System Boundary
5	LCA	Processed-based Attributional Modelling	Environmental Assessment of Building Energy-Efficient Technologies and Solar Energy Systems

1.3.1 Residential Building Energy and Thermal Modelling

The energy and thermal load were modelled using EnergyPlus (EP). EP is an energy analysis and thermal load simulation program that was used to calculate the heating and cooling, electric equipment, and lighting energy consumption of the two case-study houses. Since the free version of EP does not include a front user interface, the 3D geometry of the two case-study houses was created using OpenStudio (OS) SketchUp Plug-in, before it is exported to EP for energy and thermal load analysis (NREL et al., 2019; U.S. Department of Energy, 2019). The energy analysis was based on the occupant(s) usage of heating and cooling system, electric equipment, and lighting. The thermal load analysis uses the conduction transfer function algorithm, a transient heat conduction solution through building envelope. The internal thermal comfort is modelled using parameters such as the occupant(s) activities, air temperature and relative humidity (U.S. Department of Energy, 2019). The energy and thermal modelling techniques detailed in chapter 2 were adopted in the computational study of the two case study houses presented in chapters 3 and 4. The two case-study house energy and the thermal modelling were carried out at two levels:

- Baseline EP model: before the application of building energy-efficient technologies
- Improved EP model: after the application of building energy-efficient technologies

1.3.2 Energy Production from Solar Energy Systems

The electrical and thermal energy performance of the HCPV/T 2000x system was studied experimentally and analytically. The purpose of the experimental monitoring was to acquire onsite data to analyse the electrical and thermal performance of the operational HCPV/T 2000x system. The developed analytical model used to analyse the HCPV/T 2000x system was based on external and internal inputs. The external inputs are the uncontrollable site environmental variables such as solar radiation, ambient air temperature and atmospheric condition. The internal inputs are the design and assemble variables that characterise the HCPV/T 2000x system. The accuracy of the analytical model of the HCPV/T 2000x system was validated via comparison with experimental results.

The electrical and/or thermal energy performance of the PV and PVT systems were studied computationally. The performance of the PV system for the prediction of electricity generation was modelled using the Sandia model available in EP. The Sandia model includes mathematical equations derived from individual solar cell characteristics, based on the significant number of empirical coefficients which have been obtained from extensive experimental measurements (King et al., 2004; U.S. Department of Energy, 2019). Also, the performance of the PVT system for the prediction of electricity and heat generation was modelled using the simple PVT model available in EP. The simple PVT model reuses the Sandia model for electricity generation. The detailed experimentally and analytically study of the HCPV/T 2000x system, and computational study of the PV and PVT are presented in chapter 5.

1.3.3 Environmental Impact Study

The environmental impacts of the selected technologies as the most efficient building energy solution and solar energy system were assessed using the LCA method following the guidelines and framework of ISO 14044/40. These include goal and scope definition, inventory, impact assessment and result interpretation, as shown in Figure 1-3 (BS EN ISO, 2018, 2006). The

software used was SimaPro v8.2.3.0 software (PRé Sustainability, The Netherlands) with incorporated ReCiPe2016 environmental impact assessment method. ReCiPe2016 is the successor of Eco-indicator 99 and CML-IA methods that integrates the midpoint impact category of Eco-indicator 99 and endpoint impact category of CML-IA to interpret the lifecycle environmental impacts relevant to human health, the ecosystem and resources (PRé, 2016). The method converts lifecycle inventory emitted substances to 18 midpoint indicators (midpoint impact category) and 3 endpoint indicators (endpoint impact category), by adopting the hierarchist midpoint and endpoint characterization factors at a global scale (M.A.J. Huijbregts et al., 2017; Mark A.J. Huijbregts et al., 2017; PRé, 2016; RIVM, 2018). The environmental impact assessment technique detailed chapter 2 was adopted in the assessment of the most energy-efficient building solutions presented in chapters 6 and 7.

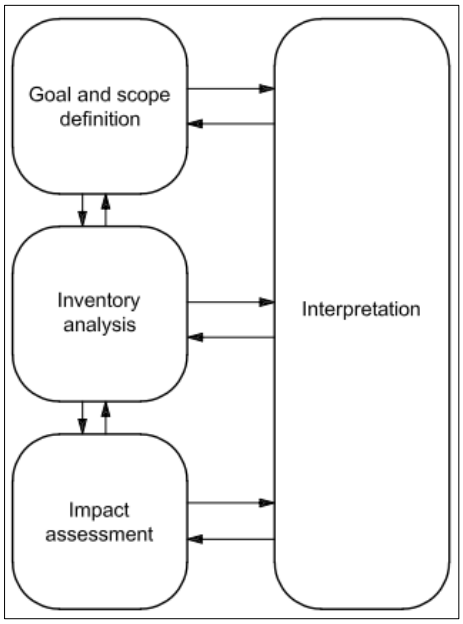

Figure 1-3: “Stages of an LCA” (BS EN ISO 14040, 2006).

1.4 Research Novelty and Significance

The research novelty resides in the approach that combines residential building energy demand, energy production by RES systems, and LCA methodology for the critical assessment of material and energy flows of energy-efficient and renewable energy technologies as retrofit solutions for residential buildings in hot countries. The research is a practical one that demonstrates the role of buildings in the global effort to reach net zero GHG by 2050. The research findings show how energy-efficient technologies can be used to reduce residential

building energy use, and the supply of energy to the residential building by locally integrated RES systems. The reduction in building energy use and energy supply by RES systems are two of the five zero-carbon-ready building energy codes that more than 85 % of global buildings (including existing ones) must comply with in the building sector pathway to net zero GHG by 2050 (IEA, 2021).

1.5 Thesis Structure

Figure 1-4 shows the thesis structure which addresses the defined 5 research objectives (Table 1-1) described and presented in 8 chapters. The contents of each chapter are summarised below:

- Chapter 1: presents the context for undertaking the research, research aim and objectives, an overview of the research methods adopted to meet the objectives and the outlined thesis structure.
- Chapter 2: presents a literature review of the research undertaken. A brief review of residential energy consumption (including cooling energy demand) in hot climates is summarised. Passive and active high energy-efficient solutions and building integrated RES systems that are applicable in hot countries to achieve low energy building and ZEB are explained in detail. The dynamic thermal modelling and LCA methods needed to perform modelling and assessment to meet the research aim and objectives are presented.
- Chapter 3: presents the experimental and computational study of the two case study houses needed to demonstrate the energy and environmental performance of energy-efficient solutions presented in chapter 2. The climate of the case study house locations, house external fabric and thermal data, experimental monitoring setup and computational model is presented in detail. The results of the validated computational model are presented.
- Chapter 4: presents the results of the case study houses energy and thermal performance, which includes energy demand of electric appliances, lights and heating and/or cooling, and surface and indoor air temperature. A comparison study was conducted by comparing the energy demand, surface (roof and ceiling) and indoor air temperature results before and after the application of the energy-efficient solutions presented chapter 2.
- Chapter 5: presents the experimental monitoring, computational and analytical assessment of the building integrated solar energy systems presented in chapter 2. The solar energy systems and experimental procedure are described, and the experimental monitoring procedure and assessment model explained in detail. A comparison study was conducted

by comparing the calculated efficiency, electrical and thermal energy production potential of the solar energy systems.

- Chapter 6: the environmental impacts of the most energy-efficient solution (cool roof) assessed in chapter 4 is presented. The system boundary and comparison of environmental impact results with other energy-efficient solutions that provide the same function is detailed.
- Chapter 7: similar to chapter 6, the environmental impacts of the most energy-efficient solar energy system (HCPV/T) assessed in chapter 5 is presented. The system boundary and comparison of environmental impact results with other solar energy systems that provide the same function is detailed.
- Chapter 8: finally, this chapter presents the overall conclusions of the research work and outlines sets of recommendations for future works.

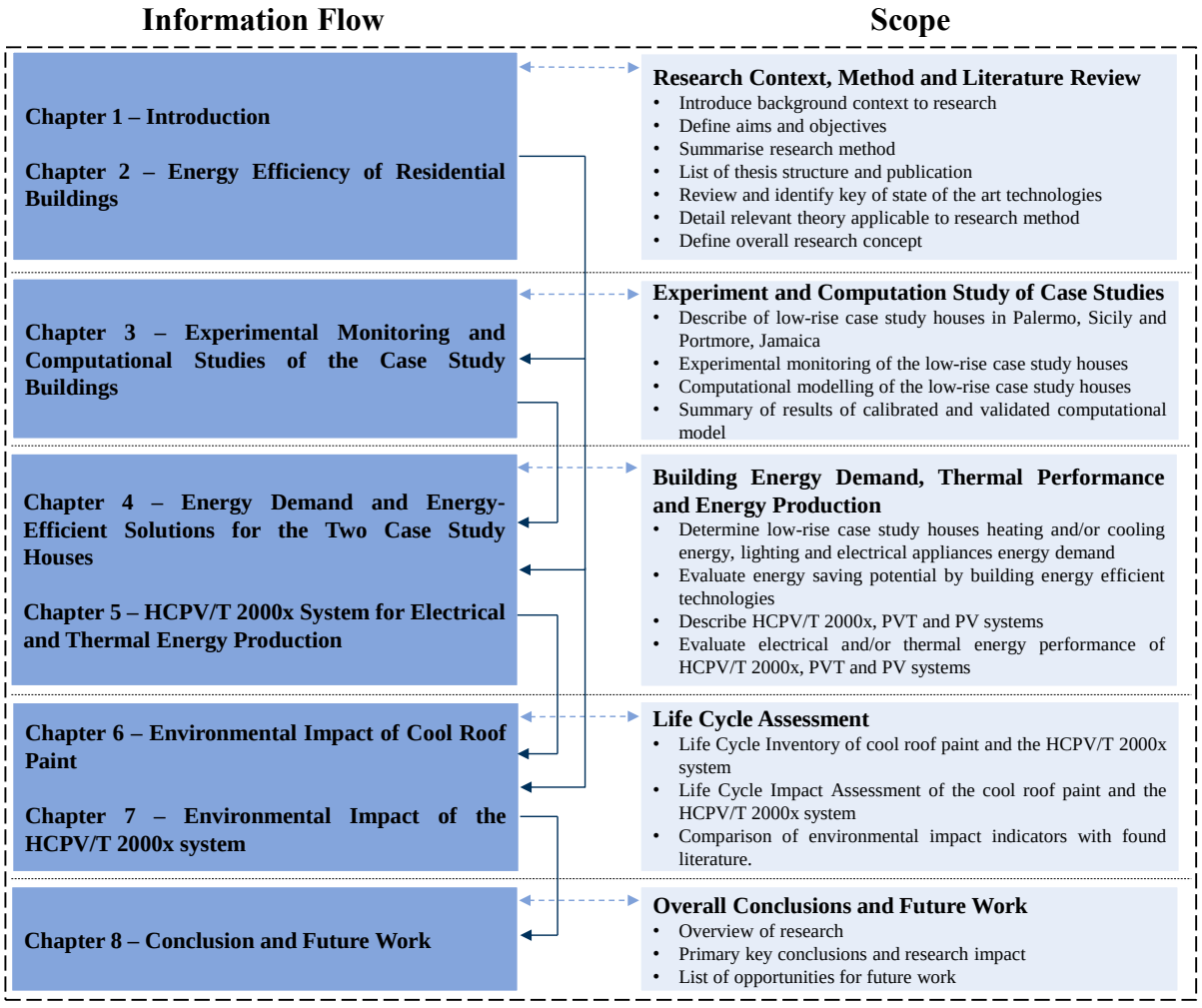

Figure 1-4: Thesis information flowchart structure and chapter interlink of research work.

1.6 Publications

The following journal papers, a conference paper and a conference poster have been published as a result of the work presented in this thesis. In addition, I contributed as chapter author to reports of the Smart GEMS project.

Journal Papers

Shittu, E., Stojceska, V., Gratton, P., Kolokotroni, M., 2020. Energy & Buildings Environmental impact of cool roof paint: case-study of house retrofit in two hot islands. Energy & Buildings 217, 110007. https://doi.org/10.1016/j.enbuild.2020.110007

Shittu, E., Kolokotroni, M., Stojceska, V., 2019a. Environmental Impact of the High Concentrator Photovoltaic Thermal 2000x System. Sustainability (Switzerland) 11, 1–21. https://doi.org/10.3390/su11247213

Kolokotroni, M., Shittu, E., Santos, T., Ramowski, L., Mollard, A., Rowe, K., Wilson, E., Filho, J.P. de B., Novieto, D., 2018. Cool roofs: High tech low cost solution for energy efficiency and thermal comfort in low rise low income houses in high solar radiation countries. Energy and Buildings 176, 58–70. https://doi.org/10.1016/j.enbuild.2018.07.005

Conferences

Shittu, E., Paredes, F., Schiavo, B., Venezia, L., Milone, S., Montagnino, F., Kolokotroni, M., 2019b. Comparison of operational performance and analytical model of high concentrator photovoltaic thermal system at 2000 concentration ratio, in: E3S Web of Conferences. p. 06007. https://doi.org/https://doi.org/10.1051/e3sconf/201911106007

Poster presentation at the SUNRISE Symposium 2020, 7th – 8th September, 2020 – Environmental Impact of the High Concentrator Thermal 2000x (HCPV/T 2000x) System

Marie Curie SMART GEMS Project Reports

Smart GEMS, 2018a. D5.1 Integration of smart grids in cities. https://cordis.europa.eu/project/id/645677/results

Smart GEMS, 2018b. D5.3 Cluster mechanisms for smart grids funding opportunities. https://cordis.europa.eu/project/id/645677/results

Smart GEMS, 2017. D4.3 Lessons learnt from the existing smart / micro grids. Guidelines for scaling-up the existing infrastructure using mobile connectivity. https://cordis.europa.eu/project/id/645677/results

Chapter 2: Energy Efficiency of Residential Buildings

Introduction

This chapter presents a review of the energy-efficient technologies for residential buildings with focus on retrofit. The review focusses on residential building energy use and related environmental issues in hot regions; these are characterised by high ambient temperature and solar radiation resulting to a significant cooling demand for buildings in comparison to heating demand. The review includes energy-efficient technologies applicable to hot countries, building retrofit, reduction of building internal heat gains and building RES system integration solutions most effective in high solar radiation regions. The review also presents the building energy modelling and environmental assessment techniques to quantify residential building energy use and environmental impacts. In the context of the research project, the key research findings to support the adoption of energy efficiency strategies in residential buildings located in hot regions are presented.

2.1 Delivering Energy Efficiency Performance in Existing Buildings

A set of roadmaps were set by the European Union (EU) to achieve net zero GHG by 2050. The 2020 EU climate and energy framework roadmap targets are to reduce GHG by 20 % from 1990 level, 20 % increase in renewables of EU's energy mix, and 20 % improvement in energy efficiency (European Commission, 2011). The 20 % improvement in energy efficiency was enacted in 2012 as stated in the Directive 2012/27/EU (European Union, 2012). The EU climate and energy framework for the period between 2020 and 2030 states that a further 40 % GHG reduction matched by 27 % renewables and 25 % energy savings, representing the lowest energy system cost for 40 % GHG reduction (European Commission, 2014).

Buildings have an important role to achieving net zero GHG by 2050, as stated in the European Green Deal (European Commission, 2019b); the key actions required are to increase building energy efficiency and decarbonise the energy sector. The European Green Deal which is a response to climate change and biodiversity loss is an integral part of the European Commission's strategy to implement the United Nation's 2030 Agenda and the 17 SDGs. Other elements of the European Green Deal (as shown in Figure 2-1) include "supplying clean,

affordable and secure energy", "mobilising industry for clean and circular economy", "preserving and restoring ecosystems and biodiversity". In the context of existing buildings, Article 7 of the Energy Performance of Buildings Directive (EPBD) 2010/31/EU, states that when buildings undergo major renovation, the energy performance of the building is upgraded in order to meet minimum energy performance requirements set in accordance with Article 4 in so far as this is technically, functionally and economically feasible (European Union, 2010). Also, energy-efficient buildings can be developed as Near Zero Energy Buildings (Near ZEB) that requires the synergy between renewable energy and energy-efficient measures that reduces building energy demand (European Union, 2016). Near ZEB are buildings with very low energy demand that is covered to a very significant extent by renewable sources, from renewable sources produced on-site or nearby. At EU level, primary energy is an indicator for numerical benchmarks for Near ZEB buildings in different EU climatic zones. For hot climate zone (with some heating demand) like the Mediterranean (Zone 1 – Catania, Athens, Larnaca, Luga, Seville and Palermo), the benchmark for the energy performance of new Near ZEB single family house is; 0 – 15 $\mathrm{kWh/m^2.year}$ of net primary energy with, typically, 50 – 65 $\mathrm{kWh/m^2.year}$ of primary energy use covered by $\mathrm{kWh/m^2.year}$ of on-site renewable sources.

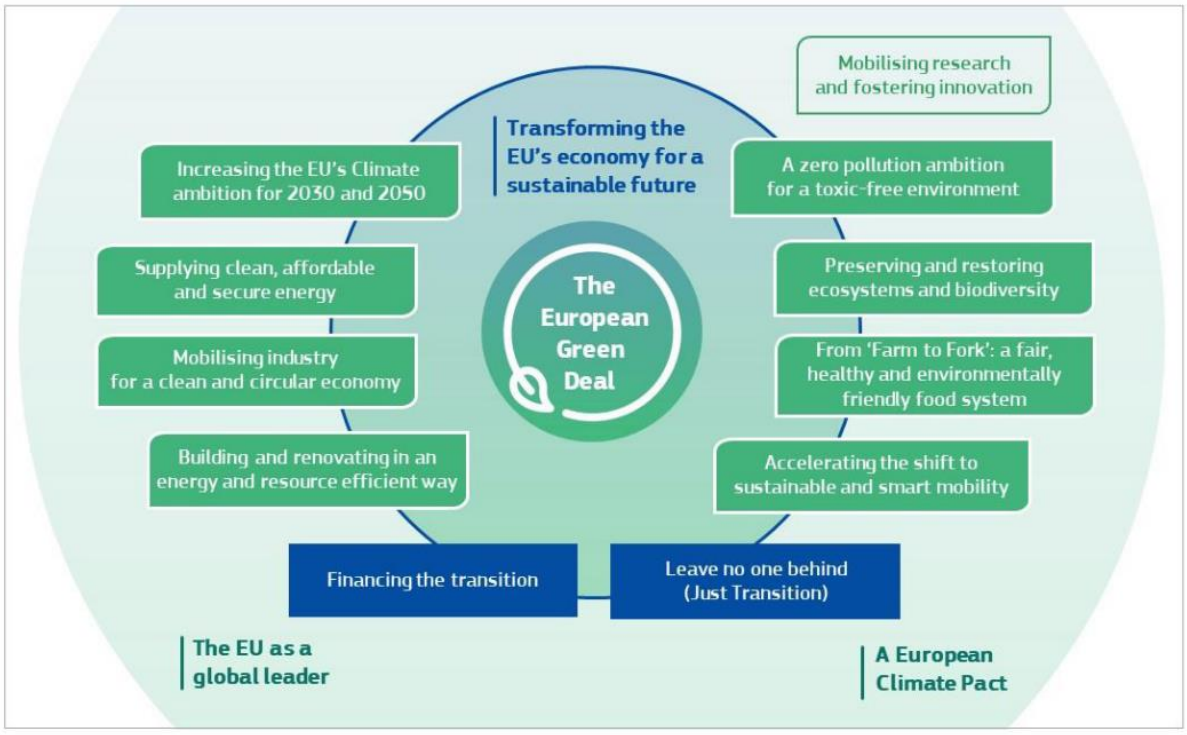

Figure 2-1: "The European Green Deal" (European Commission, 2019b).

Globally, the decarbonisation of the building and construction sector is critical to achieve the

Paris Agreement commitment and the UN SDGs. The expected doubling of building stock by 2050 (IEA, 2019) means that SDG 7 (provision of affordable and adequate housing for all) and 11 (ensure access to affordable, reliable, sustainable, and modern energy for all) (United Nations, 2018) need to be addressed. To meet SDG 7, the International Energy Agency (IEA) have a concerted effort to decarbonise and enhance energy efficiency in buildings at a rate of 3 % a year. The IEA is working with experts and policy makers in defining regionally actions across eight priority action areas to put the building and construction sector on track of decarbonisation. The eight priority action areas are building operations; appliances, lighting, cooking and systems; materials; resilience of buildings; and clean energy (IEA, 2019). For existing houses and buildings, renovations and energy efficiency actions should be facilitated by government, experts, and policy makers. Energy efficiency of existing building should increase at a rate that reduces energy consumption by 30 – 50 %. Some key challenges of building renovation are costly, further research needed to understand the effect of building fabric insulation, and the reduction of internal space (Khairi et al., 2017).

A high energy performance building is characterised by low energy demand. A low energy building is characterised with greatly reduced energy needs via good design practices and the application of energy-efficient building technologies (Cellura et al., 2014; Torcellini et al., 2006; Valladares-Rendón et al., 2017). Good design practice is a passive design strategy that is essential to reduce energy consumption (such as heating and cooling energy consumption), improve internal comfort conditions (such as thermal and air quality comforts), and ultimately increasing building energy efficiency. Passive design strategy involves the correct selection/design building envelope, orientation, and geometric/ratios. The application of energy-efficient building technologies is an active approach that focuses on reducing building energy consumption, which is achieved via the correct selection of energy-efficient technologies such as Heating, Ventilation, and Air Conditioning (HVAC), hot water, lighting, appliances and equipment. The correct application of passive design and active approach depends on the understanding of the building energy use and its interior comfort necessities (Rodriguez-Ubinas et al., 2014). Some passive and/or active solutions are presented in Figure 2-2.

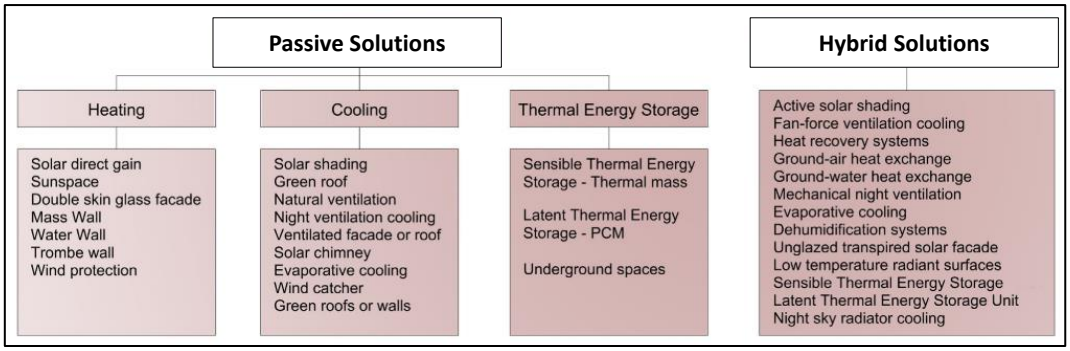

Figure 2-2: “Buildings’ passive and hybrid solutions” (Rodriguez-Ubinas et al., 2014).

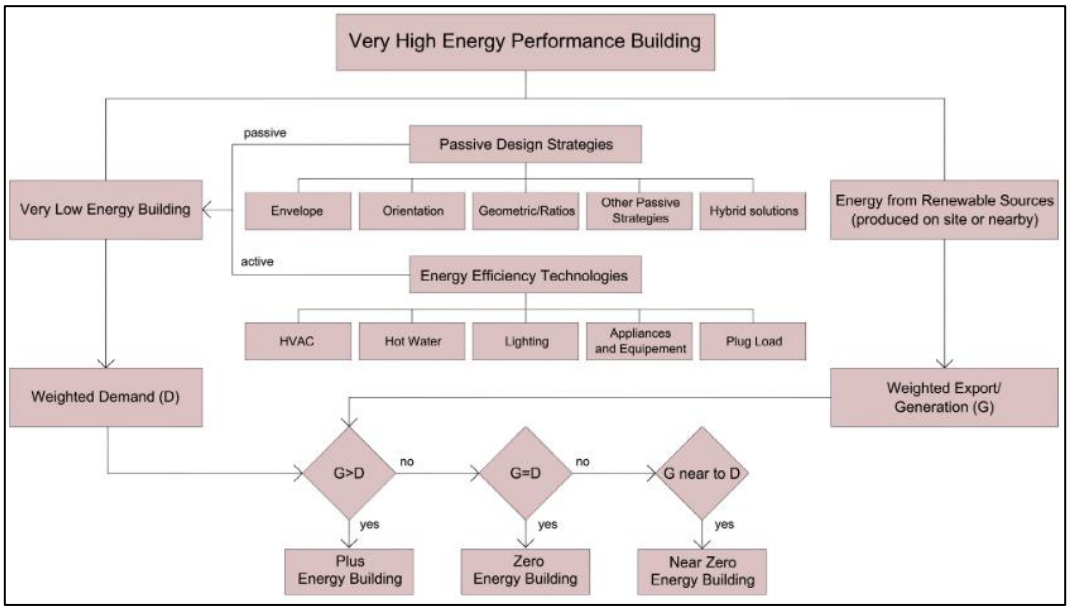

Figure 2-3: “Diagram of the ZEB approach. Passive design strategies an essential aspect to reduce the amount of energy required by the buildings” (Rodriguez-Ubinas et al., 2014).

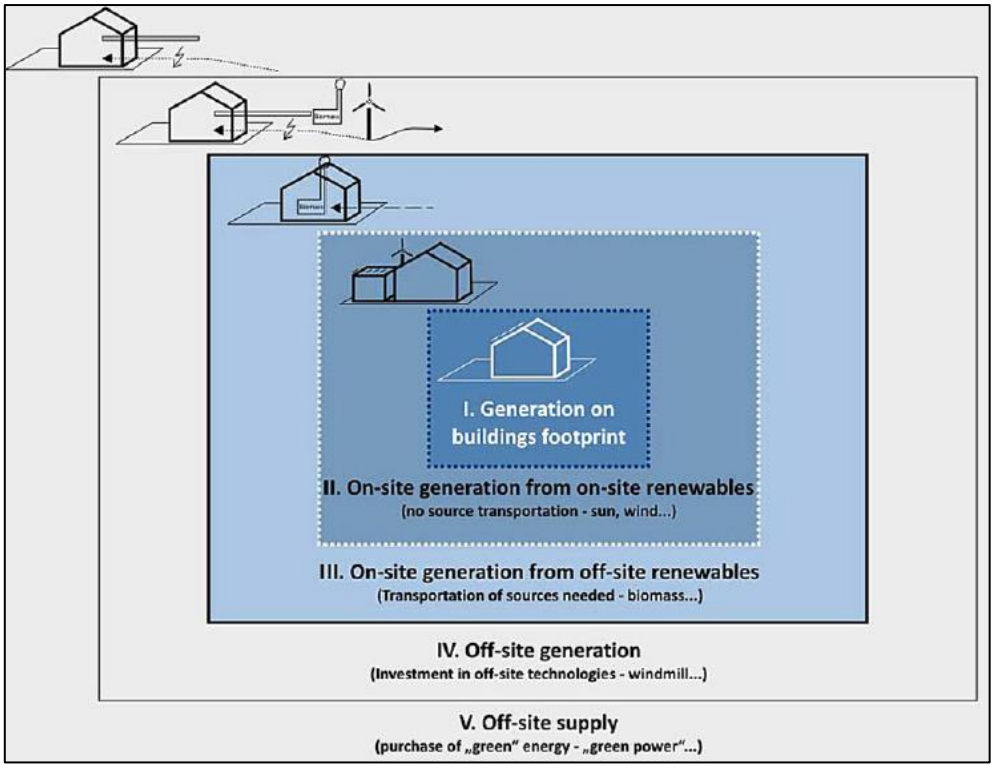

Figure 2-4: "Overview of possible renewable supply options" (Marszal et al., 2011).

The concept of ZEB evolved from a low energy building concept as described in Figure 2-3. ZEB meet most/all its operational energy needs from on-site RES system or nearby RES system. As shown in Figure 2-4, the on-site RES systems are located on or close to the building site. The on-site RES system can generate energy using on-site RES (such as sun, wind etc.) and/or off-site RES (such as biomass that needs transporting to the local site) (Marszal et al., 2011). ZEB can be classified as off-grid ZEB and on-grid ZEB. An off-grid ZEB is a stand-alone building that is not connected to any utility grid, which can supply itself energy generated from on-site RES systems (Marszal et al., 2011). There is a need for an energy storage system for the night or wintertime use or periods of peak loads (Laustsen, 2008; Marszal et al., 2011). On the other hand, an on-grid ZEB is a building connected to one or more energy grid infrastructure such as electricity, district heat and cooling system, gas pipe network, biomass, and biofuels distribution networks. As shown in Figure 2-4 and Figure 2-5, the on-grid ZEB has the possibility of taking energy from the grid (grid as a "source") and exporting its energy to the grid (grid as a "sink") and no need for an energy storage system (Iqbal, 2004; Laustsen, 2008; Marszal et al., 2011; Rosta et al., 2008; Torcellini et al., 2006). Near ZEB (also referred to as Net Minus Energy Building (NMEB)), Net Zero Energy Building (NZEB) and Net Plus Energy Building (NPEB) are on-grid ZEB as described in Figure 2-6. The NZEB is a type of building with operational energy demand that is approximately equal to the energy generated

from the on-site RES system, while NPEB and NMEB are buildings that consume less and more energy respectively, generated from on-site RES system (IPCC, 2014). Rodriguez-Ubinas *et al.*, (2014) analysed passive design strategies essential to reduce building energy consumption. The study concluded that passive design strategies can help to reach the first requisite in the path to NZEB, NPEB and NMEB; be a very low energy building. The passive design includes building envelope (also a retrofit intervention for existing residential buildings), orientation, geometrical aspects, other passive strategies and hybrid solution; these are described in Figure 2-3.

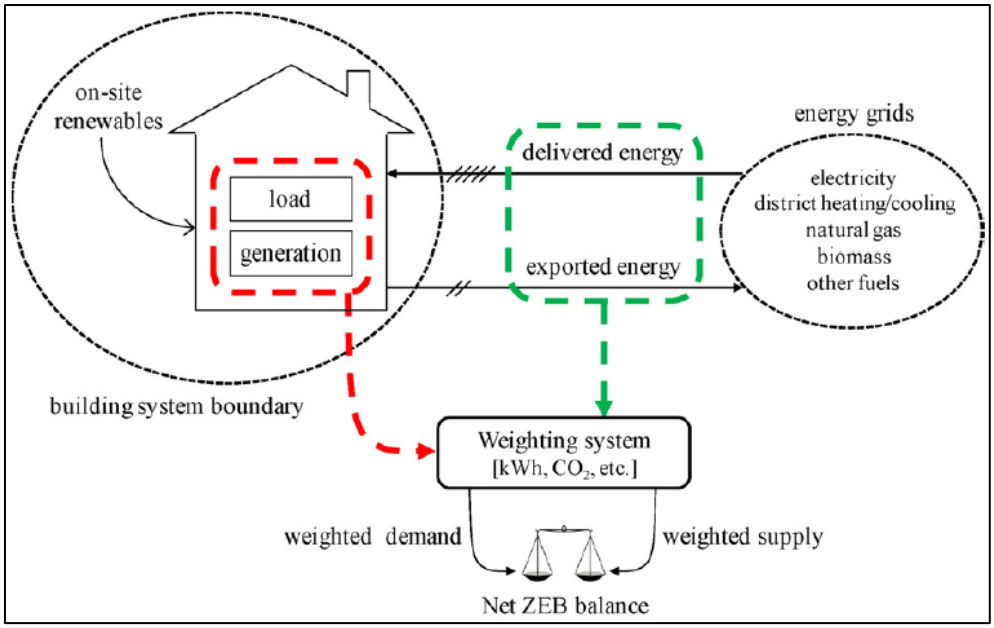

Figure 2-5: "Sketch of connection between buildings and energy grids showing relevant terminology" (Sartori et al., 2012).

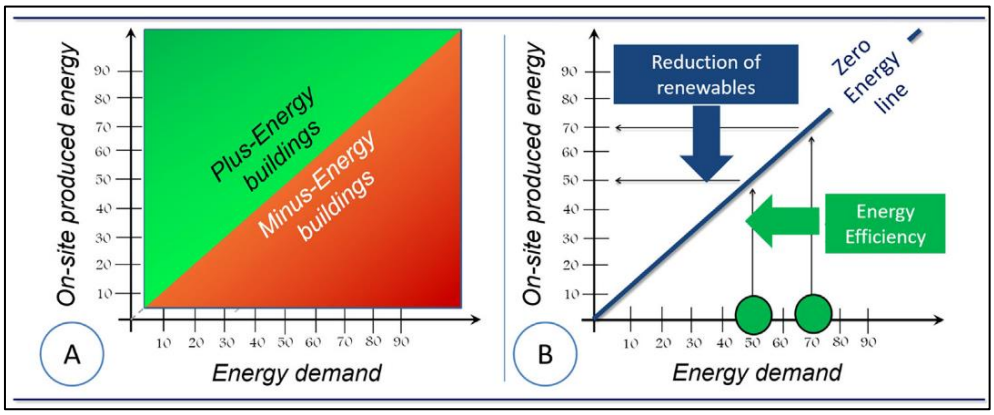

Figure 2-6: a) Definition of NZEB (is the line that separates NPEB and NMEB), NPEB and NMEB, b) "Relation between energy efficiency of envelope/active systems and need of on-site energy conversion" (Ascione et al., 2016).

Residential building integration with solar energy system is more applicable and more efficient in hot climates with high solar radiation intensity throughout the year (Ayodele et al., 2020). Feng et al., (2019) presented the energy performance of 34 case study buildings in hot and humid climates, characterised with passive design features and RES systems. The energy use and energy generation from RES for the 34 case study buildings were collected annually. The energy use of the case study buildings were reduced by employing passive design features (described in Figure 2-2). Also, since most case study buildings were in hot and humid climates that uses electricity, the energy balance analysis was based on the relationship between energy consumption and on-site renewable energy generation. The study shows that most of the case study buildings achieved NZEB or NPEB.

2.2 Energy Efficiency Strategies for Existing Residential Building

Improved building envelope and energy-efficient technologies described in Figure 2-2 and Figure 2-3 are also applicable energy efficiency strategies to existing residential buildings as shown in the literature; their energy reduction potential is summarised in section 2.2.2. This section presents applicable energy-efficient solutions for existing residential buildings in hot climates that result in energy reduction and environmental benefits. The energy-efficient solutions presented are building retrofit solutions, solutions for reducing internal heat gains and building RES system integration solutions most effective in high solar radiation regions. These solutions have the potential to address the key issue in hot climates, which is to reduce the cooling energy demand.

2.2.1 Residential Building Energy Use in Hot Climates and Related Environmental Issues

Globally, higher electricity use contributes to higher final energy consumption (Figure 2-7), with space cooling energy demand increasing by 33 % from 2010 – 2018, (space heating decreased by 1 % in the same period), energy demand by appliances and hot water increased by 18 % and 11 % respectively. At an 8 % in 2018, cooling energy demand became the fastest growing end-use in buildings since 2010, though it accounted for only a small portion of total demand at 6 % (IEA, 2019); it doubled since 2000 from 3.6 Exa-Joules (EJ) to 7 EJ due to population and economic growth, and global warming (IEA, 2018a). Therefore, offering a huge

potential energy saving. The increase in cooling energy demand increases with population, floor area, energy service demand by cooling equipment, variations in climate and how buildings are constructed and used.

Space cooling provided by air-conditioning system emits GHGs that contribute to climate change. The GHGs emissions are primarily linked to power generation from the fuel mix power generation systems. Globally, fossil fuels accounted for 65 % of total power generation in 2016 (coal for 37 %, gas 24 % and oil 4 %), resulting in average emissions of around 505 gCO_2/kWh of generation (IEA, 2018b). Cooling energy need is highly concentrated in areas located within a narrow band running roughly parallel with the equator and covering the tropics and sub-tropics. However, hot regions have higher cooling needs, and this applies to low-rise residential building which typically have a large external envelope area and comprise the most common type of residential buildings in many countries. As an example, single-family low-rise buildings in the United States consumes 80 % of the total residential building use, compare to multi-family and mobile that consumes 15 % and 5 % respectively (Kwame et al., 2020). The energy use study of single-family low-rise building in Melbourne, Florida (a hot humid region) shows that cooling energy use accounts for the highest total energy use, at 38 % (see Figure 2-8).

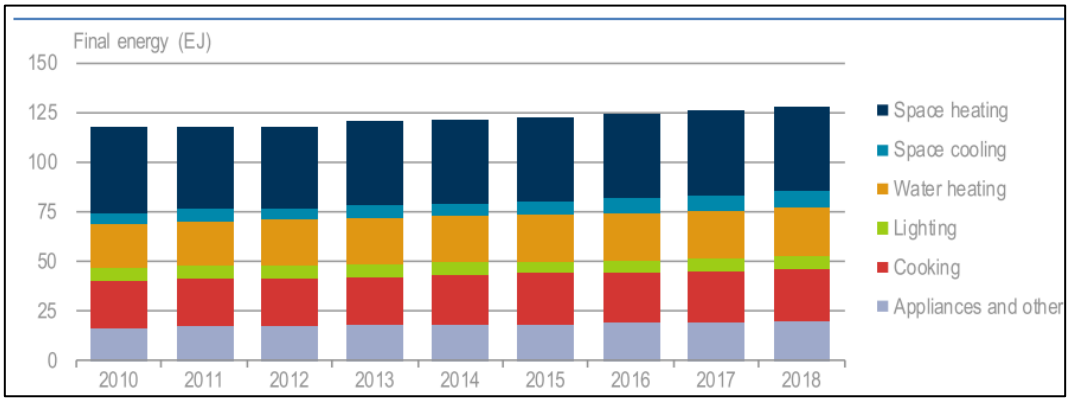

Figure 2-7: "Global buildings sector final energy consumption by end use, 2010-18" (IEA, 2019).

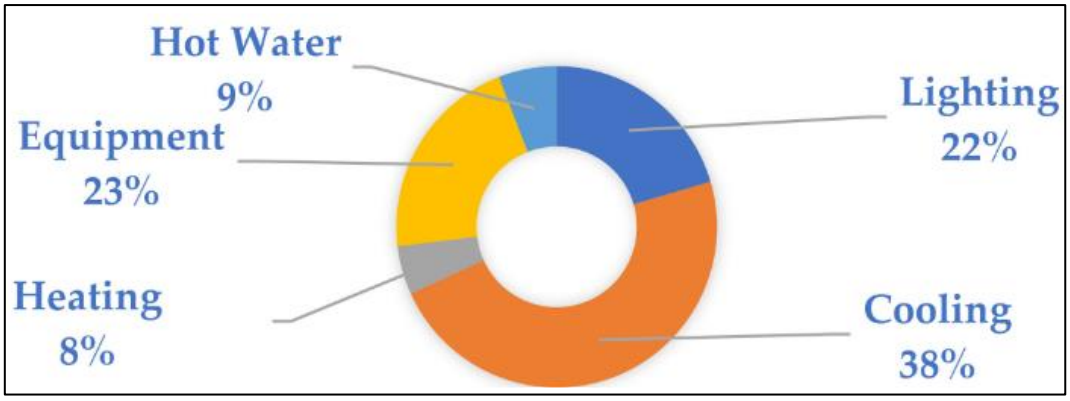

Figure 2-8: “End-use energy estimate” in a single-family house in Melbourne, Australia (Kwame et al., 2020).

2.2.2 Building Envelope Retrofit and Reduction of Internal Heat Gains

Building envelope retrofitting is a strategy to increase the energy efficiency of buildings. Buildings have a long lifecycle and a significant proportion of the total existing building stock is expected to remain in existence in 2050 (IPCC, 2014). Therefore, improvements during their life-time are necessary and these should be as energy-efficient as possible to lead to higher energy savings. In addition, energy-efficient lighting technology and appliances are crucial in reducing building energy use (IEA, 2019) as well as internal heat gains. It was reported in IPCC, (2014) that a comprehensive retrofit packages for a detached single-family house led to the reduction in total energy use by 50 – 75 % while for multi-family house such as apartment blocks space heating reduction by 80 – 90 % was possible. Despite the continuous increase in population and floor area of buildings, the highest global energy use reduction per unit floor area is the space heating (see Figure 2-9). This is due to improved building envelope and use of energy-efficient lighting and appliances; from 2010 – 2018 the global average space heating reduced by 20 %, followed by lighting energy use reduction by 17%. However, cooling energy demand continues to increase especially in hot countries, mainly due to the increased installation of cooling system (IEA, 2019, 2018a).

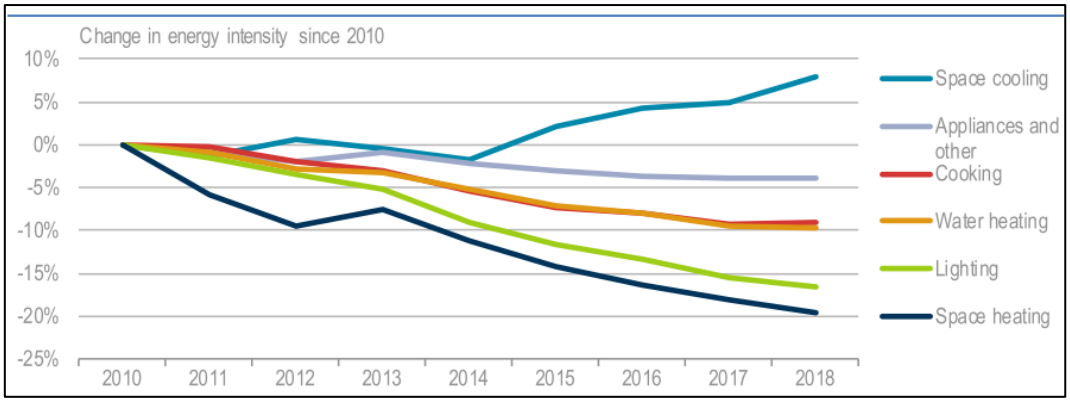

Figure 2-9: "Global buildings sector final energy intensity changes by end use, 2010-18" (IEA, 2019).

The energy performance and environmental benefit by implementing building envelope retrofit solutions is determined by heat exchange and radiative properties. The best building envelope (roof, floors, ceilings, external walls, doors, windows and foundation) retrofit solutions in hot climates are those that reject as much heat as possible, thereby reducing cooling energy demand (Desideri and Asdrubali, 2018; IEA, 2018b). (Ayodele et al., 2020; Ürge-Vorsatz et al., 2012) Ayodele *et al.*, (2020) reported retrofit interventions for residential buildings in hot climates for different building types which includes low-rise, high-rise flats and detached houses. The reported building envelope retrofit solutions are thermal insulation for roof and wall to optimise heat transfer between the indoor environment and outdoor environment of the building, solar reflective materials with high thermal emissivity and solar reflectance properties to decrease the solar thermal load, window shading and efficiently insulated double or triple glazing to optimise indoor solar heat gains and daylighting. The effort to increase energy efficiency of residential buildings in hot climates while improving thermal comfort and reducing carbon emission is most effective with roof intervention because of the high solar radiation intensity on the roof as a result of the sun's inclination. This is particularly true for low-rise houses because the area of the roof in comparison to the wall area is larger than the same ratio in high rise buildings.

Of the available envelope strategies to reduce cooling demand, a cool roof is a promising solution as documented in the literature and has been a policy recommendation in some regions (Gao et al., 2014; Pisello, 2017; Santamouris, 2014; Synnefa and Santamouris, 2012; Testa and Krarti, 2017). It has been shown that they are particularly effective in high solar radiation regions where heating is not required (Dabaieh et al., 2015; Garg et al., 2016; Radhi et al., 2017), while a heating penalty might be observed in regions with heating requirements

(Hosseini and Akbari, 2014; Kolokotroni et al., 2016). A cool roof is characterised with high solar reflectance and thermal emissivity properties to decrease the solar thermal load of a building thus reducing its energy requirements for cooling (Kolokotroni et al., 2013). A cool roof works by reflecting solar radiation (hence reducing solar heat gains), release absorbed heat, as shown in Figure 2-10. As a result, heat transfer by conduction to the internal space is reduced. The extent to which heat transfer by conduction is reduced depends on the following:

- Solar radiation magnitude,
- External and internal air and surface temperature difference, and
- Building element thermal/heat resistance.

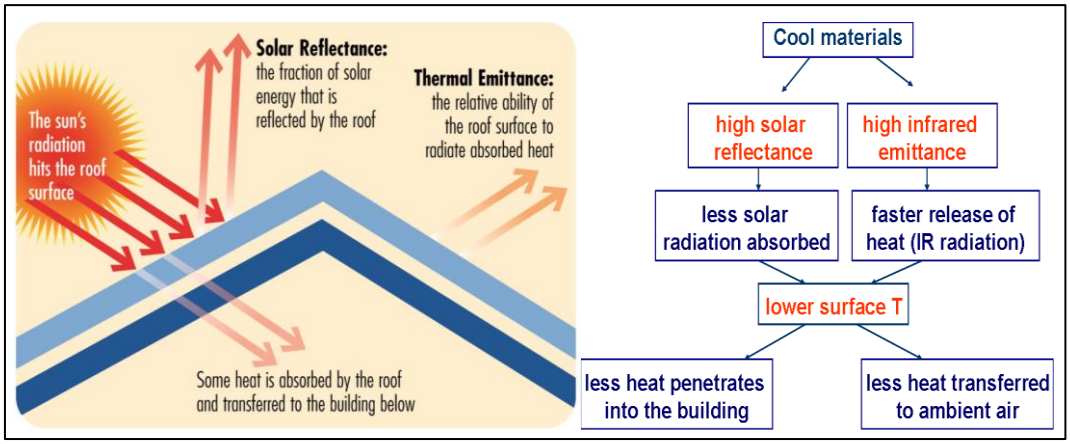

Figure 2-10: Description of Cool Roof Solar Reflectance and Thermal Emittance (CRRC, 2019; ECRC, 2019).

Other efficient strategies for the envelope are thermal insulation, window shading and insulated glazing. Thermal insulation is a poor conductor of heat with very low thermal conductivity i.e. retards the flow of heat and therefore, reduce heat transfer through the building element (Deshmukh et al., 2017). While solar radiation provides natural light and heat for buildings, an excess of it can result in overheating of the building internal space. Window shading is a form of solar control that optimise solar heat gain into the building internal space, which results in cooling energy savings, improve indoor thermal comfort, and reduce GHG (Valladares-Rendón et al., 2017). Ürge-Vorsatz *et al.*, (2012) reported previous studies on the benefit of thermal insulation, window shading and double or triple glazing to optimise indoor solar heat gains; thermal insulation can reduce heating demand by 67 % and cooling demand by 45 %, and window shading can block 90 % of incident solar radiation.

Internal heat reduction strategy is also effective to increase the energy efficiency of buildings.

Internal heat gain reduction is achieved via the introduction of efficient appliances and lighting. IPCC, (2014) reported that energy use by efficient appliances can reduce appliance energy use by 40 – 50 %. Light bulb provides artificial lighting (from electricity) to internal space, and depending on the light bulb technology, the electricity consumed can be relatively high. The artificial lighting increases space internal heat gain, and hence increase cooling demand. LED light bulb has the lowest heat emission coefficient that results in low electricity consumption and reduced cooling demand (Suszanowicz, 2017). The use of A-rated appliances (with very low power ratings) improves energy efficiency improvements in households by reducing household power consumption.

Integrated assessment and sectoral bottom-up model literature review for energy efficiency in buildings shows that the implementation of energy-efficient solutions to reduce thermal energy use (mainly heating and cooling, but sometimes hot water) is more promising compared to other building energy uses such as lighting and appliances energy consumption. Figure 2-11 presents annual modelled global total building energy demand from 2010 to 2050. Integrated Assessment Models (IAMs) are large scale computer models representation of human systems that integrates many of the most important technologies, human systems (which includes energy, economic system) and environmental impacts such as climate change. The sectoral bottom-up model is based on the perspective of specific building energy use trend (such as heating, cooling, hotwater etc.) to project future building energy use and emissions (IPCC, 2014).

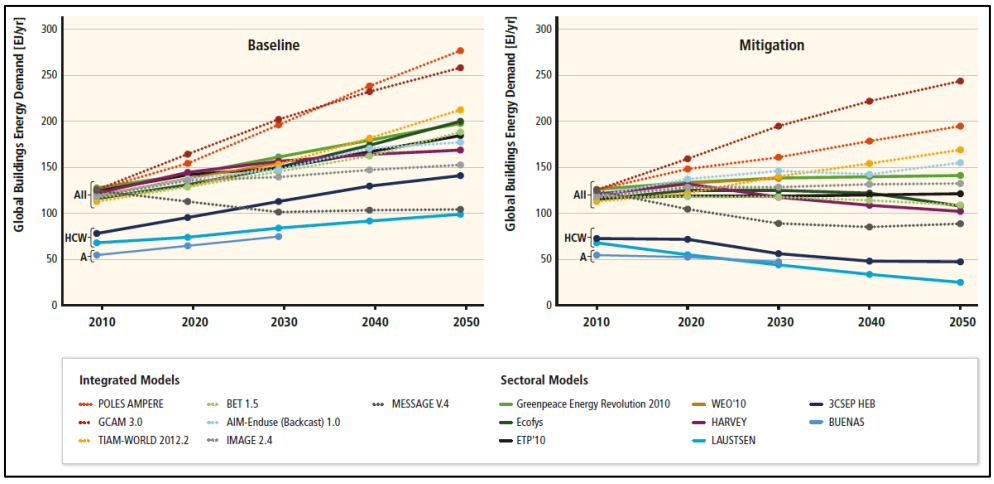

Figure 2-11: Annual baseline and mitigation global final energy demand development in the building sector by 2050 for total energy (All, heating/cooling/hot water/lighting/appliances), thermal energy (HCW, includes heating/cooling/hot water), and appliances (A).

2.2.3 Renewable Energy Source Systems

The use of RES system is the fastest growing source of building energy, yet it met less than 14 % of the global energy demand in the building sector in 2017, as describe in Figure 2-12. This is because of the yearly increase in global building energy use (1 % per year) as a result of increase in population and therefore building floor area. This increase in global energy use continues to overcome energy demand reduction from implementing building energy-efficient solutions. Therefore, the effort to continuously reduce building energy demand and environmental impacts is to accelerate the share of building integrated RES system and energy efficiency solutions (REN21, 2020).

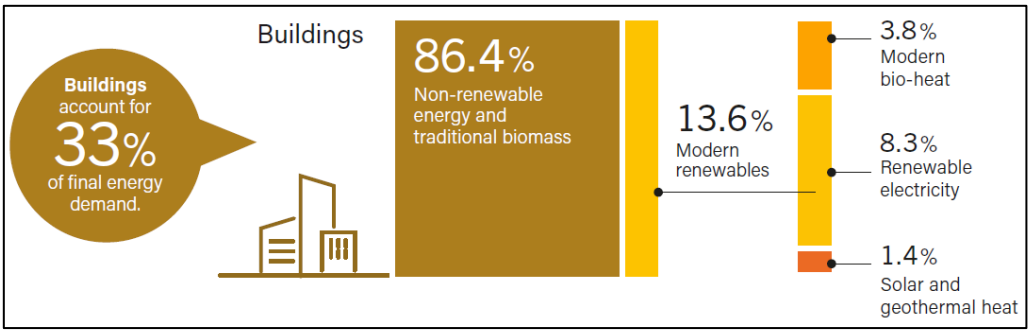

Figure 2-12: "Renewable Share of Total Final Energy Consumption in Buildings, 2017". Building accounts for 33 % of global final energy demand (REN21, 2020).

RES system converts/transform energy from sustainable energy resources that include hydroelectricity, solar energy (cleanest and most abundant RES available in the world), wind energy, geothermal energy, hydro-energy, ocean energy and bioenergy (Jha et al., 2017; Tong, 2019). Figure 2-13 presents a schematic diagram of different RES. The estimated RES system share of global electricity production is 27.3 % REN21, (2020) as shown in Figure 2-14, of which wind and solar contributes 5.9 % and 2.8 %, respectively. Solar and wind energy are more popular in the built environment because they can be harmonically integrated with buildings to provide energy need (Chel and Kaushik, 2018; REN21, 2020). Residential building integration with solar energy system is more applicable and more efficient in hot climates with high solar radiation intensity throughout the year. However, there has been drawback in the application and integration of wind energy system in the built environment due to issues surrounding the visual landscape and noise (Ayodele et al., 2020).

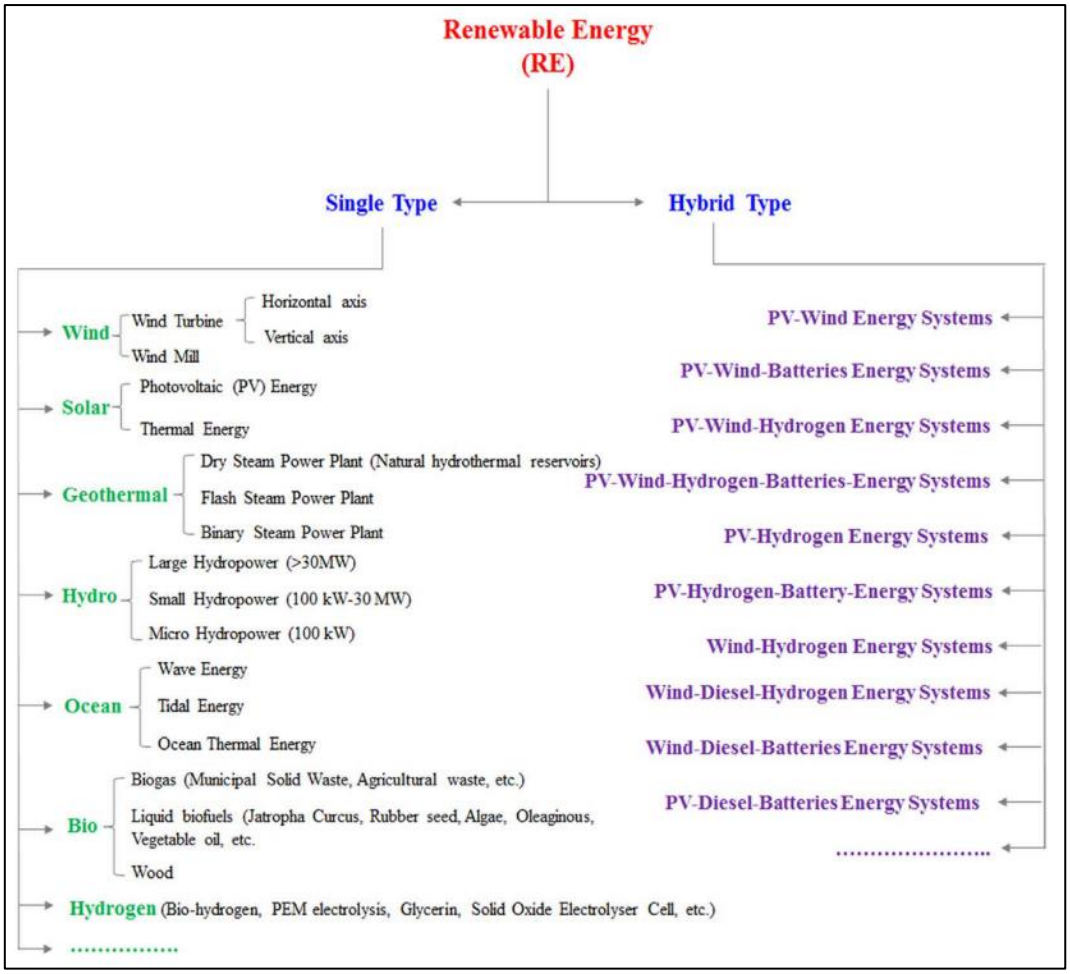

Figure 2-13: "Categories of renewable energy and their sources" (Jha et al., 2017).

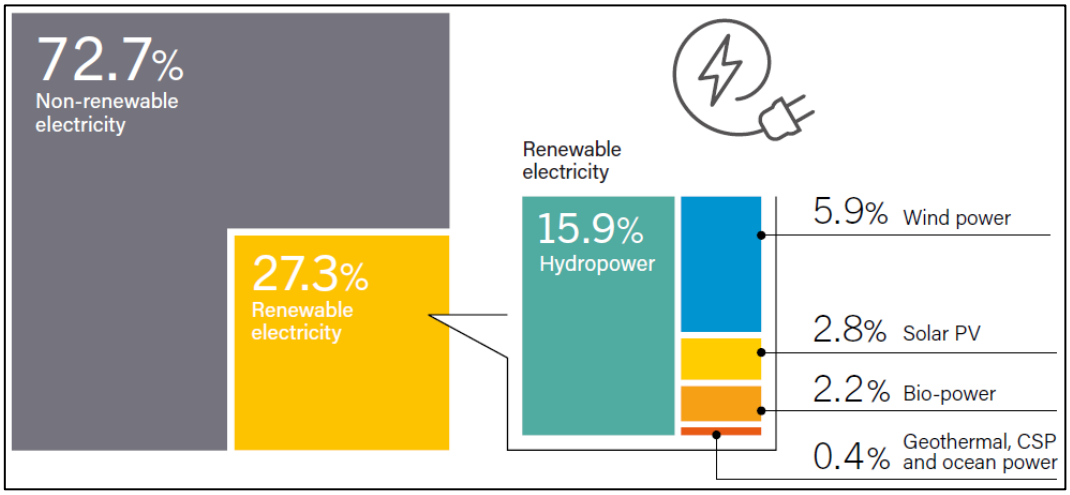

Figure 2-14: "Estimated Renewable Energy Share of Global Electricity Production, End-2019" (REN21, 2020).

Solar energy is a combination of solar radiation and heat from the sun that can be harnessed by passive (such as selected materials with favourable thermal mass or light dispersing properties that is capable of distributing energy in building space) or active solar energy systems. Active

SES uses PV solar cell and/or thermal technologies to transform solar energy to electrical and/or thermal energy. PV solar cells uses photovoltaic effect to transform solar energy to electricity. PV solar cells are integrated into modules to build PV systems that can be used for both grid and off-grid electricity generation; with efficiencies ranging from 6 – 19 % (Tong, 2019). In addition, PV solar cells are being integrated with optical concentrator (reflective and/or refractive optical device) to further increase efficiency of PV systems that exceed 30 % (Tong, 2019; Wiesenfarth et al., 2017). The most common type of this system includes Low and High Concentrator Photovoltaic (LCPV and HCPV), and Low and High Concentrator Photovoltaic Thermal (LCPV/T and HCPV/T). LCPV and HCPV are typically characterized with a concentration ratio of less than 100 and 300–1000, respectively. LCPV uses crystalline silicon PV cells to convert Direct Normal Irradiance (DNI) (and a small fraction of diffuse horizontal irradiance) into electrical energy at high efficiency, while HCPV uses Multi-Junction Solar Cell (MJSC) to convert only DNI into electrical energy at higher efficiency than LCPV (Wiesenfarth et al., 2017). LCPV/T and HCPV/T integrates solar thermal technology with LCPV and HCPV respectively, to produce electrical and thermal energy. In a typical solar thermal technology, the heat exchanger, heat sink, Heat Transfer Fluid (HTF) and thermal storage work together to simultaneously cool the PV cells and extract thermal energy (Sharaf and Orhan, 2015a, 2015b). HCPV/T has been used in a number of studies for electricity and thermal generation and it was found that the overall efficiency of the HCPV/T system can be improved to exceed 70 %, with electrical and thermal efficiency exceeding 20 % and 50 %, respectively (Sharaf and Orhan, 2015b). Additional advantages of LCPV, LCPV/T, HCPV and HCPV/T systems include low Energy Payback Time (EPBT), land use reduction, and the potential increase in power density. Concentrator Solar Power (CSP) is another type of SES system applicable for utility-scale to transform solar energy into electrical and thermal energy by using concentrators and conventional power block such as steam turbines, gas turbines and Stirling engines (Viebahn et al., 2011).

Wind energy created by the earths motion and unbalance incidence of the sun rays on earth, is converted to mechanical energy with windmills or wind turbines (Jha et al., 2017). The kinetic energy of the wind is converted to rotational kinetic energy of the wind turbine blades that is used to drive the wind turbine electricity generator. The amount of energy delivered is determined by the amount of wind available, which is often located in remote locations.

Geothermal energy, hydro-energy, ocean energy, bioenergy and hydrogen energy systems are other systems used to generate electricity and/or heating and cooling. Geothermal energy is stored in rock and in trapped vapour or liquids, used to generate electricity, heating and cooling. Hydro-energy converts the potential energy of a water source to rotational kinetic energy of the wind turbine blades that is used to drive the turbine electricity generator. Ocean energy also referred to as marine renewable energy uses wave, tides, and thermal energy of the sea to generate electricity. Bioenergy involves the use biological materials (such as wood, organic wastes, agricultural by products and wastes, algae, microorganism, vegetable oils, etc) to produce thermal energy, electricity, and fuels for transport (biofuels) through a number of different processes (REN21, 2020; Tong, 2019).

2.3 Building Energy and Thermal Assessment

The range of heat and mass transfer process that would take place in a building (as described in Figure 2-15) include conduction heat transfer through building fabric elements, convection and radiation from building walls, solar radiation transmission and conduction through window glazing, infiltration of outdoor air and air from adjoining rooms, internal heat gains (from lighting, equipment, occupants and other materials inside the building space) and heating or cooling and humidification or dehumidification provided by the HVAC system (Underwood and Yik, 2004). The basic generic principle required to calculate building heating and/or cooling energy as a result of the heat and mass transfer process is the same regardless of the calculation method. The basic generic principle is described in Figure 2-16, while the energy balance equations are presented in equations 2-1 to 2-6. Therefore, in hot climates with high cooling energy demand, the aim is to reduce internal heat gain, ϕ_{gn} (which may include heat transmission rate, ϕ_{tr} into the building) (CIBSE Guide A, 2019).

$$\phi_{ht} = \phi_{tr} + \phi_{ve} \qquad 2\text{-}1$$

where $\phi_{ht}, \phi_{tr}\ and\ \phi_{ve}$ are total heat transmission rate (W), rate of heat transmitted through the building's fabric (W) and by the ventilation system (W).

$$\phi_{gn} = \phi_{int} + \phi_{sol} \qquad 2\text{-}2$$

where $\phi_{gn}, \phi_{int}\ and\ \phi_{sol}$ are total rate of heat gain (W), rate of internal heat gain (e.g. from people, lighting and equipment) (W), and rate of solar heat gain (W).

$$\phi_H = (\phi_{ht} - \phi_{gn}) \pm \phi_c \quad \text{2-3}$$

where $\phi_H\ and\ \phi_c$ the instantaneous heating requirement (W) and heat intake (+) or release (-) from the building fabric.

$$\phi_C = (\phi_{gn} - \phi_{ht}) \pm \phi_c \quad \text{2-4}$$

where $\phi_C\ and\ \phi_c$ the instantaneous cooling requirement (W) and heat intake (+) or release (-) from the building fabric.

Therefore, the total heating energy demand, $Q_H > 0$ (kWh) and the total cooling energy demand, $Q_C > 0$ (kWh) over a long period (e.g. annual) is calculated by integrating the heat flow rates over time (in hours).

$$Q_H = \int \phi_H dt = \int (\phi_{ht} - \phi_{gn}) dt \pm \int \phi_c dt \quad \text{2-5}$$

$$Q_C = \int \phi_C dt = \int (\phi_{gn} - \phi_{ht}) dt \pm \int \phi_c dt \quad \text{2-6}$$

(a)

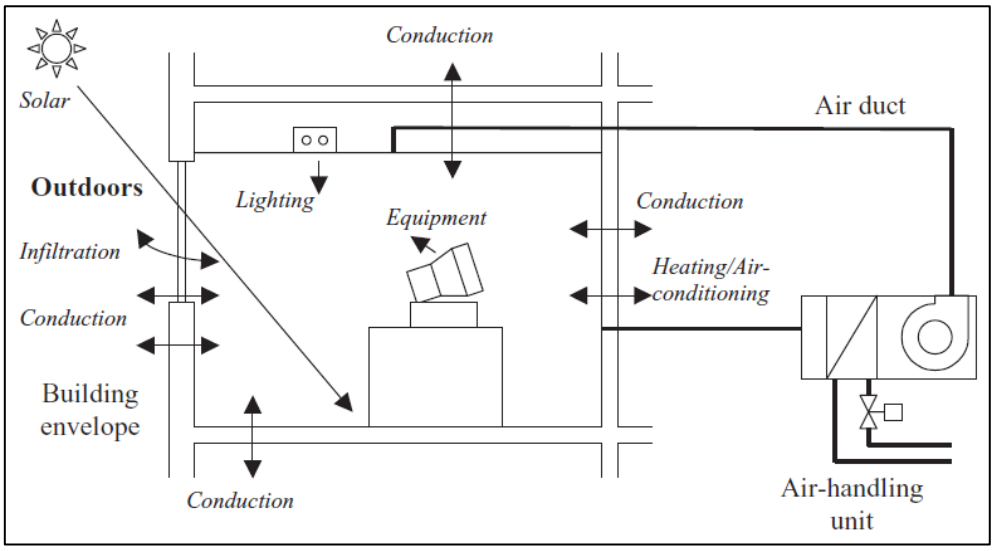

(b) (c)

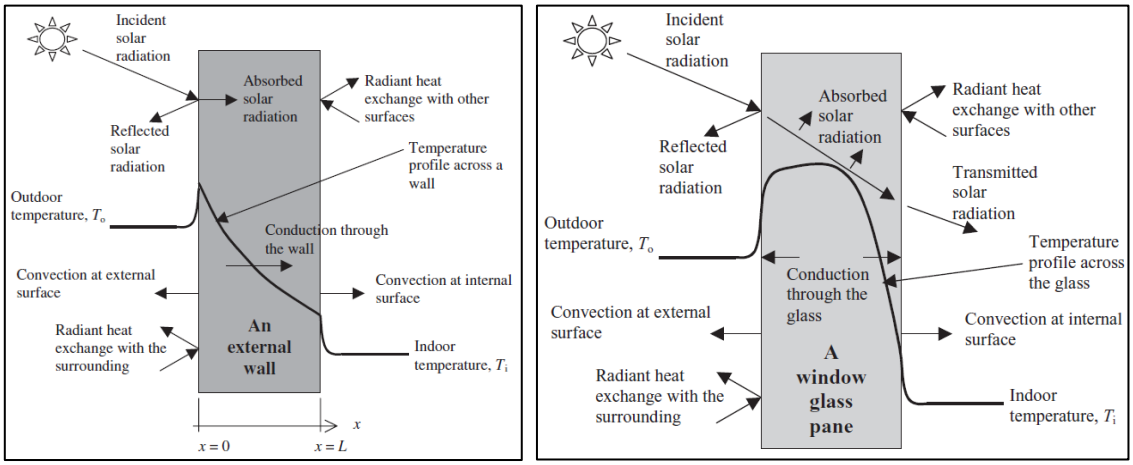

Figure 2-15: (a) “Heat and mass transfer processes involved in building energy simulation”, (b) “Heat transfer at an external wall” and (c) “Heat transfer at a window glass pane” (Underwood and Yik, 2004).

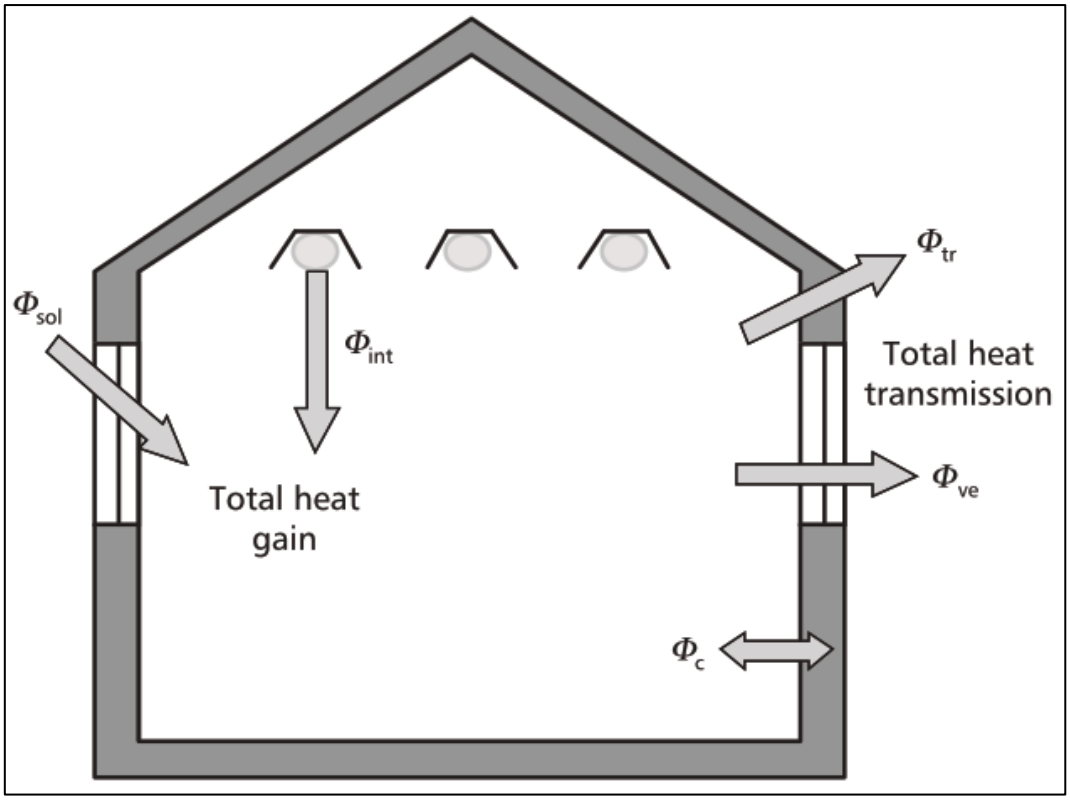

Figure 2-16: "Heat flow rates within a building". The direction of arrow is the direction of heat flow. Note that in a cooling situation the direction of the heat transmission (ϕ_{tr}) may be reversed and the sign changed, therefore becoming an additional heat gain to the building (CIBSE Guide A, 2019).

The energy performance of building is determined by passive designs and active approaches described in Figure 2-3. Figure 2-17 illustrates how building energy performance can be modelled based on three sub-models which are zone level model, system model and carbon emissions model. The zone level model is used to calculate the building energy demands determined from the "inputs of building geometry, fabric performance, heat gains, and internal and external temperatures". The system and carbon emissions models are used to calculate fuel demand and carbon emissions demand respectively (CIBSE AM11:2015, 2015). The energy demand discussed in this chapter is zone energy demand, which includes heating and cooling energy demand, lighting, and appliances energy demand. Energy demand of lighting and electric appliance can be calculated using the design level calculation method and occupant usage schedule. The design level calculation method simply requires the entry of the lighting and electric appliance design wattage level, and using the occupant hourly usage rate (U.S. Department of Energy, 2019). Thermal modelling of heating and cooling energy demand is more complex compared to the modelling of lighting and electric appliance energy demand. The complexity is due to the interrelationship between space heating and cooling loads, internal

heat gains, heat transfer mechanism and dynamic nature of energy storage in the fabric and structure of a building (CIBSE AM11:2015, 2015).

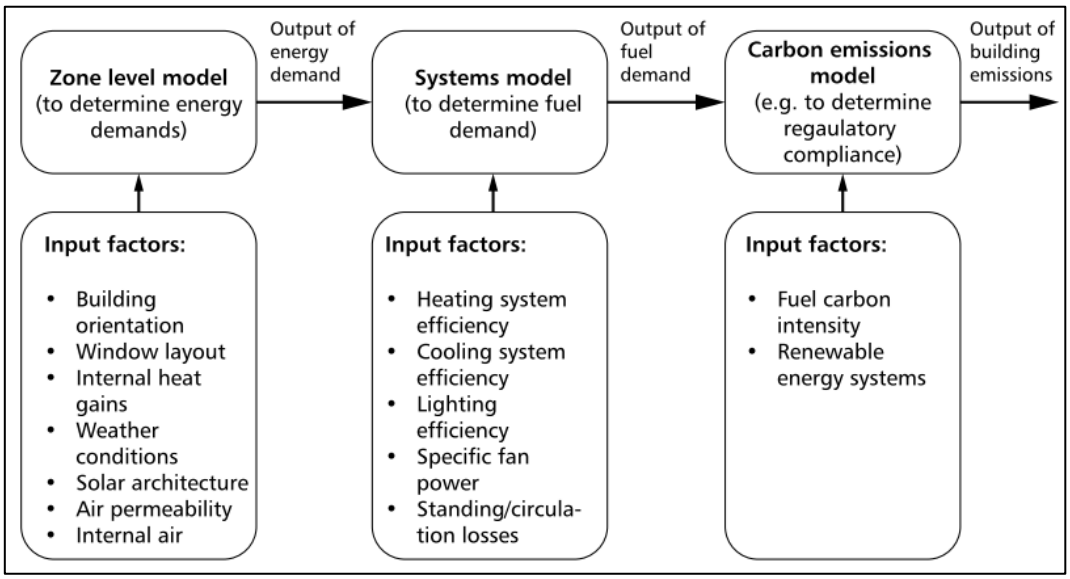

Figure 2-17: “Energy model input-output relationships” (CIBSE AM11:2015, 2015).

DTM is a model governed by parameters which varies with time (e.g. hourly or less) to calculate heating and cooling energy demand (CIBSE AM11:2015, 2015). DTM can be developed using the lumped parameter method (simplified hourly/sub-hourly method) and the numerical method (full hourly/sub-hourly). The lumped parameter method is used to represent the factors that affects the temperature of a space. The factors are represented by an equivalent network of temperature nodes that applies the Resistor – Capacity model (R-C model) shown in Figure 2-18; the network consists of resistive elements heat transfer between temperature nodes (such as air and wall surface temperature), and the a single capacitance element that represent heat storage (heat storage in building envelopes) and release characteristics of the space. The numerical method adopts the Finite Difference Method (FDM) to solve the approximation of the heat conduction equation in building envelopes, by first dividing the homogeneous building envelope material (such as a wall or floor element) into a number of a finite number of slices of equal thickness (Δx), as described in Figure 2-19. Adopting the discretisation process as defined by Underwood and Yik, (2004), the heat diffusion are presented in equations equation 2-7 to 2-10.

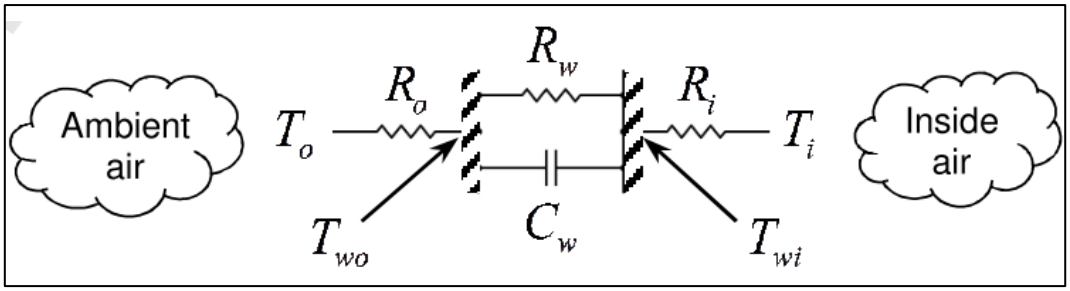

Figure 2-18: Analogous 3R1C (with 3 resistive elements and 1 capacitive element) electric circuit of a wall heat balance equation in R-C modelling. 1C model represents the heat store and release from the wall outside and inside surfaces, while 3R represents the heat transfer between the ambient air temperature node via the wall thickness and the inside air temperature node (Fayazbakhsh et al., 2015).

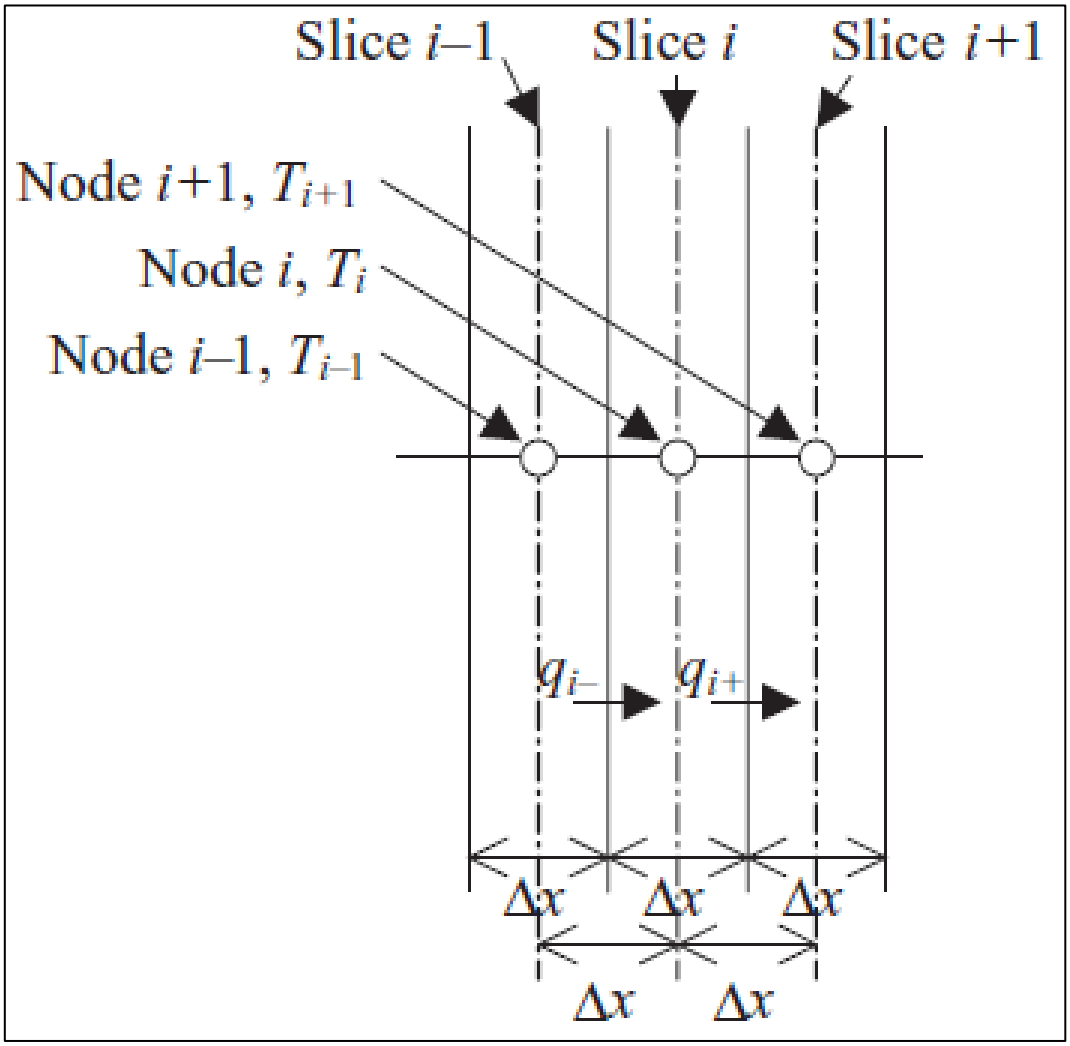

Figure 2-19: "Conduction heat transfer at an internal slice" (Underwood and Yik, 2004). T_{i-1}, T_i, and T_{i+1} are temperatures at nodes $i-1$, i, and $i+1$ respectively, located at the mid-planes of slices $i-1$, i, and $i+1$ of the homogeneous building envelope material.

The heat flux through the interface between slices $i-1$ and i (q_{i-}) and slices between the i and $i+1$ (q_{i+}):

$$q_{i-} = -k\frac{T_i - T_{i-1}}{\Delta x} \quad 2\text{-}7$$

$$q_{i+} = -k\frac{T_{i+1} - T_i}{\Delta x} \quad 2\text{-}8$$

Assuming that there are no internal heat sources or heat sinks, the heat balance on slice i is:

$$\rho c \Delta x \frac{\Delta T_i}{\Delta t} = -k\frac{T_i - T_{i-1}}{\Delta x} + k\frac{T_{i+1} - T_i}{\Delta x} \quad 2\text{-}9$$

The right hand side of equation 2-9 describes the net heat gain of the i slice due to conduction heat transfer between the slice $i-1$ and $i+1$. The left hand side describes the rate of change in the internal energy of the i slice of the slab resulting from this net conduction heat gain, which will be reflected by a rise in temperature ΔT_i at node i over the time interval Δt.

$$\frac{\Delta T_i}{\Delta t} = \alpha\frac{\Delta T_{i-1} - 2\Delta T_i + \Delta T_{i+1}}{\Delta x^2} \quad 2\text{-}10$$

where α is a collection of constants (known as thermal diffusivity, and includes ρ, c and k).

There is a number of DTM programs available such as EnergyPlus (EP) (U.S. Department of Energy, 2019), DesignBuilder (DesignBuilder, 2020), eQUEST (DOE-2, 2020), Green Building Studio (GBS) (Autodesk, 2020), TRNSYS (TrnSys, 2020), IESVE (IESVE, 2020), (Graphisoft, 2020), Modelica (The Modelica Association, 2020) and IDA-ICE (IDA-ICE, 2020). EP evolved from Building Loads Analysis and System Thermodynamics (BLAST) and DOE–2 energy and load simulation programs, both of which were developed and released in the late 1970s and early 1980s. TRNSYS is the closest alternative to EP, however, TRNSYS is vastly used to assess the electrical and thermal performance of transient systems. EP was used to assess the building energy and thermal performance of the research project building case studies (presented in chapter 4) because it is available in the public domain and includes validated subroutines that have been extensively used by researchers and designers for building retrofit studies and optimisation of energy performance.

EP is a well-established DTM program which consists of a collection of many programs that work together for energy simulation, thermal design and analysis, heating and cooling loads simulation, solar control, overshadowing, validation, lighting, LCA, lifecycle costing, scheduling etc. (U.S. Department of Energy, 2019). EP offers low-cost, easy-to-use and computational time process because it uses the Building Information Modelling based Building Energy Modelling (BIM-based BEM) method that uses the pre-designed BIM model (including the information of architectural design and mechanical loads, materials' properties, and HVAC system) to create input, as described in Figure 2-20 (Gao et al., 2019). EP provides accurate numerical results via the calibration and validation of EP model with experimental monitored data. The accuracy of the building model is very important to accurately simulate the building energy performance and thermal comfort. This can be done via model calibration, which involves the modification of the building model with experimentally monitored data. The accuracy can be statistically represented using Mean Bias Error (MBE) and Coefficient of Variance of the Root Mean Square Error (CVRMSE). CV(RMSE) tests how well the model recreates the numerical results and its indication of random error, while MBE tests how data and is also an. MBE tests how biased the model is in predicting outputs over the period the model was developed (ASHRAE, 2017).

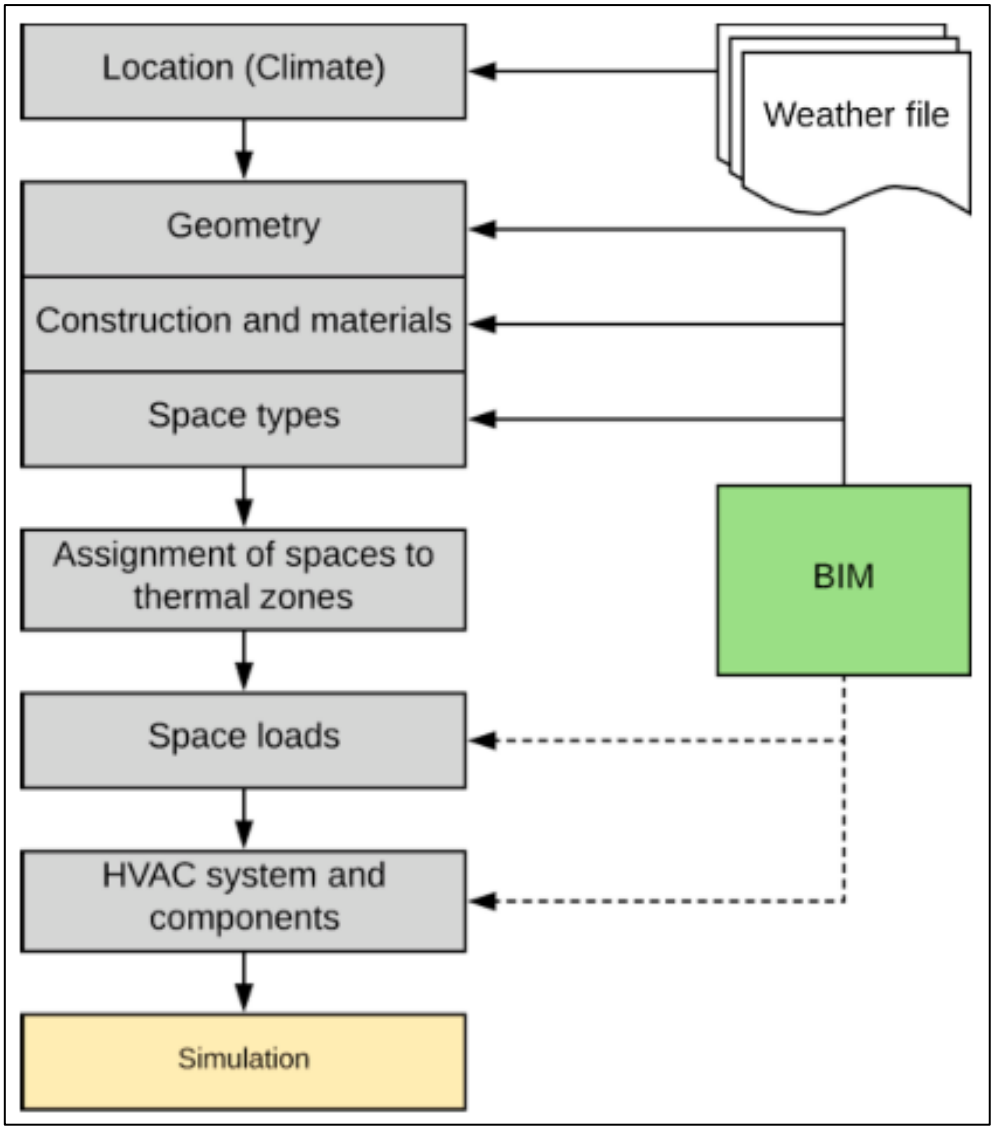

Figure 2-20: “Ideal workflow for energy performance simulation tools” (Gao et al., 2019).

2.4 Life Cycle Assessment

The application of LCA methodology described in chapter 1, is the most effective method used to assess environmental impacts of buildings; the method follows the guidelines and framework of ISO 14044/40 described in BS EN ISO (2006, 2018). Figure 1-3 describes LCA stages as goal and scope definition, inventory analysis, impact assessment and interpretation. The objective of LCA is to evaluate environmental impacts of the product system that affects human health, the ecosystem and resource depletion (European Commission, 2020). The ISO 14044/40 facilitates the LCA study performed from raw material acquisition phase through product development and manufacture, operation, and end of life of product. Figure 2-21 describes general product Life Cycle (LC) – cradle to grave. Product LCA can be conducted

using system expansion (also known as consequential modelling) that assesses environmentally relevant flows or consequences due to change in the baseline situation, and attributional modelling that assesses environmental impact of a product (or products when comparing different products of the same functional unit) or function and identify the hotspots in its LC. Commercially available software that incorporates ReCiPe (presented in section 2.4.3) includes SimaPro (PRé et al., 2016) and Gabi (Gabi, 2020). SimaPro was used to assess the environmental impact of the most energy-efficient technologies (presented in chapter 6 and 7) analysed in chapter 4 and 5. SimaPro is a user-friendly and widely used LCA software because it offers up-to-date databases with which to conduct environmental impact assessment (SimaPro, 2020).

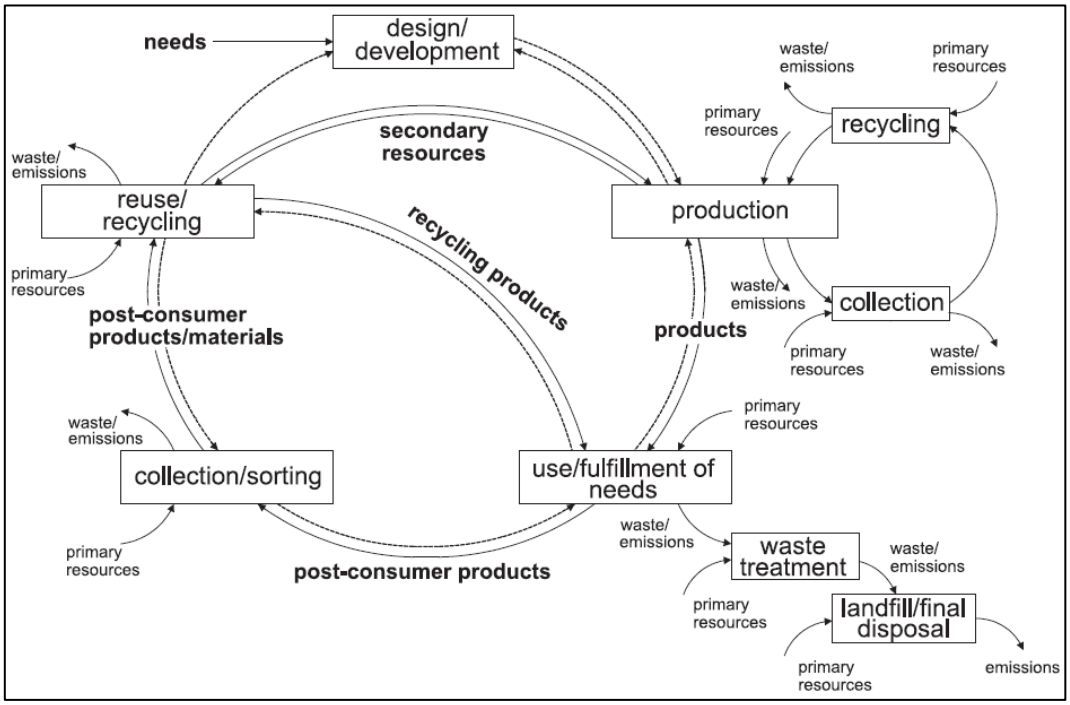

Figure 2-21: Schematic representation of a generic life cycle of a product (the full arrows represent material and energy flows, while the dashed arrows represent information flows) (Rebitzer et al., 2004).

2.4.1 Functional Unit and System Boundary

The goal defines the objective of the LCA study, while the scope defines the functional unit(s) and system boundary which ensures the goal of the study. The functional unit(s) which is consistent with the goal of the study provides a reference unit of analysing the input and output data, and comparison of LCA results of different product systems (Desideri and Asdrubali,

2018). System boundary defines the processes which are part of the product system (BS EN ISO 14044, 2018). Several factors that determine how the system boundary is defined include the product system being environmentally assessed and its application, cut-off criteria, data and cost criteria, and stakeholder (Desideri and Asdrubali, 2018).

2.4.2 Life Cycle Inventory and Impact Assessment

Life Cycle Inventory (LCI) involves data collection and modelling of the product by creating inventory of flows from and to nature, which includes “inputs of water, primary energy, and raw materials; outputs of emissions to air, land, and water; subproducts; and other releases” as described in Figure 2-22. The data collected are foreground data (technology specific data from first/second/third party) and background data (average mix market data such as ecoinvent database) (European Commission - Joint Research Centre - Institute for Environment and Sustainability, 2010). The Life Cycle Impact Assessment (LCIA) translates the LCI results to a number of midpoint environmental impact category indicators (e.g. Global Warming Potential (GWP), Ozone Depletion Potential (ODP), Fossil Depletion (FD) etc.) and endpoint damage categories which are human health, ecosystem and resource depletion. Therefore, a complete LCIA involves the assessment of midpoint impact category indicators and endpoint damage. The methods that can be used for a complete LCIA are combined midpoint and endpoint approaches which includes IMPACT 2002+, LIME, LUCAS and ReCiPe (Desideri and Asdrubali, 2018). ReCiPe is a state-of-the-art method LCIA method that assesses environmental impact at a global scale. Other LCIA methods assesses environmental impact at continental or country level (PRé, 2016).

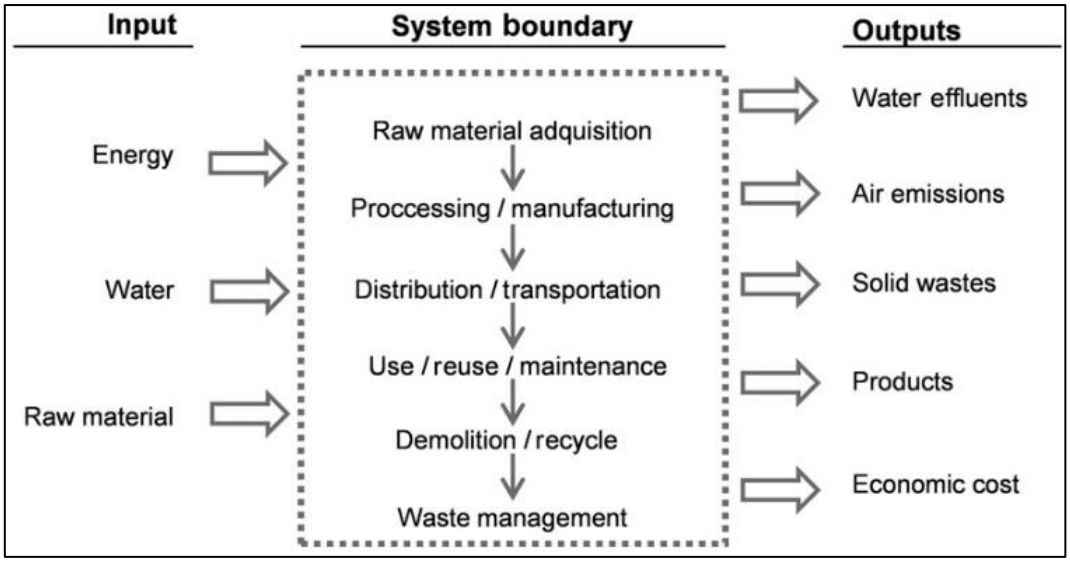

Figure 2-22: “Life-cycle inventory process applied to a system unit” (Desideri and Asdrubali, 2018).

2.4.3 ReCiPe Method

ReCiPe was first developed in 2008 via a collaborative effort between RIVM, Radboud University Nijmegen, Leiden University and Pré Consultants; the method was initially called ReCiPe2008. ReCiPe provides “a method to covert life cycle inventories to a limited number of life cycle impact scores on midpoint and endpoint level” (Mark A.J. Huijbregts et al., 2017), as shown in Figure 2-23. The life cycle inventories are lists of raw material extractions and lists of substance emissions to the soil, water and air (PRé et al., 2016).

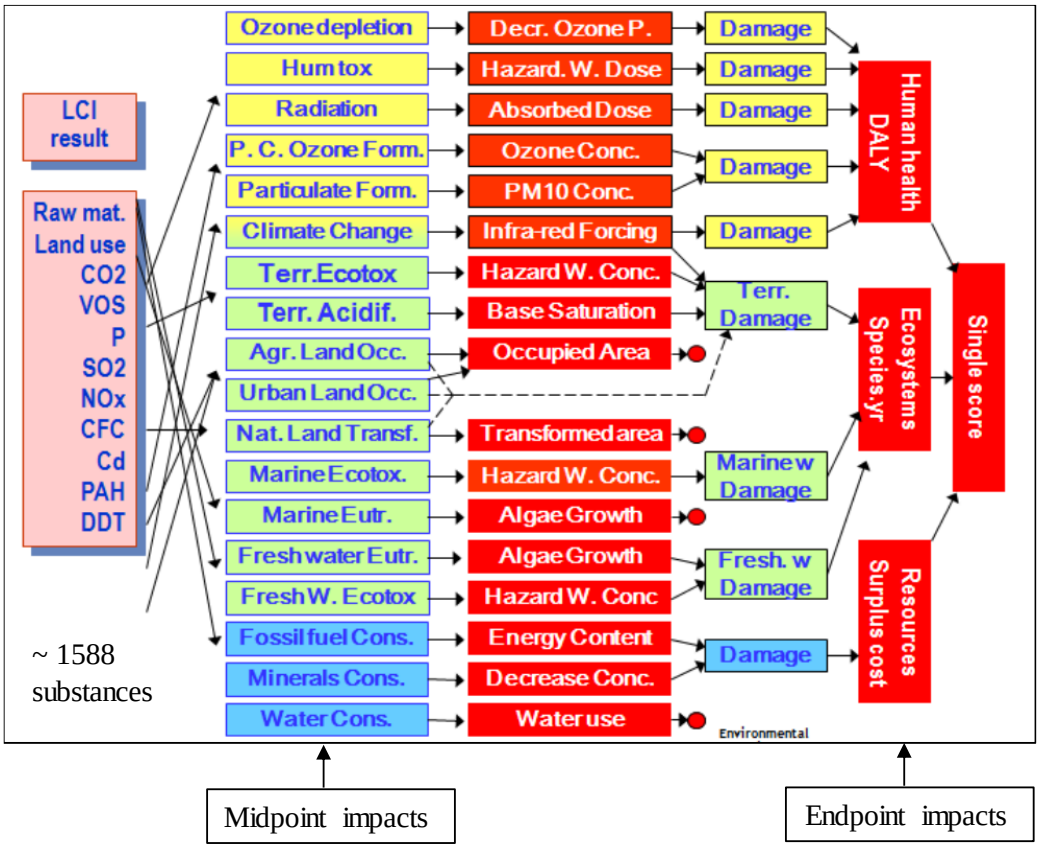

Figure 2-23: "Representation of the relations between the inventory and the midpoint categories (environmental mechanisms) and the endpoint categories, including the single score (damage model)" (PRé, 2016).

ReCiPe2016 is an update from ReCiPe2008 that provides midpoint and endpoint harmonized characterization factors that are representative for the global scale, instead of the European scale, while maintaining the possibility to carry out the characterisation of some impact categories at a continental and country level (M.A.J. Huijbregts et al., 2017). The method converts lifecycle inventory emitted substances to 18 midpoint indicators (midpoint impact category) and 3 endpoint indicators (endpoint impact category), by adopting the hierarchist perspective midpoint and endpoint characterization factors at a global scale (M.A.J. Huijbregts et al., 2017; Mark A.J. Huijbregts et al., 2017; PRé, 2016; RIVM, 2018). The ReCiPe2016 18 midpoint impact category indicators are presented in Table 2-1. The 3 endpoint indicators are:

- Human Health Potential – HHP (DALY)
- Ecosystem Potential – EP (species.yr)
- Resources Potential – RP (€)

Table 2-1: 18 ReCiPe2016 midpoint impact category indicators.

GWP	Global Warming Potential (kg CO_2-eq)
ODP	Ozone Depletion Potential (kg CFC-11-eq)
TAP	Terrestrial Acidification Potential (kg SO_2-eq)
FEP	Freshwater Eutrophication Potential (kg P-eq)
MEP	Marine Eutrophication Potential (kg N-eq)
HTP	Human Toxicity Potential (1,4 DB-eq)
POFP	Photochemical Oxidant Formation Potential (kg NMVOC-eq)
PMFP	Particulate Matter Formation Potential (kg PM_{10}-eq)
TETP	Terrestrial Ecotoxicity Potential (kg 1,4 DB-eq)
FETP	Freshwater Ecotoxicity Potential (1,4 DB-eq)
METP	Marine Ecotoxicity Potential (kg 1,4 DB-eq)
IRP	Ionising Radiation Potential (kBq U235-eq)
ALOP	Agricultural Land Occupation Potential (m^2a)
ULOP	Urban Land Occupation Potential (m^2a)
NLTP	Natural Land Transformation Potential (m^2)
WDP	Water Depletion Potential (m^3)
MDP	Metal Depletion Potential (kg Fe-eq)
FDP	Fossil Depletion Potential (kg oil-eq)

2.5 Conclusions of the Literature Review

Literature review has revealed that the combined implementation of building envelope retrofit and building integrated solar energy system solutions has the potential to increase residential building energy efficiency in hot countries, which in turn mitigates the associated building environmental impacts. Literature review has also revealed that roof retrofitting is the most effective in hot climates because of the high solar radiation intensity on the roof as a result of the sun's inclination. Results reported in the literature agree that cool roof and thermal insulation are very effective building envelope retrofit solutions in low-rise buildings where the ratio of roof area to surface area of the building is high, in regions with high solar radiation and warm conditions throughout the year so that heating needs are relatively small. Window shading is a building envelope retrofit solution that is effective in hot climates because it reduces solar gain in buildings. Also, LED lighting and A-rated appliances interventions reduces internal heat gains, and so energy consumption including cooling. To that end, the five energy-efficient solutions outlined below (categorised into external (envelope) and internal interventions) were assessed for their energy performance and environmental impacts. The house envelope solutions are:

- Cool roof paint
- Roof thermal insulation

- Window shutters

The internal interventions are:

- A-rated electric appliances
- Light Emitting Diode (LED) lighting

Literature review also shows that energy generation by building integrated and on-site solar energy systems located in hot and humid climates can meet a high percentage of energy-efficient household's energy demand. The solar energy systems studied are HCPV/T 2000x, PV and PVT. The investigated solar energy systems were enabled by the SMART GEMS European project. These systems can generate electrical and/or thermal energy.

IDEA SRL, a SMART GEMS project partner located in Sicily (a region with high solar radiation), provided access to the onsite operational HCPV/T 2000x and PV systems and data, and low-rise single family house (with some heating demand). The onsite installed PV system was not experimentally monitored due to technical issue. As a result, the PV system along with PVT system (which was not installed onsite) were numerically studied. Similarly, University of Technology, Kingston, Jamaica (a region with high solar radiation), a research partner of Brunel University London, provided access to low-rise single-family house (with no heating demand). Both locations are very good case study locations to assess the energy and environmental performance of low-rise residential buildings after the implementation of cool roof, thermal insulation, window shading, LED lighting and A-rated appliances, and solar energy systems (HCPV/T 2000x, PV and PVT). It is not clear from literature which building envelope retrofit and solar energy system solutions mentioned above has the best energy and environmental performance. Chapter 3 to chapter 8 presents studies that will allow comparison based on energy reduction potential of the interventions and environmental mitigations. EP was used to assess the building energy performance, PV and PVT energy production because of its accurate numerical results after the EP model is calibrated and validated with experimental monitored data. SimaPro (PRé et al., 2016) incorporated with state of the art ReCiPe 2016 LCIA method was used to assess the environmental impacts of the most energy-efficient solution, and compared with available literature studies of other energy-efficient solution(s) with high energy saving potential.

Chapter 3: Experimental Monitoring and Computational Studies of the Case Study Buildings

Introduction

Chapter 3 presents the experimental monitoring and computational study of the case study houses in Palermo, Sicily and Portmore, Jamaica. Section 3.1 presents the geometric description of the case study houses and climatic conditions of the case study locations. Section 3.2 presents the onsite experimental monitoring values of the case study houses carried out in 2017 and 2018. Section 3.3 presents the computation model development of the case study houses; this includes the calibrated models required to accurately investigate the building energy consumption and energy-efficient solutions presented in chapter 4.

3.1 Description of the Case Study Houses

The two case study houses are located in Palermo, Sicily and Portmore, Jamaica. Palermo is the capital of Sicily, an island in the Mediterranean Sea, located in the Southern part of Italy.

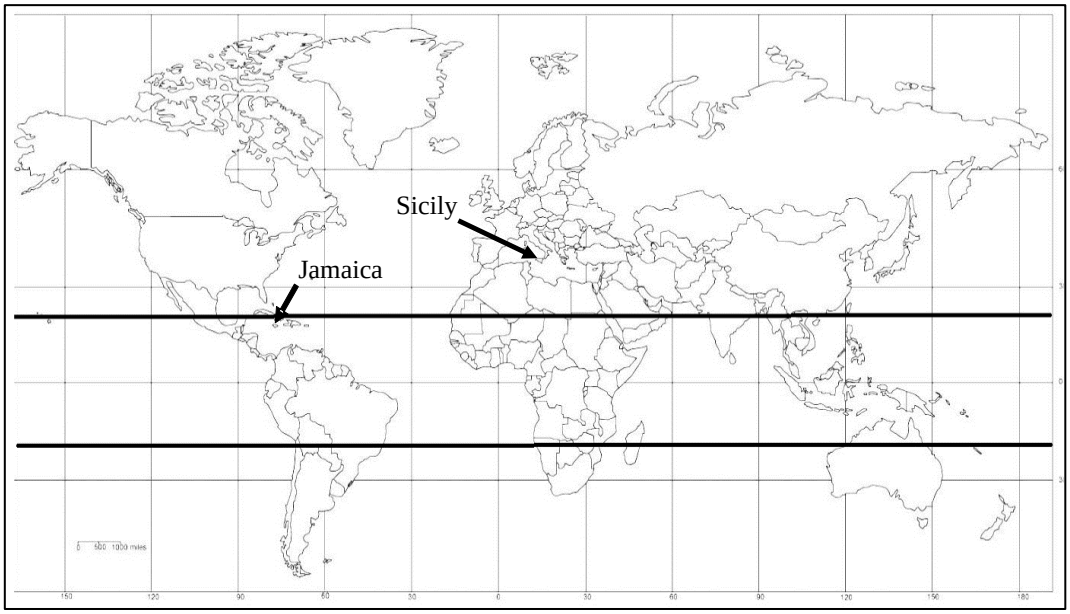

Figure 3-1: Location of case-studies

3.1.1 Climatic Conditions

Italy is divided into six climatic zones according to climatic conditions; Palermo is located in climatic zone B (Italian Government - Ministry of Economical Progress, 2015). Sicily is characterised with hot and dry summer and mild and wet winters. The average annual ambient

temperature, Global Horizontal Irradiance (GHI), Direct Normal Irradiance (DNI) and Diffuse Horizontal Irradiance (DHI) of Palermo are 19 °C, 202 W/m^2, 218 W/m^2, 101 W/m^2 and 72 W/m^2 (Meteonorm, 2019). Portmore is an urban neighbouring town to Kingston city, the capital of Jamaica; a tropical country characterised with hot and humid weather. Jamaica is located around the equator (as shown in Figure 3-1) with high solar radiation intensity throughout the year and high external air temperatures. The average annual ambient temperature, GHI, DNI and DHI of Portmore are 28 °C, 196 W/m^2, 141 W/m^2 and 101 W/m^2 (Meteonorm, 2019). The monthly distribution of the average solar radiation and ambient air temperature for both locations are shown in Figure 3-2 for a typical weather year. For Sicily, ambient temperature, GHI and DNI are highest in summer and lower in other seasons (winter being the lowest); the highest and lowest ambient temperature occurs in August and February, respectively, GHI occurs in July and December, and DNI occurs in July and February. For Jamaica, the ambient temperature, GHI and DNI show a fairly constant distribution throughout the year.

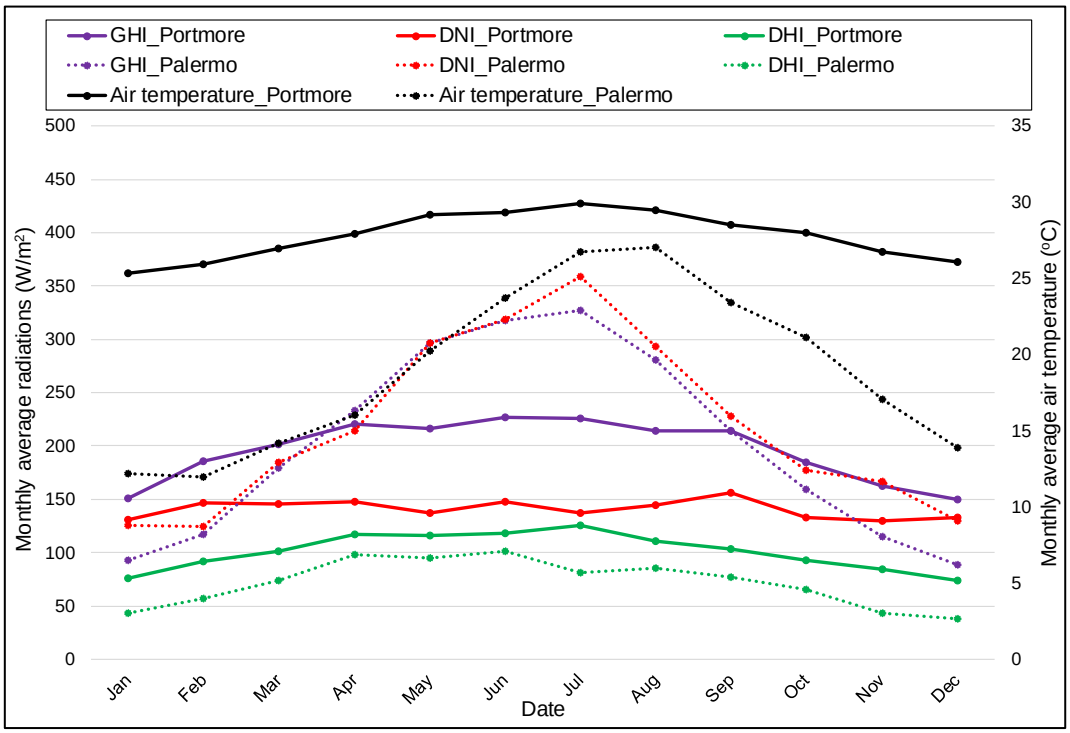

Figure 3-2: Typical monthly average ambient temperature, GHI, DNI and DHI (from Meteonorm weather file) in Palermo, Sicily Italy and Portmore, Kingston Jamaica.

3.1.2 Case Study House in Palermo, Sicily

The case study house in Palermo, Sicily is a naturally ventilated single-storey detached house with 3 occupants. The building has an installed heating system that provides heating during the cold period. The neighbouring houses are low-rise buildings with minimum shading effect to the case study house. The case study house floor plan is shown in Figure 3-3.

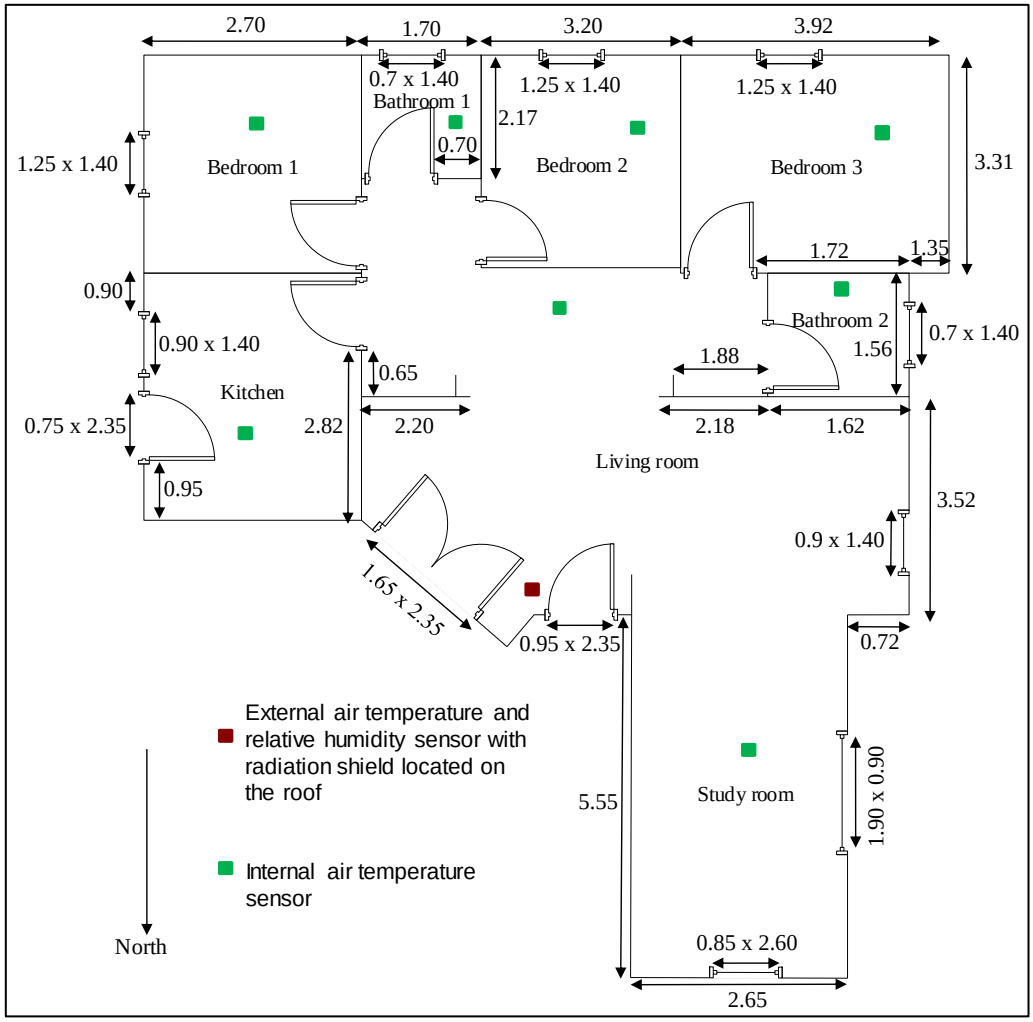

Figure 3-3: Palermo, Sicily case study house floor plan with an area of 100.4 m^2 (dimensions in m) and height of 3.00 m. Experimental monitoring devices/points indicated are described in section 3.2.

The external wall (with 0.29 m thickness) of the Palermo, Sicily house is a cavity wall construction with airspace, double glazed windows, and wooden doors. Table 3-1 provides information about the construction materials and dimensions required for computational model development in section 3.3, needed to calculate the thermal characteristics of the two case study houses (see chapter 4).

Table 3-1: External fabric and thermal data for the Palermo, Sicily case study house.

Floor/Roof area (m^2)		100.4	
Volume (m^3)		300.2	
External wall area exposed to ambient (m^2)		117.4	
Window area (m^2) – 10 double glazed windows		15.8	
1 North façade wooden door (m^2)		2.2	
1 North East glass door (m^2)		3.9	
1 Wall double glazed door (m^2)		1.78	
Occupants		3, at home night and weekends	
Internal heat gains		Lighting: 60 W (x8) Electric appliances: 3594 W	
Building envelope	Material	Thickness (m)	U-Value (W/m^2K)
External walls	Brick with plaster and airspace	0.29	1.43
Window	Double glazed glass		2.753
External door	Wood	0.05	1.97
Roof	Cast concrete, waterproof covering and plaster	0.24	2.26
Floor	Cast concrete with floor vinyl	0.23	2.14

3.1.3 Case Study House in Portmore, Jamaica

The Portmore, Jamaica case study house is a naturally ventilated single-storey house with one occupant. The neighbouring houses are low-rise buildings with minimum shading effect to the case study house. The case study house floor plan is shown in Figure 3-4.

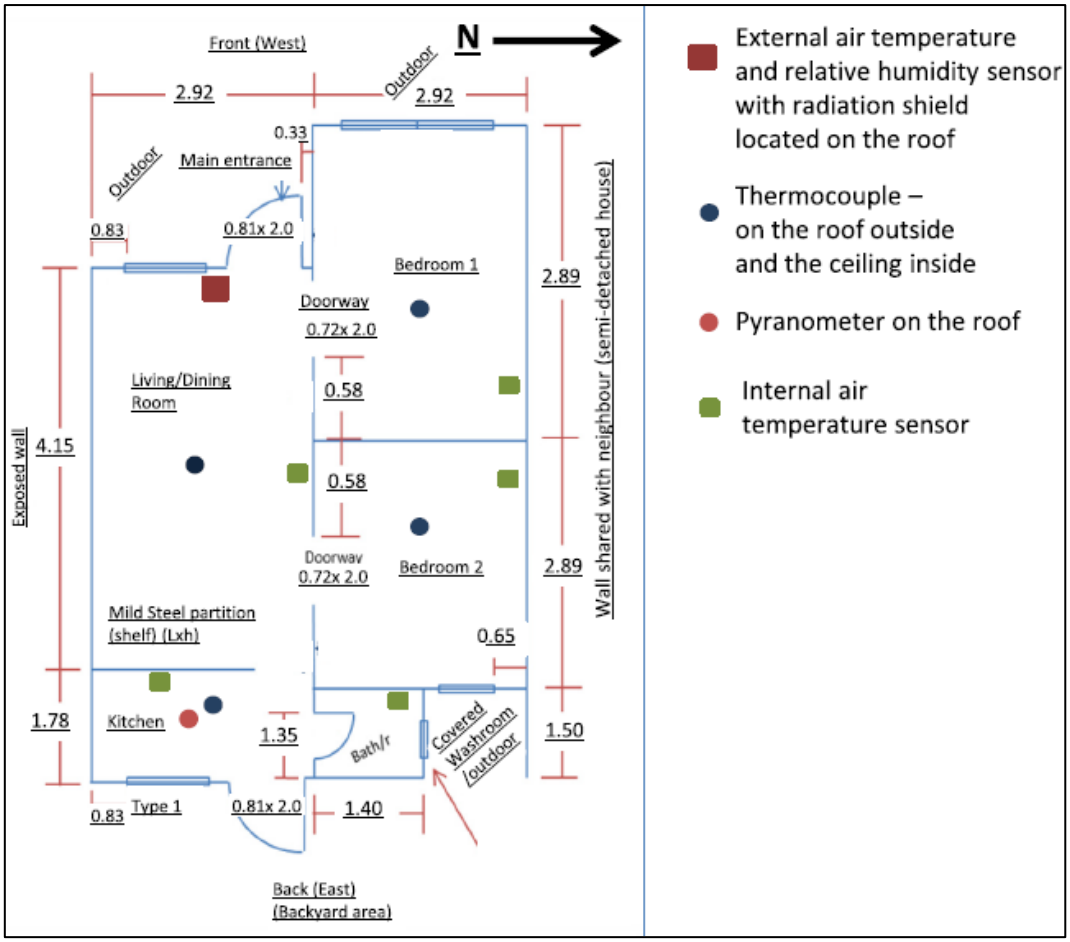

Figure 3-4: Portmore, Jamaica case study house floor plan with an area of 36 m^2 (dimensions in m) and height of 2.46 m. Experimental monitoring devices/points indicated is described in section 3.2.

The external wall (with 0.04 m thickness) of the Portmore, Jamaica case study house is a solid wall construction, single glazed windows, and wooden doors. Table 3-2 provides information about the construction materials and dimensions required for computational model development in section 3.3, needed to calculate the thermal characteristics of the two case study houses (see chapter 4).

Table 3-2: External fabric and thermal data for the Portmore, Jamaica case study house.

Floor/Roof area (m^2)		36	
Volume (m^3)		88	
External wall area exposed to ambient (m^2)		54.5	
Window area (m^2) – 6 single glazed windows		3.6	
1 West façade wooden door (m^2)		1.6	
1 East wooden door (m^2)		1.6	
Occupants		1, at home nights and weekends	
Internal heat gains		Lighting: 14 W (x5) Electric appliances: 1960 W	
Building envelope	Material	Thickness (m)	U-Value (W/m^2K)
External walls	Precast concrete	0.04	5.91
External door	Wood	0.04	6.645
Roof	Precast concrete	0.08	5.68
Floor	Concrete with tiles	0.10	4.19

3.2 Experimental Monitoring of the Case Study Houses

The purpose of the onsite experimental monitoring was to acquire values from the case study houses, needed to accurately investigate the building energy consumption and indoor thermal performance. The International Performance Measurement and Verification Protocol (IPMVP) Option D, calibration simulation was used to assess the accuracy of the measured data and the computational model. The calibration criteria used are MBE and CVRMSE values with error range of ±10 % and 30 %, respectively (CIBSE TM63, 2020) The details of the calibration simulation of the computational model is presented in sections 3.3.1 (model of Palermo, Sicily case study house) and 3.3.2 (model of Portmore, Jamaica case study house).

3.2.1 Experimental Monitoring of Case Study House in Palermo, Sicily

The experimental monitoring of the Palermo, Sicily case study house was conducted during my nine months (October 2017 to June 2018) secondment to IDEA SRL, (a SMART GEMS project partner) to study the HCPV/T 2000x system. I conducted an on-site survey of the house construction as well as equipment (including lighting) as sources of internal heat gains; the floor plan of the house was provided by the occupant. During the visit, I installed HOBO UX100-003 data loggers at different thermal zones to measure air temperature and relative humidity. The measurement of the Palermo, Sicily case study house was conducted from 25 January 2019 to 27 May 2019. The parameters measured are external air temperature and

relative humidity, and internal air temperature and relative humidity. The external air temperature and relative humidity were measured using a shielded and ventilated HOBO UX100-003 data logger (as shown in Figure 3-3 and Figure 3-5) with accuracy ±0.21 °C. The internal air and relative humidity were measured at 8 locations (2 bathrooms, 3 bedrooms, livingroom, studyroom and kitchen, as shown in Figure 3-3) with HOBO UX100-003 data logger. The onsite experimental measured values were logged at 5 minutes interval and averaged to 1 hour for the analysis.

Figure 3-5: Photos of case study house in Sicily. The position of the shielded and ventilated HOBO UX100-003 data logger.

3.2.2 Experimental Monitoring of Case Study House in Portmore, Jamaica

The measurement of the Portmore, Jamaica case study house was conducted from mid-January 2017 to mid-July 2017 by research partner at the University of Technology, Kingston, Jamaica. Prior to the measurement, an on-site survey was carried out to determine the geometry (including areas of windows and doors) and construction of the house as well as equipment (including lighting) as sources of internal heat gains. The parameters measured are GHI, roof and ceiling temperatures, external air temperature and relative humidity and internal air

temperature and relative humidity. The GHI was measured with a pyranometer CMP 3 from Kipp & Zonen; it is capable of measuring solar radiation up to 2000 W/m^2 with a wavelength from 300 to 2800 nm. The output range is 0 to 30 mV with a sensitivity of 5 to 20 $\mu V/W/m^2$. The roof and ceiling temperatures were measured with thermocouples at 4 locations outside and 4 inside (these are the roof and ceiling sections of the livingroom, 2 bedrooms and kitchen, see in Figure 3-4). Each thermocouple in the roof was protected from solar radiation using tapes, and secure using stones. The thermocouples are linked with a Campbell Scientific CR10x data logger with an accuracy of ±0.05 % of the full-scale input range. The external air temperature and relative humidity were measured using a shielded and ventilated HOBO UX100-003 data logger (as shown in Figure 3-4 and Figure 3-6). The internal air and relative humidity were measured at 4 locations (livingroom, 2 bedrooms and kitchen, as shown in Figure 3-4) with HOBO UX100-003 data logger. The onsite experimental measured values were logged at 5 minutes interval and averaged to 1 hour for the analysis.

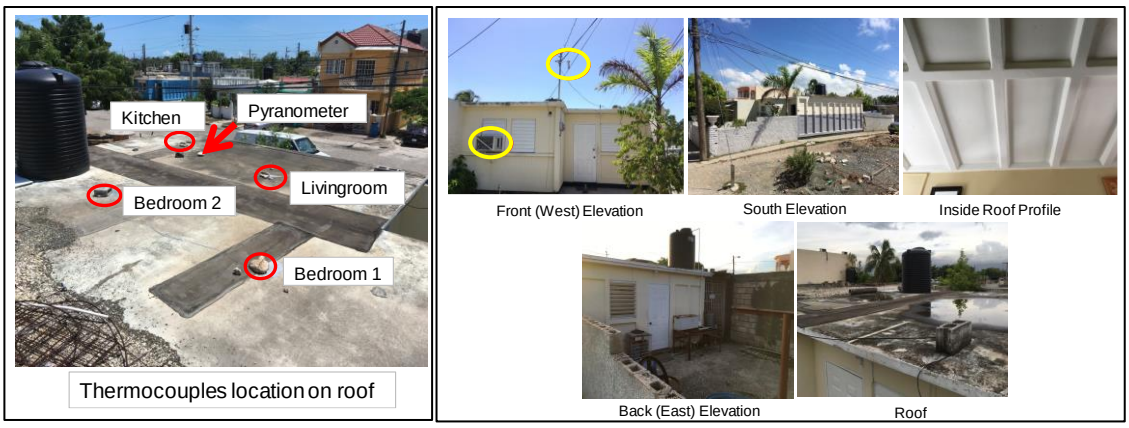

Figure 3-6: Photos of Portmore, Jamaica case study house. The position of the shielded ventilated HOBO UX100-003 data logger and the non-functioning air-conditioned unit is shown (yellow circle in the right picture) (photos provided by UTech, Jamaica).

3.3 Computational Model Development of the Case Study Houses

The purpose of the computational model development of the case study houses is to evaluate their annual energy consumption and indoor thermal conditions. The models of the case study houses were developed using OpenStudio (OS) (NREL et al., 2019) and EP (U.S. Department of Energy, 2019). OS is a collection of software tools that are used to support building energy modelling. OS SketchUp Plug-in is one of the software tools that is used in SketchUp 3D modelling tool to create geometry (including building surface geometry) to support the building

energy modelling using EP. As mentioned in chapter 2, EP is a collection of many program modules that are used to calculate building energy demand. In the context of this study, the 3D geometry surfaces created in OS SketchUp Plug-in is exported to EP to facilitate the further modelling of the two case study houses.

3.3.1 EnergyPlus Model of Case Study House in Palermo, Sicily

First, the 3D geometry surfaces created in OS SketchUp Plug-in is exported to EP and defining the annual run period starting in January. The house was modelled into eight thermal zones shown in Figure 3-7. The building envelope and internal heat gains were modelled according to the survey information obtained during the visit to the house towards the end of December 2019 (see Table 3-1). The material properties of these construction materials were obtained from CIBSE Guide A, (2019), see Appendix A.1 for the detailed EP modelling of the case study. The house is a naturally ventilated building that is controlled by the occupants. The air infiltration and natural ventilation were simulated using the EP airflow network model. The EP airflow network model provides the ability to predict multi-zone air infiltration and ventilation flows airflows driven by outdoor wind pressure (U.S. Department of Energy, 2019). Also, the airflow network model takes into account the internal divisions in the house that account for specific internal airflow paths. The pictorial description of the multi-zone airflow network is shown in Figure 3-8 (CIBSE Guide A, 2019). The air infiltration and natural ventilation through the building envelope influence the internal environment and the energy needs of buildings. The wind pressure is an important boundary condition for the EP airflow network which is expressed by pressure coefficients (C_p) in equation 3-1 (Cóstola et al., 2009).

$$C_p = \frac{P_x - P_0}{P_d}, \qquad P_d = \frac{\rho \cdot U^2}{2} \tag{3-1}$$

P_x is the static pressure at a given point on the building façade, P_0 is the static reference pressure, P_d is the dynamic pressure, ρ is the air density and U is the upstream wind speed at reference building height. The flow coefficient is a leakage characteristic that are used to further detail modelling of air infiltration through wall, ceiling, floor and window. The wind pressure coefficient data applicable to this case-study (low-rise buildings) and flow coefficient data were obtained from CIBSE Guide A (CIBSE Guide A, 2019). The detail EP model of the

multi-zone airflow network used to predict air infiltration and ventilation flows is in Appendix A.3 and A.4.

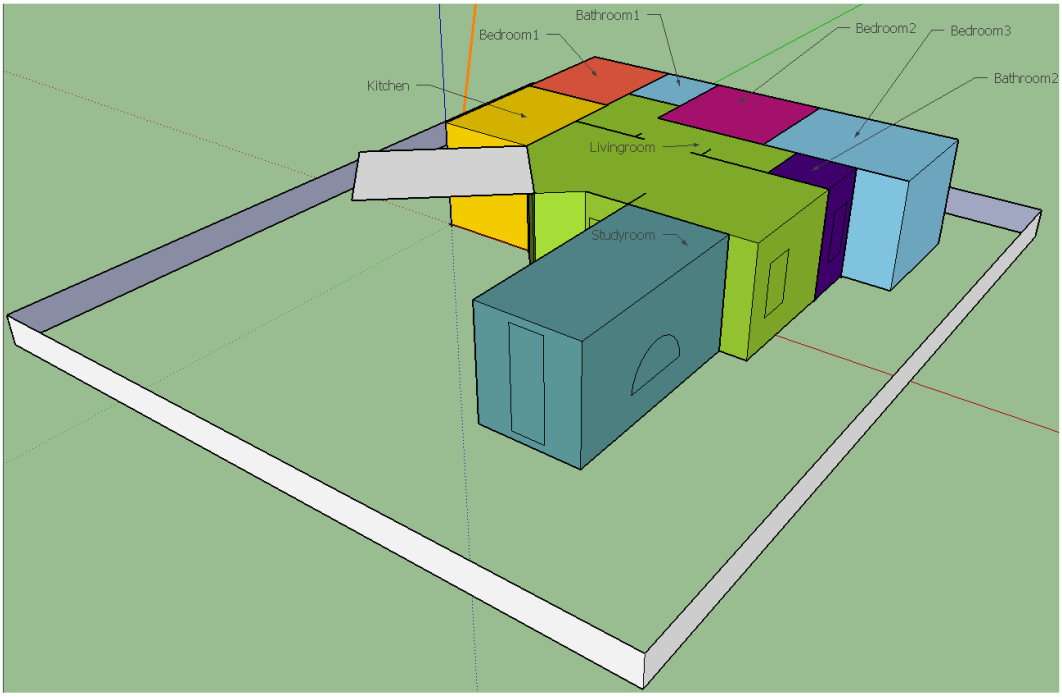

Figure 3-7: Thermal zones for the Palermo, Sicily case study house.

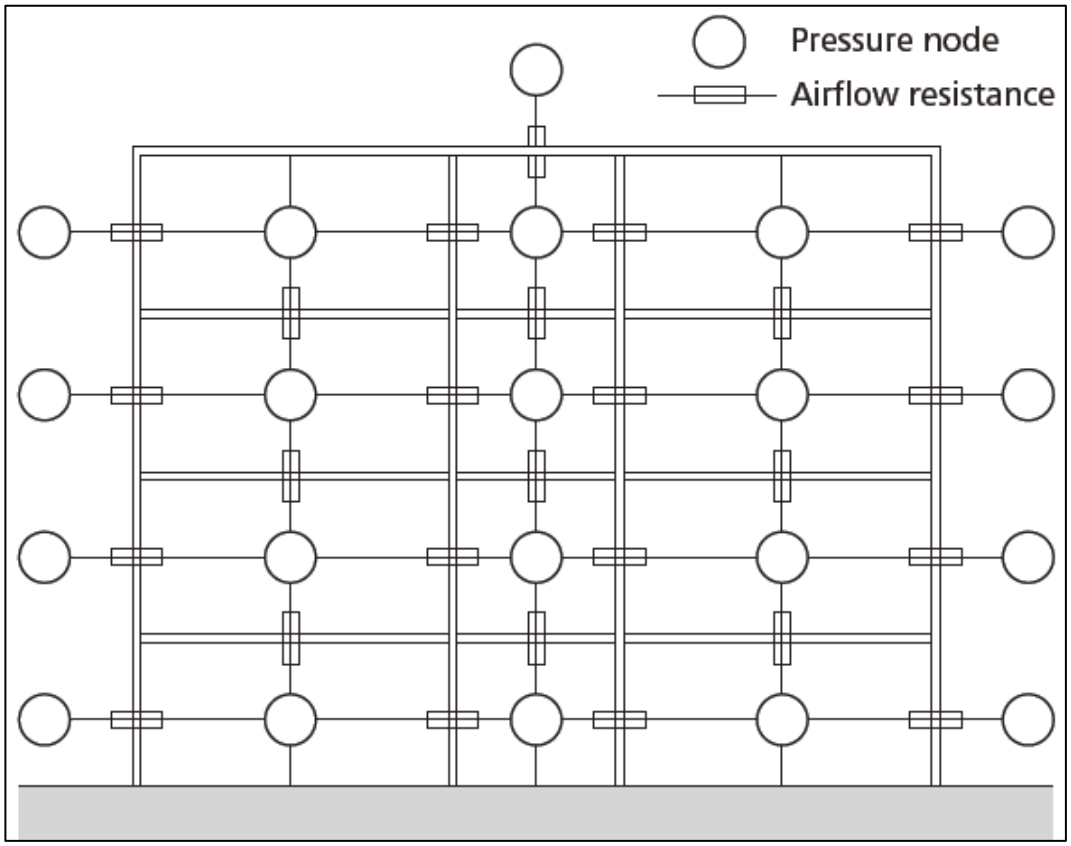

Figure 3-8: “Multi-zone flow network” (CIBSE Guide A, 2019). The pressure node represents

the inside and outside pressure reference point. The air resistance represents the building envelope and internal divisions of the house.

Finally, the Typical Meteornorm Year (TMY) weather file for Palermo, Sicily was uploaded into the EP program to calculate the external and internal surface temperature, internal air temperature, cooling and heating energy demand, and lighting and electric appliance energy consumption.

The onsite experimental measured weather values were measured to facilitate the calibration of the baseline computation model. The TMY weather file for Palermo, Sicily was modified with onsite experimental measured external air temperature and relative humidity values. The modified TMY weather file covers the period from 25 January 2019 to 27 May 2019. The modified TMY weather file was only used for calibration purpose. The DNI and DHI were not measured onsite. However, the TMY weather file DNI and DHI values were used with EP to simulate the annual building energy consumption and energy-efficient solutions studied in chapter 4. The heating period (winter) was maintained at 20 ℃ from 11 November 2018 to 31 March 2019; this means the heating system will be switched on when the temperature is below the temperature set point of 20 ℃. The house was naturally ventilated according to the occupants' schedule for the rest of the year.

A successful calibration is achieved by statistically comparing the acquired onsite experimental internal air temperature with simulated EP results. To successfully calibrate the EP model, several simulations were run by using an iterative approach during which the operation schedule details are changed (within acceptable ranges) until the recommended MBE and CVRMSE values is reached (CIBSE TM63, 2020)

The results of the calibrated model were statistically analysed and compared to the onsite measure values, using the MBE and CVRMSE in equations 3-2 and 3-3 respectively. The MBE and CVRMSE statistical values are presented in Table 3-3; which are within the recommended MBE and CVRMSE values of less than ±10 % and 30 % respectively relative to the hourly calibrated results (U.S. Department of Energy, 2015).

$$MBE = \frac{\sum_{i=1}^{N}(M_i - S_i)}{\sum_{i=1}^{N} M_i} \qquad 3\text{-}2$$

$$CVRMSE = \frac{\sqrt{\sum_{i=1}^{N} (M_i - S_i)^2 / N}}{\bar{M}} \quad 3\text{-}3$$

N is the sample data (1631 hours of measured and simulated data) starting at an instance, $i = 1$, M_i and S_i are measured and simulated data, and M is the mean of the measured data.

Table 3-3: MBE and CVRMSE of the air temperature for the Palermo, Sicily case study house.

Thermal Zones	MBE	CVRMSE
Bathroom 1	6.78 %	9.76 %
Bathroom 2	3.87 %	5.47 %
Bedroom 1	3.95 %	7.20 %
Bedroom 2	5.63 %	8.08 %
Bedroom 3	5.40 %	8.21 %
Kitchen	6.28 %	10.19 %
Living room	3.01 %	8.20 %
Study room	- 3.18 %	10.36 %

Figure 3-9 presents the onsite experimental measured values and simulated results of air temperature in the livingroom as an example. At a glance, it can be seen that the simulated results are close to the onsite experimental measured one. Additionally, Figure 3-10 presents the correlation of the onsite experimental measured values and simulated results of the ceiling and air temperature in the bathroom 1, bedroom 1 and 2, kitchen, living room and study room for 2952 hours. More than 80 % of the points are within 10 % of the MBE error. These results indicate that the case study house for Palermo, Sicily model was successfully calibrated.

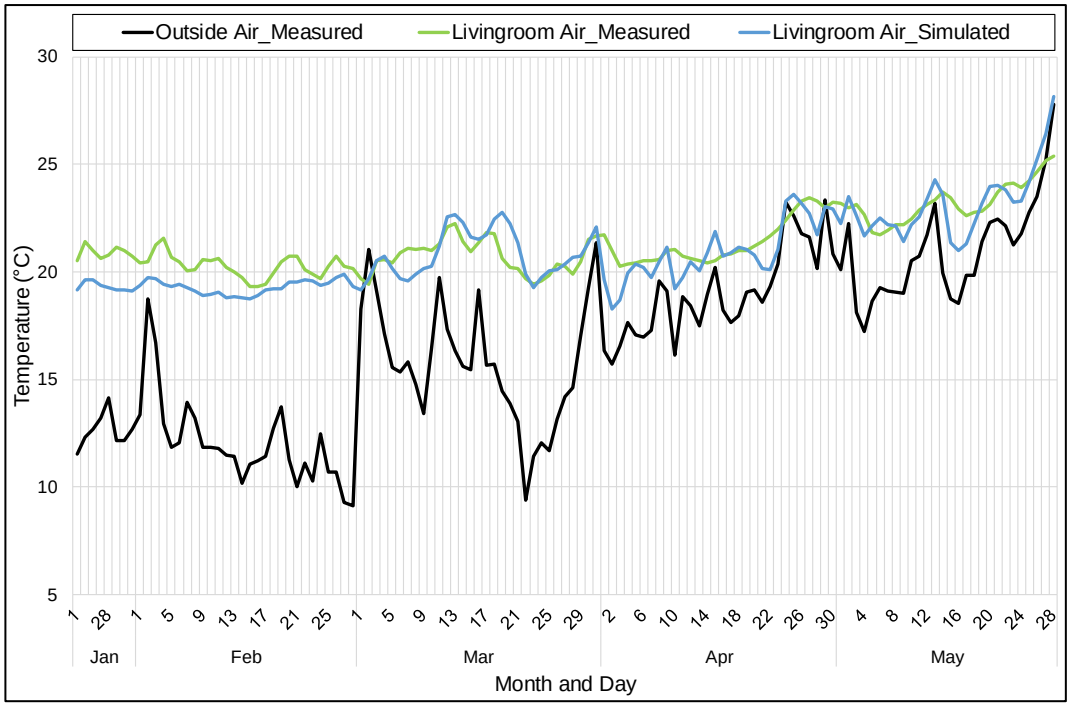

Figure 3-9: Palermo, Sicily case study house: simulated vs. onsite experimental measured air temperature of the livingroom.

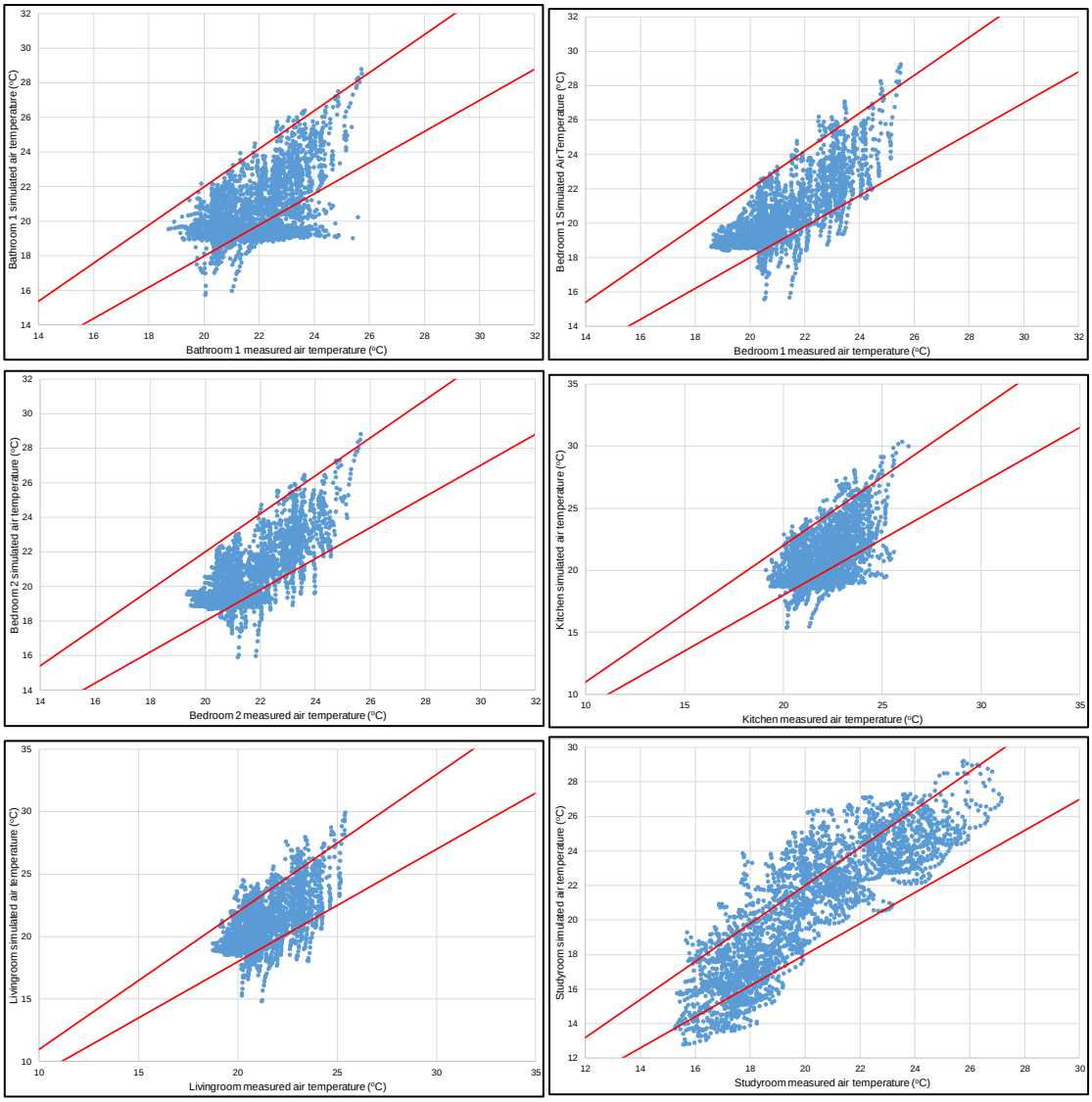

Figure 3-10: Palermo, Sicily case study house: statistical correlation; the red solid lines are the allowable ±10 % MBE margin of error) of the simulated air temperature compared to the onsite experimental measured air temperature for the bathroom 1, bedroom 1 and 2, kitchen, living room and study room.

3.3.2 EnergyPlus Model of Case Study House in Portmore, Jamaica

Firstly, the 3D geometry surfaces created in OS SketchUp Plug-in is exported to EP and defining the annual run period starting in January. The house was modelled into six thermal zones shown in Figure 3-11. The building envelope and internal heat gains were modelled according to the survey information provided by the occupant (see Table 3-2). The material properties of these construction materials were obtained from CIBSE Guide A, 2019, see Appendix A.1 for the detailed EP modelling of the case study. The modelled internal heat gain was based on the number of occupant(s), lighting, electric appliance, and gas burner. Also, the

air infiltration and natural ventilation were simulated using the EP airflow network model explained in section 3.3.1.

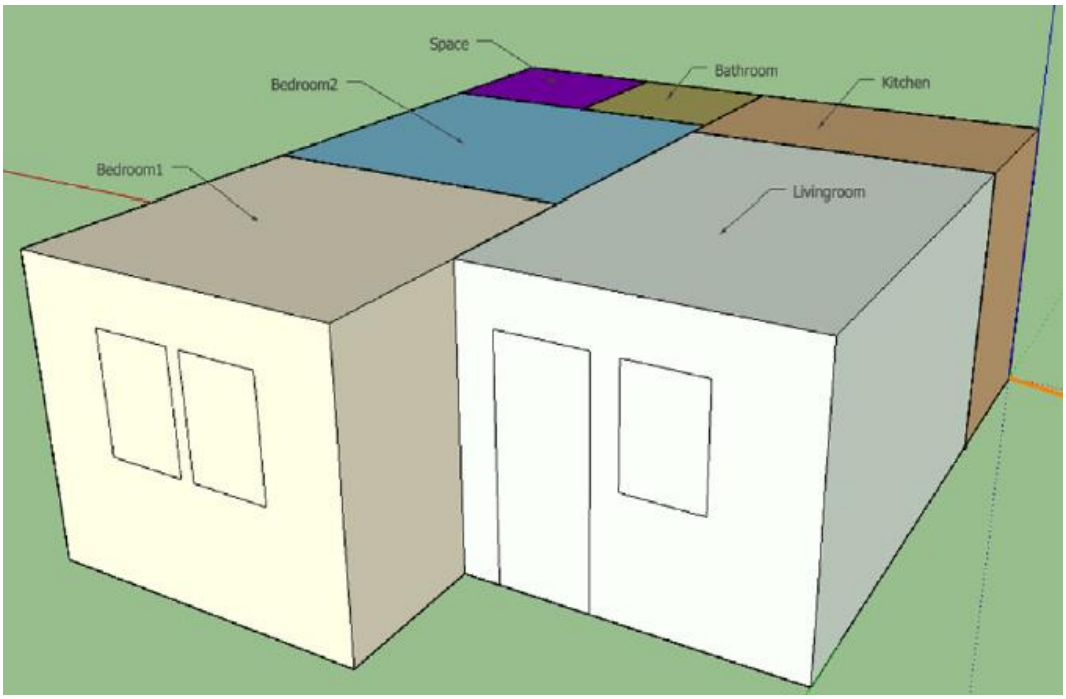

Figure 3-11: Thermal zones for the Portmore, Jamaica case study house.

Finally, the TMY weather file for Portmore, Jamaica was uploaded into the EP program to calculate the external and internal surface temperature, internal air temperature, cooling energy demand, and lighting and electric appliance energy consumption.

The onsite experimental measured weather values were measured to facilitate the calibration of the baseline computation model. The TMY weather file for Portmore, Jamaica was modified with the following acquired onsite experimental monitoring values; GHI, external air temperature and relative humidity. The modified TMY weather file covers the period from mid-January 2017 to mid-June 2017. The modified TMY weather file was only used for calibration purpose while the TMY weather file was used to model the annual building energy consumption and energy-efficient solutions studied in chapter 4. The TMY weather file DNI and DHI values required by EP, were obtained by extrapolation. Therefore, more accurate DNI and DHI values were calculated using the equation 3-4 that relates the onsite measure GHI with the DNI and DHI. For sunny days, it is reasonable to assume that 20 % and 80 % of the onsite measure GHI value by the comes from the DHI and DNI respectively (ASHRAE, 2017). In Jamaica, it is sunny throughout the year; therefore, the assumption was a reasonable one for

the period of simulation for the calibration.

$$GHI = DHI + DNI \cdot \cos(\theta), \theta \; is \; the \; zenith \; angle \qquad 3\text{-}4$$

The MBE and CVRMSE statistical values are presented in Table 3-4; which are within the recommended MBE and CVRMSE values of less than ±10 % and 30 % respectively relative to the hourly calibrated results (U.S. Department of Energy, 2015).

Table 3-4: MBE and CVRMSE of air and ceiling temperature for the Portmore, Jamaica case study house.

Thermal Zones	MBE	CVRMSE	MBE	CVRMSE
	Air temperature		Ceiling temperature	
Livingroom	7.8 %	7.6 %	8.3 %	12.0 %
Bedroom 1	8.1 %	6.3 %	8.9 %	8.4 %
Bedroom 2	8.9 %	7.5 %	9.9 %	11.1 %
Kitchen	8.8 %	7.6 %	8.2 %	10.8 %

Figure 3-12 presents the onsite experimental measured values and simulated results of the ceiling and air temperature in the livingroom, bedroom 1 and 2 for 3 days. At a glance, it can be seen that the simulated results are close to the onsite experimental measured one. Additionally, Figure 3-13 presents the correlation of the onsite experimental measured values and simulated results of the ceiling and air temperature in the livingroom, bedroom 1 and 2 for 1631 hours. More than 75 % of the points are within 10 % of the MBE error. These results indicate that the case study house for Portmore, Jamaica model was successfully calibrated.

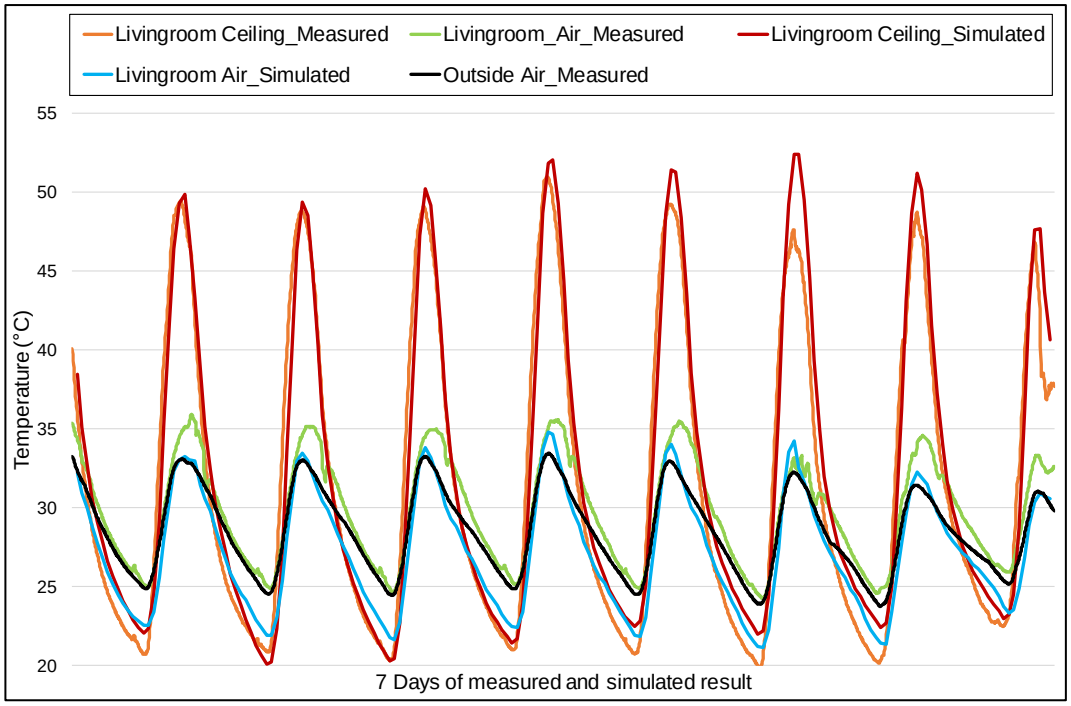

Figure 3-12: Portmore, Jamaica case study: simulated vs. onsite experimental measured air and ceiling temperature of the livingroom.

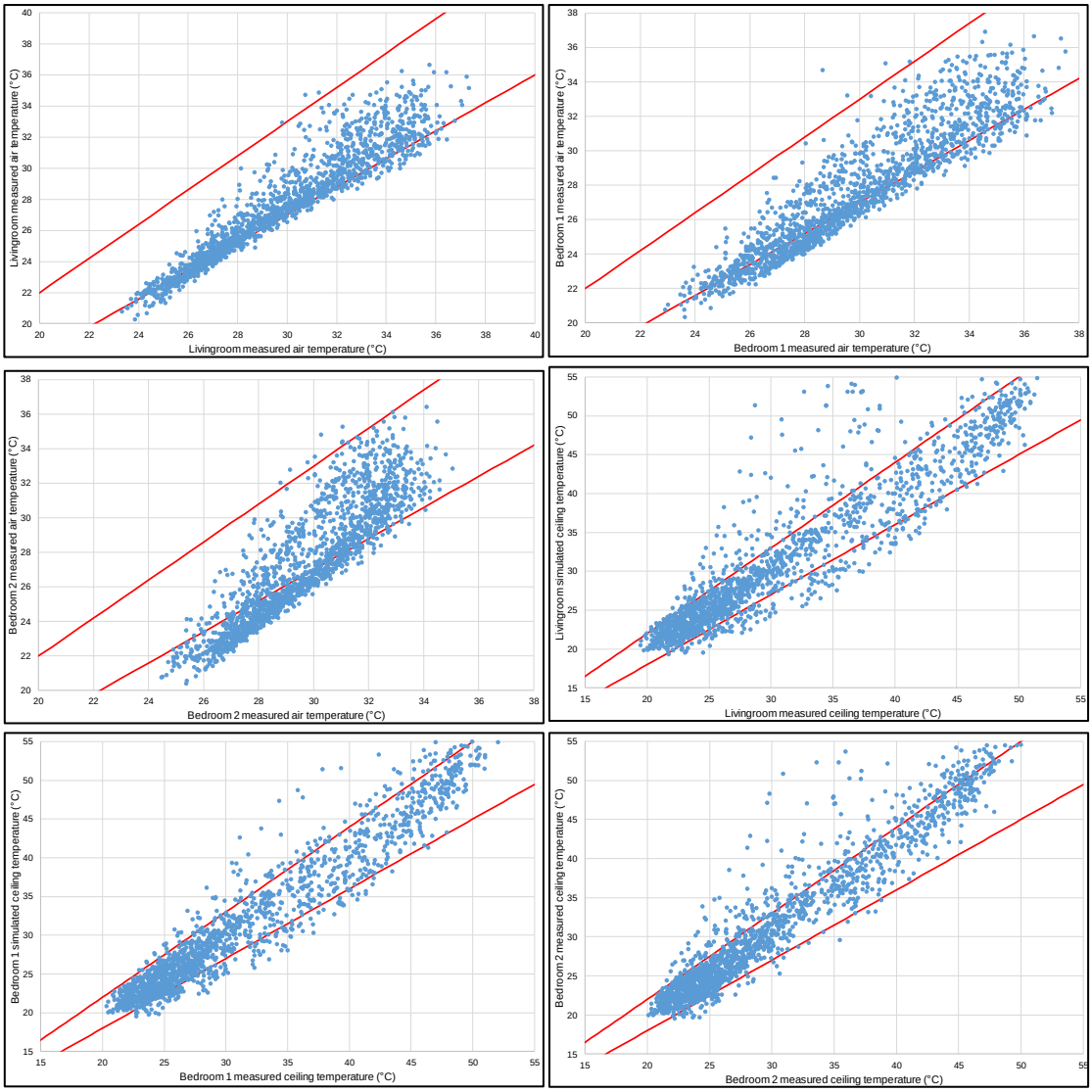

Figure 3-13: Portmore, Jamaica case study house: statistical correlation; the red solid lines are the allowable ±10 % MBE margin of error) of the simulated air temperature compared to the onsite experimental measured air temperature for the livingroom, bedroom 1 and 2 internal air temperatures and ceiling temperatures.

Chapter 3 Summary

Computational models using EP were developed for the case-study houses in Palermo, Sicily and Portmore, Jamaica. Required input parameters were acquired by on-site surveys and occupants' feedback. On-site monitoring of internal and external temperatures were carried out in the houses and were used for the calibration of the models. The computational models were successfully calibrated by comparing the simulated results with the onsite measured values. The successful calibrations of the computational models for Palermo, Sicily and Portmore, Jamaica was the first key milestone in this research project. This is because the calibrated

computational models were used to accurately assess the building energy consumption, energy savings and thermal comfort improvement by the energy-efficient solutions studied in chapter 4. The calibrated model was also used to accurately assess the energy production by the PV and PVT systems (the HCPV/T 2000x system was experimentally and analytically studied) studied in chapter 5.

Chapter 4: Energy Demand and Energy-Efficient Solutions for the Two Case Study Houses

Introduction

Chapter 4 presents the implementation of five energy-efficient solutions that were identified for residential building following the literature review presented in chapter 2. The five energy-efficient solutions are categorised into external (envelope) and internal interventions. The house envelope solutions are:

- Cool roof paint
- Roof thermal insulation
- Window shutters

The internal interventions are:

- A-rated electric appliances
- Light Emitting Diode (LED) lighting

The implementation of the five energy-efficient solutions was studied by calculating their energy savings potential and indoor thermal comfort improvement for the Palermo, Sicily and Portmore, Jamaica case study houses. Section 4.1 and section 4.2 presents the energy demand model of the case study houses and the implementation of the five energy-efficient solutions respectively. Section 4.3 presents the comparison of the energy-efficient solutions in terms of energy savings potential and indoor thermal comfort improvement.

4.1 Energy Demand of the Case Study Houses

The energy demand for the Palermo, Sicily and Portmore, Jamaica case study houses before the implementation of the five energy-efficient solutions was calculated by simulating the energy consumption of the operational electric appliances and lighting, heating and cooling energy demand using the calibrated EP model presented in chapter 3. Details and schedule of use for the electric appliances and lighting before the implementation of energy-efficient solutions were provided by the house occupants. Occupants also provided information on the use of the houses such as occupancy patterns and operation of openings and heating system in the case of Palermo. The calibrated EP model for Palermo, Sicily case study house (presented in section 3.3.1) is naturally ventilated according to the occupants' schedule from April to October, and with the heating system switched on when the indoor temperature falls below the temperature set point of 20 ℃. The calibrated EP model for Portmore, Jamaica case study house

(presented in section 3.3.2) is naturally ventilated according to the occupants' schedule throughout the year. The energy demand after the implementation of the external (envelope) interventions was calculated by editing the respective construction and material building information of the calibrated EP model. The energy demand after the implementation of the internal interventions was calculated by editing the respective design wattage level building information of the calibrated EP model.

The operational electric appliances and lighting energy demand were calculated using the EP design level calculation method and occupant usage schedule. The design level calculation method requires the entry of the operational electric appliance and lighting level. The heating and cooling energy demand were calculated using the EP "Ideal Loads Air System". The EP "Ideal Loads Air System" is a model that supplies the cooling or heating air to a zone in sufficient quantity to meet the zones load or set-point temperature (U.S. Department of Energy, 2019). The Palermo, Sicily case study house is occupied by a working family (3 occupants) that is home at night and weekend. The cooling energy was calculated with an assumed setpoint temperature of 24 ℃ from April to October; during this period, the house was naturally ventilated (the opening and closing of windows were controlled manually by the occupants) mostly in the morning and evening. The heating energy was calculated with an assumed setpoint temperature of 20 ℃ for the remaining months of the year. The Portmore, Jamaica case study house is occupied by a working occupant also at home at night and at weekends. The cooling energy was calculated with an assumed setpoint temperature of 24 ℃ all year; during this period, the house was naturally ventilated (the opening and closing of windows were controlled manually by the occupants) mostly in the morning and evening.

4.2 Energy Savings by Energy-Efficient Solutions

The energy savings potential of the five energy-efficient solutions for the Palermo, Sicily and Portmore, Jamaica case study houses were calculated using the developed and calibrated EP model presented in chapter 3 (section 3.3) and additional inputs as described in section 4.1. Results are presented in the next sections.

4.2.1 Cool Roof Paint Solution

The purpose of the computational study of cool roof paint is to calculate the cooling energy savings potential and internal air temperature reduction by cool roof paint after its applications on the roof of the Palermo, Sicily and Portmore, Jamaica case study houses. The studied cool roof paint is an economical, eco-friendly and waterborne liquid characterised with 0.84 initial solar reflectance (0.73 after three years of application), 0.90 thermal emittances (0.89 after three years of application), and initial solar reflectance index of 106 (90 after three years of application) (CRRC, 2019; ECRC, 2019). It was chosen from commercially available cool paints to have optimum characteristics described in section 2.2.2. Paint rather than a membrane was chosen for easiness of installation so that costs are kept as low as possible.

The cool roof paint for both case studies was modelled by redefining the solar absorbance of the exterior roof surface; the thickness of the cool roof paint was neglected. The approach is commonly used when modelling paints and other surface treatments with thickness up to only about 1 mm when dry (Suehrcke et al., 2008). Although the solar reflectance of the conventional roof of both case studies before cool roof paint application could not be measured as no samples are available, the solar absorptance value of the roof materials was sourced from (CIBSE Guide A, 2019). Before cool roof paint application, the solar absorptance of the roof for that of Palermo, Sicily case study was set as 0.70 because it is the value for roof waterproof covering (roof external layer), while Portmore, Jamaica case study was set as 0.85 because it is the value for the roof construction made of concrete. After the application of cool roof paint, the solar absorbance value is fixed at 0.18 for both case studies. See appendix A.1, Table A-1 and Table A-2 for the construction and material information for Palermo, Sicily and Portmore, Jamaica case study houses, respectively.

The cool roof paint intervention was additionally assessed via an experimental study of the Portmore, Jamaica case study house. The purpose of the experimental study was to acquire operational data pre- and after application of the cool roof paint. The experimental monitored data are GHI, roof and ceiling temperatures, external air temperature and relative humidity and internal air temperature and relative humidity. The house was first surveyed to determine the geometry (including areas of windows and doors) and construction of the house as well as equipment (including lighting) as sources of internal heat gains. Preliminary measurements of

the house started in September 2016; however, all monitoring sensors were installed in January 2017. The cool roof paint was applied between 22nd March 2017 and 16th April 2017. The experimental monitoring continued until July 2017. The data acquisition was carried out by research partner at the University of Technology, Kingston, Jamaica. However, I had full access to the data required to assess the cool roof paint investigation as a remote team member. Further details about the experimental monitoring of the cool roof paint is presented in appendix A.2.

4.2.2 Roof Thermal Insulation Solution

Similar to the cool roof paint study, the roof thermal insulation solution was simulated for both case studies to calculate the heating and cooling energy savings potential and thermal improvement by the roof thermal insulation after its application on the roof of the two case study houses. It was assumed that the roof thermal insulation was constructed on the external part of the roof. The roof thermal insulation was modelled in EP according to recommended U-values for better energy performance of residential buildings. The roof thermal insulation for Palermo, Sicily case study house adopted the recommended climatic zone B U-values for refurbished buildings; Palermo, Sicily is located in climatic zone B, one of the six climatic zones of Italy) (Italian Government - Ministry of Economical Progress, 2015). The roof thermal insulation for Portmore, Jamaica case study house adopted the recommended Jamaica Bureau energy code standard (Jamaica Bureau of Standards, 2019). Therefore, through trial and error by adjusting the roof thermal insulation thickness of the roof to achieve the recommended U-values presented in Table 4-1, the heat and cooling energy reduction, and internal air temperature improvement were calculated.

Table 4-1: Recommended U-values for better energy performance of residential buildings.

Recommended U-value (W/m^2K) for Palermo (Italian Government - Ministry of Economical Progress, 2015)	
Roof	0.32
Recommended U-value (W/m^2K) for Portmore (Jamaica Bureau of Standards, 2019)	
Roof	1.08

4.2.3 Window Shutter Solution

The window shutter solution was simulated for both case studies to calculate the heating and/or cooling energy savings potential and thermal improvement by the window shutter after its application on the external part of the window of the two case study houses. The window shutter was modelled as vertical oriented movable equidistance slat-type devices characterised with EP optical properties based on Simmler, Fischer and Winkelmann, 1996 (U.S. Department of Energy, 2019). The window shutter schedule was modelled according to the window opening and closing schedule. This allows the continuous natural ventilation of the house while investigating the energy savings potential and indoor thermal comfort improvement.

4.2.4 A-rated Electric Appliance and LED Light Solutions

The A-rated electric appliance and LED light solutions simulated for both case studies are household electric appliances and lights with lower energy demand ratings. The A-rated electric appliance and LED light solutions were modelled in EP by editing the power level of the operational electric appliances and lights. The simulated operational electric appliances and lights, and A-rated electric appliances and LED lights solutions are listed in Table 4-2.

Table 4-2: Operational electric appliance and light, and A-rated electric appliance and LED light solutions.

Palermo, Sicily case study		Portmore, Jamaica case study	
Operational electric appliances and lighting			
Operational appliance and light	Operational appliance and light level (W)	Operational appliance and light	Operational appliance and light level (W)
Incandescent light (x7)	60	Compact Fluorescent Lamp (x5)	14
Washing machine (x1)	740	TV (x1)	100
Fridge Freezer (x1)	60	Fan (x1)	20
Oven (x1)	1370	Fridge Freezer (x1)	352
Dishwasher (x1)	920	Microwave (x1)	293
TV (x1)	400		
Modem ADSL (x1)	7		
Desktop PC (x1)	97		
Total power level	4014 W	Total power level	835 W
A-rated electric appliances and LED lighting			
A-rated electric appliance and LED light	A-rated electric appliance and LED light level (W)	A-rated electric appliance and LED light	A-rated electric appliance and LED light level (W)
LED light (x7)	7	LED light (x5)	7
Washing machine (x1)	560	TV (x1)	50
Fridge Freezer (x1)	36	Fan (x1)	20
Oven (x1)	970	Fridge Freezer (x1)	36
Dishwasher (x1)	70	Microwave (x1)	244
TV (x1)	50		
Modem ADSL (x1)	7		
Desktop PC (x1)	48		
Total power level	1790 W	Total power level	385 W

4.3 Comparison of the Energy-Efficient Solutions

The simulation results presented in this section show the energy and indoor thermal comfort improvement due to the implementation of cool roof paint, roof thermal insulation, window shutter, A-rated electric appliances and LED lighting energy-efficient solutions.

4.3.1 Thermal Comfort Improvement

Table 4-3 presents simulated monthly reduction (negative) and/or increase (positive) of the

roof surface, ceiling surface and internal air temperature throughout the year after the implementation of cool roof paint, roof thermal insulation and window shutter for Palermo, Sicily and Portmore, Jamaica case study houses.

Results for cool roof paint

The simulated results for the implementation of cool roof paint show significant roof and ceiling surface temperature reduction, and moderate internal air temperature reduction. The highest roof surface, ceiling surface and internal air temperature reduction for Palermo, Sicily case study were -30.8 °C, -6.6 °C and -3.9 °C. The highest roof surface, ceiling surface, and internal air temperature reduction for Portmore, Jamaica case study were -32.6 °C, -24.8 °C and -5.7 °C, respectively.

In order to give a further insight of the pre and after cool roof paint application conditions, Figure 4-1 present six days simulated results of cool roof paint for Palermo, Sicily case study. The dates for the six days are 15th – 17th February (typical cold days of winter) and 6th – 8th August (typical hot days of summer). The dates 15th – 17th February have similar external average air temperature (8.3 °C, 11.5 °C and 12.6 °C respectively, Meteonorm, (2019)) and average global solar radiation intensity during daytime (226 W/m^2, 262 W/m^2 and 342 W/m^2 Meteonorm, (2019)). The dates 6th – 8th August have similar external average air temperature (25.4 °C, 24.5 °C and 25.7 °C Meteonorm, (2019)) and average global solar radiation intensity during daytime (522 W/m^2, 510 W/m^2 and 552 W/m^2 Meteonorm, (2019)). The summer days show higher roof surface, ceiling surface and internal air temperature reduction because the summer days have higher solar radiation and external air temperature as shown in Figure 3-2. For 15th – 17th February, the highest roof surface, ceiling surface and internal air temperature reduction was on the 15th February with maximum values of -9.8 °C, -2.7 °C and -1.8 °C. However, the internal air temperature reduction during the winter days results in a heating penalty. For 6th – 8th August, the highest roof surface, ceiling surface and internal air temperature reduction was on the 6th August, with maximum values of -30.4 °C, -8.00 °C and -3.8 °C. Figure 4-2 presents three days (4th – 6th May) simulated results of cool roof paint for Portmore, Jamaica case study. The dates have similar external average air temperature (29.4 °C, 29.7 °C and 29.8 °C Meteonorm, (2019)) and average global solar radiation intensity during daytime (772 W/m^2 for the three days Meteonorm, (2019)). The highest roof surface, ceiling surface and internal air temperature reduction was on the 5th May,

with maximum values of -23.0 ℃, -23.2 ℃ and -3.7 ℃. The temperature reduction for Portmore, Jamaica case study is higher because of the impact of external weather conditions and higher U-Value of the external envelope (Table 3-1 and Table 3-2, chapter 3).

Results for roof thermal insulation

The simulated results for roof thermal insulation show roof surface temperature increase, ceiling surface and internal air temperature reduction after the implementation of roof thermal insulation. For Palermo, Sicily case study, the highest roof surface temperature increase was 5.4 ℃. The ceiling surface and internal air temperature increased during the heating demand months (which includes the winter months) of January – March, November, and December. The increase was due to the heating of the house to a set-point temperature of 20 ℃, which is mostly higher than the external air temperature during this period. The highest ceiling surface and internal air temperature increase during the heating demand months were 3.7 ℃ and 2.6 ℃. The highest ceiling surface and internal air temperature reduction during the natural ventilation months (no cooling provided by cooling system) April to October were -7.0 ℃ and -3.1 ℃. For the Portmore, Jamaica case study, the highest roof surface temperature increase, ceiling surface and internal air temperature reduction were 4.0 ℃, -20.1 ℃ and -3.5 ℃ (the -8.5 ℃ in February is an anomaly) respectively. The anomaly occurred on the 2nd February, 11:00 – 12:00. The anomaly is because of the sharp increase in the hourly average global solar radiation intensity from 539 – 918 W/m^2 Meteonorm, (2019); the hourly average global solar radiation intensity between 08:00 – 09:00, 09:00 – 10:00 and 10:00 – 11:00 were 222 – 439 W/m^2, 439 – 636 W/m^2 and 636 – 539 W/m^2 (decreased) , respectively.

Further insight of the pre and after roof thermal insulation application conditions were investigated for the same days presented for pre and after cool roof paint application conditions. Figure 4-3 present simulation results of roof thermal insulation for Palermo, Sicily case study. The roof thermal insulation is characterised with high thermal absorptance (0.9 (CIBSE Guide A, 2019)), and low thermal conductivity of 0.025 $W/m.K$ (CIBSE Guide A, 2019); consequently leading to the low U-value of the roof, 0.32 W/m^2K (see Table 4-1; 0.32 W/m^2K) This causes the roof to absorb heat from the outside environment while reducing heat transfer into the house. These combined effects increase the roof surface temperature in the winter and summer days. The ceiling surface and internal air temperature increased and reduced in the winter and summer days, respectively. This is because during the winter days,

the thermal insulation prevents heat transfer from the internal space to the outside environment, and vice versa during the summer days. This is a positive effect as the operative temperature affected by radiant temperature will increase thermal comfort. For 15th – 17th February, the highest roof surface increase temperature increase was on the 16th February with maximum value of 3.6 ℃, ceiling surface and internal air temperature increase was on the 15th February with maximum values of 3.9 ℃ and 2.2 ℃. For 6th – 8th August, the highest roof surface increase, ceiling surface and internal air temperature reduction was on the 6th August with maximum values of 12.3 ℃, -6.8 ℃ and -2.8 ℃. Figure 4-4 present simulation results of roof thermal insulation for Portmore, Jamaica case study. The highest roof surface increase, ceiling surface and internal air temperature reduction was on the 5th May with maximum values of 18.6 ℃, -25.5 ℃ and -5.5 ℃. This will also have a positive impact on thermal comfort.

Results for window shutters

For the Palermo, Sicily case study, the implementation of the window shutter led to the reduction of the internal air temperature for the natural ventilation months of April to October. The highest decrease was -1.8 ℃. This is because the internal air temperature is mostly below or equivalent to the external air temperature, as shown in Figure 4-5. Therefore, the activation of the window shutter that covers all of the window glazed areas prevents the further increase in internal heat gain because of the reduction in solar heat gain via window by the external window shutter. For Portmore, Jamaica case study, the internal air temperature reduced throughout the year, as shown in Figure 4-6. The highest decrease was -0.3 ℃. The reason for the decrease is the same as that of Palermo, Sicily case study.

Further insight of the pre and after window shutter application conditions were investigated for the same days presented for pre and after cool roof paint and roof thermal insulation application conditions. Figure 4-5 present simulation results of window shutter for Palermo, Sicily case study. The internal air temperature showed no difference in winter days because of the low average global solar radiation intensity during daytime (226 W/m^2, 262 W/m^2 and 342 W/m^2 Meteonorm, (2019)), hence low solar heat gain. However, it reduced in the summer days because of the high average global solar radiation intensity during daytime (522 W/m^2, 510 W/m^2 and 552 W/m^2 Meteonorm, (2019)), hence high solar heat gain. For 6th – 8th August (winter days), the highest internal air temperature reduction was on the 6th August with maximum value of -1.5 ℃. Figure 4-6 present simulation results of window shutter for

Portmore, Jamaica case study. The highest internal air temperature reduction was on the 6th May with maximum values of -0.3 ℃.

The simulated results for the window shutter implementation indicate that it is the least beneficial in terms of indoor thermal comfort improvement compared to cool roof paint and roof thermal insulation.

Table 4-3: Reduction (-ve)/increase (+ve) of monthly average roof surface, ceiling surface and internal air temperature (°C) by cool roof paint, roof thermal insulation and window shutter.

Palermo, Sicily case study house							
Month	Cool roof paint			Roof thermal insulation			Window shutter
	Roof	Ceiling	Internal air	Roof	Ceiling	Internal air	Internal air
Jan	-21.5	-4.8	-3.0	1.5	3.5	2.6	0.0
Feb	-19.7	-3.8	-2.2	5.4	2.2	1.8	0.0
Mar	-26.2	-5.9	-3.3	3.4	0.3	0.9	0.0
Apr	-26.3	-6.2	-3.2	2.0	-3.2	-1.0	-1.7
May	-30.5	-6.5	-3.6	1.4	-5.1	-2.2	-1.5
Jun	-30.2	-6.6	-3.6	-0.3	-5.9	-2.8	-1.5
Jul	-30.8	-6.1	-3.9	0.3	-6.9	-3.1	-1.7
Aug	-30.3	-6.7	-3.7	-0.2	-7.0	-3.1	-1.7
Sep	-26.0	-5.8	-3.0	1.9	-3.6	-1.3	-1.8
Oct	-21.9	-4.8	-2.4	0.5	-2.0	-0.3	-1.8
Nov	-18.7	-4.0	-2.4	3.2	1.2	1.1	-0.3
Dec	-17.0	-3.5	-2.2	1.1	3.7	2.5	0.0
Portmore, Jamaica case study house							
Jan	-28.2	-22.0	-4.2	1.0	-14.0	-0.9	-0.3
Feb	-29.9	-22.9	-4.2	4.0	-15.0	-8.5	-0.2
Mar	-29.7	-22.6	-5.7	1.3	-17.4	-1.9	-0.2
Apr	-32.6	-24.8	-4.0	2.4	-19.3	-2.3	-0.3
May	-32.0	-24.4	-4.2	1.7	-20.1	-1.4	-0.2
Jun	-30.6	-23.4	-4.1	1.2	-17.6	-2.7	0.0
Jul	-27.2	-20.8	-2.6	4.0	-17.2	-3.3	0.0
Aug	-29.4	-22.7	-4.9	2.7	-17.7	-3.0	-0.2
Sep	-29.1	-22.4	-5.0	2.1	-17.2	-1.4	-0.1
Oct	-28.6	-22.2	-3.6	1.2	-16.3	-3.5	-0.2
Nov	-28.1	-21.6	-3.1	3.5	-15.7	-3.3	-0.1
Dec	-25.0	-19.4	-5.0	0.4	-14.5	-3.3	-0.1

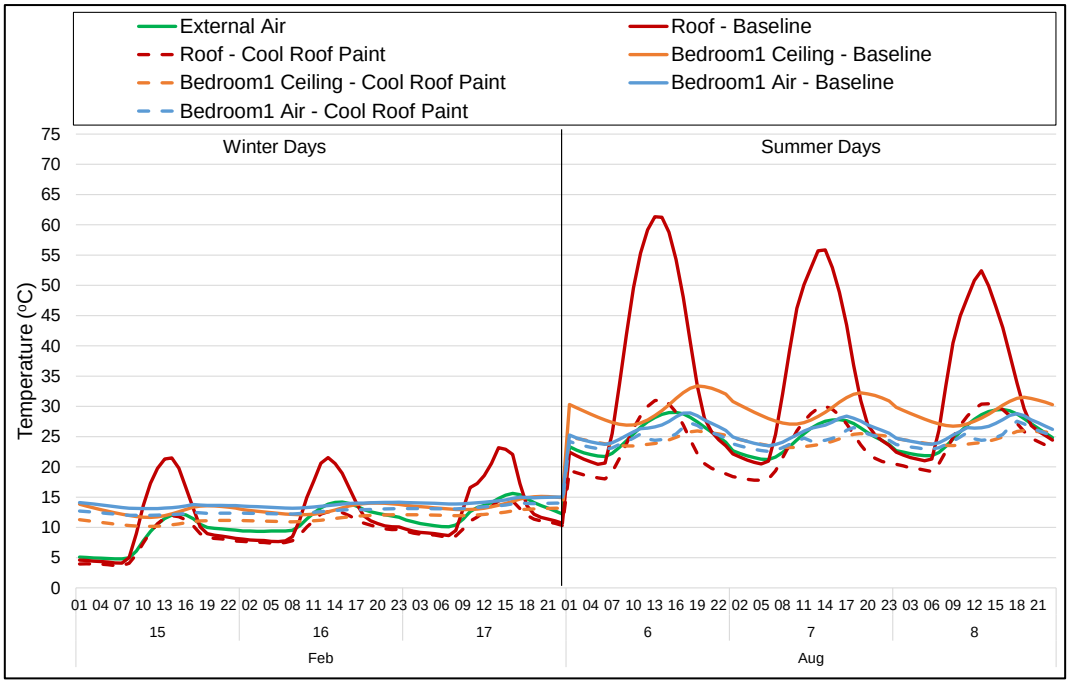

Figure 4-1: Palermo, Sicily case study house: simulated roof, bedroom1 ceiling and air temperature before and after the application of cool roof paint.

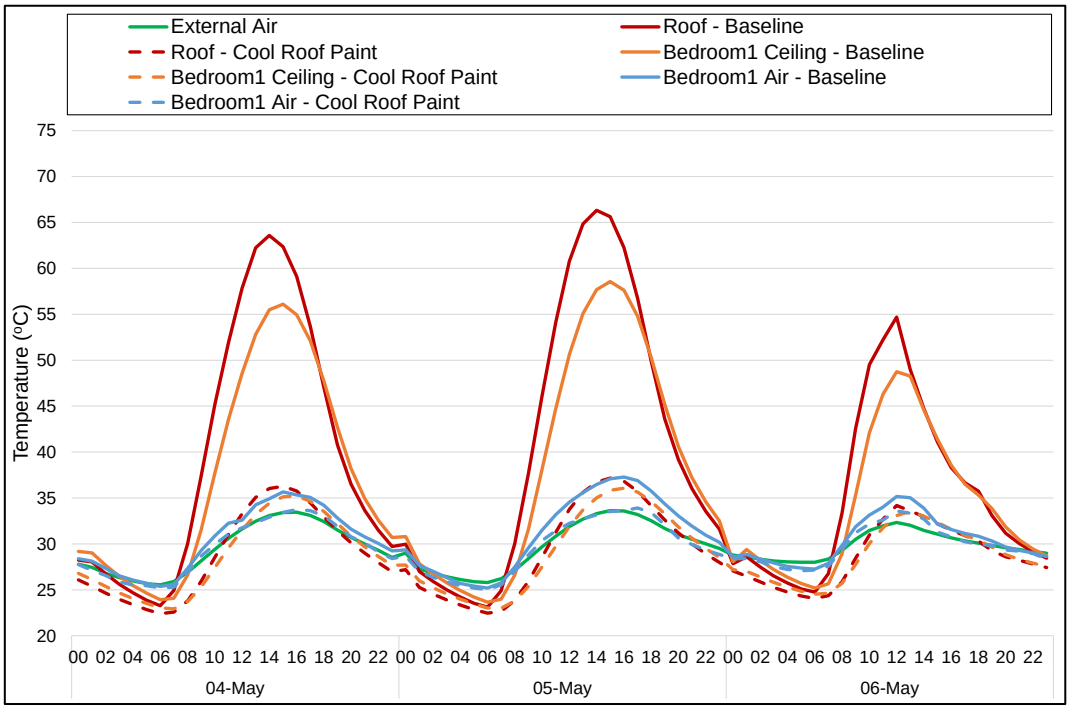

Figure 4-2: Portmore, Jamaica case study house: simulated roof, bedroom1 ceiling and air temperature before and after the application of cool roof paint.

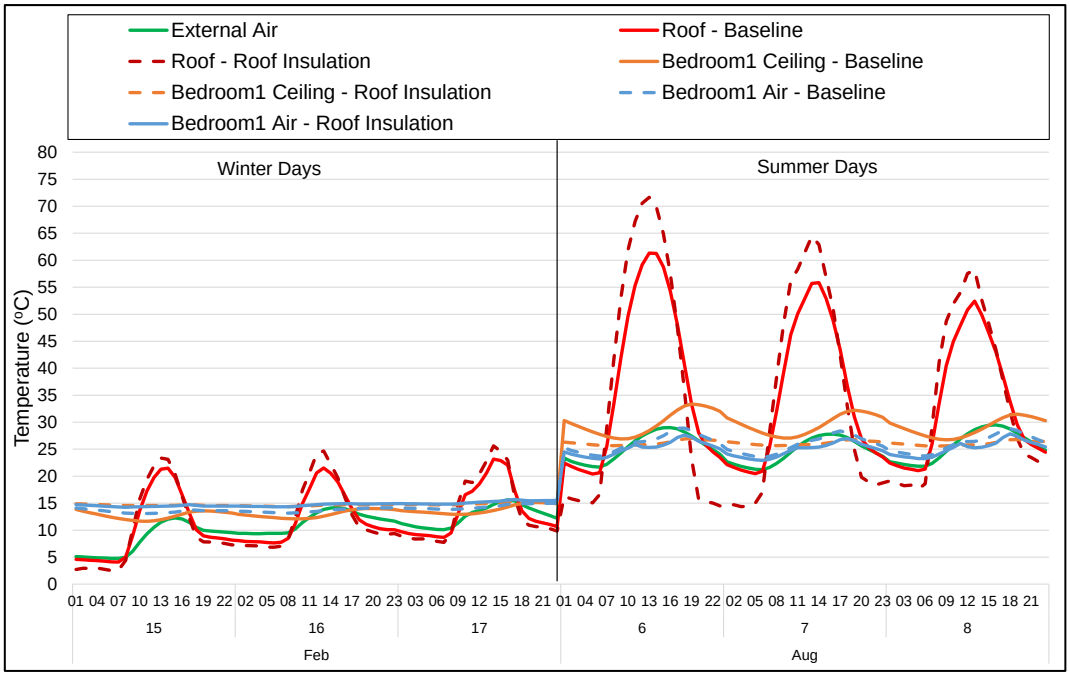

Figure 4-3: Palermo, Sicily case study house: simulated roof, bedroom1 ceiling and air temperature before and after the application of roof thermal insulation.

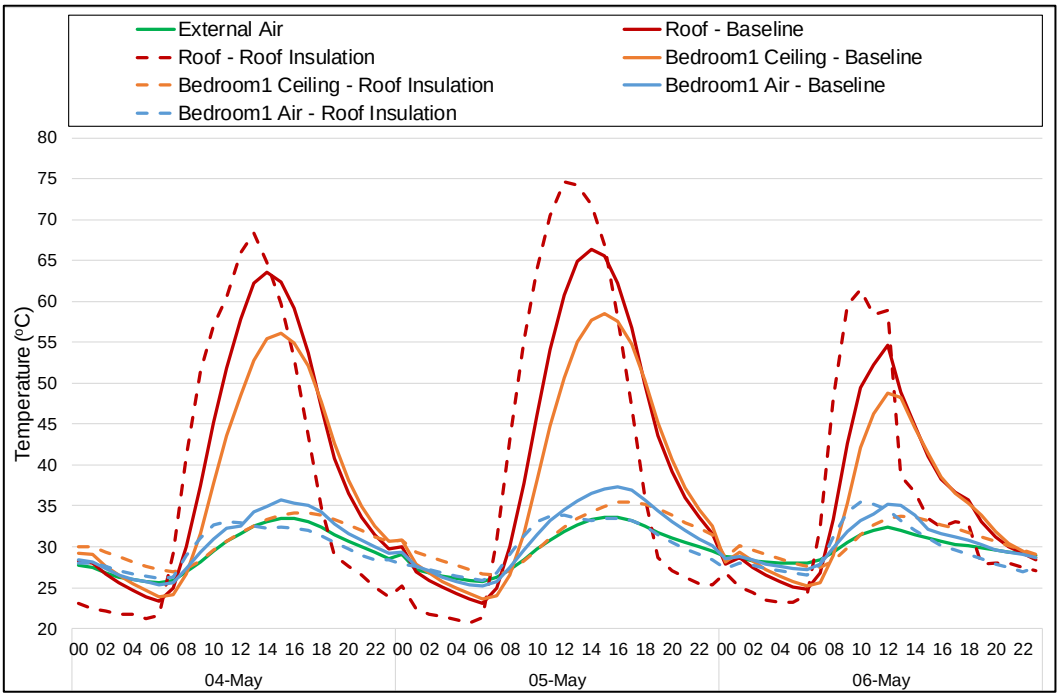

Figure 4-4: Portmore, Jamaica case study house: simulated roof, bedroom1 ceiling and air temperature before and after the application of roof thermal insulation.

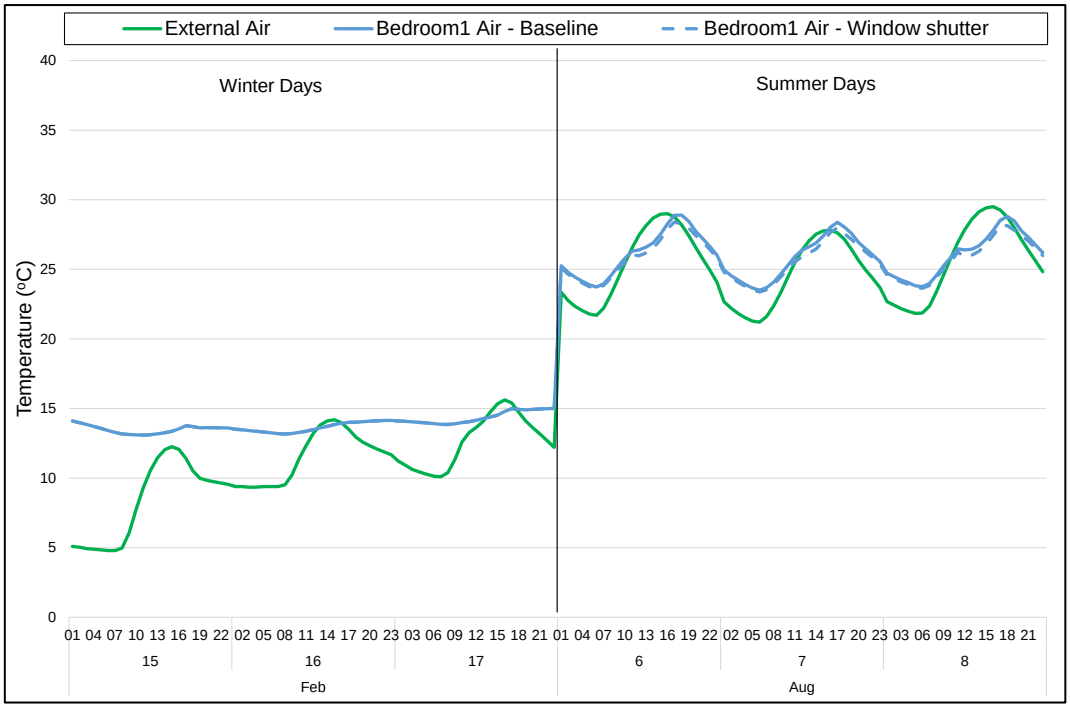

Figure 4-5: Palermo, Sicily case study house: simulated roof, bedroom1 ceiling and air temperature before and after the application of window shutter.

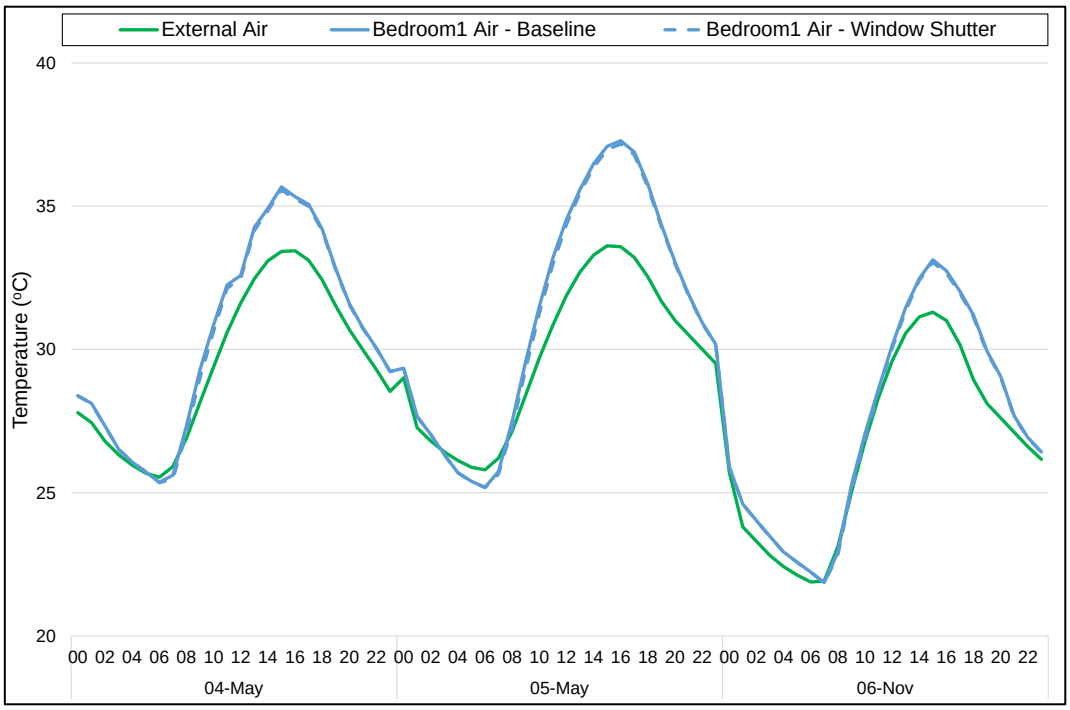

Figure 4-6: Portmore, Jamaica case study house: simulated bedroom1 ceiling and air temperature before and after the application of window shutter.

4.3.2 Energy Savings Potential

The energy savings potential after the implementation of the external interventions (cool roof paint, roof thermal insulation and window shutter) was calculated by estimating the difference between the energy demand before and after the implementation of cool roof paint, roof thermal insulation and window shutter. The energy demand difference was calculated by editing (and simulating) the respective construction and material (before the implementation of the external interventions) building information of the validated EP model. For Palermo, Sicily case study house, the cooling energy savings were calculated assuming the house was maintained at 24 °C from April to October. The heating energy savings were calculated assuming the house was maintained at 20 °C for the remaining months of the year. The annual cooling energy savings potential after the implementation of cool roof paint, roof thermal insulations and window shutter were calculated to be -29 $kWh/m^2/year$, -25 $kWh/m^2/year$ and -6 $kWh/m^2/year$. The heating energy savings potential after the implementation of roof thermal insulations was calculated to be -5 $kWh/m^2/year$. The window shutter had no effect on the heating energy savings potential. However, the cool roof paint increased the heating demand by +7 $kWh/m^2/year$; this is because the cool roof paint reflects solar radiation, thereby reducing heat transfer through the building roof. Therefore, the net cooling and heating energy savings after the application of cool roof paint is 22 $kWh/m^2/year$. For Portmore, Jamaica case study house, the cooling energy savings were calculated assuming the house was maintained at 24 °C all year. The annual cooling energy savings potential presented in Figure 4-7 and Figure 4-8 after the implementation of cool roof paint, roof thermal insulations and window shutter were calculated to be -189 $kWh/m^2/year$, -194 $kWh/m^2/year$ and -8 $kWh/m^2/year$, respectively.

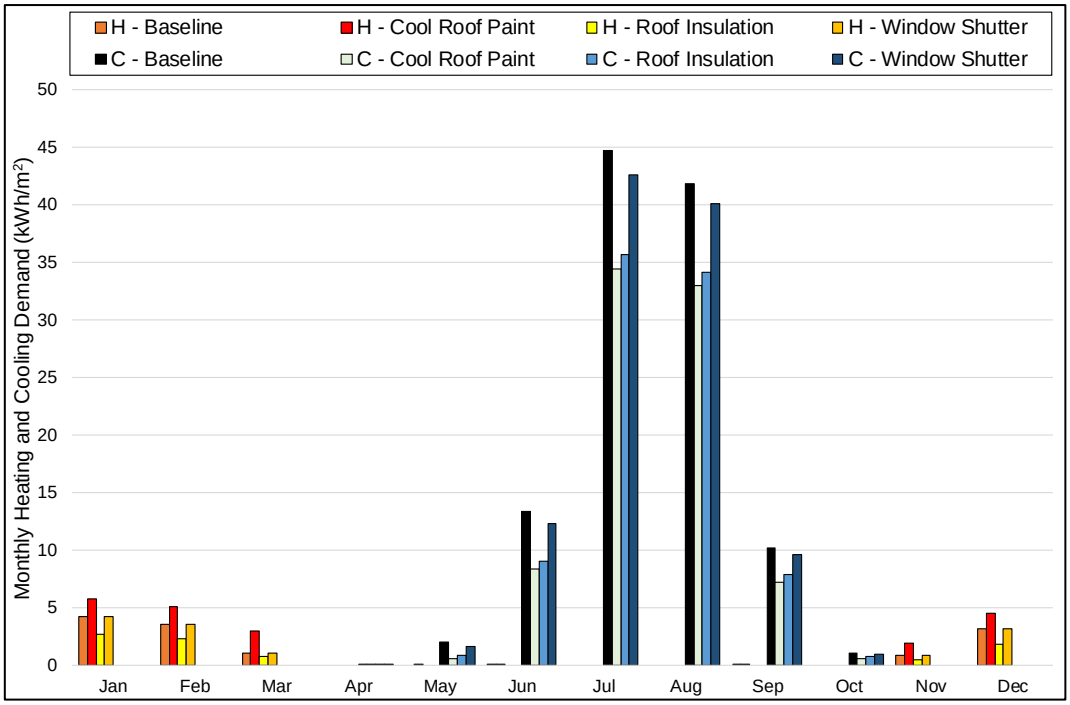

Figure 4-7: Palermo, Sicily case study house: monthly heating and cooling energy demand baseline, cool roof paint and roof thermal insulation according to local guidelines.

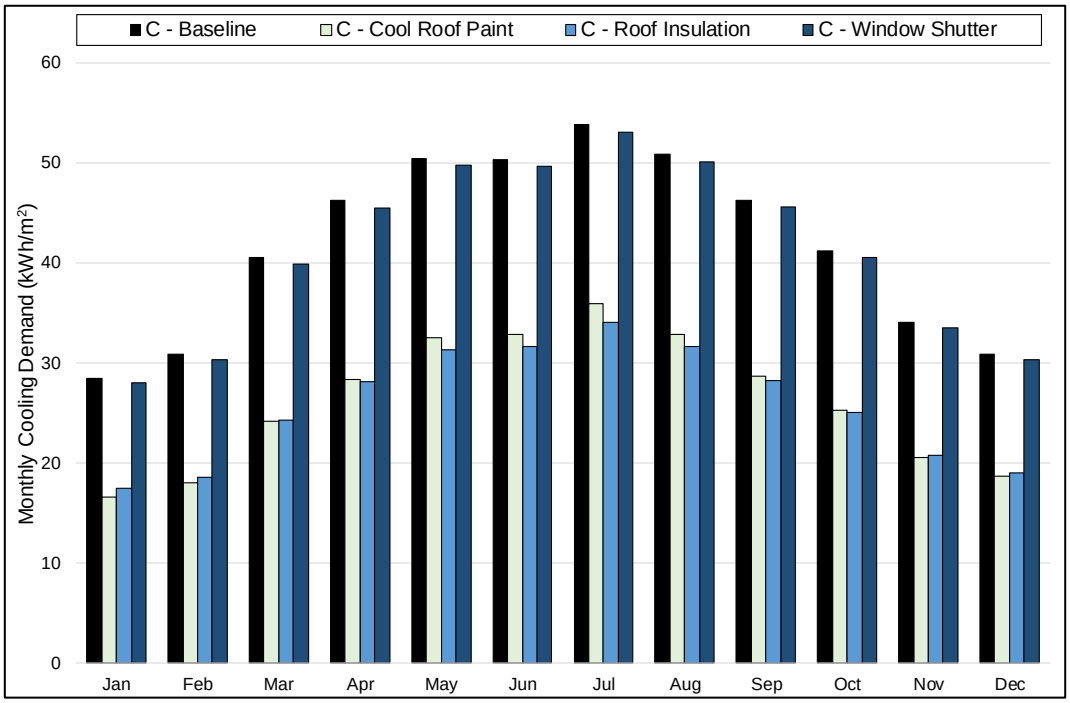

Figure 4-8: Monthly cooling energy demand of Portmore, Jamaica case study house of current, cool roof paint and roof thermal insulation according to local guidelines.

The energy savings potential after the implementation of the internal interventions (A-rated electric appliances and LED lights) was calculated by estimating the difference between the energy demand before and after the implementation of A-rated electric appliances and LED

lights. The energy demand difference was calculated by editing (and simulating) the respective operational electric appliance and light (before the implementation of the internal interventions) design wattage level of the validated EP model. The operational electric appliances and lights, and A-rated electric appliances and LED lights design wattage level are in Table 4-2.The total annual energy savings potential presented in Figure 4-9 and Figure 4-10, by the A-rated electric appliances and LED lights for Palermo, Sicily and Portmore, Jamaica case studies is -1178 kWh/year (A-rated electric appliances savings are -757 kWh/year and LED lights are -421 kWh/year) and -2998 kWh/year (A-rated electric appliances savings are -2940 kWh/year and LED lights are -58 kWh/year) and respectively.

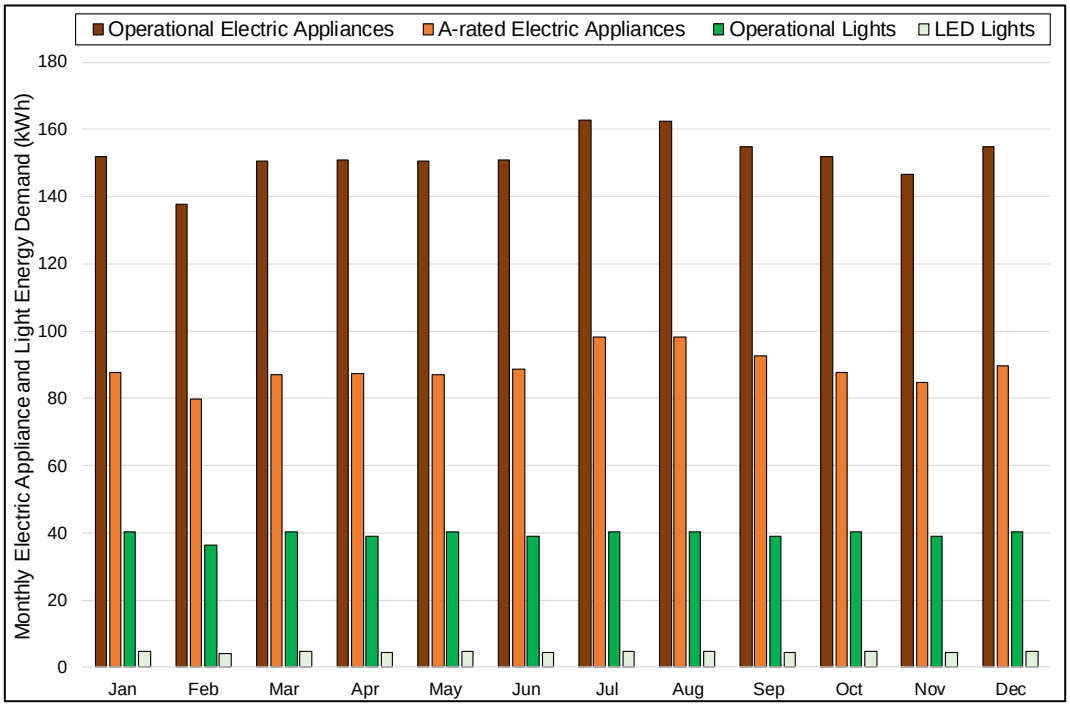

Figure 4-9: Monthly energy demand of Palermo, Sicily case study house of operational electric appliances and lights, A-rated electric appliances and LED lights.

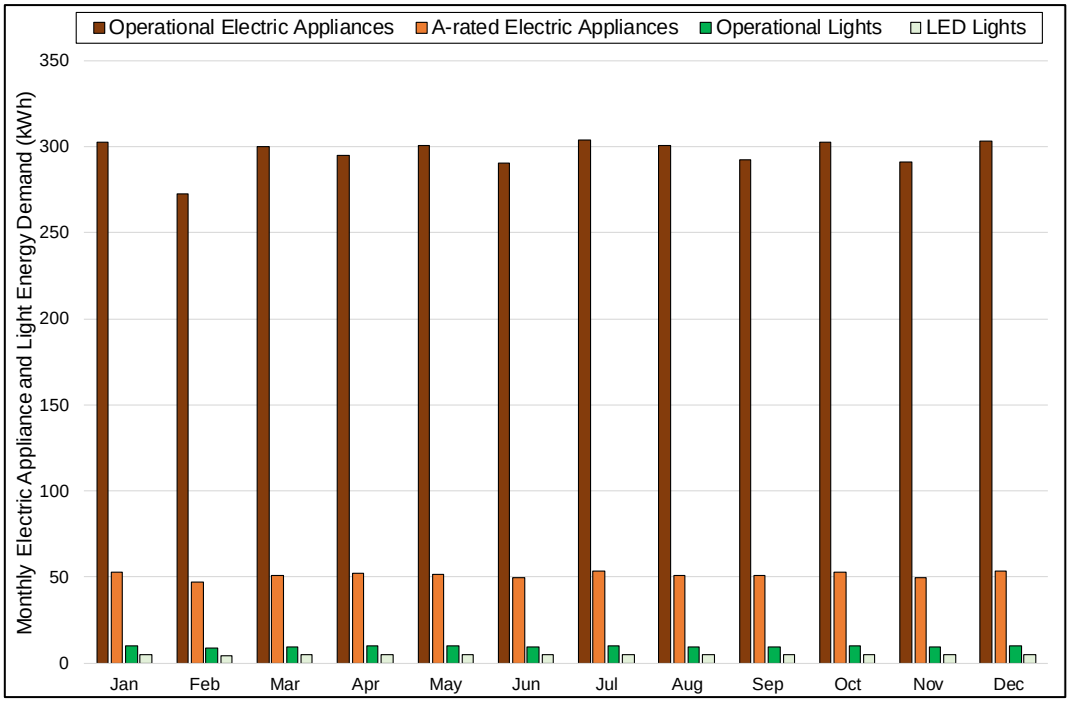

Figure 4-10: Monthly energy demand of Portmore, Jamaica case study house of operational electric appliances and lights, A-rated electric appliances and LED lights.

Table 4-4: Simulated annual energy savings potential in kWh/year by the two energy-efficient electric appliances and light solutions and three houses retrofit solutions. The cooling and heating energy savings in kWh/m^2/year are converted to kWh/year by multiply with the floor area in m^2.

Palermo, Sicily case study house (100.4 m^2 floor area)			
Energy-efficient electric appliance and light solutions		House retrofit solutions (Cooling and heating energy demand and savings in kWh/year)	
Operational electric appliances	1826	Baseline	12626
A-rated electric appliances	1069	Cool roof paint	10452
Energy savings potential	*-757*	*Energy savings potential*	-2174
Operational lights	476	Baseline	12626
LED lights	55	Roof thermal insulation	9666
Energy savings potential	-421	*Energy savings potential*	-2960
		Baseline	12626
		Window shutter	12024
		Energy savings potential	-602
Portmore, Jamaica case study house (36 m^2 floor area)			
Energy-efficient electric appliance and light solutions		House retrofit solutions (Cooling energy demand and savings in kWh/year)	
Operational electric appliances	3555	Baseline	18145
A-rated electric appliances	616	Cool roof paint	11327
Energy savings potential	*-2940*	*Energy savings potential*	-6818
Operational lights	117	Baseline	18145
LED lights	58	Roof thermal insulation	11176
Energy savings potential	-58	*Energy savings potential*	-6969
		Baseline	18145
		Window shutter	17862
		Energy savings potential	-283

Chapter 4 Summary

The simulation results show that the cool roof paint and roof thermal insulation are the two highest energy savings technologies amongst the five energy-efficient technologies that were studied for the Palermo, Sicily and Portmore, Jamaica case study houses, as shown in Table 4-4. For the studied cool roof paint, simulation results using EP models calibrated with measurements from the houses show that potential energy savings are -22 $kWh/m^2/year$ for the house in Palermo, Sicily and -189 $kWh/m^2/year$ for Portmore, Jamaica. This indicates the high energy savings potential in more poorly insulated roofs in locations with high solar radiation throughout the year and high ambient temperatures. It also shows that it is a worth-while retrofit options in locations with high solar radiation but also some heating demand. The cool roof paint energy savings were compared with savings due to roof thermal insulation according to the local guidelines (0.32 W/m^2K in Sicily and 1.08 W/m^2K in Jamaica). The simulation results show that energy savings by cool roof paint or roof thermal insulation are similar in Portmore, Jamaica (-189 $kWh/m^2/year$ with the cool roof paint and -194 $kWh/m^2/year$ with the roof thermal insulation) while the heating penalty in Palermo, Sicily results to higher energy savings with roof thermal insulation (-22 $kWh/m^2/year$ for cool roof paint and -30 $kWh/m^2/year$ for roof thermal insulation). This is also influenced by the low U-value of roof thermal insulation in Sicily. In conclusion the following points can be made:

- Cool roof paint and roof thermal insulation are effective energy-efficient solutions.
- Cool roof paint and roof thermal insulation have comparable energy saving potential.
- The indoor thermal comfort improvement by the cool roof paint is higher than the roof thermal insulation.
- Cool roof paint is an attractive low-cost house retrofit solution compared to roof thermal insulations.

The energy savings by the cool roof paint were used as input (for the defined functional unit of study) required for the lifecycle environmental impact of the cool roof paint, and comparison with roof thermal insulation for the Palermo, Sicily and Portmore, Jamaica case studies. The lifecycle environmental impact study is presented in chapter 6. Before the lifecycle environmental impact of the cool roof paint is presented, the next chapter 5 presents the experimental monitoring, computational and analytical assessment of the selected solar energy systems.

Chapter 5: HCPV/T 2000x System for Electrical and Thermal Energy Production

Introduction

As presented in chapter 2, section 2.2.3, solar energy systems are more suitable and efficient in residential buildings in hot climates with high solar radiation intensity throughout the year. They have capability to produce electrical and/or thermal energy for household demand. Chapter 5 presents the experimental monitoring and analytical model development result of the HCPV/T 2000x system. Section 5.1 presents a description of the system. Section 5.2 presents the experimental monitoring carried out in 2018, and the results from the experimental monitoring data. Section 5.3 presents the analytical model development of the system to calculate the outputs of the system for other locations. Section 5.4 presents the comparison of the output performance of the HCPV/T 2000x system with typical PV and PVT systems.

The experimental monitoring of the HCPV/T 2000x system was carried out as part of work package 5 (Integration, Innovation) of the Marie Curie SMART GEMS project. The contribution to work package 5 was achieved during my nine months (October 2017 to June 2018) secondment to IDEA SRL, (a SMART GEMS project partner) located in Palermo, Sicily. I spent the first three months working with the team of engineers in IDEA SRL to test the performance of the HCPV/T 2000x system tracking mechanism. The HCPV/T 2000x system tracking mechanism tracks the sun during operation to focus solar radiation on the solar cell at 2000x concentration ratio. The experimental monitoring of the HCPV/T 2000x system started in January 2018 until June 2018. The electrical and thermal data acquired in January and February 2018, was further used to evaluate the accuracy of the HCPV/T 2000x system tracking mechanism. The electrical and thermal data acquired from March to June 2018, was used to evaluate the electrical and thermal performance of the system.

5.1 Description of the HCPV/T 2000x System

The HCPV/T 2000x system comprises of three integrated subsystems: electrical energy system, thermal energy systems, and tracking system. The HCPV/T 2000x system is presented in Figure 5-1 and Figure 5-2 while Figure 5-3 presents a schematic diagram of the electrical and thermal systems. Figure 5-1 shows the experimental system which comprises of four modules (1–4). Each module is divided into two semi-modules and the electrical energy system (Figure 5-3) comprises of a parallel electric circuit arrangement of two semi-modules (North-side and

South-side, denoted [1a] and [1b] respectively in Figure 5-1). Each semi-module consists of 10 Indium-Gallium-Phosphide/Indium-Gallium-Arsenide/Germanium (InGaP/InGaAs/Ge) solar cells arranged in series. The electric circuit is connected to a 1 kW smart grid inverter characterized with Maximum Power Point Tracking (MPPT) to continuously generate maximum possible power. The thermal energy system consists of 20 active heat sink and a reverse return system uses flowing demineralized water to produce thermal energy. Each active heat sink contains an aluminium heat exchanger plate which is responsible for the heat transfer from the hot InGaP/InGaAs/Ge solar cells to the flowing demineralized water. The active heat sink designed with one inlet pipe and one outlet pipe was assembled in an adjacent position to the InGaP/InGaAs/Ge solar cell. The reverse return system is a type of closed-loop system used in a piping system with multiple inlet and outlet branches to maintain a constant flow rate and constant temperature change of the flowing water between the inlet and outlet of each branch (Ruch et al., 2014). As a result, the same magnitude of heat is extracted from each active heat sink that constitutes part of the thermal energy system. The active heat sink and reverse return system was adopted as an active cooling system needed to maintain the designed flowrate at 1 litre per minute, that is required to operate the InGaP/InGaAs/Ge solar cell at the designed operating temperature of 20 ℃ to 90 ℃ (maximum 110 ℃) while simultaneously extracting heat that is required for thermal energy production. The tracking system, which is made from hardware and software systems is a 2-axis tracker and is responsible for achieving the solar Concentration Ratio (CR) of 2000x. The hardware tracking system consists of an axle, structural support and reflective mirror and optical receiver that is aligned with the North-South configuration to accurately track the sun via a simultaneous rotational motion of the North-South longitudinal axle and tilting motion of the East-West transverse axle of the HCPV/T 2000x system. The rotation and tilting motions are enabled by the coaxial rotational and linear motors respectively, each connected to a magnetic encoder position sensor that is driven by suitable drivers connected to the electronic board. The accurate tracking of the sun requires the software tracking system. The electronic board is connected to a software system called Zeroplus, used to control and monitor the operational HCPV/T 2000x system. The software uses the solar position algorithm of the National Renewable Energy Laboratory (NREL). The tracking accuracy for a visible sunny or clear day is increased with the installed complementary metal oxide semiconductor webcam which is part of the tracking system.

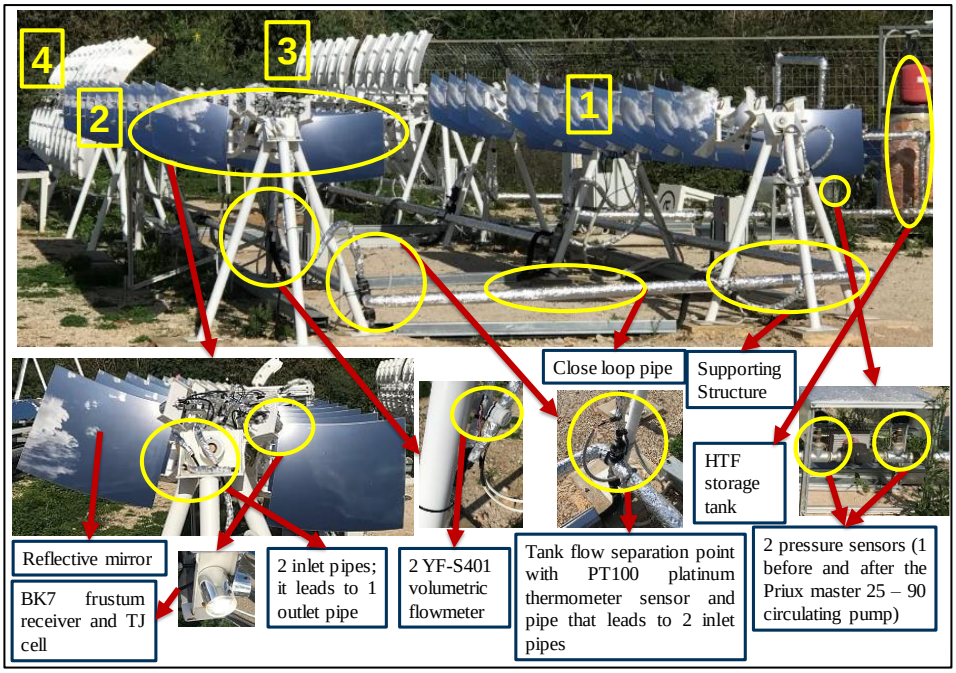

Figure 5-1: Pictorial description of the operating HCPV/T 2000x system; 1 – 4 are the HCPV/T 2000x system modules (number 2 was the experimentally study module), (a) – reflective mirror, (b) – BK7 frustum optical receiver (integrated with InGaP/InGaAs/Ge solar cell), (c) – 2 inlet pipes (it leads to 1 outlet pipe), (d) – 2 YF-SF01 volumetric flowmeter, (e) – flow separation point with PT100 platinum thermometer sensor and pipe that leads to the 2 inlet pipes, (f) – close loop pipe, (g) – structural foot support, (h) –demineralized water storage and (i) – 2 pressure sensors (1 before and after the Priux master 25 – 90 circulating pump).

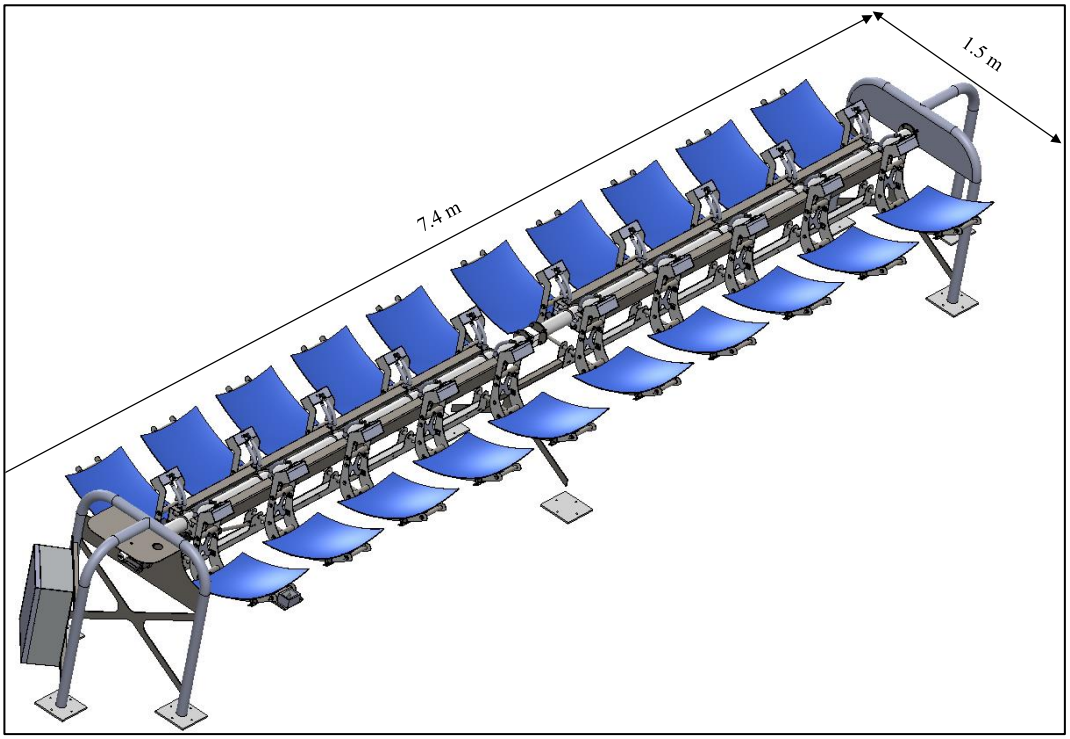

Figure 5-2: HCPV/T 2000x system Computer Aided Design (CAD) model; 11 m^2 footprint in area.

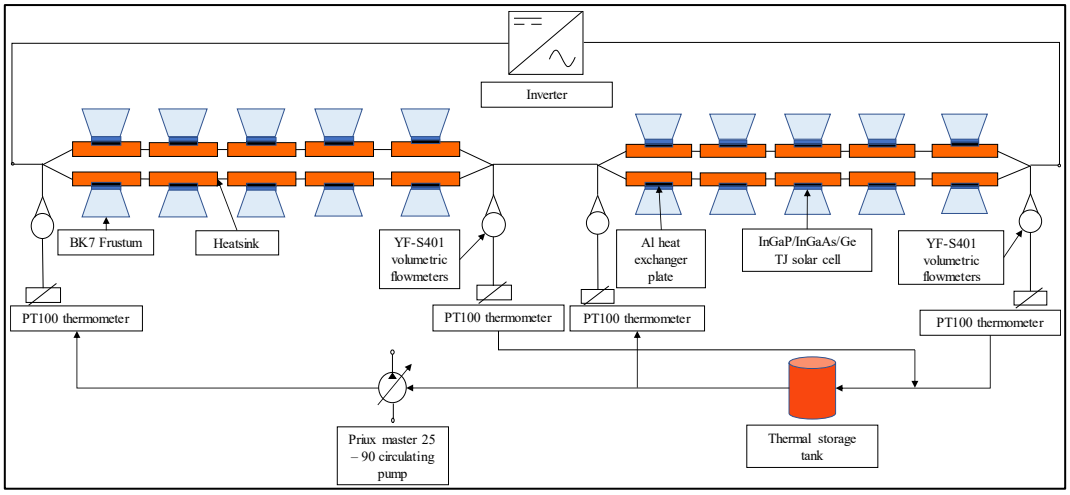

Figure 5-3: Electrical and thermal system schematic of the HCPV/T 2000x system.

5.2 Experimental Monitoring of the HCPV/T 2000x System

The aim of the experimental monitoring was to acquire data from the operational HCPV/T 2000x system to evaluate the electrical and thermal performance of the system. The electrical and thermal performance of the HCPV/T 2000x system are influenced by the InGaP/InGaAs/Ge solar cell temperature and demineralised water temperature. Two experiments were conducted to investigate the performance of the system as a function of varying demineralised water temperature; the demineralised water temperature was used as a reference parameter to characterise the behaviour of the InGaP/InGaAs/Ge solar cell with the change in temperature. In the first experiment conducted between 1 March 2018 to 22 May 2018 (electrical and thermal data were monitored between 6 am to 3 pm), the demineralised water circulating the active cooling system was not bypassed from the 0.2 m^3 demineralised water storage tank. In the second experiment conducted between 23 May 2018 to 25 June 2018 (electrical and thermal data were monitored between 6 am to 3 pm), the demineralised water was bypassed from the 0.2 m^3 demineralised water storage tank. The bypass increased the demineralised water temperature up to 53 °C, as shown in Figure 5-10. The operational HCPV/T 2000x system performance is explained in sections 5.2.1 and 5.2.2. The data collected include current (I), voltage (V), demineralised water temperature (inlet temperature (T_{in}) and outlet temperature (T_{out})), volumetric flowrate ($\dot{V}$), and onsite DNI (G_i) recorded on average six times per minute; these were used to calculate the electrical and thermal performance of the HCPV/T 2000x system.

The inlet and outlet temperatures were measured with four PT100 platinum thermometer sensors with accuracy of ±0.05 %; each semi-module has two sensors located at the inlet and outside sides (one of the sensor at the inlet is shown in Figure 5-1, labelled "(e)") of the flowing demineralised water. The volumetric flowrate was measured with two YF-S401 volumetric flowmeters located at the East and West sides of the South-side semi-module (shown in Figure 5-1, labelled "(d)"), with flowrate measurement range of 0.3 litre per minute to 6 litre per minute at water pressure of 0.8 MPa and accuracy of ±5 %. The onsite DNI was measured with the onsite installed 2-axis alt-azimuth STR-22G sun tracker (shown in Figure 5-4, (a)) with point accuracy < 0.01 °, for solar elevation of 0 to 87 °. The software control system (Zeroplus) connected to the electronic board of the HCPV/T 2000x system that controls the tracking system was also used to monitor and acquire the current, voltage, demineralised water temperature, volumetric flowrate and the onsite DNI experimental monitoring data, which were logged in MySQL database. The Zeroplus software system web interface (shown in Figure 5-4, (b)) displays the electrical, thermal, tracking (including the complementary metal oxide semiconductor webcam) and weather condition status of the operational HCPV/T 2000x system (referred to as Tracker3); the Tracker3 labelled North and South are the North and South side semi-modules respectively.

(a)

(b)

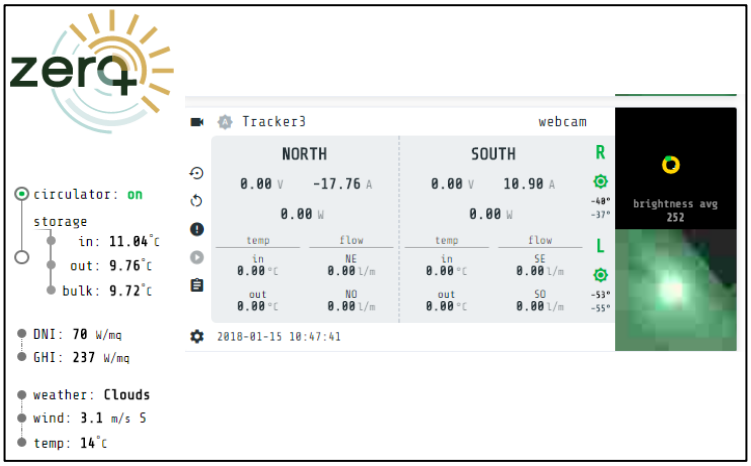

Figure 5-4: (a) Onsite 2-axis alt-azimuth STR-22G sun tracker. (b) Zeroplus software web interface. On the left-hand side is the information about the temperature of the circulating demineralised water temperature at the storage tank and weather information (DNI, GHI, wind speed, ambient temperature, and cloud condition). On the right-hand side is the information about the North and South side semi-modules, each displaying the instantaneous I and V, T_{in} and T_{out} and $\dot{V}$ of the flowing demineralised water, and the rotational and tilting position of the HCPV/T 2000x system.

5.2.1 Experimental Electrical and Thermal Energy Production

The electrical ($P_{el,p,HCPVT,exp}$) and thermal power ($Q_{th,p,HCPVT,exp}$) produced by the HCPV/T 2000x system can be calculated using equations 5-1 and 5-2 respectively, using the experimentally measured parameters. The parameters ρ_w, c_w, T_{in} and T_{out} are density of water, specific heat capacity of water, inlet and outlet temperature of the water.

$$P_{el,p,HCPVT,exp} = I \cdot V \quad 5\text{-}1$$

$$Q_{th,p,HCPVT,exp} = \rho_w \cdot \dot{V} \cdot c_w \cdot (T_{out} - T_{in}) \quad 5\text{-}2$$

The electrical power ($P_{el,p,HCPVT,der}$) produced by the HCPV/T 2000x system at any given time in a typical year can be calculated by using the derived equation 5-3. This was obtained using experimental data between 1 March 2018 and the 22 May 2018 as presented in Figure 5-5. $P_{el,p,HCPVT,exp}$, was calculated using equation 5-1 and the graph shows measured I and V versus instantaneous onsite DNI G_i; the graph shows that the coefficient of determinant, R^2 equal to 0.91 for the experimental results.

$$P_{el,p,HCPVT,der} = 0.5m^2 \cdot G_i + 71.1W, \quad for\ Gi \geq 60\ W/m^2 \quad 5\text{-}3$$

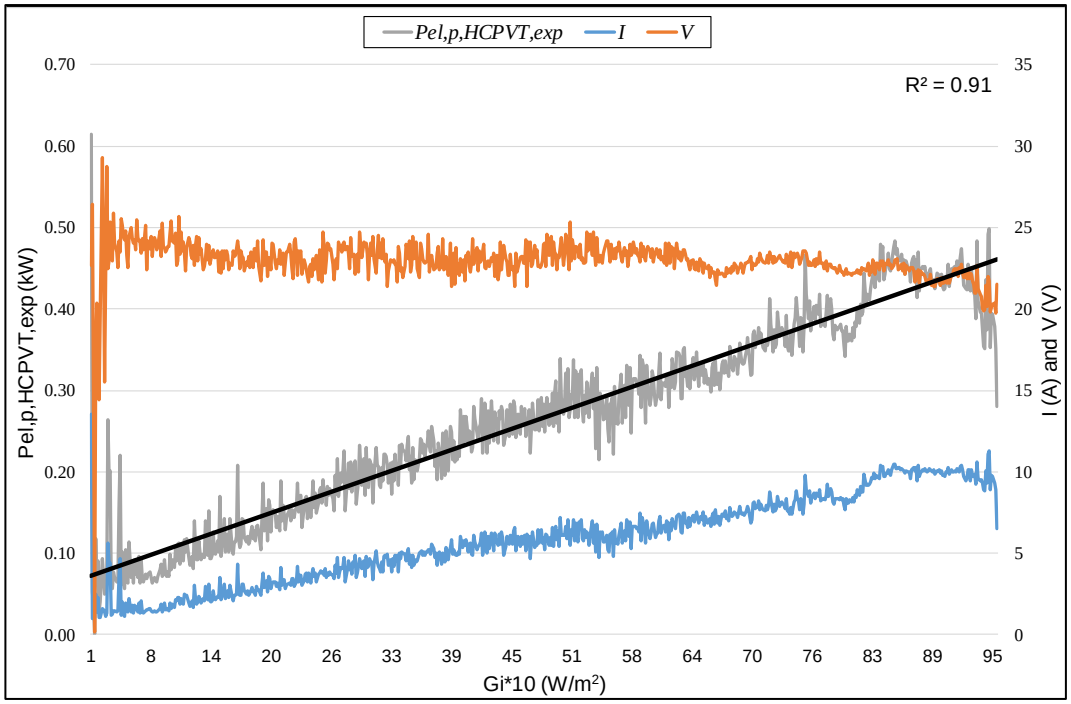

Figure 5-5: Instantaneous produced electrical power, current, and voltage versus instantaneous onsite DNI; 42 days between the 1st March 2018 and the 22nd May 2018.

The density of the demineralised water temperature decreases due to the increase in its temperature; the experimental monitored data temperature shows an increase up to 53 °C (Figure 5-6). Therefore, the density of the demineralised water was calculated as a function of water temperature in equation 5-4. The equation was obtained from Figure 5-6; graph of the specific volume of water versus its corresponding temperature (Çengel and Boles, 2015).

$$\rho_w = -0.0035 \cdot ((T_{out} + T_{in}/2)^2) - 0.0842 \cdot (T_{out} + T_{in}/2) + 1000.8 \qquad 5\text{-}4$$

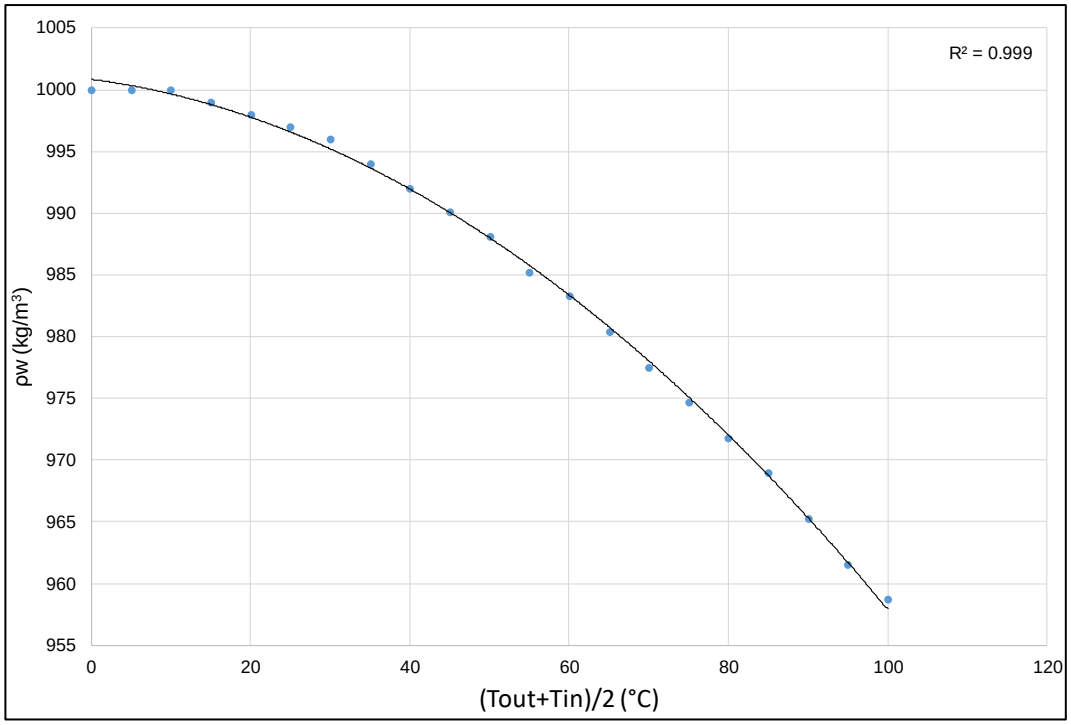

Figure 5-6: Density of demineralised water versus its temperature (average inlet and outlet).

The potential thermal power ($Q_{th,p,HCPVT,d}$) produced by the HCPV/T 2000x system at any given time in a typical year can be calculated using equation 5-2 and the derived equations 5-5 to 5-6. The equations were obtained from measurements presented in Figure 5-7, with R^2 equal to 0.93 and 0.60 respectively.

$$(T_{out} - T_{in}) = 0.0056 Km^2/W \cdot G_i + 273.69K \quad 5\text{-}5$$

$$(T_{out} + T_{in})/2 = 0.0134 Km^2/W \cdot G_i + 297.33K \quad 5\text{-}6$$

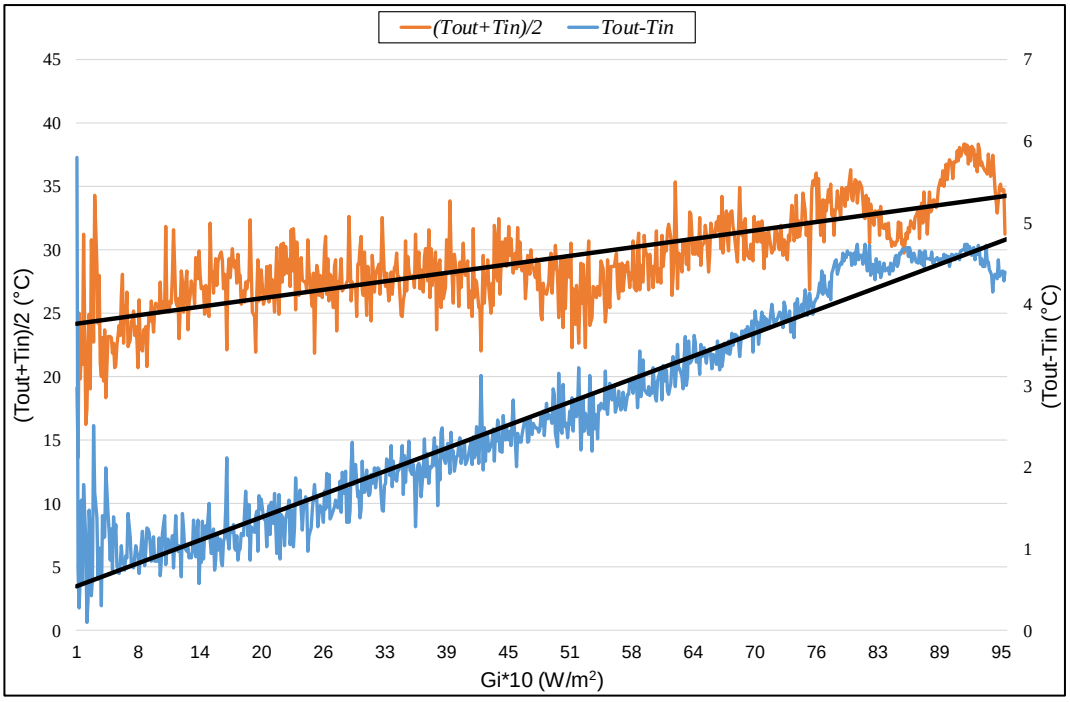

Figure 5-7: Instantaneous demineralised water temperature (average inlet and outlet, and the difference between outlet and inlet) versus instantaneous onsite DNI; 42 days between the 1st March 2018 and the 22nd May 2018.

The calculated electrical and thermal power production using measured data and equations 5-3 (electrical power) and 5-2 (thermal power) are shown in Figure 5-8. The results presented in Figure 5-8 are for 25 days of experimental monitored data; these are 16 days (1 March 2018 to 22 May 2018) when the circulating active cooling demineralized water was not bypassed from the 0.2 m^3 demineralized water storage tank, and 9 days (23 May 2018 to 25 June 2018) for when it was bypassed. The results show that the average daily produced electrical and thermal power (calculated from experimental data) follows the pattern of the average daily onsite DNI, indicating that this is the main parameter affecting them.

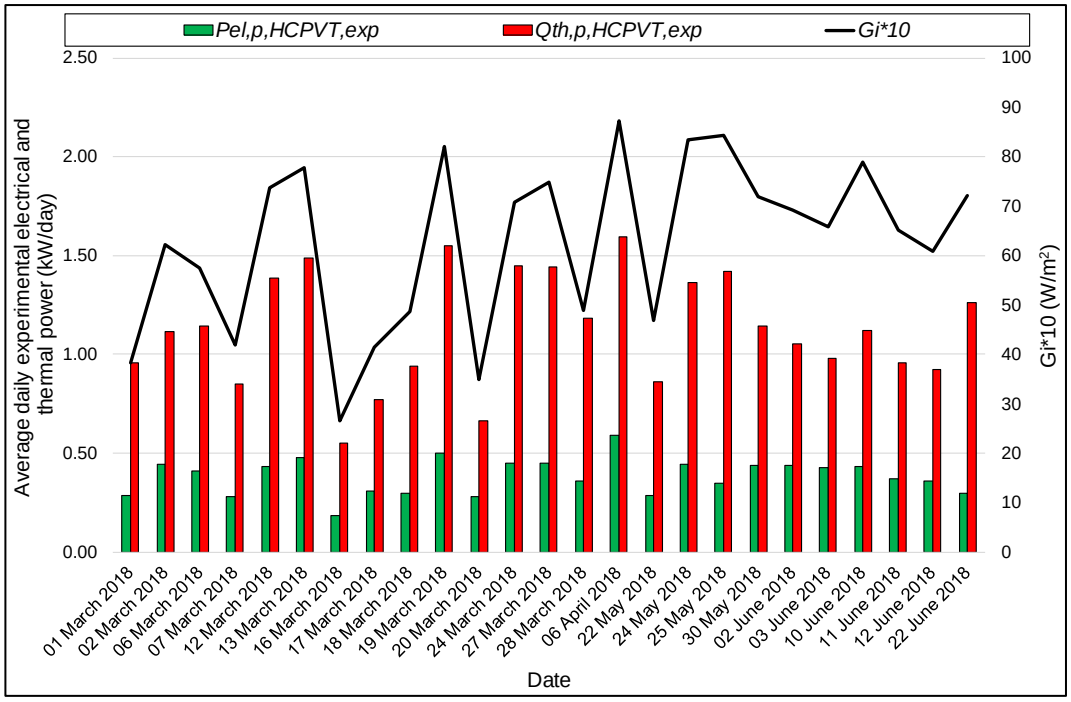

Figure 5-8: Average daily experimental electrical and thermal power production of the HCPV/T 2000x system.

5.2.2 Experimental Efficiency

The experimental HCPV/T 2000x system electrical efficiency ($\eta_{el,HCPVT,exp}$) in equation 5-7 was calculated as the ratio of the $P_{el,p,HCPVT,exp}$ to the reflected G_i by the reflective mirror.

The parameters η_{opt}, f_t, A_r and N are combined optical efficiency of the reflective mirror and optical receiver, non-ideal tracking factor of the 2-axis tracking system, the surface area of the reflective mirror and number of cells N. The parameter f_t are assumed to be 0.9 (Renno, 2014; Renno and Petito, 2013).

$$\eta_{el,HCPVT,exp} = \frac{P_{el,p,HCPVT,exp}}{\eta_{opt} \cdot f_t \cdot G_i \cdot A_r \cdot N}, \quad with\ \eta_{opt} = 0.85 \qquad 5\text{-}7$$

Where:

η_{opt} is the combined optical efficiency of the reflective mirror and optical receiver,

f_t is the non-ideal tracking factor of the 2-axis tracking system, assumed to be 0.9 (Renno, 2014; Renno and Petito, 2013),

A_r is the surface area of the reflective mirror and

N is the number of cells.

A further adjustment was made due to losses. Therefore, the experimental InGaP/InGaAs/Ge solar cell efficiency ($\eta_{c,HCPVT,exp}$) was finally calculated using equation 5-8 based on the assumption there is 10 % additional losses due to current mismatch between InGaP/InGaAs/Ge solar cell connected in series (Kribus et al., 2006).

$$\eta_{c,HCPVT,exp} = \frac{\eta_{el,HCPVT,exp}}{0.9} \quad 5\text{-}8$$

The experimental HCPV/T 2000x system thermal efficiency ($\eta_{th,HCPVT,exp}$) was calculated using equation 5-9 according to the thermal conversion efficiency proposed in (Kribus et al., 2006; Mittelman et al., 2007).

$$\eta_{th,HCPVT,exp} = \eta_{opt} \cdot \left(1 - \eta_{c,HCPVT,exp}\right) \cdot \frac{Q_{th,p,HCPVT,exp}}{Q_{th,p,HCPVT}} \quad 5\text{-}9$$

The results of efficiency calculations are shown in Figure 5-9. The graph shows that the average daily experimental electrical InGaP/InGaAs/Ge solar cell and HCPV/T 2000x system efficiencies (electrical and thermal) does not follow the pattern of the average daily onsite DNI. This is because the efficiency performance of the system is influenced by several additional factors; namely InGaP/InGaAs/Ge solar cell temperature, and demineralised water temperature. The increase in DNI values increases the demineralised water temperature (hence InGaP/InGaAs/Ge solar cell temperature), leading to a minor reduction in electrical InGaP/InGaAs/Ge solar cell efficiency; from the operating optimum demineralised water temperature of approximately 30 °C, to the maximum demineralised water temperature of approximately 53 °C.

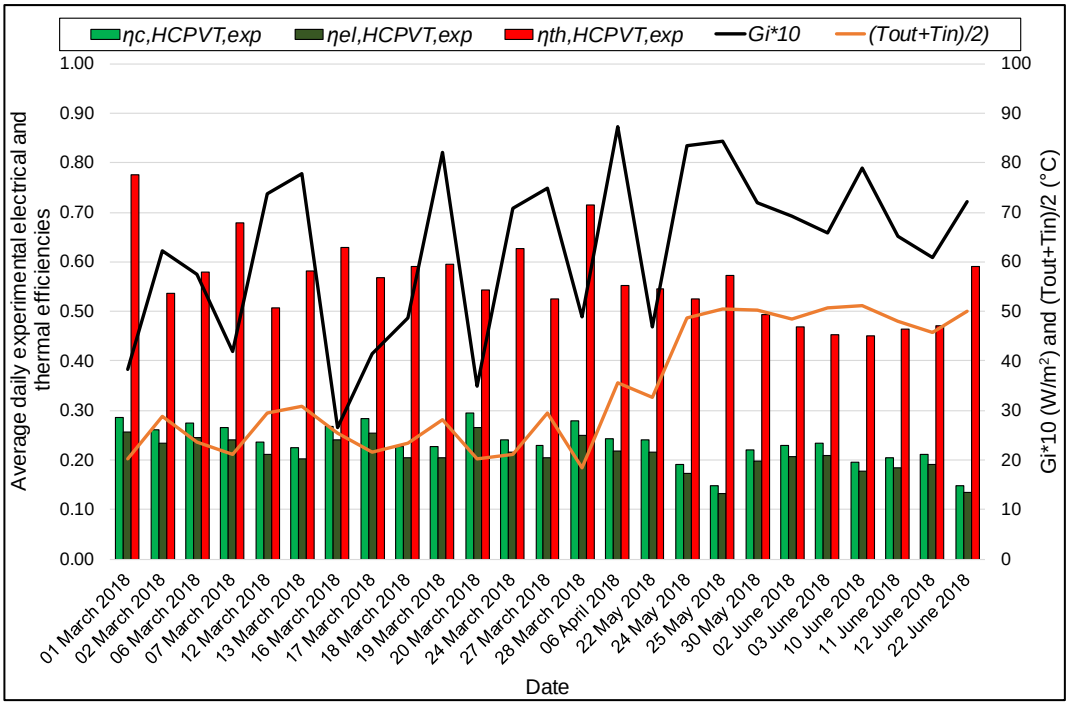

Figure 5-9: Average daily experimental electrical and thermal efficiencies of the HCPV/T 2000x system, InGaP/InGaAs/Ge solar cell efficiency, onsite DNI and demineralised water temperature (average inlet and outlet).

Since the actual operating temperature of the InGaP/InGaAs/Ge solar cell was not measured, the measured temperature of the demineralised water was used as a reference parameter to characterise the behaviour of the InGaP/InGaAs/Ge solar cell with the change in temperature as shown in Figure 5-10. The graph shows that when the circulating active cooling demineralised water was bypassed from the demineralised water storage tank, the increase in G_i values increases the demineralized water temperature (hence the cell temperature). This leads to a reduction in electrical cell efficiency; lower efficiency was achieved when the water temperature rises to approximately 53 ℃ from the optimum water temperature of approximately 30 ℃.

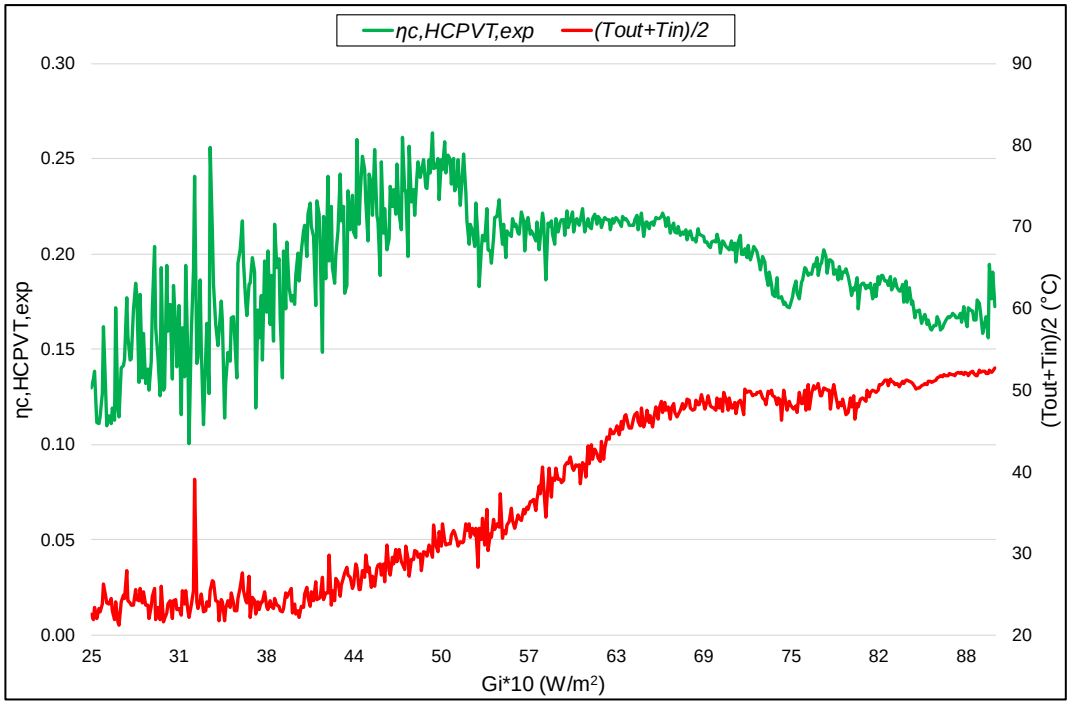

Figure 5-10: Instantaneous InGaP/InGaAs/Ge solar cell efficiency and demineralised water temperature (average inlet and outlet) versus instantaneous onsite DNI; 9 days (24th, 25th, and 30th May, and 2nd, 3rd, 10th, 11th, 12th and 22nd June 2018).

5.3 Analytical Model Development of the HCPV/T 2000x System

Based on the analysis based on experimental data, an analytical model of the HCPV/T 2000x system was developed. The analytical model requires the definition of the external and internal model inputs (Renno and Petito, 2013). The external inputs are the uncontrollable site environmental variables such as solar radiation, environment temperature and atmospheric condition. The HCPV/T 2000x system was designed and assembled with insulation materials that covers most of the components of the thermal energy system, electrical energy system and tracking system (except from the reflective mirror and optical receiver required to collect the DNI). Therefore, the environmental temperature and atmospheric condition have a negligible effect on the operational performance of the HCPV/T 2000x system. This leaves the DNI as the sole external input. The internal inputs are the variables that characterise the HCPV/T 2000x system; these are η_{opt} (the combined optical efficiency of the reflective mirror and optical receiver), f_t (the non-ideal tracking factor of the 2-axis tracking system), A_r (the surface area of the reflective mirror) and N (the number of cells).

5.3.1 Analytical Electrical and Thermal energy

The electrical ($P_{el,p,HCPVT}$) and thermal power ($Q_{th,p,HCPVT}$) by the HCPV/T 2000x system were calculated using equation 5-10 and 5-11 respectively (Renno, 2014; Renno and Petito, 2013). The parameter A_c is the cell area. The $P_{el,p,HCPVT}$ considered the assumption of 10 % losses due to current mismatch between InGaP/InGaAs/Ge solar cell connected in series (Kribus et al., 2006).

$$P_{el,p,HCPVT} = 0.9 \cdot \eta_{c,HCPVT} \cdot \eta_{opt} \cdot CR \cdot f_t \cdot A_c \cdot G_i \cdot N \qquad 5\text{-}10$$

$$Q_{th,p,HCPVT} = (1 - \eta_{el,HCPVT}) \cdot \eta_{opt} \cdot CR \cdot f_t \cdot A_c \cdot G_i \cdot N \qquad 5\text{-}11$$

The results are shown in Figure 5-11. The graph shows that the average daily analytical calculated electrical and thermal power follows the pattern of the average daily onsite DNI (also observed in section 5.2) because this is the main parameter affecting them.

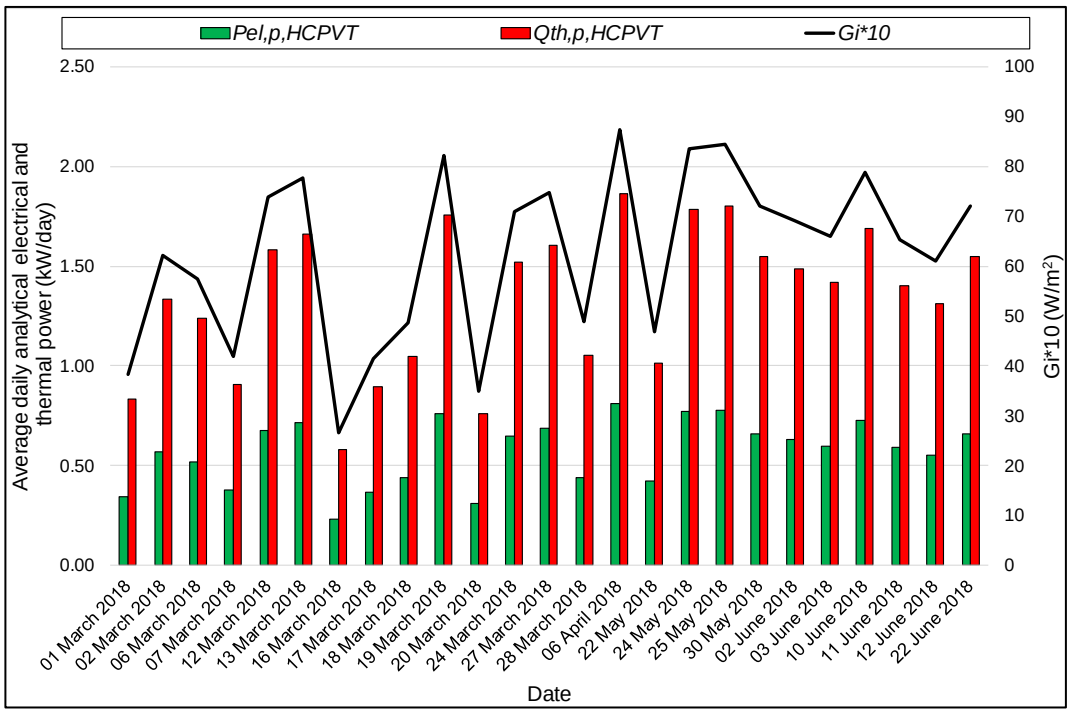

Figure 5-11: Average daily analytical electrical and thermal power production of the HCPV/T 2000x system.

5.3.2 Analytical Efficiency

The operating cell temperature is an important parameter required to calculate cell efficiency. The actual operating temperature of the InGaP/InGaAs/Ge solar cell was not used in the calculation of the cell efficiency because the assembled active heatsink does not have temperature sensor amongst its components due to its complexity. Therefore, an effective cell efficiency equation as a function of G_i was applied.

The analytical InGaP/InGaAs/Ge solar cell efficiency ($\eta_{c,HCPVT}$) was derived as a function of G_i in equation 5-12, referring to cell efficiency versus Concentration Ratio (CR, up to 1500). This was obtained from two experimental tests performed using the same type of InGaP/InGaAs/Ge solar cell installed in the HCPV/T 2000x system. The experimental tests were performed on 30.25 mm^2 (5 mm x 5 mm) and 100 mm^2 (10 mm x 10 mm) at test conditions of 25 °C, 1000 W/m^2 and 500 W/m^2 (Emcore Corporation, 2012a, 2012b). The cell efficiency versus CR characteristic obtained from both tests was extrapolated for CR up to 2000 to match the CR of the analysed HCPV/T 2000x system.

$$\eta_{c,HCPVT} = a \cdot G_i + 0.3102, \quad \text{with } a = 0.00003 m^2/W \qquad 5\text{-}12$$

The analytical HCPV/T 2000x system electrical efficiency ($\eta_{el,HCPVT}$) is in equation 5-13 which includes the additional 10 % losses caused by the unavoidable shading from the adjacent reflective mirror of the HCPV/T 2000x system.

$$\eta_{el,HCPVT} = 0.9 \cdot \eta_{c,HCPVT} \qquad 5\text{-}13$$

The analytical HCPV/T 2000x system thermal efficiency ($\eta_{th,HCPVT}$) is presented in equation 5-14. The $\eta_{th,HCPVT}$ was calculated according to the thermal conversion efficiency proposed in (Kribus et al., 2006; Mittelman et al., 2007); where η_{opt} is the combined optical efficiency of the reflective mirror and optical receiver.

$$\eta_{th,HCPVT} = \eta_{opt} \cdot \left(1 - \eta_{c,HCPVT}\right) \qquad 5\text{-}14$$

The results are shown in Figure 5-12. The graph shows that the average daily analytical

electrical InGaP/InGaAs/Ge solar cell and HCPV/T 2000x system efficiencies (electrical and thermal) does not follow the pattern of the average daily onsite DNI for the same reason explained in section 5.2.2 for Figure 5-9.

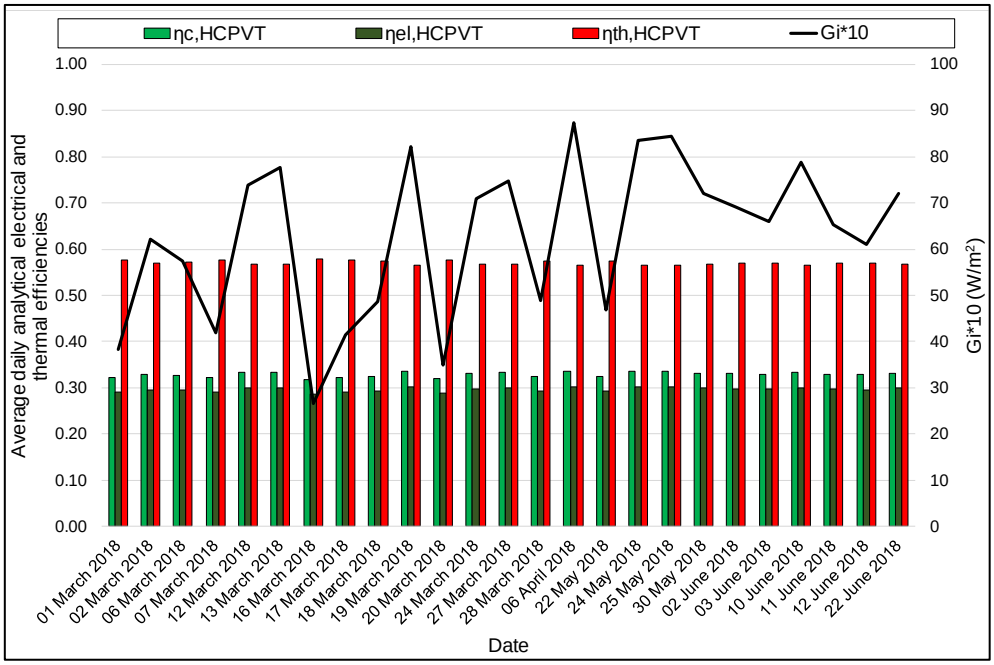

Figure 5-12: Average daily analytical electrical and thermal efficiencies of the HCPV/T 2000x system, InGaP/InGaAs/Ge solar cell efficiency and onsite DNI.

The accuracy of the analytical model of the HCPV/T 2000x system was validated by obtaining the linear regression (Figure 5-13) of experimental results versus analytical results. The analytical results show good agreement with the experimental monitoring result. The R^2 for experimental electrical and thermal results are 0.91 and 0.87, respectively. Following the validation, the monthly and annual produced electrical and thermal energy was evaluated using $G_{i,met}$ (Meteonorm, 2019), which also follows the pattern of the average monthly DNI. The months of July and February are the months with the highest and lowest electrical and thermal energy production as will be presented in section 5.4.3.

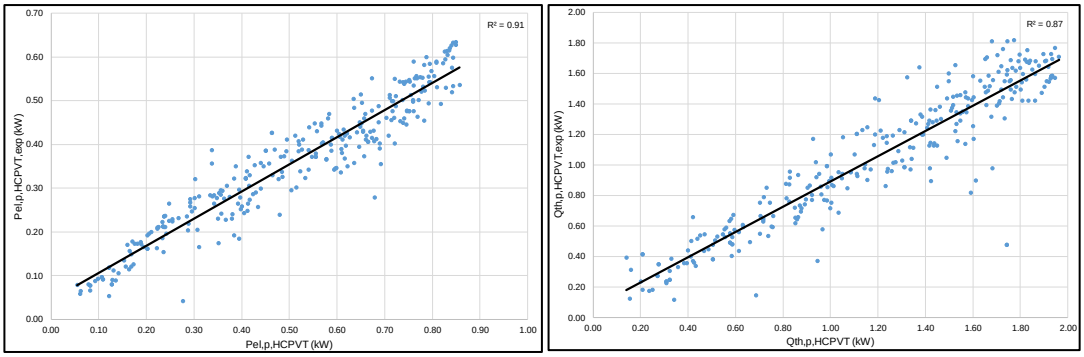

Figure 5-13: Experimental versus analytical results for the produced electrical and thermal power; 16 days (between 1st March 2018 and 22nd May 2018).

5.4 Comparison of the HCPV/T 2000x System with PV and PVT Systems

This section compares the results for the HCPV/T 2000x with results for PV and PVT systems calculated using EP modules to show the advantages of the HCPV/T 2000x system in comparison to commercially available PV systems. The comparison of the HCPV/T 2000x system with the PV and PVT system was based on the results obtained from analytical model of the HCPV/T 2000x system, and EP simulations of the PV and PVT systems for Sicily and Jamaica locations. As presented in Figure 5-12 and Figure 5-9, the average daily analytical and experimental InGaP/InGaAs/Ge solar cell efficiencies are 33 % and 25 % respectively; the maximum daily experimental InGaP/InGaAs/Ge solar cell efficiency of 30 % was achieved on the 20th March 2018. The average daily analytical and experimental efficiency of the HCPV/T system, that was calculated based on 10 % losses due to current mismatch between InGaP/InGaAs/Ge solar cell connected in series (Kribus et al., 2006) are 30 % and 23 % respectively. The average daily analytical and experimental thermal conversion efficiency are 57 % and 56 % respectively; the experimental is 56 % and 78 %. Therefore, the total average daily efficiency of is approximately 80 %.

5.4.1 PV System Model

The implementation of the Sandia model in EP (described in section 1.3.2) focusses on determining the performance at the maximum power point (P_{mp}), which is the product of current (I_{mp}) and voltage (V_{mp}) at maximum-power point. This is one of the critical five points

(with the other four points being the short-circuit current (I_{sc}), open-circuit voltage (V_{oc}), current (I_x) at module voltage of $0.5V_{oc}$ and current (I_{xx}) at module voltage of 0.5 ($V_{oc} + V_{mp}$) used to assess the *I-V* curve of a PV module as shown in Figure 5-14.

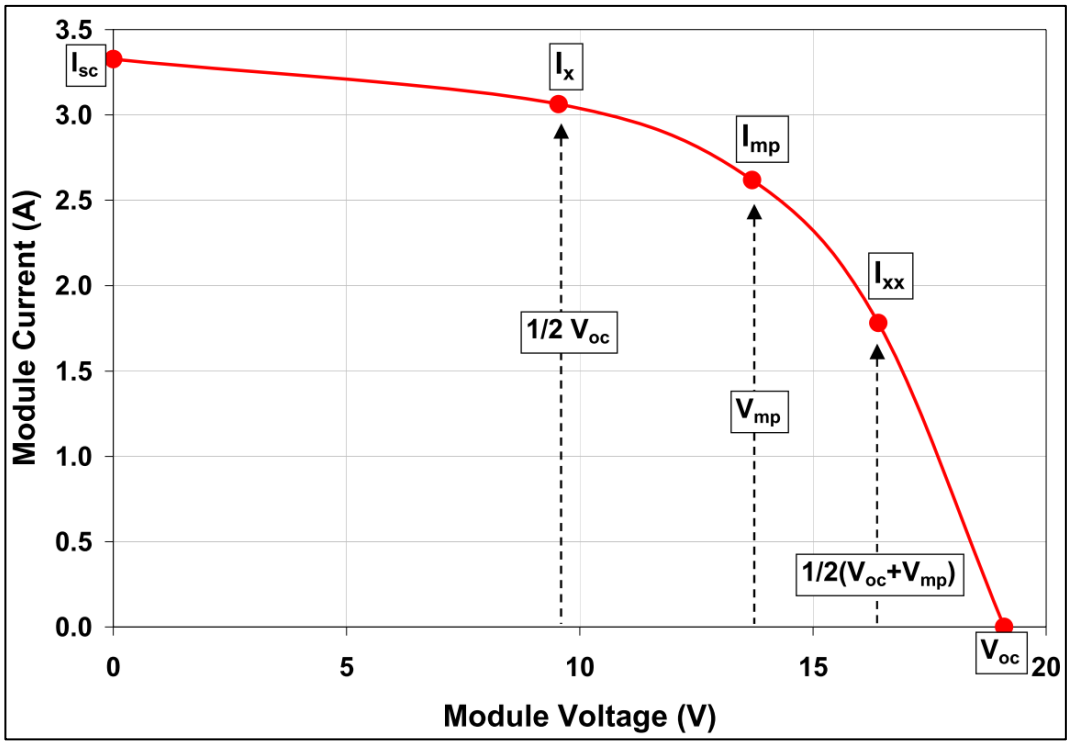

Figure 5-14: PV module I-V curve of the Sandia performance model (King et al., 2004).

The modelled PV module characterised with 72 cells has an area of 1.31 m^2 (1.62 m x 0.81 m), with tilt angle of 10 – 30 ° arrangement (Evans, 1981). Its equivalent footprint area 11 m^2 (7.4 m x 1.5 m) is the same as for the HCPV/T 2000x system. This results in a PV system that consists of 5 modules arranged in series. The mathematical description and parameters of the Sandia model used to predict electricity production by one PV module are summarised in Appendix B.

5.4.2 PVT System Model

The performance of the PVT system for the prediction of electricity and heat generation was modelled using the only simple PVT model available in EP. The PVT model is a user-defined efficiency model (U.S. Department of Energy, 2019). In this model, a fixed thermal efficiency (η_{th}) of 47.5 % was defined according to (Jessica Settino et al., 2018). A value of 0.25 (0.75 of "PV area covering factor") was assigned for the "fraction of surface area with active thermal

collector", which is a critical dimensionless input in EP for modelling PVT (Herrando et al., 2014). The PVT model reuses the Sandia model for electricity generation. The produced thermal energy of the PVT system ($Q_{th,p,PVT}$) is calculated using equation 5-15.

$$Q_{th,p,PVT} = A_{sur,PVT} \cdot f_{act,PVT} \cdot \eta_{th} \qquad 5\text{-}15$$

Where:

$A_{sur,PVT}$ is the active area,

$f_{act,PVT}$ is the fraction of surface area with active thermal collector and

η_{th} is the fixed thermal efficiency of the PVT system.

5.4.3 Comparison with HCPV/T 2000x system

A comparison of the HCPV/T 2000x, PV and PVT systems is presented in Figure 5-15 to Figure 5-17. The results presented for Sicily in Figure 5-15 and Figure 5-16, show that the HCPV/T 2000x system has higher electrical efficiency and electrical and/or thermal energy production, respectively. The electrical efficiency does not follow the pattern of the DNI/GHI because it is influenced by several additional factors mainly solar cell temperature. The electrical efficiency value shows a fairly constant value for the days presented. The produced electrical and/or thermal energy follows the pattern of the DNI/GHI, as this is the main parameter affecting them.

Figure 5-17 presents the annual produced electrical and/or thermal energy by HCPV/T 2000x system, PV and PVT for Jamaica. The produced electrical and/or thermal energy follows the pattern of the DNI/GHI, as this is the main parameter affecting them.

The annual analytically calculated electrical and/or thermal energy by the HCPV/T 2000x system is higher for Sicily (Figure 5-16) than Jamaica (Figure 5-17) because the average annual DNI for Sicily (218 W/m^2) is higher than in Jamaica (141 W/m^2) (Meteonorm, 2019). For Sicily, the production is at its highest in July (with highest DNI) and at its lowest in February (with lowest DNI), while production in Jamaica is fairly constant throughout the year, with the highest and lowest in September and November respectively. Similarly, the energy production by the PVT and PV systems are higher in Sicily than Jamaica because the average annual GHI

for Sicily (202 W/m^2) is higher than in Jamaica (196 W/m^2) (Meteonorm, 2019).

The simulated PV cell efficiency ($\eta_{c,PV}$) and PVT cell efficiency ($\eta_{c,PVT}$) presented in Figure 5-15 shows good correlation with the PV cell efficiency published in (Jessica Settino et al., 2018). The commercially available monocrystalline and polycrystalline silicon PV has an efficiency between 15 – 19 % and 15 – 19 % respectively, while the commercially available PVT technology has PV cell efficiency between 13 and 16 %. The PVT system is a similar technology to the HCPV 2000x system because it produces both electrical and thermal power. The analysed HCPV 2000x system also demonstrated higher thermal efficiency than the PVT; the thermal efficiency of the commercially available PVT is between 40 and 55 %.

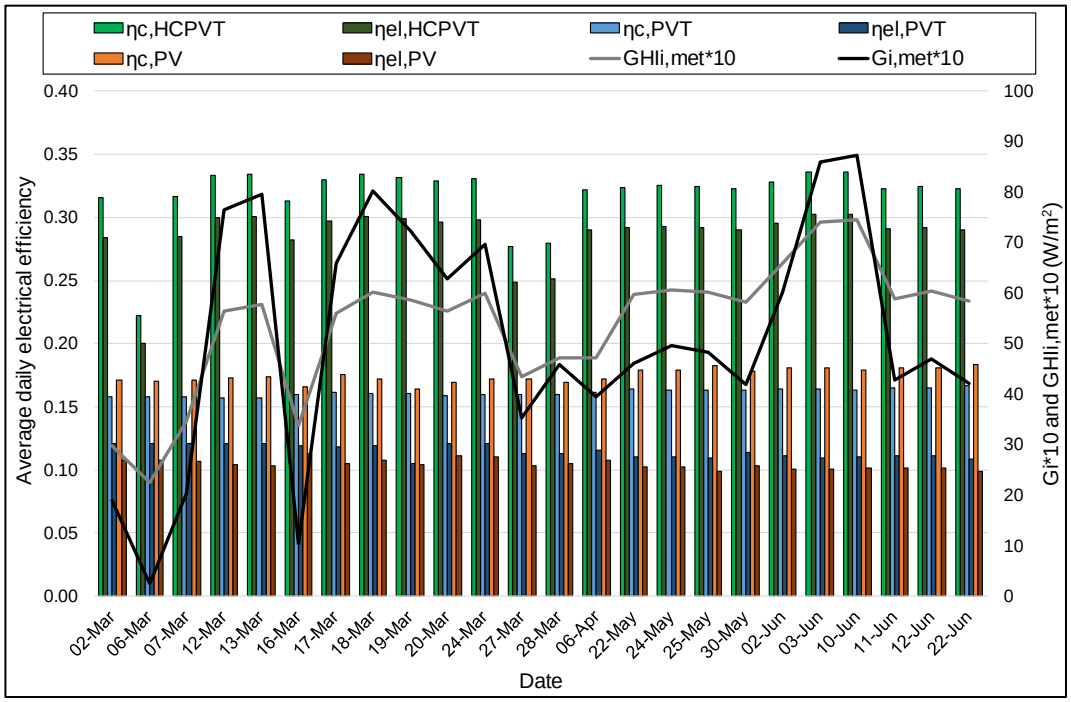

Figure 5-15: Electrical efficiency of HCPV/T 2000x system, PV and PVT; Sicily case study location.

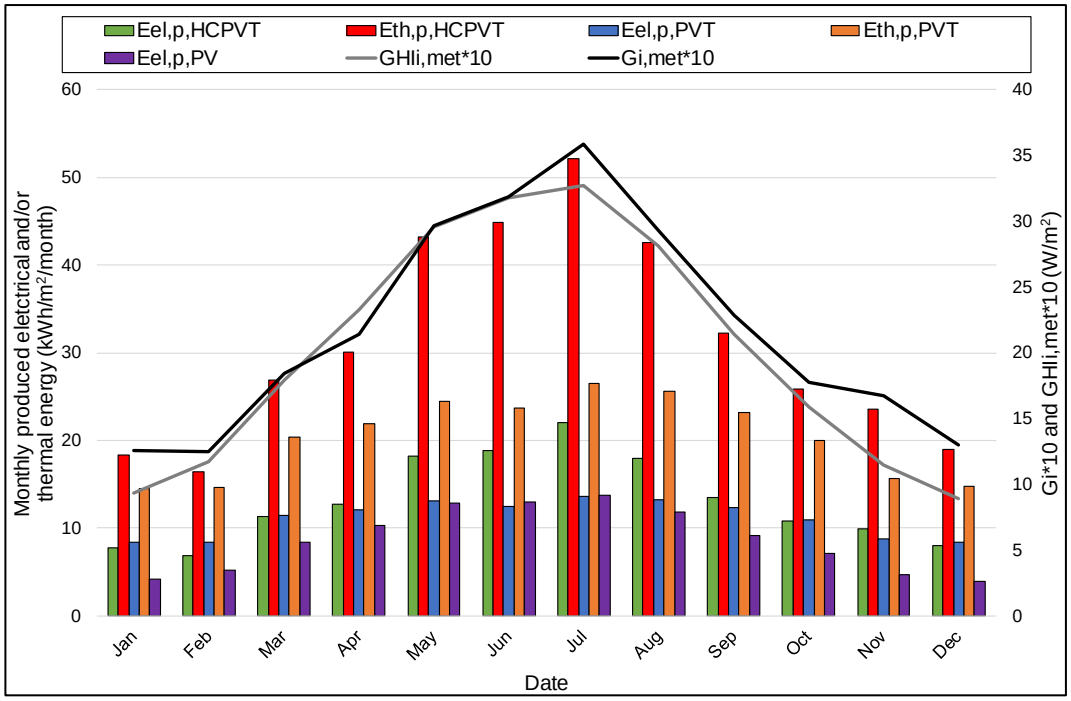

Figure 5-16: The monthly produced electrical and/or thermal energy by the HCPV/T 2000x system, PV and PVT for a typical year; Sicily case study location.

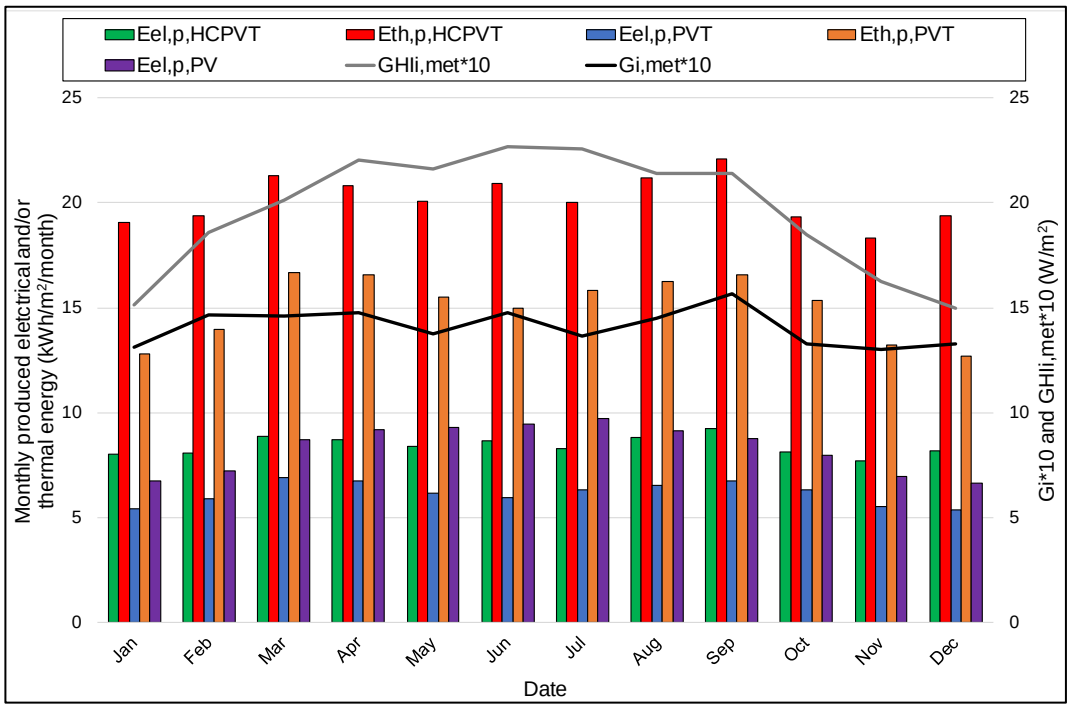

Figure 5-17: The monthly produced electrical and/or thermal energy by the HCPV/T 2000x system, PV and PVT for a typical year; Jamaica case study location.

The annual results for both Sicily and Jamaica are presented in Table 5-1 and Table 5-2. Table 5-1 shows the annual produced electrical energy by the 11 m^2 HCPV/T 2000x system, calculated analytically and experimentally. It also shows the simulated annual electrical energy

of the PV and PVT systems with equivalent footprint area. It can be seen the HCPV/T 2000x system produced the highest annual electrical energy because of it has the highest electrical efficiency. The very high electrical efficiency of the HCPV/T 2000x system is attributed to the reflective mirror CR of 2000x and optical receiver in focus to the reflective mirror. The CR of 2000x is achieved by the 2-axis tracking system of the HCPV/T 2000x system that accurately tracks the sun during operation. This meant that the InGaP/InGaAs/Ge solar cell of the HCPV/T 2000x system received very high concentrated DNI.

Table 5-2 also shows the annual produced thermal energy by the HCPV/T 2000x and PVT systems. It can be seen the HCPV/T 2000x system produced the higher annual thermal energy because of it has the higher thermal efficiency. The very high thermal efficiency of the HCPV/T 2000x system is because the InGaP/InGaAs/Ge solar cell operates at high design operating temperature of 20 ℃ to 90 ℃ (maximum 110 ℃) caused by the very high concentrated DNI it receives. This meant that the heat extracted from InGaP/InGaAs/Ge solar cell by the Al heat exchanger plate to the following demineralised water can reach a temperature of approximately 53 ℃.

Table 5-1: Annual produced electrical energy by the HCPV/T 2000x, PV and PVT systems.

Unit	Palermo, Sicily case study			Portmore, Jamaica case study		
	Analytical calculated electrical energy ($E_{el,p,HCPVT}$)					
	HCPV/T 2000x system	PV system	PVT system	HCPV/T 2000x system	PV system	PVT system
$kWh/m^2/year$	158	104	133	101	100	74
$kWh/year$	1738	1144	1463	1111	1100	814
	Experimental produced electrical energy ($E_{el,p,HCPVT,exp}$)					
$kWh/m^2/year$	144	-	-	-	-	-
$kWh/year$	1584	-	-	-	-	-

Table 5-2: Annual produced thermal energy by the HCPV/T 2000x, PV and PVT systems.

Unit	Palermo, Sicily case study			Portmore, Jamaica case study		
	Analytical calculated thermal energy ($E_{th,p,HCPVT}$)					
	HCPV/T 2000x system	PV system	PVT system	HCPV/T 2000x system	PV system	PVT system
$kWh/m^2/year$	375	-	245	242	-	180
$kWh/year$	4125	-	2695	2662	-	1980
	Experimental produced thermal energy ($E_{th,p,HCPVT,exp}$)					
$kWh/m^2/year$	390	-	-	-	-	-
$kWh/year$	4290	-	-	-	-	-

Chapter 5 Summary

The analysed operational performance of the HCPV/T 2000x system shows that the system can provide 100 % of the baseline annual heating and cooling demand for Palermo, Sicily case study house for a typical year (calculated and described in Chapter 4), or can be used to meet ~15 % of the heating and cooling energy demand (after the application of cool paint), and 100 % of A-rated appliances and LED lighting energy demand. Also, the HCPV/T 2000x system can provide ~30 % of cooling energy demand (~50 % after the application of cool roof paint) for Portmore, Jamaica case study house for a typical year, or can be used to meet ~15 % of the cooling energy demand (after the application of cool paint), and 100 % of A-rated appliances and LED lighting energy demand. The system will also provide thermal energy to cover hot water demand for the house. In conclusion, the following points can be made:

- HCPV/T 2000x, PV and PVT systems are suitable for residential buildings in high solar radiation countries.
- The HCPV/T 2000x system has the highest efficiency and annual energy production potential

The energy production by the HCPV/T 2000x system were used as input (for the defined functional unit of study) required for the lifecycle environmental impact of the HCPV/T 2000x system, and comparison with other RES and non-RES systems for the Palermo, Sicily and Portmore, Jamaica case studies. The lifecycle environmental impact study is presented in chapter 7.

Chapter 6: Environmental Impact of Cool Roof Paint

Introduction

Chapter 6 presents the estimated environmental impacts of the cool roof paint for the Palermo, Sicily and Portmore, Jamaica case studies. The purpose of chapter 6 is to investigate the environmental impacts benefit of the cool roof paint in comparison with thermal insulation, which provides equivalent energy saving potential and similar indoor thermal comfort according to the conclusion presented in chapter 4. Section 6.1 presents the goal (aim), scope and functional units of the environmental impact study. The scope defines the method of environmental impact analysis, while the functional unit quantifies the performance of the cool roof paint. Section 6.2 presents the system boundary and inventory. System boundary defines the processes which are part of the product system, while inventory consists of input and output data of the system boundary (BS EN ISO 14044, 2018). Section 6.3 presents the estimated environmental impact using "ReCiPe2016 Method – Lifecycle Midpoint and Endpoint Environmental Impact Assessment", explained in chapter 1, section 1.3.3. The ReCiPe2016 method is based on midpoint and endpoint impact category indicators. Section 6.4 presents the comparison of the estimated environmental impact indicators with a roof thermal insulation environmental impact indicators published in literature.

6.1 Goal, Scope and Functional Unit

The goals of this study were to:

- estimate the lifecycle environmental impacts of cooling energy demand reduction by the cool roof paint,
- critically evaluate the magnitude and significance of the lifecycle environmental impacts of cooling energy demand reduction by the cool roof paint.

Cradle to Grave (CTGR) approach was the scope used for the LCA study, within the LCA system boundary as shown in Figure 6-1. The system boundary includes the following:

- production of cool roof paint material/chemical inputs (including raw material acquisition),
- production of cool roof paint,
- transportation of cool roof paint material/chemical inputs to cool roof paint production site,
- transportation of cool roof paint to building case study site for application,
- application of cool roof paint,

- maintenance over service life and
- waste management (from cool roof paint production and maintenance).

The functional units (units of analysis) for a service life of 5 years, for this study, are:

- 1 kWh/m^2 of cooling energy demand reduction. The unit of measurement, kWh is in accordance with the European Commission (EC) (European Commission, 2016),
- 1 m^2 of installed cool roof paint or the climate-controlled space. The unit of measurement, m^2 is in accordance with the Council for European Producers of Materials for Construction (CEPMD) (Schiavoni et al., 2016).

The service life of 5 years was chosen according to the recommendation by cool roof paint manufacturer, Sika Corporation (http://www.sika.com, 2020), for the three cool roof paint layers applied for the Portmore, Jamaica cases study.

6.2 System Boundary Description and Inventory

Table 6-1 presents the LCI data (including assumptions) used for the LCA study of the cool roof paint. The LCI data collection based on the system boundary (Figure 6-1) was classified, as follows:

- The Foreground data – describes the LCI data that was directly sourced from the company who produced the cool roof paint (Table 6-1).
- The Background generic data – describes the materials, energy, transport and waste management data that were sourced from Ecoinvent via the SimaPro v8.2.3.0 software used for the LCA study (PRé, 2016; Steubing *et al*, 2016).
- Specific information about the system boundary (Figure 6-1) is given below. All phases are the same for Palermo, Sicily case study and Portmore, Jamaica case study houses (same cool roof paint by the same manufacturer) apart from transportation which is different as the cool roof paint is produced in different factories and transported to a different location.

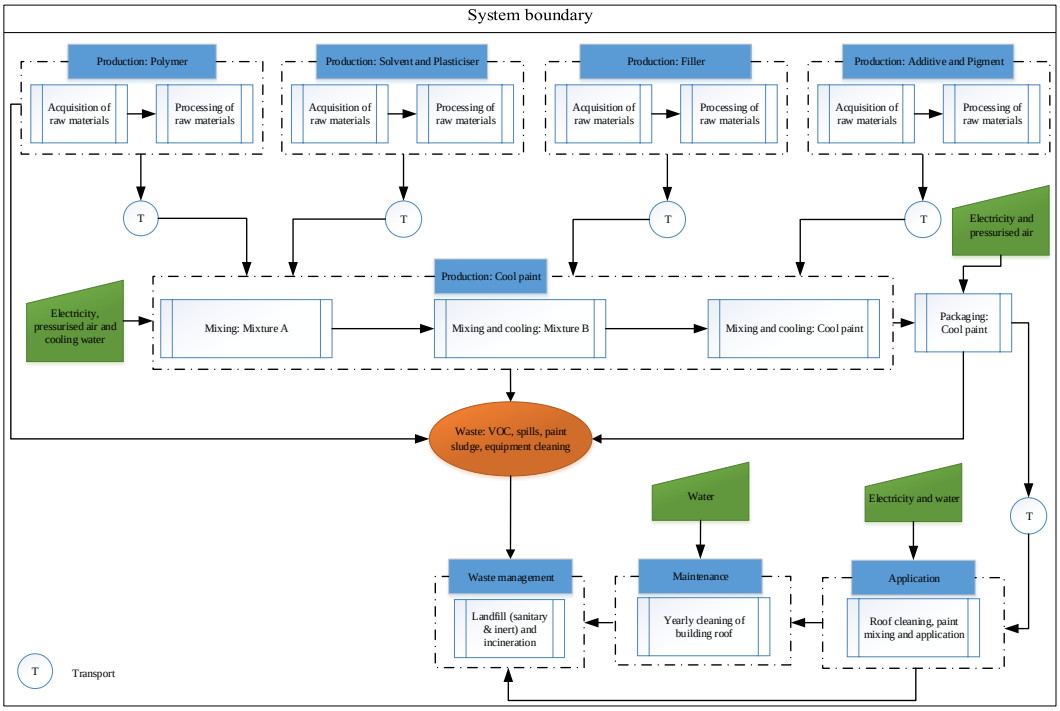

Figure 6-1: The LCA system boundary for the cool roof paint.

6.2.1 Production

The prerequisite to produce cool roof paint is the production of polymer, solvent, plasticiser, filler, additive and pigment, which are its material/chemical inputs. The production of these material/chemical inputs considers the acquisition and processing of raw materials, which includes the consumption of raw materials (and transport), energy, infrastructure, land use and waste treatment (and transport). The specific material/chemical inputs in accordance with the functionality and properties of the cool roof paint were sourced from commercially available company/literature. The production process of the specific material/chemical inputs was sourced from Ecoinvent via the SimaPro v8.2.3.0 software.

The produced material/chemical inputs were transported to the cool roof paint production site, where they are chronologically mixed in accordance with the cool roof paint manufacturer. “Mixture A” is the mixture of dispersed polymer, solvent, and plasticiser. “Mixture B” is the mixture of “Mixture A” and filler. The cool roof paint product was finally produced after the mixing of “Mixture B” with additives and pigments. It was assumed that the mixing was done with two shaft mixer-dispersers that requires cooling during the production of “Mixture B” and the final cool roof paint product. The mixing and cooling were enabled by energy, pressurised air, and cooling water inputs.

Table 6-1: Foreground inventory data to produce cool roof paint.

Material/chemical input	Value (%)	Input composition
Polymer	50	Acrylic dispersion (70 %)
Solvent	20	Water (80 %)
		Glycol ethers (20 %)
Filler	15	Barite
Pigment	10	Titanium dioxide
Additive	4	Zinc dioxide
Plasticizer	1	Phthalic anhydride

6.2.2 Application

The packaged cool roof paint was transported to the case study location where it was applied to the building roof. The building roof was prepared by cleaning the surface with water, followed by paint mixing with drill and paddle mixer, and finally the application of 1.4 kg/m^2 cool roof paint with solvent resistant skin roller.

6.2.3 Transport

The transportation phase of the LCA assesses the transportation impact during the supply of the six material/chemical inputs to the manufacturer site and then the produced cool roof paint to the case study location site. The manufacturing site was at Alcobendas, Spain for the Palermo, Sicily case study and Tocancipa, Colombias for the Portmore, Jamaica case study. The transportation during the acquisition and processing of the material/chemical inputs are embedded in the environmental impact of the production of the material/chemical inputs. The transportation modes and distances are summarised in Table 6-2. For the Palermo, Sicily case study, it was assumed that the Polymer, Solvent, Plasticizer, Additive and Pigment were acquired from a retailer/wholesaler in Tarragona, Spain, while the Filler was acquired from a retailer/wholesaler in Girona, Spain, which was supplied by road to the manufacturer site of the cool roof paint. It was also assumed that the produced cool roof paint was transported by road from the manufacturer site to the port of Valencia, Spain then by sea to the port of Palermo, Sicily and finally by road to the case study location site. For Portmore, Jamaica case study, it was assumed that the Polymer, Solvent, Plasticiser, Filler, Additive and Pigment were acquired from a retailer/wholesaler in Bogota, Colombia, which is supplied by road to the manufacturer

site of the cool roof paint. It was also assumed that the produced cool roof paint was transported by road from the manufacturer site to the port of Cartagena, Colombia then by sea to the port of Kingston, Jamaica and finally by road to the case study location site.

Table 6-2: Transportation modes and distances in the supply of all produced material/chemical inputs of cool roof paint and produced cool roof paint.

Case study	Input	Value	Transport mode
Sicily	Material/chemical to manufacturer site	1254 km	Lorry (3.5 – 7.5 t)
		377 km	Lorry (3.5 – 7.5 t)
	Packaged cool roof paint to case study site	1287 km	Transoceanic ship
		20 km	Lorry (3.5 – 7.5 t)
Jamaica	Material/chemical to manufacturer site	40 km	Lorry (3.5 – 7.5 t)
		1078 km	Lorry (3.5 – 7.5 t)
	Packaged cool roof paint to case study site	854 km	Transoceanic ship
		8 km	Lorry (3.5 – 7.5 t)

6.2.4 Maintenance

The roof is manually cleaned annually with water to remove accumulated dirt and restore it's the high solar reflectivity of the property of the cool roof paint. It was assumed that 1.4 kg/m^2 of water was used per year for the service life of 5 years.

6.2.5 Waste Management

The waste management involves landfill and incineration of waste from the production of polymer, solvent, plasticiser, filler, additive, pigment, production and packaging of cool roof paint, application and end of life (assuming the building was demolished and landfilled; this only considers landfilling of the cool roof paint). The waste management process was sourced from Ecoinvent via the SimaPro v8.2.3.0 software.

6.3 Midpoint and Endpoint Environmental Impact Category Indicators and Identification of Hotspots

The most relevant lifecycle stages are those that contribute over 80 % (starting from the largest to the smallest contributions; before normalisation and weighting) to any of the baseline impact category indicators, while the hotspot at lifecycle stages are those that cumulatively contribute

at least 50 % to any of the baseline impact category indicators (European Commission, 2016; Zampori et al., 2016). As described in chapter 2 (section 2.4.3) these are the midpoint and endpoint environmental impacts. The midpoint environmental impacts are listed in Table 2-1. The endpoint environmental impacts are, Human Health Potential – HHP (DALY), Ecosystem Potential – EP (species.yr) and Resources Potential – RP (€).

Table 6-3 presents the results of the midpoint environmental impacts per m^2 of applied cool roof paint and kWh/m^2 of cooling demand for Palermo, Sicily and Portmore, Jamaica case studies. The impact indicators differ slightly for the two cases mainly because of transportation. Figure 6-2 and Figure 6-3 present the percentage contribution of the midpoint environmental impacts while Figure 6-4 presents the endpoint environmental impacts.

At the midpoint impact category level as shown in Figure 6-2 and Figure 6-3, the production of polymer and pigment and transport are the main contributors to the following 11 impact category indicators: GWP, FEP, ODP, TAP, MEP, POFP, PMFP, IRP, ULOP, NLTP, MDP and FDP. The production of polymer and pigment and waste management are the main contributors to the HTP, FETP and METP. The production of polymer and pigment are the main contributors to MEP. The main contributors to ALOP and WDP are production of polymer, pigment, and cool roof paint.

Therefore, at the midpoint level across the 18 environmental midpoint impact category indicators, the most relevant lifecycle stages contributing over 80% of the environmental impacts are the acquisition and processing of raw material, contributed by production of polymer (45 %), production of pigment (20 %), production of cool roof paint (7 %), and transport (15 %).

At endpoint level the main difference between the endpoint environmental impacts of the cool roof paint for the Palermo, Sicily and Portmore, Jamaica case studies is solely due to impacts from the transport of the cool roof paint to the building application site. As shown in Figure 6-4, the production: of polymer and pigment, and transport are the main contributors to the EP and RP while the main contributors to HHP are the same plus waste management. Therefore, at the endpoint level, the acquisition and processing of raw materials are the identified hotspots, contributing at least 50 % of the environmental impacts. The production of polymer

contribution to the environmental impacts are mostly due to the acquisition and processing of titanium dioxide (TiO_2), acrylic binder, toluene diisocyanate and polyol, which are the raw materials used for its production. The contribution by the production of pigment is mostly due to the acquisition and processing of TiO_2.

Across the three environmental endpoint impact category indicators, the most relevant lifecycle stages contributing over 80 % of the environmental impacts are the acquisition and processing of raw materials, contributed by production polymer (49 %) and production of pigment (18 %), production of cool roof paint (6 %), and transport (16 %).

In conclusion, across all the midpoint and endpoint environmental impacts, the identified hotspots contributing at least 50 % of the environmental impacts are acquisition and processing of raw materials.

Table 6-3: Midpoint cradle to grave environmental impacts of cool roof paint in Palermo, Sicily and Portmore, Jamaica case studies.

Impact indicators	per 1 m^2 Palermo, Sicily	per 1 m^2 Portmore, Jamaica	per 1 kWh/m^2 Palermo, Sicily	per 1 kWh/m^2 Portmore, Jamaica
GWP	4.92E+00	5.04E+00	2.59E-02	2.65E-02
ODP	4.48E-07	4.69E-07	2.36E-09	2.47E-09
TAP	2.59E-02	2.60E-02	1.36E-04	1.37E-04
FEP	1.53E-03	1.54E-03	8.03E-06	8.10E-06
MEP	1.75E-03	1.75E-03	9.19E-06	9.22E-06
HTP	2.75E+00	2.79E+00	1.45E-02	1.47E-02
POFP	1.66E-02	1.68E-02	8.75E-05	8.84E-05
PMFP	1.18E-02	1.19E-02	6.20E-05	6.26E-05
TETP	7.82E-04	8.17E-04	4.12E-06	4.30E-06
FETP	8.50E-02	8.58E-02	4.47E-04	4.52E-04
METP	8.05E-02	8.15E-02	4.24E-04	4.29E-04
IRP	3.52E-01	3.61E-01	1.85E-03	1.90E-03
ALOP	2.92E-01	2.94E-01	1.54E-03	1.55E-03
ULOP	6.93E-02	7.36E-02	3.65E-04	3.87E-04
NLTP	9.03E-04	9.48E-04	4.75E-06	4.99E-06
WDP	1.60E-01	1.60E-01	8.41E-04	8.43E-04
MDP	2.12E-01	2.19E-01	1.12E-03	1.15E-03
FDP	1.60E+00	1.64E+00	8.43E-03	8.65E-03

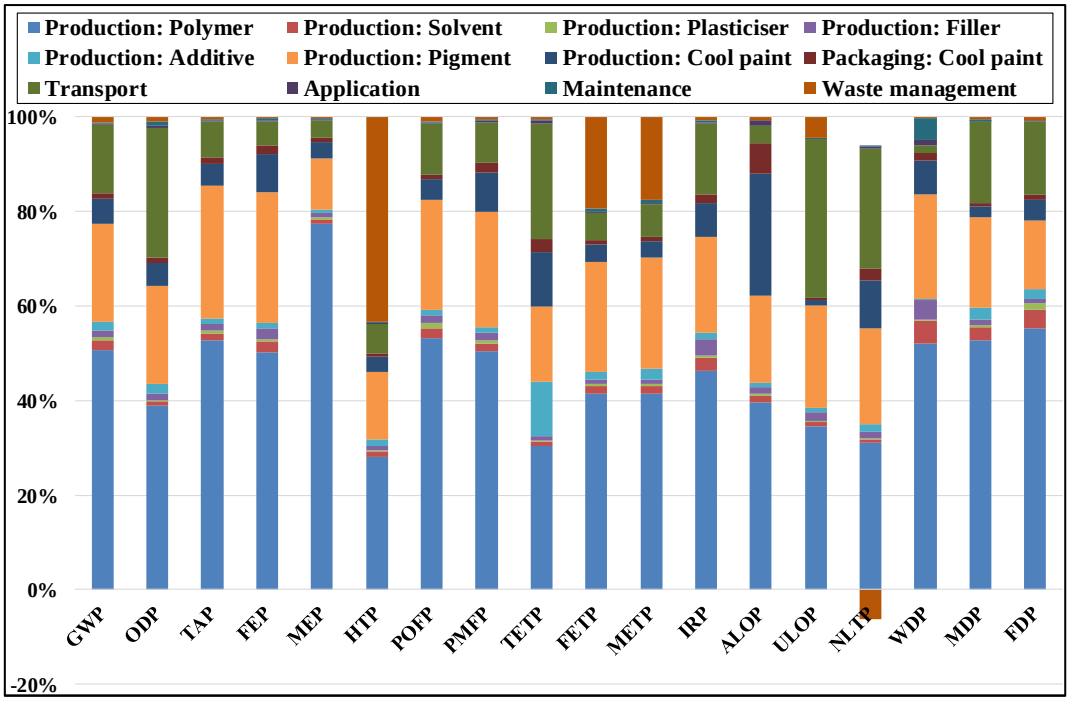

Figure 6-2: Midpoint cradle to grave percentage contribution by the lifecycle phases of the cool roof paint for the Palermo, Sicily case study.

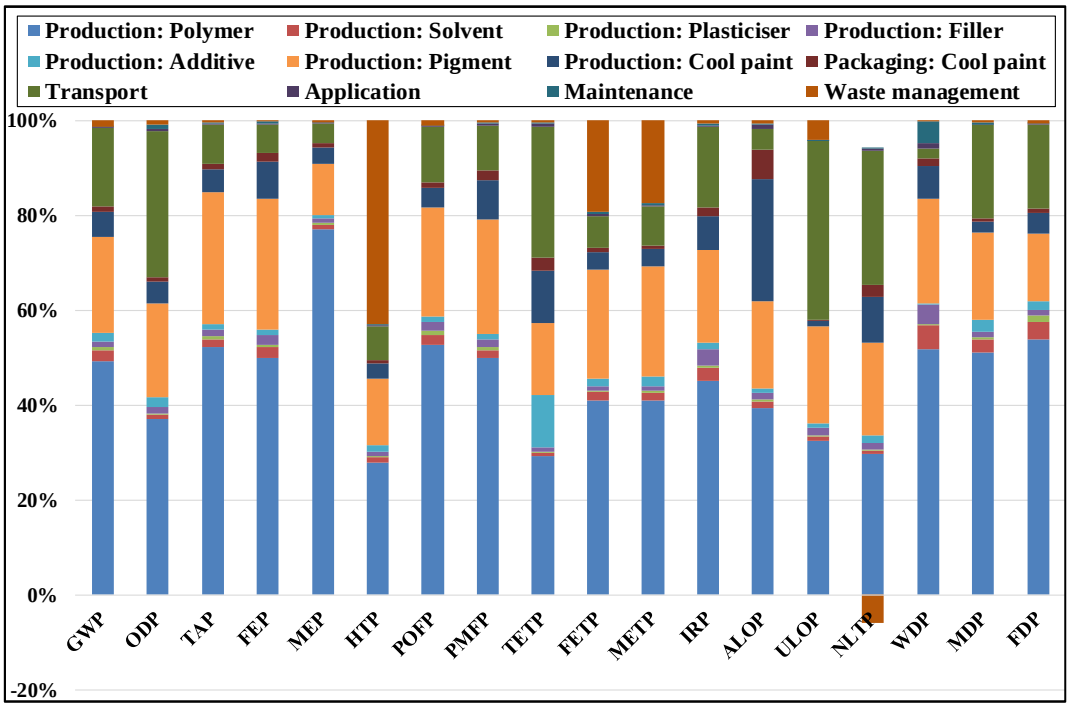

Figure 6-3: Midpoint cradle to grave percentage contribution by the lifecycle phases of the cool roof paint for the Portmore, Jamaica case study.

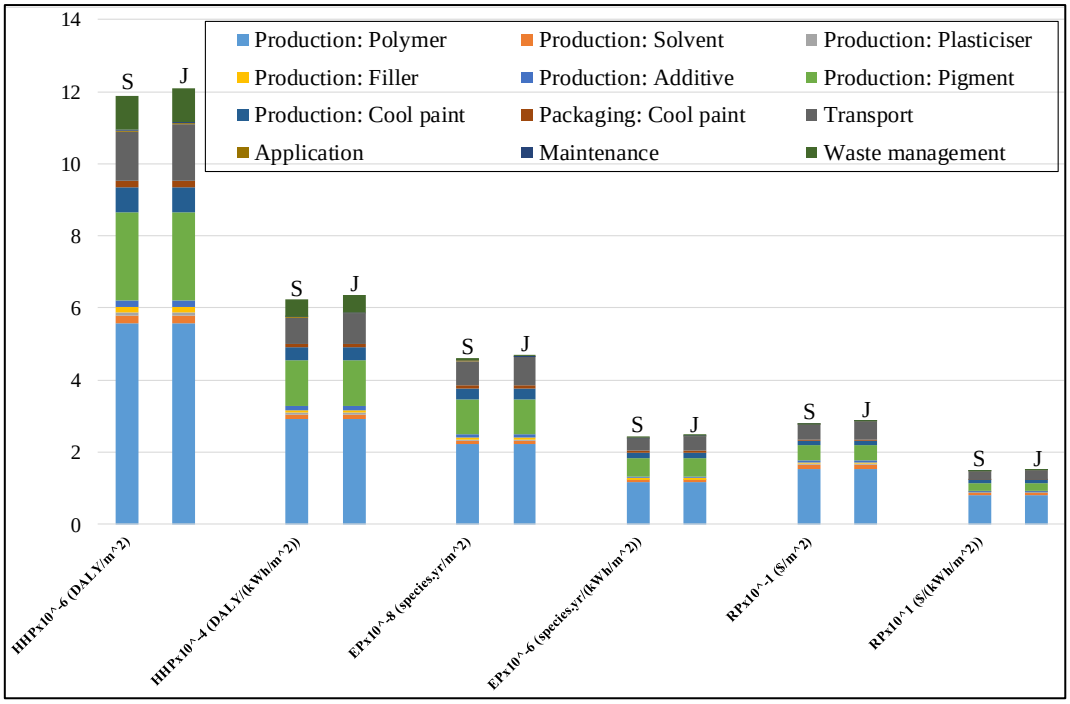

Figure 6-4: Endpoint cradle to grave lifecycle impacts of the cool roof paint for the Palermo, Sicily (S) and Portmore, Jamaica (J) case studies.

6.4 Comparison with LCA Studies of Thermal Insulation

The environmental impact comparison of cool roof paint was conducted for Palermo, Sicily only because of the availability of literature studies for case study locations in Europe. The environmental impact of cool roof paint is compared to literature studies of environmental impact of thermal insulation materials. As presented in chapter 4, the thermal insulation material provides equivalent energy saving potential and similar indoor thermal comfort as the assessed cool roof paint.

For this comparison, different LCA indicators were used depending on the available data in the literature for thermal insulation. The following were used:

- Cradle to Gate – CTGA; raw material acquisition and production,
- Cradle to Site – CTSI; raw material acquisition and production, transportation to the building site and installation, and
- CTGR approaches were used for the comparison.

Data were sourced from three public sources and are presented in Table 6-4 and Table 6-5 in comparison to the cool roof paint results. The sources are (Žigart et al., 2018), (Densley Tingley

et al., 2015) and (Sierra-Pérez et al., 2016). The results were normalised per 1 m^2; the functional unit of climate-controlled space according to the Council for European Producers of Materials for Construction (CEPMD) (Schiavoni et al., 2016).

Table 6-4 presents the CTGA GWP and TAP of the cool roof paint compared with the CTGA of the Rock Wool (RW), Expanded Polystyrene (EPS) and Wood Fibre (WF) for wall and/or roof of low-rise buildings in Central Europe (Žigart et al., 2018). It also compares CTGA GWP, ODP, POFP, TEP, FEP, MEP and WDP of the cool roof paint compared with the CTGA of EPS, Mineral Wool (MW) and Phenolic Foam (PF) (Densley Tingley et al., 2015).

Žigart *et al.*, (2018) studied different external wall elements (structural materials, thermal insulation materials and surface finishing) for different types of constructions. Therefore, the average GWP and TAP contribution by the studied thermal insulations were calculated according to the stated percentage share stated for thermal insulations. As a result, the GWP and TAP of the cool paint were 4–7-fold and 6–17-fold lower, than all the thermal insulation materials.

Densley Tingley, Hathway and Davison, (2015) found that the GWP, ODP, FEP, MEP and POFP of the cool roof paint were similar and up to 9-fold lower than EPS, MW and PF, while the WDP of the cool roof paint is 4–26-fold higher. The main contributing emission substances by cool paint to GWP are CO_2 (90 %) and methane (CH_4; 9 %), while sulphur dioxide (SO_2) (76 %) and nitrogen oxides (NO_x) (23 %) are the contributing substances to TAP. Similarly, the contributing emission substances by the thermal insulations to GWP are CO_2 and CH_4, while SO_2 and NO_x are the contributing substances to TAP. The higher (mostly) or lower environmental impact category indicators of the thermal insulations compared to the cool roof paint is probably because of the production phase; thermal insulator materials with high material density has a high environmental impact due to high primary energy demand during the acquisition (which includes transportation) and processing of raw materials.

Table 6-5 presents the CTSI GWP, ODP and TAP of the cool roof paint compared with the CTSI of the Extruded Polystyrene (XPS), EPS, Polyurethane (PU), Stone Wool (SW) and Spray Foam (GW) in Spain (Sierra-Pérez et al., 2016). The TAP of the cool roof paint was

found to be similar and up to 6.5-fold lower than all thermal insulation materials, GWP were 2–3-fold lower than XPS and EPS, and 40 % and up to 2-fold higher than PU, SW and GW, while ODP were similar and up to 7-fold lower than XPS, EPS and SW, and up to 77 % higher than XPS, PU and GW.

The midpoint environmental impact indicators of the cool roof paint from this study were compared with the results reported in the literature that investigated the midpoint environmental impact of thermal insulation. The average values of the study of (Žig*art et al*, 2018) were reported in Table 6-4 because different U-values of thermal insulation construction were assessed. From the comparison presented in Table 6-4 and Table 6-5, it can be seen that the CTGA/CTSI environmental impacts of the cool roof paint are lower than thermal insulation. The higher CTGA/CTSI environmental impact of insulation materials is mainly due to the fossil fuel consumption required during the production phase, which includes raw material acquisition and processing.

Table 6-4: Midpoint cradle to gate environmental impacts (per 1 m^2) comparison of cool paint with thermal insulation.

Impact indicators	This study	Central Europe case study (U-value = 0.25 W/m^2K) (Žigart et al., 2018)			UK case study location (U-value = 0.33 W/m^2K) (Densley Tingley et al., 2015)		
	Cool roof paint, Sicily	RW	EPS	WF	EPS	MW	PF
GWP	4.13E+00	3.22E+01	1.69E+01	1.94E+01	1.44E+01	1.55E+01	1.71E+01
ODP	3.14E-07				4.51E-07	7.60E-07	7.15E-07
TAP	2.36E-02	4.04E-01	1.60E-01	2.61E-01			
FEP	1.43E-03				1.60E-03	5.50E-03	4.70E-03
MEP	1.67E-03				8.70E-03	1.50E-02	1.10E-02
POFP	1.46E-02				7.90E-02	5.20E-02	8.50E-02
WDP	1.47E-01				5.60E-03	2.30E-02	3.20E-02

Table 6-5: Midpoint cradle to site environmental impacts (per 1 m^2) comparison of cool paint with thermal insulation.

Impact indicators	This study	Spain case study (U-value = 0.25 W/m^2K) (Sierra-Pérez et al., 2016)				
	Cool roof paint, Sicily	XPS	EPS	PU	SW	GW
GWP	4.84E+00	8.50E+00	1.40E+01	1.10E+01	2.10E+00	3.90E+00
ODP	4.39E-07	4.60E-07	6.80E-07	1.10E-07	3.20E-06	3.00E-07
TAP	2.57E-02	3.00E-02	4.60E-02	4.60E-02	1.70E-01	3.20E-02

Chapter 6 Summary

The use of LCA to estimate lifecycle environmental impact category indicators of the cool roof paint shows that the production of polymer and pigment lifecycle phase are the main hotspots responsible for most environmental impacts at both midpoint (45 % polymer and 20 % pigment) and endpoint (49 % polymer and 18 % pigment) categories. The contribution to the environmental impacts is mostly due to the acquisition and processing of raw materials to produce the material/chemical inputs. The comparison of the findings of this study with the results reported in the literature found that the lifecycle environmental impacts of the cool roof paint are lower than thermal insulation materials.

The study output of this chapter is the second key milestone in this research project. The study completed in this chapter complements the study conducted in chapter 4 in terms of the combination of energy demand, and environmental impacts for the critical assessment of material and energy flows of energy-efficient solutions for residential buildings. Further to the conclusion presented in chapter 4, this chapter buttresses the attractiveness of a cool roof paint retrofit solution because its environmental impact is lower than thermal insulation materials.

Chapter 7: Environmental Impact of the HCPV/T 2000x System

Introduction

Chapter 7 presents the estimated environmental impacts of the HCPV/T 2000x system for the Palermo, Sicily and Portmore, Jamaica case studies. The purpose of chapter 7 is to investigate the environmental impacts benefit of the HCPV/T 2000x system and compare them with PV and PVT. Section 7.1 presents the goal (aim), scope and functional units of the environmental impact study. The scope defines the method of environmental impact analysis, while the functional unit quantifies the performance of the HCPV/T 2000x system. Section 7.2 presents the system boundary and inventory. System boundary defines the processes which are part of the product system, while inventory consists of input and output data of the system boundary (BS EN ISO 14044, 2018). Section 7.3 presents the estimated environmental impact using "ReCiPe2016 Method – Lifecycle Midpoint and Endpoint Environmental Impact Assessment", explained in chapter 1, section 1.3.3. The ReCiPe2016 method is based on midpoint and endpoint impact category indicators. Section 7.4 presents the comparison of the estimated environmental impact indicators with the RES and non-RES electrical and/or thermal energy generation systems as reported in the literature.

7.1 Goal, Scope and Functional Unit

The goals of this study were to:

- estimate the lifecycle environmental impacts of electrical and thermal energy generation from HCPV/T 2000x system,
- critically evaluate the magnitude and significance of the lifecycle environmental impacts of electrical and thermal energy generation from HCPV/T 2000x system.

CTGR approach was the scope used for the LCA study, within the LCA system boundary as shown in Figure 7-1. The system boundary includes the following:

- raw materials acquisition and production,
- component manufacturing,
- transportation components to the installation site,
- installation of HCPV/T 2000x system, operation and maintenance over the service life, and
- end of life waste management (recycling and landfilling).

The functional units (units of analysis) for this study are:

- 1 kWh of electrical energy generated for a service life of 25 years,
- 1 kWh of thermal energy generated for a service life of 25 years.

The estimated lifecycle environmental impacts were allocated based on the total electrical and thermal energy production potential of the 11 m^2 HCPV/T 2000x system for a service life of 25 years. The service life of 25 years was used to assess the lifecycle environmental impacts of the HCPV/T 2000x system because CPV installations are typically warranted for 25 years as with standard PV systems (Wiesenfarth et al., 2017). The energy production potential of the HCPV/T 2000x system is presented in section 5.4 of chapter 5. For Palermo, Sicily case study, the total electrical energy production potential is 39,600 kWh (1584 kWh/year) and the total thermal energy production potential is 107,250 kWh (4290 kWh/year); consequently, the energy-based fraction of the lifecycle environmental impacts attributed to electrical and thermal energy are 0.37 and 0.63, respectively. For Portmore, Jamaica case study, the total electrical energy production potential is 27,500 kWh (1100 kWh/year) and the total thermal energy production potential is 66,550 kWh (2662 kWh/year); consequently, the energy-based fraction of the lifecycle environmental impacts attributed to electrical and thermal energy are 0.41 and 0.59, respectively.

7.2 System Boundary Description and Inventory

The assumptions, compilation and analysis of LCI data (Figure 7-1) used for this study are based on the system boundary for the HCPV/T 2000x system. LCI data collection for the HCPV/T 2000x system was classified, as follows:

- The Foreground data describe the HCPV/T 2000x system that was sourced directly from the company who designed and built the system (Table 7-1).
- The Background generic data describe the materials, energy, transport, and waste management related to the HCPV/T 2000x system. Those data were sourced from Ecoinvent via the SimaPro v8.2.3.0 software used in assessing the LCA of the HCPV/T 2000x system (PRé, 2016; Steubing et al., 2016).

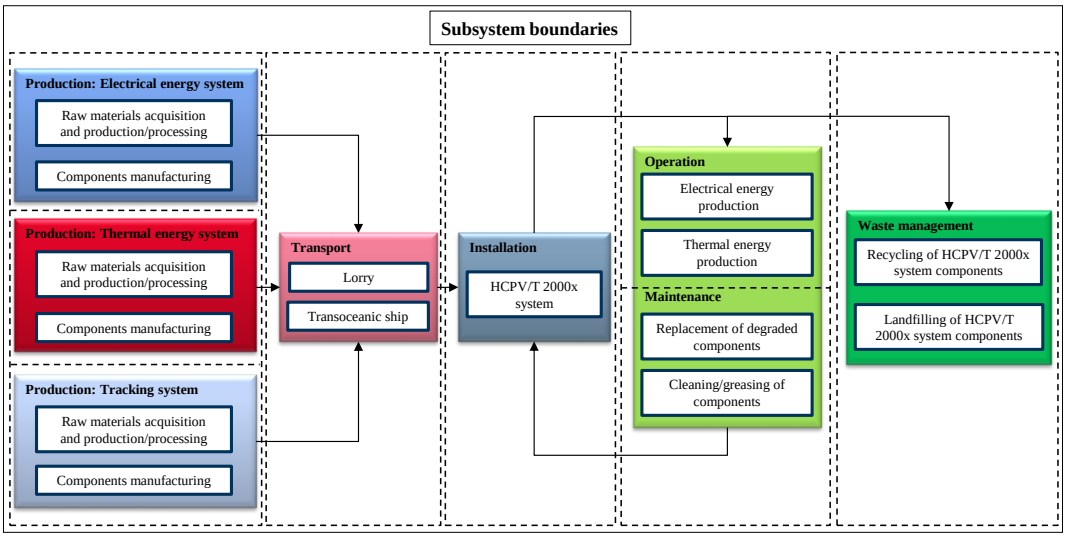

Figure 7-1: The LCA system boundary for the HCPV/T 2000x system.

The HCPV/T 2000x system boundary for the Palermo, Sicily and Portmore, Jamaica case studies consists of five subsystems: production and installation, operation and maintenance, and waste management (Figure 7-1). The production and installation subsystem involves raw materials acquisition and production, components manufacturing, components transportation to the installation site and assembly/installation of the HCPV/T 2000x system. The operation and maintenance subsystem involves the generation of electrical and thermal energy, replacement of degraded HCPV/T 2000x system component, cleaning, and greasing. Finally, the waste management subsystem involves recycling and landfilling according to the waste management policy and regulation of the case study location. Specific information on the five systems and sources of data are given below.

Table 7-1: Foreground inventory data for the electrical energy system, thermal energy system and tracking system.

Component (No of Components)	Value	Material
Thermal energy system		
Heat sink (x20)		
Top, bottom and side covers	1.72 kg	Aluminium alloy
Internal supporting structure	0.17 kg	Aluminium alloy
Countersunk fasteners (x80)	0.0040 kg	Steel
Internal and external rings (x40)	0.0062 kg	Synthetic rubber
G1-8 I-FESTO and G1-8 L-FESTO connectors (x40)	0.1700 kg	Steel
Reverse return system (1)		
12.7 mm and 38.1 mm cylindrical pipes, and 3.2 mm square pipe	8.83 kg	Steel
6 mm pipe	81.65 kg	Perfluoroalkoxy (vinyl ether) (PFA)
22 mm corrugated hose	0.6243 kg	Polyvinyl chloride (PVC)
Circulating pump (x1)	5.30 kg	Various: mainly iron, steel and copper
0.2 m^3 demineralized water storage tank (x1)	86 kg	Various: mainly steel and glass wool
Aignep 1120 fitting (x46)	0.8200 kg	Nickel-plated brass
PT100 platinum thermometer sensor (x4)	0.2500 kg	Various; mainly steel and wiring components (Polytetrafluoroethylene (PTFE) insulated screened lead)
0.2 m^3 demineralized water (x1)	200 kg	Demineralized water
Tracking energy system		
Axle		
Rotational longitudinal axle (2)	42.76 kg	Iron-base superalloy
Upper (x10) and lower (x10) tilting transverse axles	15.20 kg	Iron-base superalloy
Internal (x2) and external (x2) longitudinal transmission rods	24.17 kg	Iron-base superalloy
Longitudinal transmission rod connector (1)	1.68 kg	Iron-base superalloy
CMOS webcam	0.0590 kg	Various (including glass filter)
Electronic and software connections		Various
Reflective mirror and optical receiver		
Optical receiver (20)	0.38 kg	BK7 frustum
Reflective mirror (20)	23.30 kg	Ultraclean glass with a silver coating
Rotational and linear motor		
Rotational motor	0.1600 kg	Various (including steel)
Linear motor	0.1500 kg	Various (including steel)
Gearbox	1.4400 kg	Various (including steel)
AN8 magnet	0.0051 kg	Various (including iron)
Structural support		
Axle support	17.41 kg	Iron-base superalloy, nylon and steel
Central, north and south side foot supports	122.95 kg	Iron-base superalloy and steel
CMOS webcam support	0.54 kg	Iron-base superalloy and steel
Electronic connection support	11.23 kg	Iron-base superalloy and steel
Reflective mirror and optical receiver support	129.96 kg	Iron-base superalloy, nylon, and steel
Rotational and linear motor support	0.7974 kg	Iron-base superalloy
Electrical energy system		
InGaP/InGaAs/Ge solar cell (x20)		
Area of one InGaP/InGaAs/Ge solar cell	107.90 m^2	
Mass of one InGaP/InGaAs/Ge solar cell	7.80×10^{-3} kg	
Inverter (x1)		
Electrical capacity	1 kW	
Mass	2.30 kg	
1 Li-ion battery (x1) – 26 kg		

7.2.1 Production

This section presents specific information on the three systems and sources of data that make up the production of the HCPV/T 2000x system components.

Electrical energy system: The electrical energy system comprises InGaP/InGaAs/Ge solar cells, 1 kW variable load inverter, Lithium (Li) ion battery and electric wire connections. Although a Li-ion battery is not installed as part of the HCPV/T/2000x system at the case study location, it was assumed that it is part of the HCPV/T/2000x system. The background LCI data of InGaP/InGaAs/Ge solar cell were sourced from commercially available company/literature data, and adapted Silicon (Si) wafer and Czochralski processes from Ecoinvent; these processes were adapted by substituting element/process data related Si with In, Ga, P, As and Ge (PRé, 2016; Steubin*g et al*, 2016).

Thermal energy system: The thermal energy system comprises of active heat sinks and a reverse return system.

Tracking system: The tracking system comprises of structural support, axle, CMOS webcam, electronic and software connection, reflective mirrors, optical receiver, rotational and linear motor.

7.2.2 Transport

The transportation phase of the LCA assesses the transportation impact during the supply of system components to the case-study location site. The transportation impact during raw materials acquisition and component production is not included in the phase. Instead, it is embedded in the environmental impact at the raw materials acquisition and component production. The transportation modes and distances are summarized in Table 7-2: Transportation modes and distances in the supply of all HCPV/T 2000x system components. For the Palermo, Sicily case study, it was assumed that all the system components (except the InGaP/InGaAs/Ge solar cell) were manufactured and supplied from the industrial area of Italy (the north). The InGaP/InGaAs/Ge solar cells were manufactured and supplied from Taiwan to Palermo, Sicily, Italy. It was assumed that the InGaP/InGaAs/Ge solar cells were transported

by road from the manufacturer to the port of Kaohsiung, Taiwan then by sea to the port of Palermo, Italy. It was also assumed that the components from the north of Italy were transported by road to the port of Genova then by sea to the port of Palermo. For the Portmore, Sicily case study, it was assumed that all the system components (except the InGaP/InGaAs/Ge solar cell) were manufactured and supplied from the industrial area of Mississippi (southern USA state). The InGaP/InGaAs/Ge solar cells were manufactured and supplied from Germany to Portmore, Jamaica. It was assumed that the InGaP/InGaAs/Ge solar cells were transported by road from the manufacturer to the port of Bremen, Germany then by sea to the port of Kingston, Jamaica. It was also assumed that the components from the industrial area of Mississippi were transported by road to the port of New Orleans, then by sea to the port of Kingston.

Table 7-2: Transportation modes and distances in the supply of all HCPV/T 2000x system components.

Case study	Components	Value	Transport Mode
Sicily	InGaP/InGaAs/Ge solar cells	325 km	Lorry (3.5–7.5 t)
		16433 km	Transoceanic ship
	The rest of the system components	100 km	Lorry (3.5–7.5 t)
		963 km	Transoceanic ship
Jamaica	InGaP/InGaAs/Ge solar cells	589	Lorry (3.5–7.5 t)
		11708	Transoceanic ship
	The rest of the system components	467	Lorry (3.5–7.5 t)
		2759	Transoceanic ship

7.2.3 Installation

The installation phase of the LCA assesses the potential land use and electricity consumption of installing 11 m^2 HCPV/T 2000x system.

7.2.4 Operation and Maintenance

The current challenge facing the deployment of the CPV and CPV/T (or HCPV/T) systems is the lack of procedures and regulatory standards for the development and maintenance gates of the system product lifecycle. Currently, the only available information is the findings published by (Sanchez *et al*, 2010) based on theoretical aspects of the different elements to identify the critical components of the CPV system. The elaboration of those findings, which are related to the identified critical components based on the CPV system operation and maintenance data were collected from 2009 to 2016 (Gil et al., 2017). The identified critical

components accounting for 85 % of the operational and maintenance incidences are tracker, control software and electrical connections, of which the tracker accounts for more than 50 % of the operational and maintenance incidence (Sanchez et al., 2010). The findings published by (Gil et al., 2017) show a significant reduction in operational and maintenance incidences from 2009 to 2016, which resulted with increasing the reliability and availability of the system to 99.5 %. Therefore, it was assumed that the HCPV/T 2000x systems reliability and maintenance is 99.5 % and that the required operation and maintenance were based on the replacement of degraded components and yearly maintenance of structural components (

Table 7-3). A state-of-the-art Li-ion battery available in MWh nominal capacity was adopted as part of the HCPV/T 2000x system. Li-ion batteries have a long lifetime depending on their management and depth of discharge. They are recommended for home systems with PV electricity generation in hot climates (Charles et al., 2019); although costs are still high their environmental impact is lower than acid-lead batteries (Diouf and Avis, 2019). We propose a Lithium Ferro Phosphate battery with claimed discharge cycles of 10,000 at 80 % depth of discharge (Spirit Energy, 2017) complemented by a management system to minimize cycles and depth of discharge. Therefore, the battery will not be replaced during the HCPV/T 2000x system service life of 25 years.

Table 7-3: Operational and maintenance of the HCPV/T 2000x system for a service life of 25 years.

Components	Value	Assumption
InGaP/InGaAs/Ge solar cells	0.0096 kg	Replacement of one cell per year caused the failure or damaged due to the high CR (=2000) from the reflective mirror
Demineralized water	5000 kg	Assuming 200 kg of water is used for cleaning the reflective mirror, and for refilling the thermal storage tank
Optical receiver	0.38 kg	Replacement of all the optical receiver halfway through the service life (Costa *et al*, 2011)
Reflective mirror	23.3 kg	Replacement of all the reflective mirror halfway through the service life
Structural support	125 kg	Assuming 5 kg of lithium grease is used to grease structural components
Li-ion battery	26 kg	The battery is assumed to function for the 25 years of system's life equipped by a management system to minimise cycles and depth of discharge.

7.2.5 Waste Management

This case study assumes that after 25 years of service, the HCPV/T 2000x system components, which include the components replaced during maintenance and their different material types/parts (Table 7-4) will be recycled and landfilled (Figure 7-1). Italy as a member of the

EU is obliged to follow the EU's waste policy and legislation set up by the EC (European Commission, 2019c).

Table 7-4: Waste management of HCPV/T 2000x system. Due to lack of data, waste treatment of InGaP/InGaAs/Ge solar cell was not assessed.

Components/Material Type	Value
Ferrous metal; waste management	
Recycling	80 % (UN*EP et al*, 2011)
Landfilling	20 %
Non-ferrous metal; waste management	
Recycling	90 % (IAI, 2009)
Landfilling	10 %
Glass; waste management	
Recycling	73 % (FEVE, 2015)
Landfilling	27 %
Plastic, PFA and synthetic rubber; waste management	
Recycling	30 % (EU, 2018)
Landfilling	70 %
Li-ion battery, inverter, pump, circulating pump and demineralized water storage tank; waste management	
Recycling	These components were made of different types of material. However, recycling/landfilling was assessed based on the main material type and Ecoinvent database.
Landfilling	

7.3 Midpoint and Endpoint Environmental Impact Category Indicators and Identification of Hotspots

The results of midpoint environmental impacts are presented in Table 7-5 (presented numerically in the first two columns for Palermo, Sicily and Portmore, Jamaica case studies). Figure 7-2 and Figure 7-3 present the percentage contribution (presented in Table 7-5) by the subsystem boundaries. The endpoint environmental impacts are presented in Figure 7-4 and Figure 7-5 for Palermo, Sicily and Portmore, Jamaica case studies respectively. The results are presented separately for the Electrical Energy Impact Allocation (EEIA) and Thermal Energy Impact Allocation (TEIA) for the defined functional units of 1 kWh for the electrical energy and 1 kWh for the thermal energy.

At the midpoint level as shown in Figure 7-2 and Figure 7-3, the *production: thermal energy* and *tracking systems* are the main contributors to the following 13 impact category indicators: GWP, ODP, TAP, FEP, MEP, HTP, POFP, PMFP, FETP, IRP and FDP. The main contributors to TETP, WDP and ALOP are the *operation and maintenance* and *production: thermal energy*

system. The main contributors to METP are *production: thermal and electrical energy* and *tracking systems*. Finally, the main contributors to NLTP are *operation and maintenance* and *installation*.

At the endpoint level as shown in Figure 7-4 and Figure 7-5, the main contributors to HHP and RP are the *production: thermal energy* and *tracking systems* while the main contributors to EP are the *production: thermal energy system* and *operation and maintenance*. The *production: thermal energy system* contribution to the environmental impacts are mostly due to the raw materials acquisition/production and manufacturing of the demineralized water storage tank that is mostly accounted for by metalworking (mainly hot steel alloy rolling), welding and glass wool manufacturing process. Also, the *production: tracking system* contribution is mostly due to the raw materials acquisition/product and manufacturing of the structural support and axle that are mostly accounted for by metalworking (mainly hot steel alloy rolling). The *production: electrical energy system* contribution can be traced to the raw materials acquisition/production and manufacturing of the electrical wire connections. The contribution towards *operation and maintenance* was due to the use of on-site land, demineralized water for thermal energy extraction and cleaning of the reflective mirror, and lithium for greasing the metallic structural support while the *installation* was due to the use of on-site land and energy consumed by during the installation of the HCPV/T 2000x system.

Table 7-5: Midpoint system boundary environmental EEIA (per 1 kWh) and/or TEIA (per 1 kWh) for Palermo, Sicily and Portmore, Jamaica case studies; comparison with the cradle to grave of the WB-CHP (González-garcía and Bacenetti, 2019) and AD-CHP-ORC (Bacenetti et al., 2019) systems in Italy and SE-micro-CHP (Stamford et al., 2018) and industrial CHP (Kelly et al., 2014) systems conducted in the UK.

Midpoint Impact Indicator	HCPV/T 2000x System Palermo, Sicily		HCPV/T 2000x System Portmore, Jamaica		WB-CHP	AD-CHP-ORC	SE-Micro-CHP		Industrial CHP
	EEIA	TEIA	EEIA	TEIA	EEIA	EEIA	EEIA	TEIA	EEIA
GWP	1.30E-01	8.19E-02	2.12E-01	1.25E-01	1.41E-01	2.02E-01	3.66E-01	2.32E-01	1.93E-01
ODP	3.04E-08	1.92E-08	4.96E-08	2.91E-08		1.31E-08			
TAP	3.32E-03	2.09E-03	5.36E-03	3.15E-03	3.64E-03	4.91E-03	3.44E-04	−1.59E-04	
FEP	1.13E-04	7.10E-05	1.82E-04	1.07E-04	1.27E-05	3.46E-05			
MEP	5.38E-05	3.39E-05	8.71E-05	5.11E-05	3.69E-04	2.33E-03			
HTP	1.78E-01	1.12E-01	2.87E-01	1.68E-01	4.38E-02	2.81E-02			
POFP	7.26E-04	4.58E-04	1.18E-03	6.93E-04	2.31E-03	6.70E-04			
PMFP	1.07E-03	6.75E-04	1.73E-03	1.01E-03	1.01E-03	7.90E-04			
TETP	1.08E-04	6.84E-05	1.76E-04	1.03E-04					
FETP	8.96E-03	5.65E-03	1.45E-02	8.48E-03					
METP	8.59E-03	5.42E-03	1.39E-02	8.14E-03					
IRP	9.48E-03	5.98E-03	1.55E-02	9.11E-03					
ALOP	2.59E-02	1.64E-02	4.18E-02	2.45E-02					
ULOP	2.59E-03	1.63E-03	4.27E-03	2.51E-03					
NLTP	1.14E-04	7.19E-05	1.85E-04	1.09E-04					
WDP	2.55E-03	1.61E-03	4.12E-03	2.42E-03					
MDP	2.02E-01	1.27E-01	3.25E-01	1.91E-01		1.13E-02			
FDP	2.89E-02	1.82E-02	4.77E-02	2.80E-02	3.34E-02	3.76E-02			

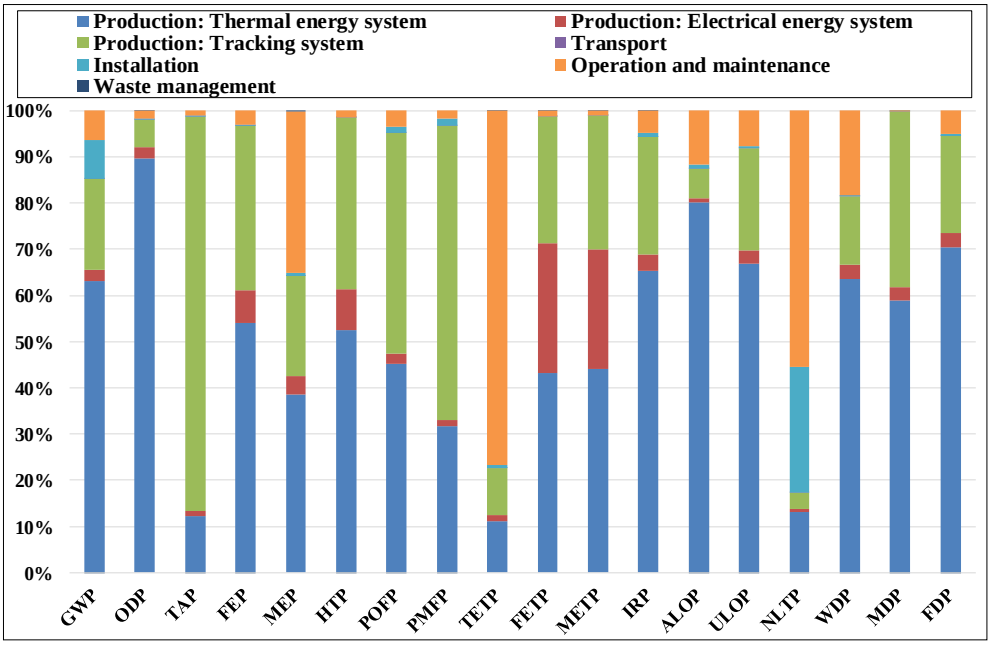

Figure 7-2: Midpoint EEIA and TEIA percentage contribution by the subsystem boundaries of the HCPV/T 2000x system for the Palermo, Sicily case study.

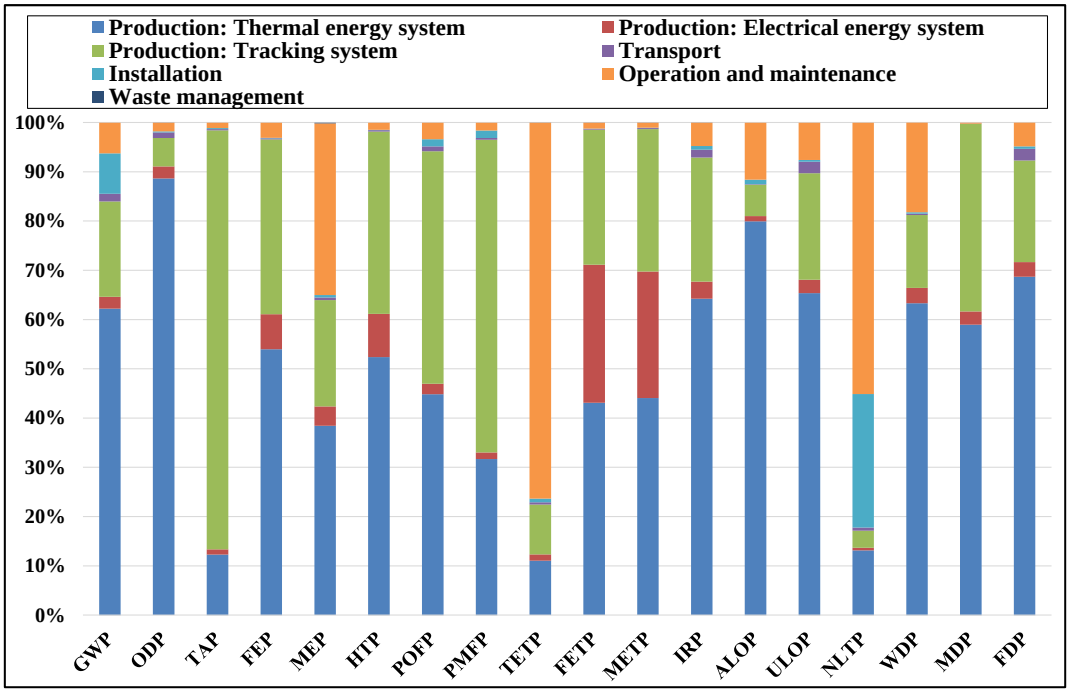

Figure 7-3: Midpoint EEIA and TEIA percentage contribution by the subsystem boundaries of the HCPV/T 2000x system for the Portmore, Jamaica case study.

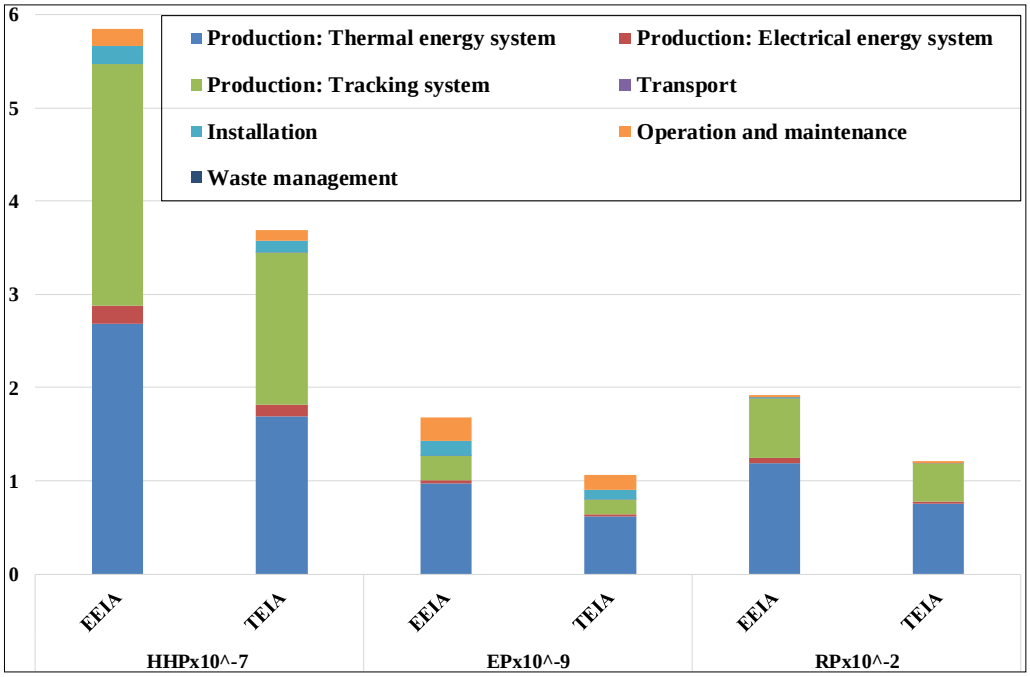

Figure 7-4: Endpoint system boundary EEIA and TEIA of the HCPV 2000x system for the Palermo, Sicily case study. The units of the endpoint impacts are HHP (DALY/kWh), EP (species. yr/kWh) and RP ($/kWh).

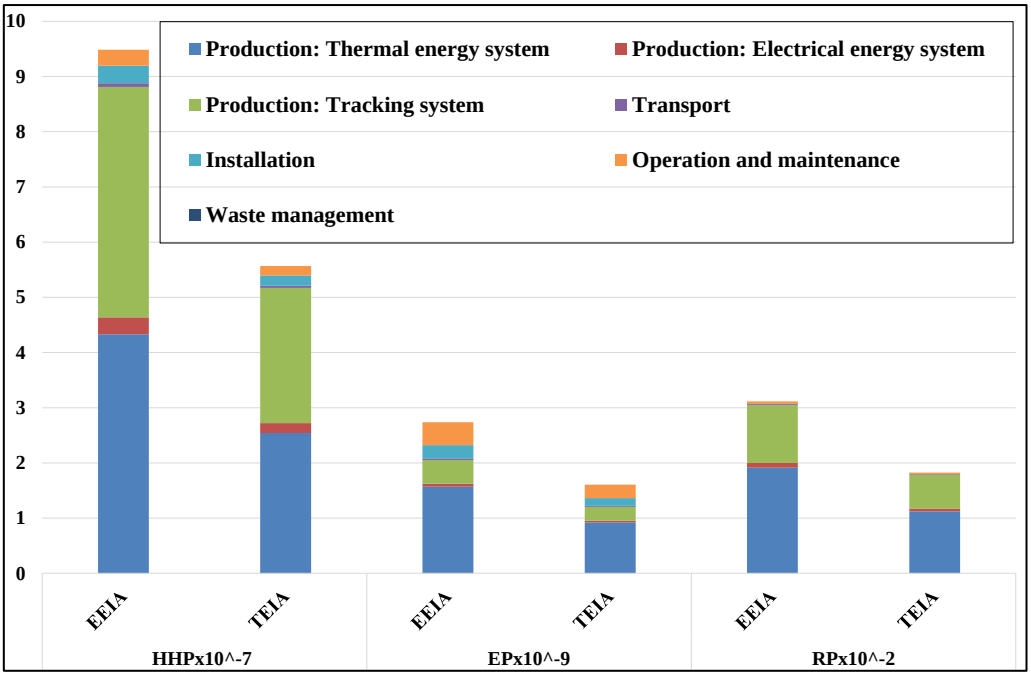

Figure 7-5: Endpoint system boundary EEIA and TEIA of the HCPV 2000x system for the Portmore, Jamaica case study. The units of the endpoint impacts are HHP (DALY/kWh), EP (species.yr/kWh) and RP ($/kWh).

These results were used to identify the hotspots within the system boundary in accordance to the EC (European Commission, 2016; Zampo*ri et al*, 2016), which state that the most relevant lifecycle stages are those that contribute over 80 % (before normalization and weighting) to any of the baseline impact category indicators. The percentage contribution of the estimated environmental impacts of the HCPV/T 2000x system, by each subsystem of the system boundary (presented in Figure 7-1) is the same as presented in Figure 7-2 and Figure 7-3. However, the estimate environmental impacts values are different as presented in Table 7-5. At the midpoint level, the *production: thermal energy system*, *production: tracking system*, *operation and maintenance* subsystem boundaries are the identified hotspots because on average across the 18 environmental impact category indicators, they are responsible for 92 % of the environmental impacts (50 %, 29 % and 13 % respectively). At the endpoint level, the *production: thermal energy system* and *production: tracking system* subsystem boundaries are the identified hotspots because on average across the 3 environmental impact category indicators, they are responsible for 87 % of the environmental impacts (55 % and 32 % respectively). The identification of *production: tracking system* as a hotspot and its cause is in agreement with (Nishimura et al., 2010; Sturm et al., 2010) who reported that the LCA study of HCPV system identifies the tracking system as a hotspot.

7.4 Comparison of Midpoint Impact Indicator Results with Literature

The midpoint environmental impact indicators of the HCPV/T 2000x system from this study were compared with the results reported in the literature that investigated the midpoint environment impact of the cogeneration systems for the case studies in Italy, Mexico and the UK (Table 7-5 and Table 7-6). Also, Table 7-7 and Figure 7-6 show the comparison of the lifecycle environmental impacts of this study in comparison to RES and non-RES technologies in six world regions (China, OECD Europe, OECD North America, Latin America, Africa and the Middle East), and the global scale. The median values of the literature case studies were reported in Table 7-6 and Table 7-7 and Figure 7-6 because different scenarios (SC) or types of energy system technology were studied and it was less affected by outliers. To maintain consistency, the impact indicator units of MWh were converted to kWh.

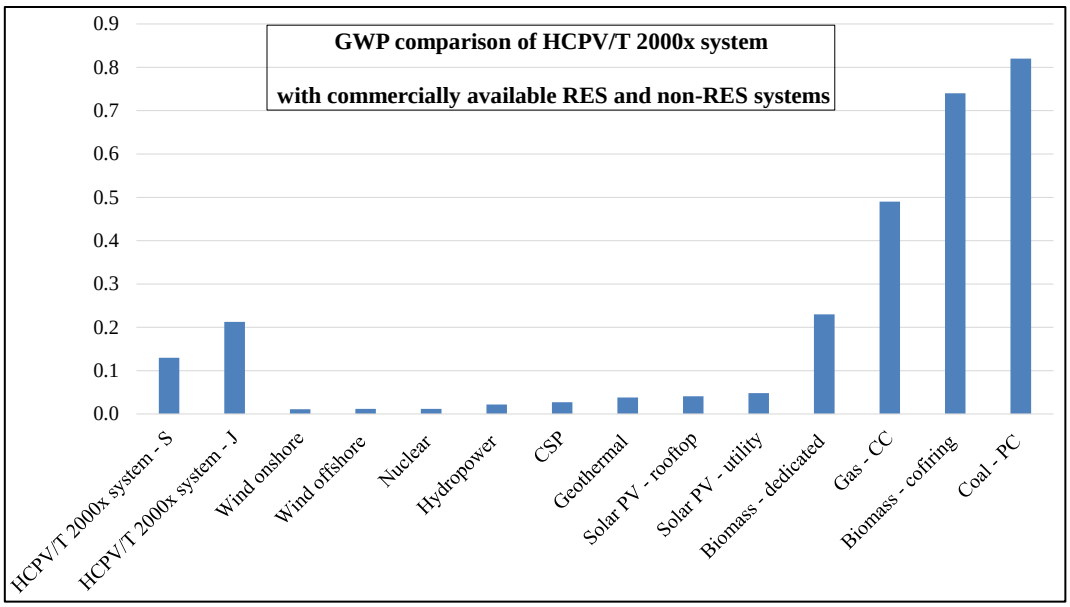

Figure 7-6: System boundary GWP ($kg\,CO_2 - eq/kWh$) for EEIA Palermo, Sicily (S) and Portmore, Jamaica (J) case study comparison with commercially available RES and non-RES systems; based on the global average of lifecycle GWP (IPCC, 2014). The abbreviations CC and PC means Combined Cycles and Pulverized Coal, respectively.

Table 7-6: Midpoint operation and maintenance subsystem boundary environmental EEIA and TEIA for Palermo, Sicily and Portmore, Jamaica case studies; comparison with an operational lifecycle stage of the ST-CHP, GT-HRSG-CHP and GT-PCC-HRSG-CHP systems case studies conducted in Mexico (Mora et al., 2019).

Midpoint Impact Indicator	HCPV/T 2000x System Palermo, Sicily		HCPV/T 2000x System Portmore, Jamaica		ST-CHP		GT-HRSG-CHP		GT-PCC-HRSG-CHP	
	EEIA	TEIA	EEIA	TEIA	EEIA	TEIA	EEIA	TEIA	EEIA	TEIA
GWP	8.27E-03	5.22E-03	1.33E-02	7.82E-03	1.09E-01	5.17E-01	8.03E-02	3.80E-01	5.95E-03	3.07E-02
ODP	5.50E-10	3.47E-10	8.86E-10	5.20E-10						
TAP	3.81E-05	2.40E-05	6.14E-05	3.60E-05	9.74E-04	4.61E-03	6.30E-04	2.98E-03	2.55E-04	1.32E-03
FEP	3.51E-06	2.21E-06	5.66E-06	3.32E-06					7.09E-06	3.65E-05
MEP	1.88E-05	1.19E-05	3.04E-05	1.78E-05	8.73E-06	4.13E-05	5.24E-06	2.48E-05	4.25E-06	2.19E-05
HTP	2.61E-03	1.65E-03	4.21E-03	2.47E-03	1.17E-04	5.53E-04	5.24E-05	2.48E-04	5.37E-03	2.77E-02
POFP	2.49E-05	1.57E-05	4.01E-05	2.35E-05	5.17E-04	2.44E-03	3.35E-04	1.58E-03	3.54E-05	1.83E-04
PMFP	1.75E-05	1.11E-05	2.82E-05	1.66E-05	2.18E-04	1.03E-03	1.41E-04	6.68E-04	5.67E-05	2.92E-04
TETP	8.32E-05	5.25E-05	1.34E-04	7.87E-05			1.75E-06	8.25E-06	5.67E-06	2.92E-05
FETP	1.09E-04	6.87E-05	1.75E-04	1.03E-04	1.57E-05	7.43E-05			3.83E-04	1.97E-03
METP	9.11E-05	5.75E-05	1.47E-04	8.62E-05	1.40E-05	6.60E-05			1.13E-04	5.84E-04
IRP	4.60E-04	2.90E-04	7.42E-04	4.35E-04	4.54E-05	2.15E-04			7.09E-05	3.65E-04
ALOP	3.02E-03	1.90E-03	4.86E-03	2.85E-03						
ULOP	2.02E-04	1.27E-04	3.25E-04	1.91E-04					1.42E-05	7.31E-05
NLTP	6.33E-05	3.99E-05	1.02E-04	5.99E-05						
WDP	4.67E-04	2.94E-04	7.52E-04	4.41E-04	1.89E-04	8.91E-04	7.16E-05	3.38E-04	1.70E-04	8.77E-04
MDP	4.70E-04	2.96E-04	7.57E-04	4.44E-04	8.73E-06	4.13E-05			9.92E-05	5.11E-04
FDP	1.45E-03	9.12E-04	2.33E-03	1.37E-03	2.82E-02	1.33E-01	1.82E-02	8.61E-02	1.18E-02	6.09E-02

Table 7-7: Midpoint system boundary environmental EEIA for Palermo, Sicily and Portmore, Jamaica case studies; comparison with lifecycle environmental impacts of RES and non-RES systems (Hertwich et al., 2015).

Midpoint Impact Indicator	HCPV/T 2000x System Palermo, Sicily	HCPV/T 2000x System Portmore, Jamaica	PV	CSP	Hydropower	Wind	Coal	Natural Gas
GWP	1.30E-01	2.12E-01	2.25E-02	2.79E-02	4.22E-02	1.11E-02	5.27E-01	3.87E-01
TAP	3.32E-03	5.36E-03	1.40E-04	1.39E-04	2.39E-04	7.23E-05	1.08E-03	4.23E-03
FEP	1.13E-04	1.82E-04	1.84E-05	9.04E-06	2.06E-06	8.32E-06	5.30E-04	7.75E-06
HTP	1.78E-01	2.87E-01	2.84E-02	9.21E-03	4.32E-03	1.70E-02	1.18E-01	1.00E-01
POFP	7.26E-04	1.18E-03	7.99E-05	1.14E-04	4.16E-04	6.17E-05	8.21E-04	6.93E-04
PMFP	1.07E-03	1.73E-03	4.12E-05	4.80E-05	1.13E-04	3.96E-05	3.25E-04	8.37E-04
FDP	2.89E-02	1.44E-01	1.44E-02	1.17E-02	2.44E-03	1.16E-02	9.60E-04	3.89E-04

7.4.1 Discussion on results presented in Table 7-5

Table 7-5 presents several system boundary environmental EEIA of the HCPV/T 2000x system compared with the cradle to grave of the Wood Biomass-Combined Heat and Power (WB-CHP) (González-garcía and Bacenetti, 2019) and Anaerobic Digestion-Combined Heat and Power-Organic Rankine Cycle CHP (AD-CHP-ORC) (Bacenetti et al., 2019) systems located in Italy. The WB-CHP system uses wood-based biomass from the forest and agricultural activities as a source of heat to produce electrical energy. The analyzed WB-CHP considered four alternative SC of biomass sources: “residues from natural regeneration forestry and industrial activities as feedstock” (SC1), rotation forestry of poplar (SC2), rotation forestry of willow (SC3) and “residues from natural forests and traditional poplar plantations” (SC4). It

was found that the GWP, TAP, FDP, POFP and MEP of the HCPV/T 2000x system were up to 68-fold lower than the WB-CHP system. In opposite, the remaining impact indicators were 6 % – 89 % higher than WB-CHP system. The main reason for the higher environmental impacts seems to be the processes that include: biomass transportation from forest stands to the power plant site, biomass combustion in CHP system and diesel consumption in forest machinery for the production of biomass feedstock used in SC2, SC3 and SC4, all of which contributes to the emission of substances; mainly NO), CO_2 and Particulate matter (PM) (González-garcía and Bacenetti, 2019). The AD-CHP-ORC system uses the AD process as a source of low-grade heat to produce electrical energy. The FDP, TAP, GWP, and MEP of the HCPV/T 2000x system were up to 43-fold lower while the remaining impact indicators were 8 % – 94 % higher than the AD-CHP-ORC system. The main reason for increasing of the environmental impacts of the AD-CHP-ORC system is probably as a result diesel consumption for feedstock production and transport (resulting in the emission of NO_x, CO_2, PM), and methane (CH_4) and Nitrogen Dioxide (NO_2) emissions from digestate during storage (Bacenetti et al., 2019; González-garcía and Bacenetti, 2019).

Table 7-5 also presents system boundary GWP and/or TAP for EEIA and TEIA of the HCPV/T 2000x system compared with the cradle to grave of the Stirling Engine micro-CHP (SE-micro-CHP) (Stamford et al., 2018) and industrial CHP systems (Kelly et al., 2014) for the case studies in the UK. The SE-micro-CHP system is similar in shape and size to a residential domestic gas boiler while the industrial CHP plant is an operational plant that both produces electrical and thermal energy. The system boundary GWP for EEIA and TEIA of the HCPV/T 2000x system was 19-fold lower, while the TAP was 90 % and 11-fold respectively, compared to the SE-micro-CHP system. The system boundary GWP for EEIA of the HCPV/T 2000x system showed to be 49 % lower comparing to the industrial CHP. The main reason for the higher GWP of SE-micro-CHP system is probably as a result of fuel (natural gas) combustion (Kelly et al., 2014; Stamford et al., 2018).

7.4.2 Discussion on results presented in Table 7-6

Table 7-6 presents several operations and maintenance subsystem boundary environmental EEIA and TEIA of the HCPV/T 2000x system compared with the operational lifecycle stage of the Steam Turbine-CHP (ST-CHP), Gas Turbine- Heat Recovery Steam Generator-CHP

(GT-HRSG-CHP), Gas Turbine-Post Combustion Carbon Capture-CHP and (GT-PCC-HRSG-CHP) systems for the case studies in Mexico (Mora et al., 2019). The ST-SHP system is a conventional plant, which uses high-pressure steam, while the GT-HRSG-CHP and GT-PCC-HRSG-CHP systems retrofitted from the ST-SHP system are gas turbine systems incorporated with HRSG, and PCC-HRSG respectively. It was found that the HCPV/T 2000x system operation and maintenance subsystem boundary EEIA and TEIA GWP, TAP, POFP, PMFP and FDP were 9 – 155-fold lower than the ST-CHP and GT-HRSG-CHP systems. Also, the HCPV/T 2000x system operation and maintenance subsystem boundary EEIA and TEIA TAP, HTP, POFP, PMFP, FETP, METP and FDP were up to 66-fold lower than GT-PCC-HRSG-CHP system. The main reason for the higher environmental impacts of ST-CHP, GT-HRSG-CHP and GT-PCC-HRSG-CHP systems is probably as a result of fuel (natural gas) combustion, which contributes to the emission of substances; mainly NO_x, CO_2, carbon monoxide (CO), PM, CH_4, and Volatile Organic Compounds (VOC). The ST-CHP and GT-PCC-HRSG-CHP systems have the highest and lowest environmental impacts respectively, because of the reduction in fuel (natural gas) for combustion by the GT-PCC-HRSG-CHP systems (Mora et al., 2019).

7.4.3 Discussion on results presented in Table 7-7

Table 7-7 presents several system boundary environmental EEIA of the HCPV/T 2000x system compared with the lifecycle environmental impacts of RES (PV, CSP, Hydropower and Wind power) and non-RES (Coal and Natural gas) systems respectively, for six world regions; China – Coal and Natural gas systems, OECD Europe – Wind power systems, OECD North America – PV systems, Latin America – Hydropower systems, and Africa and Middle East – CSP systems. It can be seen that for all impacts, the PV systems are 50 % – 96 %, CSP systems 60 % – 96 %, hydropower systems 43 % – 98 % and wind systems 60 % – 98 % lower than the HCPV/T 2000x system. The higher environmental impact of the HCPV/T 2000x system is probably as a result of higher input of raw materials, energy and heating processes during the production of the thermal energy and tracking systems. The non-RES systems in comparison with HCPV/T 2000x system presented different values for the different EEIA, as follows: the GWP, FEP and POFP of Coal systems were up to 4-fold lower while TAP, HTP, PMFP and FDP of the HCPV/T 2000x system 34 % – 97 % higher; the GWP and TAP of Natural gas systems up to 2-fold lower while FEP, HTP, POFP, PMFP and FDP of the HCPV/T 2000x

system 5 % – 99 % higher (IPCC, 2014). The environmental impact of the HCPV/T 2000x system is higher probably as a result of the higher primary energy demand required during raw materials acquisition/production and manufacturing of the thermal energy and tracking systems.

7.4.4 Discussion on results presented in Figure 7-6

Figure 7-6 presents the system boundary GWP for EEIA compared with commercially available RES and non-RES systems based on the global average of lifecycle GWP. The RES technologies are wind offshore, solar PV – rooftop, wind onshore, CSP geothermal and solar PV – utility while the non-RES technologies are nuclear, coal power plant (pulverized plant), gas power plant (combined cycle), biomass power plant (co-firing), biomass power plant and hydropower. The GWP of the RES systems is 63 – 92 % lower than the HCPV/T 2000x system. The GWP of the non-RES technologies (except for nuclear) is up to 6-fold higher than the HCPV/T 2000x system while the GWP of the nuclear is 91 % lower. The main reason for the higher GWP of the non-RES systems is probably as a result of fossil fuel combustion (IPCC, 2014) while for the RES systems, it is as a result of the higher primary energy demand required during raw materials acquisition/production and manufacturing of the thermal energy and tracking systems (Nishimura et al., 2010; Sturm et al., 2010).

7.4.5 Summary of Comparison of HCPV/T 2000x with other Systems

The system boundary (including the operation and maintenance subsystem boundary) environmental impacts (including GWP) of the HCPV/T 2000x system is lower than lifecycle environmental impacts of the non-RES systems (including fuel-based CHP systems). This is mainly due to the fuel (natural gas and diesel) combustion/consumption by the CHP system. However, comparison with RES systems shows higher environmental impacts in most categories. In many cases, there are explanations of why and need to be looked at system by system.

As an example, the system boundary GWP of HCPV/T 2000x system for EEIA (estimated at 130 $\mathrm{g\,CO_2-eq/kWh}$) was compared with the literature findings. The estimated GWP for HCPV systems was found to be no more than 50 $\mathrm{g\,CO_2-eq/kWh}$ (Lamnatou and Chemisana,

2017). It should be noted that those literature case studies did not include a reverse return system, which is the most significant contributor to the thermal energy system of the HCPV/T 2000x system. As mentioned in Table 7-1, the reverse return system consists of several components that include an active heat sink, and pipes with supply and return the connection to the demineralized water storage tank. The demineralized water storage tank is the main contributor to the reverse return system due to the raw materials acquisition/production and manufacturing of the demineralized water storage tank; that are mostly accounted for by metalworking (mainly hot steel alloy rolling), welding and glass wool manufacturing process. The discontinuation of the GWP by the reverse return system (82 $\mathrm{g\,CO_2-eq/kWh}$) leads to the reduced GWP of 48 $\mathrm{g\,CO_2-eq/kWh}$ which is similar to CPV/HCPV systems (Lamnatou and Chemisana, 2017).

Chapter 7 Summary

The use of LCA to estimate lifecycle environmental impact category indicators of the HCPV/T 2000x system shows that the "production: thermal energy system", "production: tracking system", "operation and maintenance" subsystem boundaries are the main hotspots responsible for most environmental impacts at both midpoints (with 50%, 29% and 13% contribution respectively) and endpoint (with 55 %, 32 %, and 7 % contribution respectively) categories. The contribution to the environmental impacts is mostly due to the raw materials acquisition/production and manufacturing of the thermal energy and tracking systems.

The findings of this study were compared with results reported in the literature. It was found that the estimated GWP of HCPV/T 2000x system for EEIA was below the threshold of 50 $\mathrm{g\,CO_2-eq/kWh}$ (Lamnatou and Chemisana, 2017). Also, it was found that the lifecycle environmental impacts (including GWP) of the HCPV/T 2000x system are lower than fuel-based CHP and non-RES systems. Although the lifecycle environmental impact for EEIA of the HCPV/T 2000x system is higher than RES systems, the combined lifecycle environmental impact for EEIA and TEIA is potentially lower if the defined thermal energy functional unit of 1 kWh is met by fuel-based CHP system or non-RES system.

The study output of this chapter is the final milestone in this research project. The study completed in this chapter complements the study conducted in chapter 5 in terms of the combination of energy production, and environmental impacts for the critical assessment of material and energy flows of RES solutions for residential buildings. The HCPV/T 2000x system environmental impact is lower than fuel-based CHP and non-RES systems.

Chapter 8: Conclusion and Future Work

8.1 General Overview

This thesis presented work carried out to investigate energy efficiency strategies suitable for retrofit and their environmental impacts for low-rise single use residential buildings in hot countries. The research approach adopted two methods for investigation; to (a) increase energy efficiency and indoor thermal comfort in these buildings and (b) improve their environmental impacts. The investigation was conducted via experimental monitoring and computational study of two case study houses (located in Palermo, Sicily and Portmore, Jamaica), energy production study and lifecycle environmental impact study. The investigation involved the quantification of energy use, energy reduction and penalty due to the implementation of building energy-efficient technologies, improved thermal comfort and energy production by the solar energy systems, focussed on the case study houses. It also carried out environmental impact studies of the identified most suitable energy-efficient technology and solar energy system and compared them with other technologies based on data sourced through the literature.

The building energy-efficient technologies studied are cool roof paint, roof thermal insulation, window shading, A-rated appliances, and LED lighting. The cool roof paint, roof thermal insulation and window shading are retrofit solutions for building envelopes. Each energy-efficient technology was studied separately through thermal/energy modelling using the dynamic thermal simulation program EnergyPlus with the models calibrated with measured data. Their energy reduction potential was compared to the corresponding baseline energy demand of each case-study without the energy-efficient technologies. The cooling energy reduction potential and heating energy penalty by the cool roof paint was compared to the baseline cooling and heating energy demand. Similarly, the cooling and heating energy reduction potential by the roof thermal insulation was compared to the baseline. Finally, the replacement of typical appliances and lighting with A-rated appliances and LED lighting was compared to the baseline. The studied energy-efficient technologies showed varying energy reduction potential presented in Chapter 4.

A novel solar energy system was identified suitable for residential applications. This system was studied in detail at an experimental installation in Palermo Italy. This was enabled by the SMART GEMS European project. The system studied was the HCPV/T 2000x system,

comprising of three integrated subsystems: electrical energy system, thermal energy systems, and tracking system capable of producing electrical and thermal energy production. The electrical and thermal energy production of the HCPV/T 2000x system was assessed experimentally and analytically. It was compared to potential production of PV and PVT systems using dynamic thermal simulation; this is presented in Chapter 5.

The environmental impacts of the most energy-efficient building envelope technology (cool paint) and solar energy system (HCPV/T 2000x) were studied in detail. Cradle to Grave (CTGR) environmental impacts of the cool paint and HCPV/T 2000x system were assessed using the LCA method following the guidelines and framework of ISO 14044/40; this include goal and scope definition, inventory, impact assessment and result interpretation, described in chapter 1, Figure 1-**3**. SimaPro v8.2.3.0 software (PRé Sustainability, The Netherlands) with incorporated ReCiPe2016 environmental impact assessment method was used to assess the environmental impacts. This work is presented in Chapters 6 and 7.

The work followed the defined research objectives as presented in chapter 1, section 1.2, which were achieved; the results were presented in chapters 3 – 7. The key conclusions mapped to the objectives are presented in the next section.

8.2 Primary Conclusions

The summary of the five key conclusions presented below addresses the original five objectives of the research work defined in chapter 1, section 1.2.

Conclusion 1 (objectives 1 and 2): *Cool roof paint, roof thermal insulation, window shading, A-rated appliances and LED lighting are effective energy-efficient technologies suitable for retrofit of existing residential buildings in hot countries. HCPV/T 2000x, PV and PVT systems are solar energy systems with relatively high electrical and/or thermal energy efficiency also suitable for residential buildings in countries with high solar radiation.*
Cool roof paint and roof thermal insulation were the two most effective energy-efficient technologies amongst the five technologies studied, particularly suited for low rise buildings in which the roof area comprises a high percentage of the external area of the building envelope. Solar energy systems are suitable for built environment as they can be harmonically integrated

with buildings to provide household energy demand. They are especially applicable and efficient in hot climates with high solar radiation intensity throughout the year. HCPV/T 2000x, PV and PVT systems are solar energy systems that can be integrated with residential buildings to reduce dependency on non-RES systems, hence the potential to further reduce building environmental impacts.

The two case study low-rise houses (characterised with high ratio of roof area to the total surface area of the building) located in hot climates (Palermo, Sicily and Portmore, Jamaica), with high solar radiation intensity on the roof were used to assess the energy-efficient technologies and solar energy systems. The high solar radiation intensity on the roof is a result of the sun's inclination angle. Therefore, the application of the cool roof paint and roof thermal insulation are very effective in reducing cooling and/or heating energy demand. Also, high solar radiation increases the efficiency and the annual energy production potential of the HCPV/T 2000x, PV and PVT systems.

Conclusion 2 (objective 3): *The cool roof paint and roof thermal insulation demonstrated comparable cooling energy reduction potential and indoor thermal improvement for both case study houses. There was a heating energy penalty for cool roof paint application for Palermo, Sicily case study house*.

The simulated results obtained from the EP models calibrated using in-situ measurements, indicate that the two highest energy saving technologies are cool roof paint and roof thermal insulation. The energy savings by cool roof paint or the roof thermal insulation are similar. For Palermo, Sicily case study, the energy savings for cool roof paint and roof thermal insulation are -22 $kWh/m^2/year$ and -30 $kWh/m^2/year$ respectively, while for the Portmore, Jamaica case study, the energy savings are -189 $kWh/m^2/year$ and -194 $kWh/m^2/year$. The results indicate that energy savings are higher in poorly insulated roofs in locations with high solar radiation throughout the year and high ambient temperatures. Also, the cool roof paint showed a higher monthly indoor thermal improvement than roof thermal insulation for both case study houses. It can be concluded that cool roof paint is a more attractive and low-cost house retrofit solution than roof thermal insulation energy savings and indoor thermal comfort.

Conclusion 3 (objective 3): *The efficiency and annual energy production potential of the HCPV/T 2000x system is higher than PV and PVT systems*.

The HCPV/T 2000x and the PVT systems produce electrical and thermal energy. The HCPV/T

2000 system achieved a total average daily efficiency of ~80 %; 30 % for electrical efficiency and 50 % for thermal efficiency. The PVT system achieved electrical and thermal efficiency of 11 % and 47.5 %. The PV system that produces only electrical energy had an efficiency of 10 %. Based on the result, the HCPV/T 2000x system is an attractive solar energy system that can be integrated with residential buildings to meet heating and/or cooling energy demand, and lighting and appliances electrical demand.

Conclusion 4 (objectives 4 and 5): *The environmental impact of the cool roof paint is lower than a variety of thermal insulation materials.*

The cool roof paint being the most attractive low-cost house retrofit solution was investigated further for its environmental impact. The lifecycle environmental impact based on ReCiPe2016 method was compared with found literature studies of environmental impact of thermal insulation, a retrofit solution that demonstrated comparable energy savings to cool roof paint. The comparison showed that the lifecycle environmental impacts of the cool roof paint is lower than the variety of thermal insulation materials. The higher environmental impact of the thermal insulation materials is mainly due to production phase (which includes raw material acquisition and processing) of the system boundary. The main hotspot responsible for most of the environmental impacts of the cool roof paint are the production of polymer and pigment lifecycle phases, accounting for 49 % and 18 % respectively, at the endpoint category.

Conclusion 5 (objectives 4 and 5): *The environmental impact of the HCPV/T 2000x system is lower compared to fuel-based CHP and non-RES systems.*

The HCPV/T 2000x system being the most efficient solar energy system solution was investigated further for its environmental impact. The lifecycle environmental impact based on ReCiPe2016 method was compared with found literature studies of environmental impact of fuel-based CHP, non-RES and RES systems. The comparison showed that the lifecycle environmental impacts of the HCPV/T 2000x system are lower than fuel-based CHP and non-RES systems (which includes coal and natural gas systems). The HCPV/T 2000x system lifecycle environmental impacts are potentially lower than RES (which includes wind, solar PV – rooftop and nuclear), if thermal energy demand is met by met by fuel-based CHP system or non-RES system. Also, the main hotspot responsible for most of the environmental impacts of the HCPV/T 2000x system are “production: thermal energy system”, “production: tracking

system", "operation and maintenance" subsystem boundaries, accounting for 55 %, 32 % and 7 % respectively, at the endpoint category.

8.3 Research Impact on Academic and Industrial Sectors

The research project led to academic contribution via the publications of journal papers, a conference paper, and a conference poster. The integration of thermal modelling and Life Cycle Assessment (LCA) method used in this research project, can be used by researchers to investigate building energy-efficient technologies to improve energy performance and environmental impacts of residential buildings.

Academic and professionals in the built environment, including policy makers can make use of the information presented in this thesis to improve building energy and environmental performance. The cool roof paint can be used to address the growing cooling energy concern in hot countries, by retrofitting poorly insulated low-rise existing building roof. The cool roof paint can also be used on the roof of new low-rise building instead of roof thermal insulation because it is a low-cost solution with similar energy savings potential. The integration of HCPV/T 2000x system in residential buildings can be used as a step to improving environmental impact in the building sector. This is because it reduces the dependency on non-RES systems, which according to found literature studies have high environmental impact (including climate change).

8.4 Future Work

The opportunities to extend the research work in the future are summarised below.

Life Cycle Costing of the Cool Roof Paint and the HCPV/T 2000x System

The Life Cycle Costing (LCC) of the cool roof paint and the HCPV/T 2000x system aims to assess their economic sustainability. Economic sustainability is one of the three pillars of sustainability: environmental, economic, and social sustainability. The economic sustainability ensures that businesses or countries efficiently and sustainably use its resource to sustain a profit generation in the long term. LCC is an economic assessment tool that employs a life cycle approach to assess the financial costs and benefits of a product or service from the

investment cost (which includes materials and labour costs), operational maintenance and replacement costs during the use phase, financial benefit during the use phase, and end-of-life waste management costs and/or financial benefits. LCC of cool roof paint and HCPV/T 2000x system will help to identify the life cycle financial cost main contributors and establish the relationship between the life cycle financial and life cycle environmental main contributors. Also, the financial benefits can be calculated. In the case of the cool roof paint, the energy saving (-22 $kWh/m^2/year$ and -189 $kWh/m^2/year$ for the Palermo, Sicily, and Portmore, Jamaica case studies, respectively) financial benefit during the use phase can be assessed. The energy cost from RES systems including solar energy systems continues to decrease as the installation capacity increases. Therefore, there is a financial benefit of using energy from RES systems. In the case of the HCPV/T 2000x system, the financial benefit per kWh of the electrical and thermal energy from the HCPV/T 2000x system can be assessed.

Energy System Flexibility with Energy Storage

Energy system flexibility is important to ensure the continuous deployment of RES systems in the electrical and thermal distribution grid at the national/district level. The primary purpose of the energy system flexibility is to maintain a balance between energy demand and supply in a cost-effective and sustainable approach. Due to the intermittency of clean energy from RES systems, energy storage is continuously being developed for both off-grid and on-grid energy system applications. Energy storage helps to balance energy demand and supply, by storing the energy (or excess) generated from RES systems when it is available and supply the energy when needed. The integration of energy storage systems with RES systems has the potential to increase the efficiency of RES systems and improve their environmental impact potentials. Therefore, the energy performance and the environmental impacts of the HCPV/T 2000x system should be further studied for when it is integrated with energy storage systems. Electrical energy storage (such as mechanical, chemical, and electrochemical) and thermal energy storage (sensible heat, latent heat, and thermochemical) systems should be considered as potential storage systems.

Consequential LCA of the Cool Roof Paint, and the HCPV/T 2000x System

Consequential LCA (CLCA) aims to capture the direct and indirect environmental impact consequence of a certain activity compared to a baseline situation. The implementation of cool roof paint reduces the cooling energy demand consumption from the utility grid. Also, the implementation of the HCPV/T 2000x system (including the necessary energy storage systems)

displaces the electrical and thermal energy from the utility grid. Therefore, the indirect environmental impact consequence is the displaced electrical and/or thermal energy from the grid. The CLCA of the cool roof paint can be conducted by adopting system expansion; the cool roof paint system boundary (presented in Figure 6-**1**) is expanded to include the materials and energy flow of a cooling system such as air conditioning systems. The direct and indirect environmental impacts from the cool roof paint and the cooling system, respectively, can be critically assessed. Similarly, the CLCA of the HCPV/T 2000x system can be conducted by adopting the system expansion. The HCPV/T 2000x system boundary (presented in Figure 7-1) is expanded to include the materials and energy flows of the utility grid, energy storage system, and the energy demand and supply dynamics between the utility grid, energy storage system, and the load energy system.

References

Ascione, F., Bianco, N., Böttcher, O., Kaltenbrunner, R., Vanoli, G.P., 2016. Net zero-energy buildings in Germany: Design, model calibration and lessons learned from a case-study in Berlin. Energy Build. 133, 688–710. https://doi.org/10.1016/j.enbuild.2016.10.019

ASHRAE, 2017. Handbook, Fundamentals.

Autodesk, 2020. Green Building Studio. Available online: https://gbs.autodesk.com/GBS/ (accessed 12.5.20).

Ayodele, T.T., Taki, A., Oyinlola, M., Subhes, B., 2020. A review of retrofit interventions for residential buildings in hot humid climates. Int. J. Environ. Sci. Dev. 11, 251–257. https://doi.org/10.18178/IJESD.2020.11.5.1258

Bacenetti, J., Fusi, A., Azapagic, A., 2019. Environmental sustainability of integrating the organic Rankin cycle with anaerobic digestion and combined heat and power generation. Sci. Total Environ. 658, 684–696. https://doi.org/10.1016/j.scitotenv.2018.12.190

BS EN ISO 14040, 2006. Environmental management - Life cycle assessment - Principles and framework.

BS EN ISO 14044, 2018. Environmental management - Life cycle assessment - Requirements and guidelines.

Cellura, M., Guarino, F., Longo, S., Mistretta, M., 2014. Energy life-cycle approach in Net zero energy buildings balance: Operation and embodied energy of an Italian case study. Energy Build. 72, 371–381. https://doi.org/10.1016/j.enbuild.2013.12.046

Çengel, Y.A., Boles, M.A., 2015. Thermodynamics: An Engineering Approach, 8th editio. ed. McGraw-Hill.

Charles, R.G., Davies, M.L., Douglas, P., Hallin, I.L., Mabbett, I., 2019. Sustainable energy storage for solar home systems in rural Sub-Saharan Africa – A comparative examination of lifecycle aspects of battery technologies for circular economy, with emphasis on the South African context. Energy 166, 1207–1215. https://doi.org/10.1016/j.energy.2018.10.053

Chel, A., Kaushik, G., 2018. Renewable energy technologies for sustainable development of energy efficient building. Alexandria Eng. J. 57, 655–669. https://doi.org/10.1016/j.aej.2017.02.027

CIBSE AM11:2015, 2015. Building performance modelling.

CIBSE Guide A, 2019. Environmental design.

CIBSE TM63, 2020. Operational performance: Building performance modelling and calibration for evaluation of energy in-use. CIBSE.

Costa, F., Fregonese, D., Agnello, S., Cannas, M., 2011. Stability of sol-gel silica glass for CPV and ultraviolet LED applications. Glas. Technol. Eur. J. Glas. Sci. Technol. Part A 52, 185–189.

Cóstola, D., Blocken, B., Hensen, J.L.M., 2009. Overview of pressure coefficient data in building energy simulation and airflow network programs. Build. Environ. 44, 2027–2036. https://doi.org/10.1016/j.buildenv.2009.02.006

CRRC, 2019. Rated Products Directory. Available online: https://coolroofs.org/products/results (accessed 6.28.19).

Dabaieh, M., Wanas, O., Hegazy, M.A., Johansson, E., 2015. Reducing cooling demands in a hot dry climate: A simulation study for non-insulated passive cool roof thermal performance in residential buildings. Energy Build. 89, 142–152. https://doi.org/10.1016/j.enbuild.2014.12.034

Densley Tingley, D., Hathway, A., Davison, B., 2015. An environmental impact comparison of external wall insulation types. Build. Environ. 85, 182–189. https://doi.org/10.1016/j.buildenv.2014.11.021

Deshmukh, G., Birwal, P., Datir, R., Patel, S., 2017. Thermal Insulation Materials: A Tool for Energy Conservation. J. Food Process. Technol. 08. https://doi.org/10.4172/2157-7110.1000670

Desideri, U., Asdrubali, F., 2018. Handbook of Energy Efficiency in Buildings: A Life Cycle Approach. Elsevier Science & Technology.

DesignBuilder, 2020. DesignBuilder. Available online: https://designbuilder.co.uk/ (accessed 8.31.20).

Diouf, B., Avis, C., 2019. The potential of Li-ion batteries in ECOWAS solar home systems. J. Energy Storage 22, 295–301. https://doi.org/10.1016/j.est.2019.02.021

DOE-2, 2020. Available online: http://www.doe2.com/equest/ (accessed 12.5.20).

ECRC, 2019. Product Rating Programme. Available online: https://coolroofcouncil.eu/#section0 (accessed 6.28.19).

Emcore Corporation, 2012a. Triple-junction solar cell for terrestrial applications. CTJ photovoltaic cell – 5.5 mm x 5.5 mm. Datasheets Emcore.

Emcore Corporation, 2012b. Triple-junction solar cell for terrestrial applications. CTJ photovoltaic cell – 10 mm x 10 mm. Datasheets Emcore.

EU, 2018. Plastic waste and recycling in the EU: facts and figures. Available online:

http://www.europarl.europa.eu/news/en/headlines/society/20181212STO21610/plastic-waste-and-recycling-in-the-eu-facts-and-figures (accessed 3.20.19).

European Commission, 2020. An introduction to Life Cycle Assessment (LCA). Available online: https://www.buildup.eu/en/node/58457 (accessed 7.25.20).

European Commission, 2019a. Energy efficiency in buildings. Available online: https://www.buildup.eu/en/practices/publications/energy-efficiency-buildings (accessed 8.21.20).

European Commission, 2019b. The European Green Deal. COMMUNICATION FROM THE COMMISSION TO THE EUROPEAN PARLIAMENT, THE EUROPEAN COUNCIL, THE COUNCIL, THE EUROPEAN ECONOMIC AND SOCIAL COMMITTEE AND THE COMMITTEE OF THE REGIONS.

European Commission, 2019c. Review of Waste Policy and Legislation. Available online: http://ec.europa.eu/environment/waste/target_review.htm (accessed 3.20.19).

European Commission, 2016. Product Environmental Footprint Pilot Guidance - Guidance for the implementation of the EU Product Environmental Footprint (PEF) during the Environmental Footprint (EF) pilot phase - version 5.2 (pp. 95). Available online: http://ec.europa.eu/environment/eussd/smgp/pdf/Guidance_products.pdf (accessed 3.29.19).

European Commission, 2014. Grant Agreement number: 645677 — Smart Grids Energy management Staff (SMART GEMS).

European Commission - Joint Research Centre - Institute for Environment and Sustainability, 2010. International Reference Life Cycle Data System (ILCD) Handbook: General guide for Life Cycle Assessment - Provisions and Action Steps. Eur 24378 en - 2010, European Commission. https://doi.org/10.2788/94987

Evans, D.L., 1981. Simplified method for predicting photovoltaic array output. Sol. Energy 27, 555–560. https://doi.org/10.1016/0038-092X(81)90051-7

Fayazbakhsh, M.A., Bagheri, F., Bahrami, M., 2015. A Resistance – Capacitance Model for Real-Time Calculation of Cooling Load in HVAC-R Systems. J. Therm. Sci. Eng. Appl. https://doi.org/https://doi.org/10.1115/1.4030640

Feng, W., Zhang, Q., Ji, H., Wang, R., Zhou, N., Ye, Q., Hao, B., Li, Y., Luo, D., Lau, S.S.Y., 2019. A review of net zero energy buildings in hot and humid climates: Experience learned from 34 case study buildings. Renew. Sustain. Energy Rev. 114. https://doi.org/10.1016/j.rser.2019.109303

FEVE, 2015. Glass recycling hits 73 % in the EU. Available online: https://feve.org/wp-

content/uploads/2016/04/Press-Release-EU.pdf (accessed 3.20.19).

Gao, H., Koch, C., Wu, Y., 2019. Building information modelling based building energy modelling: A review. Appl. Energy 238, 320–343. https://doi.org/10.1016/j.apenergy.2019.01.032

Gao, Y., Xu, J., Yang, S., Tang, X., Zhou, Q., Ge, J., Xu, T., Levinson, R., 2014. Cool roofs in China: Policy review, building simulations, and proof-of-concept experiments. Energy Policy 74, 190–214. https://doi.org/10.1016/j.enpol.2014.05.036

Garg, V., Kotharkar, R., Sathaye, J., Rallapalli, H., Kulkarni, N., Reddy, N., Rao, P., Sarkar, A., 2016. Assessment of the impact of cool roofs in rural buildings in India. Energy Build. 114, 156–163. https://doi.org/10.1016/j.enbuild.2015.06.043

Gil, E., Martinez, M., Rubia, O. De, 2017. Operation and maintenance results from ISFOC CPV plants, in: AIP Conference Proceedings 1881. https://doi.org/https://doi.org/10.1063/1.5001405

González-garcía, S., Bacenetti, J., 2019. Exploring the production of bio-energy from wood biomass. Italian case study. Sci. Total Environ. 647, 158–168. https://doi.org/10.1016/j.scitotenv.2018.07.295

Graphisoft, 2020. EcoDesigner. Available online: https://graphisoft.com/downloads/ecodesigner/ecodesigner_download (accessed 12.5.20).

Herrando, M., Markides, C.N., Hellgardt, K., 2014. A UK-based assessment of hybrid PV and solar-thermal systems for domestic heating and power : System performance 122, 288–309. https://doi.org/10.1016/j.apenergy.2014.01.061

Hertwich, E.G., Gibon, T., Bouman, E.A., Arvesen, A., Suh, S., Heath, G.A., Bergesen, J.D., Ramirez, A., Vega, M.I., Shi, L., 2015. Integrated life-cycle assessment of electricity-supply scenarios confirms global environmental benefit of low-carbon technologies. Proc. Natl. Acad. Sci. 112, 6277–6282. https://doi.org/10.1073/pnas.1312753111

Hosseini, M., Akbari, H., 2014. Heating energy penalties of cool roofs: the effect of snow accumulation on roofs. Adv. Build. Energy Res. 8, 1–13. https://doi.org/10.1080/17512549.2014.890541

http://www.sika.com, 2020. http://www.sika.com. Available online: http://www.sika.com (accessed 10.25.20).

Huijbregts, Mark A.J., Steinmann, Z.J.N., Elshout, P.M.F., Stam, G., Verones, F., Vieira, M., Zijp, M., Hollander, A., van Zelm, R., 2017. ReCiPe2016: a harmonised life cycle impact assessment method at midpoint and endpoint level. Int. J. Life Cycle Assess. 22,

138–147. https://doi.org/10.1007/s11367-016-1246-y

Huijbregts, M.A.J., Steinmann, Z.J.N., Elshout, P.M.F., Stam, G., Verones, F., Vieira, M.D.M., Hollander, A., Zijp, M., Zelm, R. van, 2017. ReCiPe 2016 v1.1 A harmonized life cycle impact assessment method at midpoint and endpoint level Report I: Characterization. Available online: https://www.rivm.nl/en/life-cycle-assessment-lca/downloads (accessed 12.19.18).

IAI, 2009. Global Aluminium Recycling : A Cornerstone of Sustainable Development. Available online: http://www.world-aluminium.org/media/filer_public/2013/01/15/fl0000181.pdf (accessed 2.18.19).

IDA-ICE, 2020. IDA-ICE. Available online: https://www.equa.se/en/ida-ice

IEA, 2021. Net Zero by 2050. A Roadmap for the Global Energy Sector.

IEA, 2019. 2019 Global Status Report for Buildings and Construction. Towards a zero-emissions, efficient and resilient buildings and construction sector Foreword, United Nations Environment Programme.

IEA, 2018a. Energy Efficiency 2018 - Analysis and Outlooks to 2040.

IEA, 2018b. The Future of Cooling. Opportunities for energy efficient air conditioning 92.

IESVE, 2020. https://www.iesve.com/. Available online: https://www.iesve.com/ (accessed 8.23.20).

IPCC, 2018. Global Warming of 1.5°C. An IPCC Special Report on the impacts of global warming of 1.5°C above pre-industrial levels and related global greenhouse gas emission pathways, in the context of strengthening the global response to the threat of climate change,.

IPCC, 2014. Climate Change 2014: Mitigation of Climate Change. Contribution of Working Group III to the Fifth Assessment Report of the Intergovernmental Panel on Climate Change [Edenhofer, O., R. Pichs-Madruga, Y. Sokona, E. Farahani, S. Kadner, K. Seyboth, A. Adler,. Cambridge University Press, Cambridge, United Kingdom and New York, NY, USA. https://doi.org/https://doi.org/10.1017/CBO9781107415416

Iqbal, M.T., 2004. A feasibility study of a zero energy home in Newfoundland. Renew. Energy 29, 277–289. https://doi.org/10.1016/S0960-1481(03)00192-7

Italian Government - Ministry of Economical Progress, 2015. Interministerial Decree of 26 June 2015 - Adaptation of national guidelines for the energy certification of buildings. Available online: https://www.mise.gov.it/index.php/it/normativa/decreti-interministeriali/ 2032968-decreto-interministeriale-26-giugno-2015-adeguamento-linee-guida- nazionali- per- la- certificazione- energetica- degli- edifici (accessed

1.17.20).

Jamaica Bureau of Standards, 2019. Jamaican Standard Jamaica Application Document for the International energy conservation code.

Jessica Settino, Sant, T., Micallef, C., Farrugia, M., Staines, C.S., Licari, J., Micallef, A., 2018. Overview of solar technologies for electricity, heating and cooling production. Renew. Sustain. Energy Rev. 90, 892–909. https://doi.org/10.1016/j.rser.2018.03.112

Jha, S.K., Bilalovic, J., Jha, A., Patel, N., Zhang, H., 2017. Renewable energy: Present research and future scope of Artificial Intelligence. Renew. Sustain. Energy Rev. 77, 297–317. https://doi.org/10.1016/j.rser.2017.04.018

Kelly, K.A., Mcmanus, M.C., Hammond, G.P., 2014. An energy and carbon life cycle assessment of industrial CHP (combined heat and power) in the context of a low carbon UK. Energy 77, 812–821. https://doi.org/10.1016/j.energy.2014.09.051

Khairi, M., Jaapar, A., Yahya, Z., 2017. The application, benefits and challenges of retrofitting the existing buildings. IOP Conf. Ser. Mater. Sci. Eng. 271, 0–8. https://doi.org/10.1088/1757-899X/271/1/012030

King, D.L., Boyson, W.E., Kratochvill, J.A., 2004. SANDIA REPORT Photovoltaic Array Performance Model 43.

Kolokotroni, M., Gowreesunker, B.L., Giridharan, R., 2013. Cool roof technology in London: An experimental and modelling study. Energy Build. 67, 658–667. https://doi.org/10.1016/j.enbuild.2011.07.011

Kolokotroni, M., Wines, C., Babiker, R.M.A., Da Silva, B.H., 2016. Cool and Green Roofs for Storage Buildings in Various Climates. Procedia Eng. 169, 350–358. https://doi.org/10.1016/j.proeng.2016.10.043

Kribus, A., Kaftori, D., Mittelman, G., Hirshfeld, A., Flitsanov, Y., Dayan, A., 2006. A miniature concentrating photovoltaic and thermal system. Energy Convers. Manag. 47, 3582–3590. https://doi.org/https://doi.org/10.1016/j.enconman.2006.01.013

Kwame, A.B.O., Troy, N. V, Hamidreza, N., 2020. A Multi-Facet Retrofit Approach to Improve Energy Efficiency of Existing Class of Single-Family Residential Buildings in Hot-Humid Climate Zones.

Lamnatou, C., Chemisana, D., 2017. Concentrating solar systems : Life Cycle Assessment (LCA) and environmental issues. Renew. Sustain. Energy Rev. 78, 916–932. https://doi.org/10.1016/j.rser.2017.04.065

Laustsen, J., 2008. Energy Efficiency Requirements in Building Codes , Energy Efficiency Policies for New Buildings. Buildings 1–85. https://doi.org/10.1.1.378.1012

Marszal, A.J., Heiselberg, P., Bourrelle, J.S., Musall, E., Voss, K., Sartori, I., Napolitano, A., 2011. Zero Energy Building - A review of definitions and calculation methodologies. Energy Build. 43, 971–979. https://doi.org/10.1016/j.enbuild.2010.12.022

Meteonorm, 2019. Global meteorological database for Engineers, Planners and 403 Education, Meteotest, Bern, Switzerland. Available online: https://meteonorm.com/ (accessed 1.17.20).

Mittelman, G., Kribus, A., Dayan, A., 2007. Solar cooling with concentrating photovoltaic/thermal (CPVT) systems. Energy Convers. Manag. 48, 2481–2490. https://doi.org/https://doi.org/10.1016/j.enconman.2007.04.004

Mora, M.A.M., Vergara, C.F.P., Delgadillo, S.A.M., Nolasco, C.I.C., 2019. Environmental assessment of a combined heat and power plant configuration proposal with post - combustion - CO2 capture for the Mexican oil and gas industry. Clean Technol. Environ. Policy 21, 213–226. https://doi.org/10.1007/s10098-018-1630-3

Nishimura, A., Hayashi, Y., Tanaka, K., Hirota, M., Kato, S., Ito, M., Araki, K., Hu, E.J., 2010. Life cycle assessment and evaluation of energy payback time on high-concentration photovoltaic power generation system. Appl. Energy 87, 2797–2807. https://doi.org/10.1016/j.apenergy.2009.08.011

NREL, ANL, LBNL, ORNL, PNNL, 2019. Open Studio Support Software for Building Energy Modelling. Available online: http://nrel.github.io/OpenStudio-user-documentation/img/pdfs/openstudio_interface_quickstart.pdf (accessed 3.14.20).

Pisello, A.L., 2017. State of the art on the development of cool coatings for buildings and cities. Sol. Energy 144, 660–680. https://doi.org/10.1016/j.solener.2017.01.068

PRé, 2016. SimaPro Database Manual; Methods Library.

PRé, Goedkoop, M., Oele, M., Leijting, J., Ponsioen, T., Meijer, E., 2016. Introduction to LCA with SimaPro. Available online: https://www.pre-sustainability.com/download/SimaPro8IntroductionToLCA.pdf (accessed 2.3.17).

Radhi, H., Sharples, S., Taleb, H., Fahmy, M., 2017. Will cool roofs improve the thermal performance of our built environment? A study assessing roof systems in Bahrain. Energy Build. 135, 324–337. https://doi.org/10.1016/j.enbuild.2016.11.048

Rebitzer, G., Ekvall, T., Frischknecht, R., Hunkeler, D., Norris, G., Rydberg, T., Schmidt, W.P., Suh, S., Weidema, B.P., Pennington, D.W., 2004. Life cycle assessment Part 1: Framework, goal and scope definition, inventory analysis, and applications. Environ. Int. 30, 701–720. https://doi.org/10.1016/j.envint.2003.11.005

REN21, 2020. Renewables 2020 Global Status Report, REN21 Secretariat.

Renno, C., 2014. Optimization of a concentrating photovoltaic thermal (CPV/T) system used for a domestic application. Appl. Therm. Eng. 67, 396–408. https://doi.org/10.1016/j.applthermaleng.2014.03.026

Renno, C., Petito, F., 2013. Design and modeling of a concentrating photovoltaic thermal (CPV/T) system for a domestic application. Energy Build. 62, 392–402. https://doi.org/10.1016/j.enbuild.2013.02.040

RIVM, 2018. LCIA: The ReCiPe Model. Available online: https://www.rivm.nl/en/life-cycle-assessment-lca/recipe (accessed 3.13.19).

Rodriguez-Ubinas, E., Montero, C., Porteros, M., Vega, S., Navarro, I., Castillo-Cagigal, M., Matallanas, E., Gutiérrez, A., 2014. Passive design strategies and performance of Net Energy Plus Houses. Energy Build. 83, 10–22. https://doi.org/10.1016/j.enbuild.2014.03.074

Rosta, S., Hurt, R., Boehm, R., Hale, M.J., 2008. Performance of a zero-energy house. J. Sol. Energy Eng. Trans. ASME 130, 0210061–0210064. https://doi.org/10.1115/1.2844429

Ruch, R., Ludwig, P., Maurer, T., 2014. Balancing Hydronic Systems in Multifamily Buildings. Available online: https://www.nrel.gov/docs/fy14osti/62388.pdf (accessed 11.26.19).

Sanchez, D., Martinez, M., Gil, E., Rubio, F., Pachon, J.L., Banda, P., 2010. First experiences of ISFOC in the maintenance of CPV plants. New York: American Institute of Physics, 1970-2012.

Santamouris, M., 2014. Cooling the cities - A review of reflective and green roof mitigation technologies to fight heat island and improve comfort in urban environments. Sol. Energy 103, 682–703. https://doi.org/10.1016/j.solener.2012.07.003

Sartori, I., Napolitano, A., Voss, K., 2012. Net zero energy buildings: A consistent definition framework. Energy Build. 48, 220–232. https://doi.org/10.1016/j.enbuild.2012.01.032

Schiavoni, S., D'Alessandro, F., Bianchi, F., Asdrubali, F., 2016. Insulation materials for the building sector: A review and comparative analysis. Renew. Sustain. Energy Rev. 62, 988–1011. https://doi.org/10.1016/j.rser.2016.05.045

Serrano, S., Ürge-Vorsatz, D., Barreneche, C., Palacios, A., Cabeza, L.F., 2017. Heating and cooling energy trends and drivers in Europe. Energy 119, 425–434. https://doi.org/10.1016/j.energy.2016.12.080

Sharaf, O.Z., Orhan, M.F., 2015a. Concentrated photovoltaic thermal (CPVT) solar collector systems : Part I – Fundamentals , design considerations and current technologies. Renew. Sustain. Energy Rev. 50, 1500–1565. https://doi.org/10.1016/j.rser.2015.05.036

Sharaf, O.Z., Orhan, M.F., 2015b. Concentrated photovoltaic thermal (CPVT) solar collector systems : Part II – Implemented systems , performance assessment , and future directions. Renew. Sustain. Energy Rev. 50, 1566–1633. https://doi.org/10.1016/j.rser.2014.07.215

Sierra-Pérez, J., Boschmonart-Rives, J., Gabarrell, X., 2016. Environmental assessment of façade-building systems and thermal insulation materials for different climatic conditions. J. Clean. Prod. 113, 102–113. https://doi.org/10.1016/j.jclepro.2015.11.090

SimaPro, 2020. LCA. Available online: https://simapro.com/business/life-cycle-assessments/ (accessed 8.23.20).

Spirit Energy, 2017. Guide to Residential Battery Storage. Available online: https://www.spiritenergy.co.uk/residential-solar-storage (accessed 11.19.19).

Stamford, L., Greening, B., Azapagic, A., 2018. Life cycle environmental and economic sustainability of Stirling engine micro-CHP systems. Energy Technol. 6, 1119–1138. https://doi.org/https://doi.org/10.1002/ente.201700854

Steubing, B., Wernet, G., Reinhard, J., Bauer, C., Moreno-ruiz, E., 2016. The ecoinvent database version 3 (part II): analyzing LCA results and comparison to version 2. Int. J. Life Cycle Assess. 3, 1269–1281. https://doi.org/10.1007/s11367-016-1109-6

Sturm, M., Ag, S.I., Box, P.O., Butturi, M.A., Srl, C., Traversagno, V., 2010. Environmental sustainability of concentrator pv systems: preliminary lca results of the apollon project, in: World Conference on Photovoltaic Energy Conversion.

Suehrcke, H., Peterson, E.L., Selby, N., 2008. Effect of roof solar reflectance on the building heat gain in a hot climate 40, 2224–2235. https://doi.org/10.1016/j.enbuild.2008.06.015

Suszanowicz, D., 2017. Internal heat gain from different light sources in the building lighting systems. E3S Web Conf. 19. https://doi.org/10.1051/e3sconf/20171901024

Synnefa, A., Santamouris, M., 2012. Advances on technical, policy and market aspects of cool roof technology in Europe: The Cool Roofs project. Energy Build. 55, 35–41. https://doi.org/10.1016/j.enbuild.2011.11.051

Testa, J., Krarti, M., 2017. A review of benefits and limitations of static and switchable cool roof systems. Renew. Sustain. Energy Rev. 77, 451–460. https://doi.org/10.1016/j.rser.2017.04.030

The Modelica Association, 2020. Modelica. Available online: https://www.modelica.org/ (accessed 12.5.20).

Tong, C., 2019. Introduction to Materials for Advanced Energy Systems. https://doi.org/https://doi.org/10.1007/978-3-319-98002-7

Torcellini, P., Pless, S., Deru, M., Crawley, D., 2006. Zero Energy Buildings: A Critical Look at the Definition.

TrnSys, 2020. TrnSys. Available online: http://www.trnsys.com/ (accessed 7.29.20).

U.S. Department of Energy, 2019. EnergyPlusTM Documentation, Engineering Reference, The Reference to EnergyPlus Calculations available online. Available online: https://energyplus.net/sites/all/modules/custom/nrel_custom/pdfs/pdfs_v9.2.0/Engineerin%0AgReference.pdf (accessed 3.14.20).

U.S. Department of Energy, 2015. M & V Guidelines: Measurement and Verification for Performance-Based Contracts Version 4.0 1–306.

Underwood, C.P., Yik, F.W.H., 2004. Modelling Methods for Energy in Buildings, Modelling Methods for Energy in Buildings. https://doi.org/10.1002/9780470758533

UNEP, Graedel, T.E., Allwood, J., Birat, J.-P., Reck, B.K., Sibley, S.F., Sonnemann, G., Buchert, M., Hagelüken, C., 2011. Recycling Rates of Metals – A Status Report, A Report of the Working Group on the Global Metal Flows to the International Resource Panel. Available online: https://europa.eu/capacity4dev/unep/document/recycling-rates-metals-status-report (accessed 2.18.19).

United Nations, 2018. The Sustainable Development Goals Report.

United Nations Department of Global Communications, 2020. GUIDELINES FOR THE USE OF THE SDG LOGO INCLUDING THE COLOUR WHEEL, AND 17 ICONS.

Ürge-Vorsatz, D., Eyre, N., Graham, P., Harvey, D., 2012. Energy End-Use: Buildings.

Valladares-Rendón, L.G., Schmid, G., Lo, S.L., 2017. Review on energy savings by solar control techniques and optimal building orientation for the strategic placement of façade shading systems. Energy Build. 140, 458–479. https://doi.org/10.1016/j.enbuild.2016.12.073

Viebahn, P., Lechon, Y., Trieb, F., 2011. The potential role of concentrated solar power (CSP) in Africa and Europe-A dynamic assessment of technology development, cost development and life cycle inventories until 2050. Energy Policy 39, 4420–4430. https://doi.org/10.1016/j.enpol.2010.09.026

Wiesenfarth, M., Philipps, S.P., Bett, A.W., Horowitz, K., Kurtz, S., 2017. Current Status of Concentrator Photovoltaic Technology, Natl. Renew. Energy Lab. Available online:https://www.ise.fraunhofer.de/content/dam/ise/de/documents/publications/studies/cpv-report-ise-nrel.pdf (accessed 11.25.19).

Zampori, L., Saouter, E., Schau, E., Cristobal, J., Castellani, V., Sala, S., 2016. Guide for interpreting life cycle assessment result, Joint Research Centre.

https://doi.org/10.2788/171315

Žigart, M., Kovačič Lukman, R., Premrov, M., Žegarac Leskovar, V., 2018. Environmental impact assessment of building envelope components for low-rise buildings. Energy 163, 501–512. https://doi.org/10.1016/j.energy.2018.08.149

Appendix A Building Case Study Information

A.1 Construction and Material Properties of Building Envelope

Table A-1 and Table A-2 present the construction and material for Palermo, Sicily and Portmore, Jamaica case study houses respectively.

Table A-1: Construction and material for Palermo, Sicily case study house.

	Material												
Name	External wall brick	External wall surface plaster	External wood door	Floor cast concrete	Floor screed	Floor vinyl covering	Internal wall brick	Internal wall surface plaster	Internal wood door	Roof cast concrete	Roof internal surface plaster	Roof screed	Roof waterproof covering
Thickness (m)	0.105	0.013	0.105	0.15	0.075	0.005	0.105	0.013	0.105	0.15	0.013	0.075	0.0015
Conductivity (W/m. K)	0.77	0.57	0.14	1.33	0.46	0.17	0.56	0.18	0.14	1.33	0.57	0.46	0.23
Density (kg/m^3)	1750	1300	600	2000	1200	1390	1750	600	600	2000	1300	1200	110
Specific Heat (J/kg. K)	1000	1000	1700	1000	1000	900	1000	1000	1700	1000	1000	1000	1000
Thermal Absorptance	0.9	0.91	0.9	0.9	0.91	0.9	0.9	0.91	0.9	0.9	0.91	0.91	0.9
Solar Absorptance	0.5	0.4	0.7	0.725	0.73	0.7	0.5	0.4	0.7	0.725	0.4	0.73	0.7
Visible Absorptance	0.5	0.4	0.7	0.725	0.73	0.7	0.5	0.4	0.7	0.725	0.4	0.73	0.7

	Material					
Name	External detailed window glazing	External front (north) door	External side (east) detailed door glazing	External wall	Internal floor	Roof
Layer 1 (Outer)	Detailed window glazing	External wood door - 0.05 m	Detailed glass door glazing	External wall surface plaster - 0.013 m	Floor vinyl covering - 0.005 m	Roof waterproof covering - 0.00150 m
Layer 2				External wall brick - 0.105 m	Floor screed - 0.0750 m	Roof screed - 0.0750 m
Layer 3				External airspace - 0.050 m	Floor cast concrete - 0.150 m	Roof cast concrete 0.150 m
Layer 4				External wall brick - 0.105 m		Roof internal surface plaster - 0.013 m
Layer 5 (Inner)				Internal wall surface plaster - 0.013 m		

Table A-2: Construction and material for Portmore, Jamaica case study house.

Construction	External and internal door	External wall	Internal wall	Floor	Roof
Material	Steel panel	Precast concrete slab	Precast concrete slab	Precast concrete slab and terrazzo Tile	Precast concrete slab
Thickness	0.04	0.04	0.04	0.1	0.08
Conductivity	50	2.06	1.93	1.3	2.06
Density	7800	2400	2400	2400	2400
Specific heat	450	840	840	840	840
Thermal absorptance	0.93	0.93	0.93	0.93	0.93
Solar absorptance	0.85	0.85	0.85	0.85	0.85
Visible absorptance	0.7	0.7	0.7	0.7	0.7

A.2 Experimental Monitoring Pre- and After Application of Cool Roof Paint – Portmore, Jamaica Case Study House

First, the building roof was prepared by cleaning the surface with water. Thereafter, a primer coat was applied on the roofs precast concrete slab on 22nd March 2017. However, due to the bad weather condition, the application of the required three layers of the cool roof paint was prolonged and therefore applied from the 31st March 2017 to 16th April 2017. Figure A-1 shows the roof before and after the application of cool paint. The experimental monitoring before the application of the cool paint started in January 2017, while the monitoring after application continued until July 2017. The experimental monitoring parameters after the application of the cool roof paint are the same as that measured before the application, presented in section 3.2.2. The measured parameters are GHI, roof and ceiling temperatures, external air temperature and relative humidity and internal air temperature and relative humidity. The measured data were used to calibrate the EP model to accurately calculate the cooling energy savings potential and internal air temperature reduction by the cool roof paint. The accuracy of the simulated results compared to the measured results for the overall measurement period (presented in Figure A-2 and Table A-3) after the application of cool roof paint shows good agreement, with 99.3% of the hourly points within the recommended MBE statistical value of less than ±10 % (U.S. Department of Energy, 2015).

Figure A-1: Application of cool roof paint on the roof of Portmore, Jamaica case study house. The cool roof paint application was carried out by research partner at the University of Technology, Kingston, Jamaica.

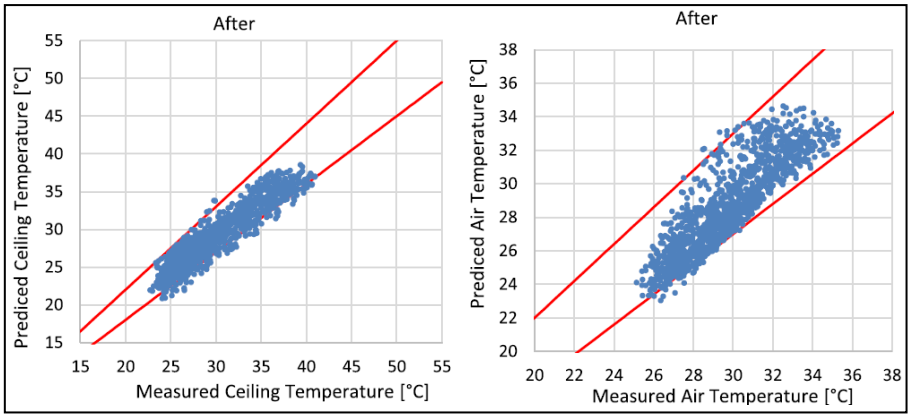

Figure A-2: Simulated vs. measured values of the ceiling and internal air temperatures after the application of cool roof paint for Portmore, Jamaica case study house.

Table A-3: MBE and CVRMSE of air and ceiling temperature for the Portmore, Jamaica case study house, after cool roof paint application.

Thermal Zones	MBE	CVRMSE	MBE	CVRMSE
	Air temperature		Ceiling temperature	
Livingroom	3.9 %	4.5 %	5.7 %	7.6 %
Bedroom 1	5.1 %	5.8 %	4.8 %	6.0 %
Bedroom 2	5.9 %	6.8 %	8.9 %	12.6 %
Kitchen	5.1 %	5.6 %	4.4 %	5.6 %

Figure A-3 and Figure A-4 are measured and simulated results for the indoor thermal comfort benefit of cool roof paint for Portmore, Jamaica case study house. Figure A-3, a graph of measured solar radiation, livingroom ceiling and air temperature; shows that the ceiling temperature and air temperature are lower after the application of cool roof paint (16th April 2017 to 25th April 2017). The average solar radiation and external air temperature during daytime were lower in March (average of 407 W/m ^{2} and 27.4 °C), period before (13th March 2017 to 23rd March 2017) cool roof paint was applied. The average solar radiation and external air temperature during the day time in April were averages of 428 W/m ^{2} and 27.9 °C. Figure A-4 present a further insight of the application of cool roof paint by showing two days (with similar average solar radiation and external air temperature during day time) of measured results before and after its application The first day, 13th March 2017 before cool roof paint application has an average of 413 W/m ^{2} and 27.3 °C, while the second day (24th April 2017) after cool roof paint application has an average of 428 W/m ^{2} and 28.2 °C. The result shows that livingroom ceiling temperature was higher on the 13th March 2017 by a maximum and average values of 18.6 °C and 6.8 °C respectively. The livingroom air temperature was higher on the 13th March 2017 by an average value of 2.3 °C.

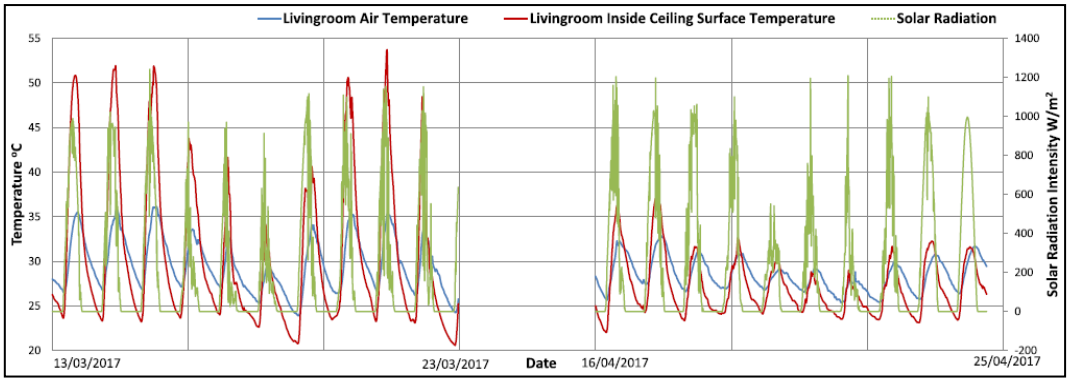

Figure A-3: Measured solar radiation, livingroom air and ceiling temperature before (13th March 2017 to 23rd March 2017) and after the application (16th April 2017 to 25th April 2017) of cool roof paint for Portmore, Jamaica case study house.

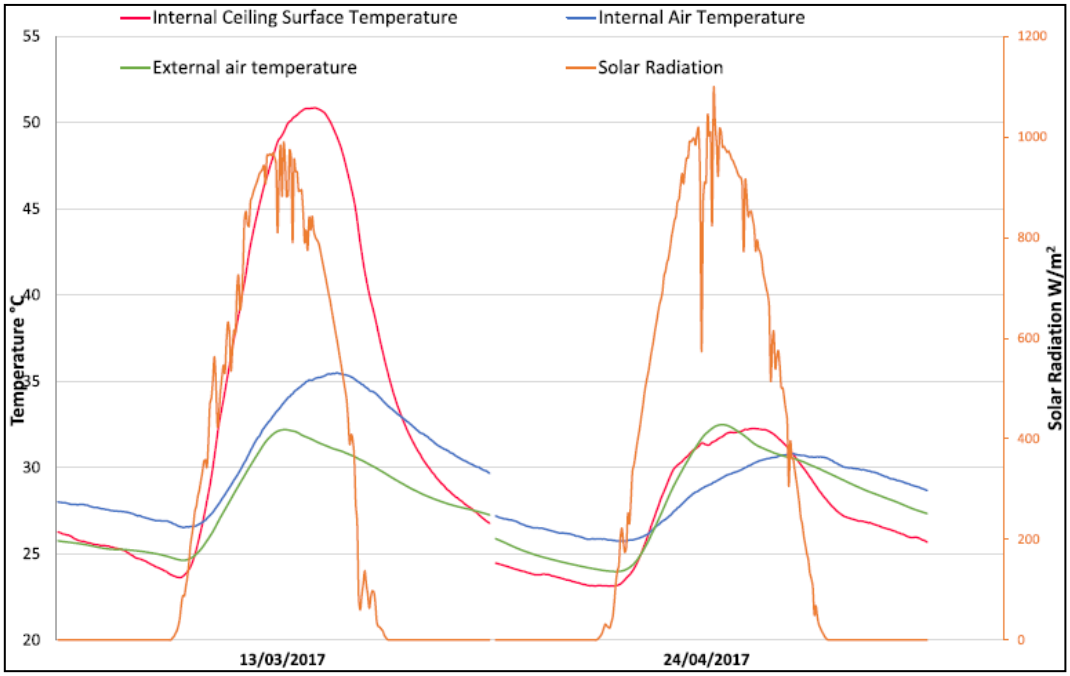

Figure A-4: Two days measured results of solar radiation, livingroom air and ceiling temperature before (13th March 2017) and after the application (24th April 2017) of cool roof for Portmore, Jamaica case study house.

A.3 Multi-Zone Airflow Network Modelling: Infiltration

Table A-4 and Table A-5 specify the properties of airflow through windows and doors when they are open for Palermo, Sicily and Portmore, Jamaica case study houses respectively. The air mass flow coefficient and air mass flow exponent are properties for when the window or door is closed, while the minimum density difference for two-way flow and discharge coefficient are properties for when the window or door is open. The opening allows for two-

way flow due to temperature difference, resulting in density difference. This creates a positive pressure difference at the top of the opening and negative pressure difference at the bottom, and vice versa (U.S. Department of Energy, 2019).

Table A-4: Infiltration airflow properties for Palermo, Sicily case study house.

Name	Window and door
Air Mass Flow Coefficient When Opening is Closed (kg/s.m)	0.000018
Air Mass Flow Exponent When Opening is Closed	0.65
Minimum Density Difference for Two-Way Flow (kg/m^3)	0.0001
Discharge Coefficient	1

Table A-5: Infiltration airflow properties for Portmore, Jamaica case study house.

Name	Window and door
Air Mass Flow Coefficient When Opening is Closed (kg/s.m)	0.001
Air Mass Flow Exponent When Opening is Closed	0.65
Minimum Density Difference for Two-Way Flow (kg/m^3)	0.0001
Discharge Coefficient	1

A.4 Multi-Zone Airflow Network Modelling: Natural Ventilation

Table A-6 and Table A-7 present the Wind Pressure Coefficient (WPCs) defined for different wind angle direction for Palermo, Sicily and Portmore, Jamaica case study houses respectively. Equation 3-1 defines the equation for pressure difference.

Table A-6: Natural ventilation airflow WPCs for Palermo, Sicily case study house.

Wind direction (angle)	WPC-North	WPC-South	WPC-East	WPC-West
0	0.4	-0.2	-0.3	-0.3
45	0.1	-0.35	0.1	-0.35
90	-0.3	-0.3	0.4	-0.2
135	-0.35	0.1	0.1	-0.35
180	-0.2	0.4	-0.3	-0.3
225	-0.35	0.1	-0.35	0.1
270	-0.3	-0.3	-0.2	0.4
315	0.1	-0.35	-0.35	0.1

Table A-7: Natural ventilation airflow WPCs for Portmore, Jamaica case study house.

Wind direction (angle)	WPC-North	WPC-South	WPC-East	WPC-West
0	-0.6	-0.6	-0.5	0.25
45	0.2	-0.5	-0.6	0.06
90	0.4	-0.3	-0.35	-0.35
135	0.2	-0.5	0.06	-0.6
180	-0.6	-0.6	0.25	-0.5
225	-0.5	0.5	0.06	-0.6
270	-0.3	0.4	-0.35	-0.35
315	-0.5	0.2	-0.6	0.06

Appendix B Sandia Model Parameters and Values

Table B-1 below contains the values and definition of parameters of the five critical five points (described in chapter 5, Figure 5-14), which mathematically describes the Sandia model described mathematically in equations B-1 to B-8. These values are available in EnergyPlus data sets (King et al., 2004; U.S. Department of Energy, 2019).

$$I_{sc} = I_{sco} \cdot f_1(AM_a) \cdot \left\{\left(E_b \cdot f_2(AOI) + f_d \cdot E_{diff}\right)/E_o\right\} \cdot \{1 + \alpha_{Isc} \cdot (T_c - T_o)\} \quad \text{B-1}$$

$$I_{mp} = I_{mpo} \cdot \{C_o \cdot E_e + C_1 \cdot E_e^2\} \cdot \left\{1 + \alpha_{Imp} \cdot (T_c - T_o)\right\} \quad \text{B-2}$$

$$V_{oc} = V_{oco} + N_s \cdot \delta(T_c) \cdot \ln(E_e) + \beta_{Voc}(E_e) \cdot (T_c - T_o) \quad \text{B-3}$$

$$V_{mp} = V_{mpo} + C_2 \cdot N_s \cdot \delta(T_c) \cdot \ln(E_e) + C_3 \cdot N_p \cdot \{\delta(T_c) \cdot \ln(E_e)\}^2 + \beta_{Vmp}(E_e) \cdot (T_c - T_o) \quad \text{B-4}$$

$$P_{mp} = I_{mp} \cdot V_{mp} \quad \text{B-5}$$

$$Fill\ Factor\ (FF) = P_{mp}/\left(I_{sc} \cdot V_{oc}\right) \quad \text{B-6}$$

$$I_x = I_{xo} \cdot \{C_4 \cdot E_e + C_5 \cdot E_e^2\} \cdot \{1 + \alpha_{Isc} \cdot (T_c - T_o)\} \quad \text{B-7}$$

$$I_{xx} = I_{xxo} \cdot \{C_6 \cdot E_e + C_7 \cdot E_e^2\} \cdot \left\{1 + \alpha_{Imp} \cdot (T_c - T_o)\right\} \quad \text{B-8}$$

Table B-1: Sandia performance input data for PV modelling (King et al., 2004; U.S. Department of Energy, 2019).

Parameters	Definitions	Values
I_{sc}	Short-circuit current (A)	4.8
I_{mp}	Current at maximum power point (A)	4.4
V_{oc}	Open-circuit current (V)	43.4
V_{mp}	Voltage at maximum power point (A)	4.4
I_x	Current at module voltage of $0.5V_{oc}$	4.79
I_{xx}	Current at module voltage of 0.5 $(V_{oc} + V_{mp})$	3.12